PHYSI

VOLUME 87 N

THE PHYSICAL REVIEW

A journal of experimental and theoretical physics established by E. L. Nichols in 1893

Published by the American Institute of Physics for the

AMERICAN PHYSICAL SOCIETY

Officers

President

J. H. VAN VLECK
Harvard University
Cambridge, Massachusetts

Vice-President

ENRICO FERMI
Institute for Nuclear Studies
University of Chicago
Chicago 37, Illinois

Secretary

K. K. DARROW
Bell Telephone Laboratories
Office:
Columbia University
New York 27, New York

Treasurer

G. B. PEGRAM
Columbia University
New York 27, New York

Local Secretary for the Pacific Coast

J. KAPLAN
University of California at Los Angeles
Los Angeles, California

Managing Editor

S. A. GOUDSMIT
Brookhaven National Laboratory
Upton, Long Island
New York

BOARD OF EDITORS

Editor

S. A. GOUDSMIT

Assistant Editor

S. FLÜGGE

Associate Editors

HARVEY BROOKS
R. F. CHRISTY
C. L. CRITCHFIELD
M. DEUTSCH
T. H. JOHNSON
BRUNO ROSSI
M. GOLDHABER
R. HOFSTADTER
A. W. LAWSON
A. PAIS
R. SERBER
C. H. TOWNES
W. P. ALLIS
F. G. BECKWITH
W. B. FRETTER
CONYERS HERRING
H. W. LEVERENZ
ARNOLD NORDSIECK

Manuscripts for publication should be submitted to S. A. Goudsmit, Brookhaven National Laboratory, Upton, Long Island, New York. The authors' institutions are requested to pay a publication charge of $15 per page which, if honored, entitles them to 100 free reprints. Instructions will be sent with galley proofs.

Proof and all correspondence concerning papers in the process of publication should be addressed to the Publication Manager, American Institute of Physics, 57 East 55 Street, New York 22, New York.

Subscription Price

United States and Canada.....$30.00
Elsewhere.....$32.00

Back Numbers[1]

Yearly back number rate when complete year is available:
Prior to 1949: $25.00
Thereafter: $33.00
Single copies: $3.00 each, prior to July, 1929;
$1.50 each, July, 1929–December, 1941;
$3.00 each, January, 1942–December, 1946;
$1.50 each, thereafter.
General index, 1893–1920: $4.00.

Subscriptions, renewals, and orders for back numbers should be addressed to the American Institute of Physics, 57 East 55 Street, New York 22, New York.

Changes of address in the case of members of the American Physical Society should be addressed to the Treasurer; in the case of other subscribers to the American Institute of Physics.

[1] For Series 1 inquire of Physics Department, Cornell University, Ithaca, New York.

The Physical Review is published semi-monthly at Prince and Lemon Streets, Lancaster, Pennsylvania.

Entered as second-class matter March 6, 1917, at the Post Office at Lancaster, Pennsylvania, under the Act of March 3, 1879.

Acceptance for mailing at special rate of postage provided for in paragraph (d-2), section 34.40, P. L. & R. of 1948, authorized January 27, 1925.

THE
PHYSICAL REVIEW

A journal of experimental and theoretical physics established by E. L. Nichols in 1893

SECOND SERIES, VOL. 87, NO. 2 JULY 15, 1952

Angular Correlations in the $Li^6(d,p)Li^{7*}(\gamma)Li^7$ Reaction

C. M. CLASS AND S. S. HANNA
*Department of Physics, The Johns Hopkins University, Baltimore, Maryland**
(Received January 30, 1952)

The yield of radiation in the $Li^6(d,p)Li^{7*}(\gamma)Li^7$ reaction has been measured as a function of angle in correlation with protons observed in the direction of the beam and with the beam alone. No anisotropy was detected in either observation. The only plausible theoretical explanation of these results is the assignment of $I=1/2$ to the first excited state of Li^7 in agreement with other recent observations.

I. INTRODUCTION

DIRECTIONAL effects in the emission of particles from nuclei are an important source of information on the properties of nuclear energy levels. The direction of emission may be correlated with the direction of an incoming particle initiating the reaction[1–3] or with the direction of some other emitted particle.[3,4] It has been pointed out[3,5] that the two cases are similar in their formal aspects. General rules have been given[3,5] which govern the complexity of the correlation between any two particles, either incoming or outgoing, in a nuclear process, provided no other directional information is supplied in the experiment.

In a reaction frequently encountered, particle P enters a nucleus to form a compound system, which decays by emission of particle Q to an excited state in a final nucleus and then by γ-emission to the ground state. Angular distributions of the type (P,Q) and (P,γ) have been studied in a number of instances.[6] The angular correlation (Q,γ) has also been investigated in reactions in which particle P enters as an s wave and thus has no influence on the subsequent correlation measurement.[7,8] When the entering wave is not isotropic, however, the correlation (Q,γ) is in reality a correlation (P,Q,γ) among all three particles, since the direction of the incident particle P is generally specified by the experimental arrangement. The situation is equivalent to the (γ,γ,γ) or the (P,γ,γ) correlations which have been treated by Beidenharn, Arfken, and Rose.[9] If the assumption is made that the angular momenta associated with the motion of the particles and with the state of the compound nucleus are all unique, the only additional complexity in the present case arises when particle Q as well as particle P has a spin. The most general case which might be encountered, however, may involve overlapping states in the compound nucleus and multiple values of orbital angular momenta for the particles. The calculation of the correlation function is then exceedingly complex, and the result will include interference terms and a large number of unknown parameters.

The interference effects which involve only magnetic substates and are peculiar to the triple process may be eliminated by observing any two of the radiations in parallel or antiparallel directions.[9,10] The most convenient arrangement for studying states in the final nucleus is to observe the particles Q in the same direction as the beam particles P, a process which we shall designate by $(PQ;\gamma)$. The correlation function may

* Assisted by a contract with the AEC.
[1] R. D. Myers, Phys. Rev. **54**, 361 (1938); E. Gerjuoy, Phys. Rev. **58**, 503 (1940); C. L. Critchfield and E. Teller, Phys. Rev. **60**, 10 (1941); D. R. Inglis, Phys. Rev. **74**, 21 (1948).
[2] E. Eisner and R. G. Sachs, Phys. Rev. **72**, 680 (1947); L. Wolfenstein and R. G. Sachs, Phys. Rev. **73**, 528 (1948).
[3] C. W. Yang, Phys. Rev. **74**, 764 (1948).
[4] D. R. Hamilton, Phys. Rev. **58**, 122 (1940); G. Goertzel, Phys. Rev. **70**, 897 (1946); D. L. Falkoff and G. E. Uhlenbeck, Phys. Rev. **79**, 323 (1950); S. P. Lloyd, Phys. Rev. **80**, 118 (1950); J. A. Spiers, Phys. Rev. **80**, 491 (1950).
[5] L. Eisenbud, Phys. Rev. **76**, 185 (1949).
[6] See the review by Hornyak, Lauritsen, Morrison, and Fowler, Revs. Modern Phys. **22**, 291 (1950).
[7] B. Rose and A. R. W. Wilson, Phys. Rev. **78**, 68 (1950).
[8] W. R. Arnold, Phys. Rev. **80**, 34 (1950); Barnes, French, and Devons, Nature **166**, 145 (1950).
[9] Biedenharn, Arfken, and Rose, Phys. Rev. **83**, 586 (1951).
[10] B. A. Lippmann, Phys. Rev. **81**, 162 (1951).

then be written

$$W(\theta)=\sum_{m_2}\sigma_{m_2}(0)\sum_{m_3}P_{m_2m_3}(\theta), \qquad (1)$$

where $\sigma_{m_2}(0)$ is the partial cross section for the formation of the substate m_2 in the residual nucleus following the emission of particle Q in the direction $\theta=0$; and $P_{m_2m_3}(\theta)$ expresses the relative probability of a transition from the sublevel m_2 of the excited state with angular momentum I_2 to the sublevel m_3 of the final state with angular momentum I_3, by means of 2^{L_2} pole radiation in the direction θ.[11]

Even in those cases in which it seems impractical to calculate the quantities $\sigma_{m_2}(0)$, the correlation function (1) can provide useful information. Since the function

$$U_{m_2}(\theta)=\sum_{m_3}P_{m_2m_3}(\theta) \qquad (2)$$

will be a polynomial in $\cos^2\theta$ of degree not greater than L_2 or I_2, whichever is smaller, a measurement of the correlation function makes it possible to set a lower limit on the value of the spin I_2. A unique assignment of spin may not be possible, even when $L_2>I_2$, since it can happen in rare cases that the function (2) will not attain the maximum allowed complexity.[12] It is also possible that the (P, Q) transition will limit the complexity of the correlation function (1). Except for accidental cancellations, however, it is possible to predict the extent of this limitation for any given case. As has been shown by Biedenharn, Arfken, and Rose,[9] the maximum power of $\cos^2\theta$ in the correlation function cannot exceed either L_0+L_1 or I_1+L_1, whichever is smaller, where L_0 and L_1 are the orbital angular momenta associated with P and Q, respectively, and I_1 is the angular momentum of the compound nucleus.[13] Thus in the triple process the complexity will exceed that allowed by L_1, provided there are no other limitations, and it is possible to have an anisotropic correlation even with $L_1=0$.

TABLE I. Angular distribution of radiation emitted in the transition from the substate m_2 of the state I_2 to the state $I_3=3/2$. The functions have the proper relative weight within each group.

I_2	Radiation	m_2	$U_{m_2}(\cos^2\theta)$
1/2	MD	$\pm1/2$	1
1/2	EQ	$\pm1/2$	1
3/2	MD	$\pm3/2$	$6-3\cos^2\theta$
		$\pm1/2$	$4+3\cos^2\theta$
3/2	EQ	$\pm3/2$	1
		$\pm1/2$	1
5/2	MD	$\pm5/2$	$5+5\cos^2\theta$
		$\pm3/2$	$7-\cos^2\theta$
		$\pm1/2$	$8-4\cos^2\theta$
5/2	EQ	$\pm5/2$	$35-45\cos^2\theta+40\cos^4\theta$
		$\pm3/2$	$17+105\cos^2\theta-120\cos^4\theta$
		$\pm1/2$	$32-60\cos^2\theta+80\cos^4\theta$

[11] The quantity $\sigma_{m_2}(0)$ may be calculated in the manner used in the references given in 1 and will in general involve many unknown parameters. The calculation of $P_{m_2m_3}(\theta)$ is straightforward and includes only known quantities. See, for example, references in 4.

[12] Arfken, Biedenharn, and Rose, Phys. Rev. **84**, 89 (1951).

A particularly simple application is to the case of an isotropic $(PQ;\gamma)$ correlation. Since $L_2\geqslant1$, the isotropy probably arises either from the condition $I_2<1$ or from a limitation imposed by the (P, Q) transitions. For the latter to be the case L_1 must equal 0 and either $L_0=0$ or $I_1<1$. In either event the angular distribution of Q relative to P must also be isotropic. If, therefore, the $(PQ;\gamma)$ correlation is isotropic while the (P, Q) correlation is not, the only possible formal limitation is $I_2<1$. In a similar manner the angular distribution of the γ-rays relative to the particles P with Q unobserved is also informative.[14] In this case the complexity of the (P, γ) distribution is limited by the smallest of the quantum numbers (L_0, I_1, I_2, L_2).[9] If again the (P, γ) correlation is isotropic while the (P, Q) correlation is not, the spin I_2 provides the only possible formal limitation.

II. THE $Li^6(d,p)Li^{7*}(\gamma)Li^7$ REACTION

In two reactions it has been established that radiation from the first excited state of Li^7 is emitted isotropically. Littauer[15] has observed an isotropic distribution relative to the incident proton beam in the $Li^7(p,p')Li^{7*}(\gamma)Li^7$ reaction. Unless $L_0=0$ for the entering protons or $I_1=0$ for the compound nucleus Be^8, this result would indicate a spin $I_2<1$, or in the case of Li^7, $I_2=1/2$.† Rose and Wilson[7] have measured the angular correlation between the radiation and the alpha-particles in the $B^{10}(n,\alpha)Li^{7*}(\gamma)Li^7$ reaction, and they find it to be isotropic. In this instance the entering slow neutrons have $L_0=0$ so that the correlation is a simple (α,γ) process, for which quantitative correlation functions can be calculated. The likely possibilities have been examined by Feld[16] and by Devons,[17] and only the case $I_2=1/2$ gives an isotropic correlation function[18] in accordance with the rules discussed above, if the radiation is taken to be either pure magnetic dipole or pure electric quadrupole. Since, however, for the case $I_2=5/2$ (or 7/2) the parity and angular momentum selection rules give $L_1=1$ for the alpha-particles, the correlation function is limited to a $\cos^2\theta$ complexity for

[13] If the values of L_0, I_1, and L_1 are not unique, this statement will apply separately to each part of the correlation function corresponding to a particular L_0, I_1, and L_1, but it must be modified appropriately for the terms in which values of L_0, I_1, or L_1 are mixed.

[14] S. S. Hanna, Phys. Rev. **76**, 686 (1949).

[15] R. M. Littauer, Proc. Phys. Soc. (London) **A63**, 294 (1950).

† *Note added in proof:*—A. H. Bethel and R. E. Segel in this laboratory have obtained evidence that the inelastic protons in this reaction are not emitted isotropically, thereby strengthening the assignment of $I_2=1/2$.

[16] B. T. Feld, Phys. Rev. **75**, 1618 (1949).

[17] S. Devons, Proc. Phys. Soc. (London) **A62**, 580 (1949).

[18] See, however, the case $I=3/2$ below.

both types of radiation. Accordingly, it is possible to obtain a cancellation of the $\cos^2\theta$ term by a somewhat unlikely mixture of magnetic dipole and electric quadrupole radiation.[17,19]

In the $Li^6(d,p)Li^{7*}(\gamma)Li^7$ reaction the angular distribution of protons relative to the entering deuterons has been measured at bombarding energies from 0.3 to 1.4 Mev.[20] The measured angular yield functions contain terms as high as $\cos^4\theta$. The odd terms which are observed are indicative of interference between waves of opposite parity. It seems likely therefore that incoming deuterons with $L_0=0$, 1, 2 contribute to the reaction. There is evidence perhaps in these distributions that the (d,p) stripping process contributes partially to the reaction. A forward peak, characteristic of the theory of Butler,[21] begins to form above 1 Mev but is inconspicuous at lower energies, where we shall assume the reaction involves primarily the compound nucleus.

In order to investigate the complexity which may be attained by the yield function of the gamma-rays correlated either to the protons observed in the direction of the deuteron beam or to the beam alone, the distribution functions (2) are listed in Table I for magnetic dipole and electric quadrupole radiation, taking $I_3=3/2$ (odd parity) for the ground state of Li^7 and three choices, $I_2=1/2$, 3/2, 5/2 (all odd parity), for the excited state. It is seen that these functions attain their maximum complexity, except for the case of quadrupole radiation and $I_2=3/2$.[12] With a knowledge of these functions and the rules discussed above it is possible to predict the maximum power allowed in the correlation functions for any particular choice of L_0, I_1, L_1, I_2, and L_2. An examination of all possible cases reveals that a nonisotropic correlation $W(\theta)$ is expected unless $I_2=1/2$ or $I_2=3/2$ (quadrupole). Furthermore, the gamma distribution function relative to the beam is found to be at least as complex as the proton distribution, except for the same two cases. Actual correlation functions $W(\theta)$ have been calculated for a variety of choices of L_0, I_1, and L_1, for $I_2=5/2$ and 3/2 (dipole). In each instance the maximum power of $\cos^2\theta$ was that predicted by the rules. The numerical coefficients ranged from 0.2 to 2.5 times the isotropic term, and in the dipole case were almost uniformly negative for $I_2=5/2$. For all the cases examined involving $L_0=2$, which seems required by the evidence from the (d,p) angular distributions, and for some with $L_0=0,1$, the quadrupole expression involved a term in $\cos^4\theta$. Undoubtedly the real correlation function would include terms corresponding to several choices of L_0, I_1, and L_2, as well as some in which values of these quantities were mixed. Below a bombarding energy of 1 Mev, however, the yield of the reaction indicates the presence of a fairly strong resonant state in the compound nucleus.[20] No matter what assignment is made to this resonance, one could expect to find a nonisotropic correlation for the "resonant" part of the reaction, except for $I_2=1/2$ or for pure quadrupole radiation and $I_2=3/2$.

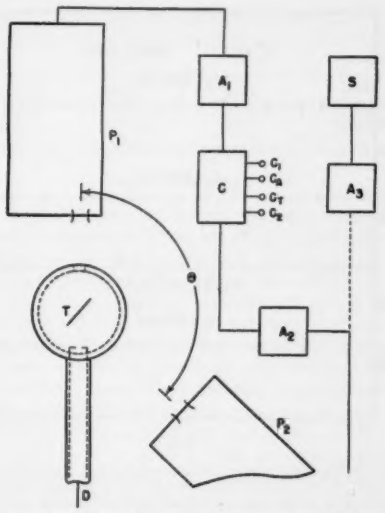

FIG. 1. Schematic diagram of the apparatus: (D) deuteron beam; (T) lithium target on thin backing; (P_1) fixed proton counter; (P_2) rotating gamma-counter; (θ) correlation angle; (A_1, A_2) 10-mc linear amplifiers; (C) coincidence circuit; (C_1, C_2) single channel registers; (C_T, C_A) total and accidental coincidence registers; (A_3) 3-mc linear amplifier; (S) single channel discriminator. The last two circuits were used to obtain energy resolution of the radiation observed in the experiment.

III. EXPERIMENTAL APPARATUS

The energy of the deuteron beam, supplied by the electrostatic accelerator of the Department of Physics, was in the range 600 to 900 kev for which the remarks of the preceding section would apply. In an effort to decrease single channel counting rates enriched Li^6 targets were used in the correlation measurements. One was prepared in a small mass spectrograph,[22] available in the laboratory, with provision for transporting the target without breaking vacuum to the beam tube of the accelerator in order to minimize oxygen contamination. A second target was prepared with lithium sulfate compound[23] having a Li^6/Li^7 ratio of 20. The first target was reasonably thin (less than 0.1 mg/cm^2) and relatively free from oxygen. The

[19] D. R. Inglis, Phys. Rev. **81**, 914 (1951).
[20] Krone, Hanna, and Inglis, Phys. Rev. **75**, 335 (1949); **80**, 603 (1950); W. Whaling and T. W. Bonner, Phys. Rev. **79**, 258 (1950); D. N. F. Dunbar and F. Hirst, Phys. Rev. **83**, 164 (1951).
[21] S. T. Butler, Proc. Roy. Soc. (London) **A208**, 559 (1951).
[22] Built according to the design of Smyth, Rumbaugh, and West, Phys. Rev. **45**, 724 (1934).
[23] Produced by Carbide and Carbon Chemicals Division, Oak Ridge National Laboratory, Y-12 Area, Oak Ridge, Tennessee and obtained on allocation from the Isotopes Division of the AEC.

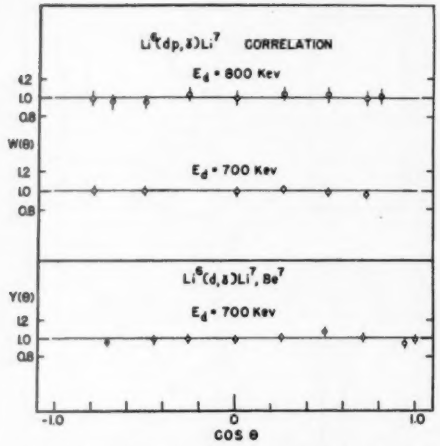

FIG. 2. Measured angular correlations in the $Li^6(d,p)Li^{7*}(\gamma)Li^7$ reaction: (Top) gamma-rays correlated with protons emitted in the direction of the deuteron beam. (Bottom) gamma-rays from Li^{7*} and Be^{7*} correlated only with the deuteron beam.

sulfate target was appreciably thicker (containing roughly the same amount of lithium), but it had relatively less Li^7 (owing principally to a faulty alignment in the lithium separator in the preparation of the first target) and gave a reduced gamma-ray intensity resulting from Li^7 bombardment.

The experimental arrangement is shown schematically in Fig. 1. The aluminum wall surrounding the target was $\frac{1}{8}$ inch thick. Thin aluminum windows were provided for observing charged particles, but one side of the chamber was free for observation of the gamma-rays. The protons and the gamma-rays were detected with anthracene and sodium iodide crystals, respectively, in conjunction with the RCA 5819 photomultiplier tube. In order to reduce gamma and neutron background the anthracene was in the form of a thin, 5-mil flake. Appropriate tests showed that this system, shielded by suitable foils, was an efficient detector of the two proton groups from the Li^6 reaction with unimportant contributions from other radiations. The NaI(Tl) crystal was a $\frac{3}{4}$-inch cube mounted in a Lucite cup, containing mineral oil and making good optical contact with the photomultiplier. Aluminum foil served as a reflector. The efficiency for 0.5-Mev radiation was found to be roughly 50 percent. The proton counter was fixed at zero degrees to the beam, while the gamma-counter was free to rotate in a horizontal plane. Both counters were shielded with lead and aluminum to reduce background. The solid angles of the detectors, about 2×10^{-4} steradian for the gamma-counter and 10^{-4} steradian for the proton counter, produced coincidence rates of about 10/min and total single channel rates on the order of 10^3/sec.

Pulses from the cathode followers of the counters passed through 10-mc amplifiers having gains of about 100. Sensitive trigger circuits were employed in conjunction with blocking oscillators to produce uniform pulses which were mixed on the grids of a pentode for coincidence detection. Single channel rates were obtained directly from the blocking oscillators. Resolving times down to 30 or 40 millimicroseconds were used without excessive loss of true coincidences. In the experiment the background of uncorrelated phenomena in each detector produced an appreciable accidental coincidence rate, which was monitored by feeding the output of each blocking oscillator to a second coincidence detector which received only random pulses. This was accomplished by introducing a 0.5-microsecond delay into the line from one of the blocking oscillators. This procedure is particularly desirable because the unsteadiness of the beam produces an unsteady source of radiation from the target, which results in a higher accidental rate than would be calculated from the resolving time and the single counter rates. In operation it is important to know only the ratio of the resolving times of the two coincidence detectors. This value was measured over long periods of time and found to be subject to only negligible drifts.

IV. THE (dp,γ) CORRELATION[24]

The correlation measurements were obtained by observing the (p,γ) coincidence rate from the $Li^6(d,p)Li^{7*}(\gamma)Li^7$ reaction at angles of the gamma-counter from 35° to 145°. Despite the fact that symmetry about 90° is expected, measurements were obtained in both the front and back quadrants as a check on geometric and scattering effects. The integrated beam intensity was measured with a beam current integrator and also with the total proton count from the fixed proton counter; the two measurements agreed satisfactorily. For each observation the coincidence rate was corrected for slight variations in the distance of the gamma-counter. In all some 100 observations were made at nine angles of the gamma-counter, and approximately 45,000 real coincidences were observed. The measurements were compatible with an isotropic distribution, the observed fluctuations being consistent with the expected statistical uncertainty. The data, presented in Fig. 2, are the results of two separate observations taken several months apart with different targets (see above), somewhat different bombarding energy, and with alterations in counters, circuitry, and geometry. Effects of scattering were investigated by placing lead absorbers in strategic places and by observing the decay of the coincidence counting rate

[24] A brief account of part of the measurements reported in this section has been given in Nature **168**, 429 (1951). Measurements on the (p,γ) correlation in which the protons were observed at 90° have been reported by J. O. Newton, Proc. Phys. Soc. (London) **A64**, 938 (1951). See also W. H. Burke and J. R. Risser, Phys. Rev. **85**, 741 (1952); and Phillips, Heydenburg, and Cowie. Phys. Rev. **85**, 742 (1952).

when various thicknesses of lead were interposed between the target and the gamma-counter.

V. THE (d,γ) ANGULAR DISTRIBUTION

In order to obtain additional evidence for the isotropy of radiation from the excited state under study, a brief investigation was made of the angular distribution of such radiation relative only to the direction of the incident deuteron beam. Energy discrimination was employed in order to discard radiation from target impurities, but the 480- and the 430-kev gamma-rays from Li^{7*} and Be^{7*}, respectively, were not resolved. In these mirror nuclei there is little doubt as to the identical nature of the first excited states.[25] Since the (d,γ) distribution with the proton (or neutron) unobserved will in general differ from the (dp,γ) correlation, unless of course they are both necessarily isotropic, a measurement of the former should provide additional evidence. On the other hand, if the isotropy of the Li^{7*} radiation is conceded, the observation will serve to confirm the expected isotropy of Be^{7*} radiation. The relative yield of Li^{7*} and Be^{7*} radiation was not determined quantitatively in the present experiment, but from observations reported in the literature[6] it can be estimated very roughly that the yields are comparable.

The radiation from the lithium target was detected with a NaI(Tl) crystal similar to the one used in the correlation measurements with minor changes in the mounting to improve the resolving characteristics of the system. All shielding was removed from around the counter assumbly, except for a lead collimator which served greatly to reduce annihilation radiation coming from the walls of the target chamber (arising from the positron activity induced by deuteron bombardment of carbon). The pulses from the photomultiplier after amplification were analyzed in a single channel discriminator[26] with a 1.5 volt channel width. The system was calibrated with annihilation radiation from a Na^{22} source. The angular measurements were obtained by recording the unresolved photopeak of the Li^{7*} and Be^{7*} radiation at several angles with respect to the deuteron beam. No significant angular effects were observed in these measurements, either in the height of the peaks or in the area under the peaks. The data, corrected for geometric effects and small contributions from annihilation radiation, are shown in Fig. 2.

[25] Brown, Snyder, Fowler, and Lauritsen, Phys. Rev. **82**, 159 (1951); D. R. Inglis, Phys. Rev. **82**, 181 (1951).
[26] K. I. Roulston, Nucleonics **7**, 27 (1950).

TABLE II. Coefficients in the series $1+A_1\cos\theta+A_2\cos^2\theta$.

	E_d	A_1	A_2
(dp,γ)	800 kev	0.040	−0.029
(dp,γ)	700 kev	0.009	−0.011
(d,γ)	700 kev	0.023	−0.078

VI. DISCUSSION

As presented the data include the instrumental and geometric corrections. There are in addition small corrections (~1 percent) arising from the motion of the recoiling Li^{7*} nucleus at the instant of emission of the radiation. After applying these corrections the data were analyzed into series of the form $1+A_1\cos\theta+A_2\cos^2\theta$ by the method of least squares. The results are given in Table II. The coefficients obtained differ from zero by amounts which are easily compatible with the uncertainties in the measurements. In view of the definite and fairly complex asymmetry observed in the (d,p) process, it is striking that in both processes involving the gamma-ray no asymmetry can be detected. Although it is conceivable that an isotropic (or nearly isotropic) correlation function could be constructed for a spin $I_2>1/2$, it seems very unlikely that at the same time the (d,γ) process would not display a detectable anisotropy or vice versa. The most reasonable conclusion is that the lack of anisotropy arises from the nature of the gamma distribution functions, Table I. The choice is between $I_2=1/2$ with either dipole or quadrupole radiation or both and $I_2=3/2$ with pure quadrupole radiation. The latter choice is unlikely in view of the lifetime[27] (~10^{-13} sec) of the radiating state, which indicates that magnetic radiation probably predominates and in addition $I_2=3/2$ seems rather implausible theoretically.[28] The assignment $I_2=1/2$ to the first excited states of Li^7 and Be^7 is the only reasonable explanation for the isotropy of the radiation in the present two observations as well as in the $B^{10}(n,\alpha\gamma)Li^7$ and $Li^7(p,p'\gamma)Li^7$ reactions.

Our thanks are due Paul W. Milich for the construction and care of a considerable part of the equipment used in the experiment, H. M. Watts of the Radiation Laboratory of The Johns Hopkins University for valuable discussions in connection with the circuits employed, and S. M. Shafroth for assistance in measuring the (d,γ) angular distributions.

[27] L. G. Elliott and R. E. Bell, Phys. Rev. **76**, 168 (1949).
[28] H. H. Hummel and D. R. Inglis, Phys. Rev. **81**, 910 (1951).

Beta-Spectra and Internal Conversion Coefficients for Co^{60}, Nb^{95}, Au^{198}, and Hf^{181}

CHANG-YUN FAN*
Department of Physics, University of Chicago, Chicago, Illinois
(Received January 14, 1952)

Using a double-lens beta-ray spectrometer, the beta-spectra and the internal conversion coefficients for Co^{60}, Nb^{95}, Au^{198}, and Hf^{181} were investigated. All the beta-spectra were found to be of allowed shape with end-point energies 0.306±0.005 Mev, 0.160±0.003 Mev, 0.97±0.01 Mev, and 0.408±0.008 Mev, respectively. The extra activity presented in Au^{198} was identified to be Au^{199}, and the slow neutron absorption cross section of Au^{199} was estimated to be about 10^6 barns.

The internal conversion coefficients indicate that both of the gamma-rays from Co^{60} are E-2^2 radiations; the 0.77-Mev gamma-ray from Nb^{95} is either an M-2^1 or an E-2^2 radiation or a mixture of both; the 0.411-Mev gamma-ray from Au^{198} is an E-2^2 radiation; the 0.474-Mev gamma-ray from Hf^{181} is an E-2^2 radiation, the 0.134-Mev and 0.340-Mev gamma-rays are M-2^1 radiations, and the 0.130-Mev gamma-ray is doubtful but seems to be an E-2^2 radiation.

The results are discussed from the point of view of the beta-decay theory and the shell structure model (Mayer, Haxel, Jensen, and Suess).

I. INTRODUCTION

WITHIN the past few years the theory of internal conversion has been worked out in some detail by several investigators, and a complete table of the K-shell internal conversion coefficients was published recently by Rose and his collaborators.[1] The general purpose of such calculations is to evaluate the probability of the transition of K, L, etc., atomic electrons to states of the continuum under the influence of the electromagnetic radiation emitted by the nucleus when an isomeric transition occurs. An essential feature is that the probability of the transition depends upon the intensity of the electromagnetic field in the vicinity of the nucleus where the field decreases with a power of r determined by the multipole order of the radiation. Hence the measurement of the probability of the transition of atomic electrons from different shells affords a method of exploring the multipole order of the transition.

Two selection rules govern the nature of the electromagnetic radiation, from which it becomes possible to draw some conclusions about the nuclear states involved in the transition. The first is the rule that the photon which is emitted from a 2^l electric or magnetic multipole has angular momentum lh with respect to the position of the multipole.[2,3] Thus, if I and I' are the angular momenta in units of h of the initial and final states of the radiating system, then l must have the value

$$|I+I'| \geqslant l \geqslant |I-I'|, \tag{1}$$

with the lowest value of l most probable.

The second selection rule governs the parity change between initial and final states. Electric 2^l-pole and/or magnetic 2^{l-1}-pole radiation occur only between states of the same parity if l is even, and only between states of opposite parity if l is odd.[2,3]

This paper describes the study of a number of cases in which a nucleus A is transformed by beta-decay into an excited state of a stable nucleus B. The transition from the excited state of B occurs by the emission of an internally converted gamma-ray.

In so far as Fermi's theory of beta-decay applies, it is usually possible to draw some conclusion about the spin and parity changes involved in the beta-ray process from the shape of the beta-spectrum and the ft-value.[4,5] Such studies of the beta-spectrum together with the coefficients of internal conversion provide a check of the theoretical predictions of the spins and parities of nuclei A and B, such as those given by the shell structure model.[6] The present work was undertaken to provide sufficient accuracy in the experimental determination of beta-spectra and internal conversion coefficients so that a significant test of the shell theory could be made.

II. APPARATUS AND CALIBRATION

1. Beta-Ray Spectrometer

All the measurements were carried out by using the double-lens beta-ray spectrometer[7] of this laboratory (Fig. 1). The spectrometer consists of two current carrying coils 95.8 cm apart. The source was placed at the center of one coil and the detector was placed at the center of the other. Electrons from the source were detected only when their trajectories were of the first order,[7] those having trajectories of higher orders being eliminated by a helical baffle at the center of the instrument. The transmission and the resolving power of the instrument were controlled by two iris diaphragms situated in close contact with the ends of the helical baffle. Because of the large dimensions of the instrument, scattering from the side walls was practically absent. Scattering from the helical baffle was eliminated

* Now at Yerkes Observatory, Williams Bay, Wisconsin.
[1] Rose, Goertzel, Spinrad, Harr, and Strong, Phys. Rev. **83**, 79 (1951).
[2] W. Heitler, Proc. Cambridge Phil. Soc. **32**, 112 (1936).
[3] E. Segrè and A. C. Helmholz, Revs. Modern Phys. **21**, 271 (1949).
[4] E. Fermi, Z. Physik **88**, 161 (1934).
[5] E. J. Konopinski, Revs. Modern Phys. **15**, 209 (1943).
[6] M. G. Mayer, Phys. Rev. **78**, 16 (1950).
[7] H. Agnew and H. L. Anderson, Rev. Sci. Instr. **20**, 869 (1949).

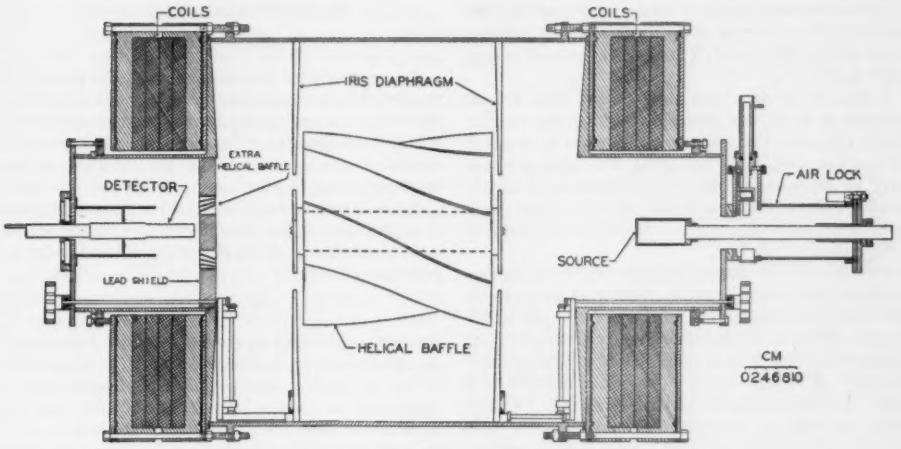

FIG. 1. The beta-ray spectrometer.

by introducing an extra helical baffle in front of the detector. The Compton electrons produced by gamma-rays from the source were reduced to a negligible amount when this device was installed.

2. Calibration

Although the spectrometer makes use of an iron shell to shield the orbits from the earth's magnetic field, its linearity is not noticeably impaired thereby and a single constant $k=I/p$ relates the momentum p with the current in the coil I. This constant was checked by observing the current at which the maxima of the conversion lines of Cs^{137} (624 kev)[8] and of Co^{60} (1163.1 kev and 1323.2 kev)[9] appeared. Values of the constant k from these calibration points were 16.92, 16.91, and 16.90, where p is in units of mc and I is in amperes. The value $k=16.91$ was adopted in the calculations.

The transmission of the spectrometer was determined by a beta-gamma coincidence measurement using a Co^{60} source. With the source and the beta-ray counter in the standard position in the spectrometer, a gamma-ray counter having a 2-mm brass window was placed 2 cm behind the source. The gamma-ray counting rate N_γ, the beta-ray counting rate N_β, and the beta-gamma coincidence rate $N_{\beta\gamma}$ were measured for various values of current in the spectrometer. Co^{60} decays by emitting a beta-ray followed by two gamma-rays in cascade; thus, at any given value of the current,

$$N_{\beta\gamma}/N_\beta=\epsilon_1(1-\alpha_1)+\epsilon_2(1-\alpha_2) \quad (2)$$

and

$$N_\gamma=\epsilon_1(1-\alpha_1)N+\epsilon_2(1-\alpha_2)N, \quad (3)$$

where ϵ_1 and ϵ_2 are the efficiencies of the counter for counting gamma-rays 1 and 2, respectively, α_1, α_2 are the total internal conversion coefficients corresponding to the two gamma-rays, respectively, and N is the total number of beta-disintegrations per second. Here, the possible beta-gamma angular correlation is taken to be zero.[10] The absolute strength of the source is given by

$$N=N_\beta N_\gamma/N_{\beta\gamma}. \quad (4)$$

Using this value and the area A under the momentum spectrum of Co^{60}, which is equal to the product of N, the resolution w, and the transmission t of the instrument [Eq. (6)], the transmission can be determined.

It was found that when the counter position was fixed, the transmission depended very sensitively on the source position. Thus, the position of the source and the control diaphragms were carefully adjusted to get (1) sufficient resolution and (2) the highest possible transmission. For a source 4 mm in diameter, the transmission was 1 percent with a resolution of 2 percent.

3. The Counter

A spherical G-M counter was originally used for the detector. This type of counter was designed particularly for a system in which low energy electrons receive an accelerating voltage at the detector to aid them in the penetration of the thin window.[7] Later, a cylindrical counter was used which had an efficiency which was more nearly independent of the energy of the electrons. Figure 2 shows a sketch of the cylindrical counter. It was constructed of a 4 in. long brass tubing with twenty-two $\frac{1}{16}$ in.$\times\frac{1}{2}$ in. slots distributed around the circumference, and a center wire along the axis of the tubing. Nylon foils, made conducting by evaporating

[8] L. M. Langer and R. D. Moffat, Phys. Rev. **78**, 75 (1950).
[9] Lind, Brown, and DuMond, Phys. Rev. **76**, 591 (1949).
[10] R. L. Garwin, Phys. Rev. **76**, 1876 (1949).

5 $\mu g/cm^2$ of aluminum on them, were used for the window.[11] The thickness of the window ranged between 80 $\mu g/cm^2$ to 100 $\mu g/cm^2$; it stopped electrons of energy below 5 kev.

A mixture of neon and amyl-acetate with a total pressure of 8 cm was generally used for the counter filling. On several occasions, ethyl-acetate at pressure 2.4 cm was used. With the latter, the vapor pressure could be kept constant by dipping liquid ethyl-acetate into ice, and the thickness of the counter window could be reduced to 50 $\mu g/cm^2$ which corresponds to a cut-off energy about 3 kev.[12]

The efficiency of counters was also studied at various pressures. Let m be the number of electrons per molecule and p be the pressure (in cm Hg) of the gas in the counter. It was found that the efficiency of the particular counter used was almost proportional to mp for beta-particles of energy ≈ 0.6 Mev when $mp < 70$. For $mp \geqslant 70$, the efficiency of the counter reached its maximum and remained constant. The value of mp for 8 cm of neon is 80, and it is 115 for 2.4 cm of ethyl-acetate.

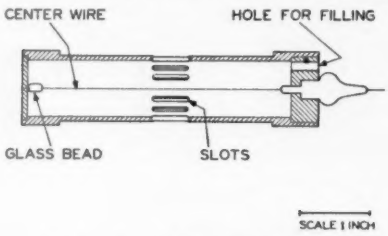

FIG. 2. A sketch of the cylindrical counter.

100 percent efficiency for electrons for the whole range in beta-ray spectrometer work was therefore assumed.

4. Sources

Sources were deposited on 15 $\mu g/cm^2$ Nylon foils having a thin backing of evaporated aluminum. The weight of the sources was determined by controlling the total amount of liquid deposited, and the uniformity was checked by radio-autograph. All the samples reported here were obtained from Oak Ridge National Laboratory except those mentioned specially.

[11] The method used to wrap thin foils on a cylinder was as follows: A wet foil was laid on a rectangular frame of a width slightly smaller than the length of the counter and a length slightly longer than that of the circumference of the counter. Then the counter, whose surface was painted with clear glyptal, was placed at one end of the frame. The foil could then be picked up and glued to the surface when the counter was rolled carefully over the frame. It was necessary to leave enough space on the counter shell without slots for the overlapped ends of the foil.

[12] The ethyl-acetate filling permitted the use of thinner window and more stable gas pressure. However, it was found that the counters with the ethyl-acetate filling had several minor drawbacks. They needed higher applied voltage (1700 v); they produced pulses less uniform in height and having a longer dead time (≈ 100 μsec). The plateau was also shorter, viz., having about 30 volts with a 2 percent slope.

III. EXPERIMENTAL METHOD

1. Momentum Spectrum

By a momentum spectrum is meant the plot of the number of beta-disintegrations $n(p)$ per unit momentum interval per second *vs* the corresponding momentum p of the beta-particles. The quantity $n(p)$ cannot be measured directly because of the finiteness of the resolving power of a beta-ray spectrometer. However, it can be shown that $n(p)$ is related to the counting rate N_c of the detector, the transmission t, and the resolution w of the beta-ray spectrometer by the following approximate equation:

$$n(p) = N_c/pwt = kN_c/Iwt, \tag{5}$$

where k is the constant previously defined. Equation (5) is a good approximation for $0 < p < p_{max}(1-w)$ provided (1) an originally monoenergetic line of momentum p' appears as an isosceles triangle, and (2) the resolution w which is defined as the ratio of the width of the triangle at the half-maximum, $\Delta p'$, to the momentum p' is a constant. A detailed discussion is given in the appendix.

In the present measurement, the assumption (1) was justified by the shapes of single conversion lines measured, and the assumption (2) was justified by the linear relationship found between the coil current I and the magnetic rigidity p as shown in Agnew and Anderson's paper.[7] Since p was proportional to the coil current I, a momentum spectrum was thus obtained by plotting N_c/I *vs* p or $H\rho$. Consequently, the area under the momentum spectrum is

$$A = Nwt, \tag{6}$$

where N is the total number of beta-disintegrations per second.

2. Maximum Energy of a Beta-Spectrum

The maximum energy of a beta-spectrum was determined by means of a Fermi plot. Since Eq. (5) is no longer correct and the counting rate is low for p near p_{max}, experimental points near the end of the beta-spectrum were ignored in curve-fitting according to the method of least squares. The percentage errors in the final results were obtained by the standard statistical method.[13]

3. Internal Conversion Coefficient

The ratio of the number of K-shell electrons ejected per second, N_K, to the number of gamma-quanta emitted per second, N_γ, is defined to be the K-shell internal conversion coefficient, α_K, and similar definitions hold for α_L, etc. The ratio of the total number of internal conversion electrons ejected per second, N_e,

[13] H. Margenau and G. Murphy, *The Mathematics of Physics and Chemistry* (D. Van Nostrand Company, Inc., New York, 1943), pp. 487–502.

to N_q is called the total internal conversion coefficient α. However, in older literature, the internal conversion coefficient was defined as the ratio of the internal conversion electrons to the number of radiative transitions N_γ, i.e., $\alpha' = N_e/N_\gamma = N_e/(N_q+N_e)$, where the "primed" quantity denotes the older definition. In this paper, the former definition is followed in agreement with the more recent custom.[14]

The measurement of the internal conversion coefficients for a given isotope does not require a knowledge of the true activity of the source if the decay scheme is known. Let N be the total number of beta-disintegrations per second. The area under the curve of the plot of the momentum spectrum is $A = Nwt$ according to Eq. (6) provided that the window absorption of the counter is negligible. The area under the K-shell internal conversion peak in the momentum spectrum is equal to $A_K = \alpha_K' N_\gamma wt$. Therefore,

$$\alpha_K' = A_K N / A N_\gamma, \tag{7}$$

where the quantity N_γ/N can be determined from the known decay scheme. The value of α_K is thus given by the following expression:

$$\alpha_K = \alpha_K'/(1-\alpha'), \tag{7'}$$

which is used to compare with the theoretical values of Rose *et al.*

A Fermi plot of the momentum spectrum is essential to decide what part of the curve is due to the beta-rays and what part is due to the conversion electrons, and to make the correction at low energies for the cutoff of the counter window. Accordingly, such plots were made in every instance. Where some degree of forbiddenness was revealed in a lack of straightness using the simple Fermi rules, an appropriate correction factor was applied.[5] However, because of the distortions due to the source thickness and the uncertainty of Fermi's theory over the low energy range, a correction curve for the window absorption thus obtained might not be correct. Hence, one-half of the difference of the area under the measured spectrum and that under the corrected spectrum was taken as the possible error of the measurement.

IV. RESULTS

1. Co^{60}

5.3-year Co^{60} decays into an excited state of Ni^{60} by negatron emission, with a maximum energy of 0.31 Mev. Subsequently two gamma-rays of energy 1.1715 Mev and 1.3316 Mev, respectively, are emitted in cascade. The beta-spectrum was found to be of allowed shape down to 0.17 Mev.[15]

The coefficients of internal conversion for Co^{60} were measured first by Deutsch and Siegbahn[16] and then by Waggoner, Moon, and Roberts.[17] Their measurements indicate that the two gamma-rays are both due to electric quadrupole radiations. However, in all these measurements, thick window counters were used. It was considered worth-while to study the same problem with thin window counters.

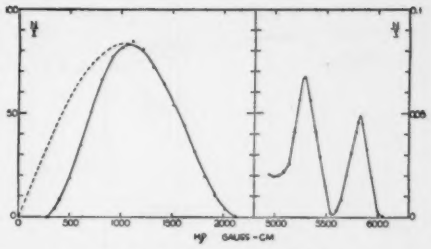

FIG. 3. The beta-spectrum of Co^{60}.

The measured beta-spectrum of Co^{60} is shown in Fig. 3. A 10-microcurie source of 0.2-mg/cm² thickness and 0.5-cm diameter was used. The internal conversion peaks are shown in the same figure with the scale enlarged 1000 times. The rising background on the left side of the first peak is known to be caused by Compton electrons produced in the source. It was found that the beta-spectrum is allowed down to 70 kev with an end-point energy 0.306±0.005 Mev as shown in Fig. 4. The dotted curve in Fig. 3 is the extension of the beta-spectrum corresponding to the extrapolation to zero energy of the straight Fermi plot. The total internal conversion coefficient is found to be $(1.72\pm0.17)\times10^{-4}$ for the 1.17-Mev gamma-ray and $(1.24\pm0.12)\times10^{-4}$ for the 1.33-Mev gamma-ray, where the experimental errors are taken according to the assumption stated in Sec. III. A comparison of the present measurement with those of the other authors is given in Table I, where the experimental errors assumed by the latter are also indicated.

The values of α_K are unknown because the K lines were not resolved from L, etc., lines. However, the

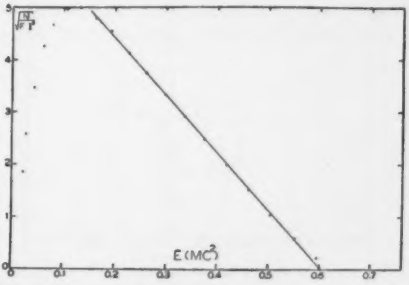

FIG. 4. The Fermi plot for the beta-spectrum of Co^{60}.

[14] See, for example, J. R. Reitz, Phys. Rev. **77**, 10 (1950).
[15] Deutsch, Elliot, and Roberts, Phys. Rev. **68**, 193 (1945).
[16] M. Deutsch and K. Siegbahn, Phys. Rev. **77**, 680 (1950).
[17] Waggoner, Moon, and Roberts, Phys. Rev. **80**, 420 (1950).

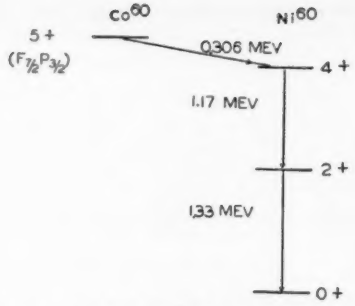

FIG. 5. The decay scheme of Co^{60} and the suggested level values.

values of α_K/α_L can be roughly estimated from Goldhaber and Sunyar's empirical curves;[18] they are high for all multipole radiations. If $\alpha_K/\alpha_L \approx 10$ is assumed for both gamma-rays, $\alpha_K=(1.55\pm0.15)\times10^{-4}$ for the 1.17-Mev gamma-ray and $\alpha_K=(1.12\pm0.11)\times10^{-4}$ for the 1.33-Mev gamma-ray. A comparison of these values with the theoretical ones in Table II[1] permits one to assign both gamma-rays to be more likely E-2^2 radiations. This is in agreement with the angular correlation measurement[19] and the polarization-direction correlation measurement[20] which assigned the states of Ni^{60} involved in the decay of Co^{60} as 0+, 2+, and 4+, respectively. However, the internal conversion measurements alone would not rule out the possibility of M-2^1 or mixed M-2^1 and E-2^2 transitions, if one interprets the experimental uncertainties rather conservatively.

The Fermi plot of the beta-spectrum is straight down to 70 kev. This, together with the absence of beta-gamma angular correlation,[10] allows one to conclude that the transition is allowed, though the ft-value is rather high ($\log ft=7.5$). This means, accepting the assignment 4+ for the state of Ni^{60} for Co^{60} decay, that

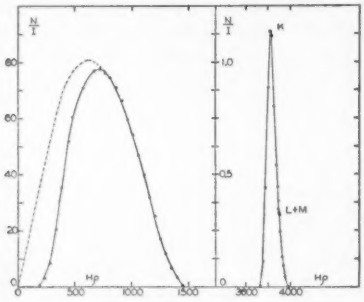

FIG. 6. The beta-spectrum of Nb^{95}.

[18] M. Goldhaber and A. W. Sunyar, Phys. Rev. **83**, 906 (1951).
[19] E. L. Brady and M. Deutsch, Phys. Rev. **78**, 558 (1950).
[20] F. Metzger and M. Deutsch, Phys. Rev. **78**, 551 (1950).

Co^{60} has a 5+, 4+, or 3+ ground state according to the G-T selection rules. The possibility of a 3+ state can be ruled out by the fact that there is no evidence for transitions from Co^{60} to the lower excited state of Ni^{60}. The experimental evidence at hand does not permit one to decide between the assignments 4+ and 5+. Shell structure model predicts 5+ for Co^{60} [21] and is thus not inconsistent with our results. A tentative conclusion about the level values involved in the decay of Co^{60} is shown in Fig. 5.

TABLE I. Total internal conversion coefficient$\times10^4$.

	1.17 Mev	1.33 Mev
Deutsch and Siegbahn	2.32±0.6	1.83±0.5
Waggoner *et al.*	1.73±0.061	1.286±0.035
The present measurement	1.72±0.17	1.24±0.12

2. Nb^{95}

The decay scheme of 37-day Nb^{95} is simple. The work of Mandeville, Scherb, and Keighton[22] indicates indeed that beta-decay of Nb^{95} into Mo^{95} is followed by a single gamma-ray. The beta-spectrum and the internal conversion coefficient have been determined by Hudgens and Lyon.[23] Figure 6 shows the beta-spectrum of Nb^{95} obtained from the present measurement using a two-microcurie source of 0.05-mg/cm^2 thickness and 0.5-cm diameter. The purity of the source was checked by observing the decay rate over 9 half-lives and was found to be sufficient for the purpose of the experiment. The internal conversion peak is plotted in the same figure on a scale enlarged eighty times. The Fermi plot is seen in Fig. 7 to be straight down to 40 kev. The dotted curve in Fig. 6 is the extrapolation of the beta-spectrum corresponding to a straight Fermi plot down to zero energy. The present results differ in some respects from those of Hudgens and Lyon. A comparison is given in Table III.

TABLE II. K-internal conversion coefficients$\times10^4$.

	E-2^1	E-2^2	E-2^3	M-2^1	M-2^2
1.17 Mev	0.72	1.55	3.01	1.38	2.87
1.33 Mev	0.58	1.17	2.07	1.03	2.07

The L and M conversion line can only barely be resolved from the K conversion line. By comparing the heights of the two tips as indicated in Fig. 6, or by decomposing the conversion line into two isosceles triangles and comparing their area, one obtains as a rough estimate for $\alpha_K/\alpha_L \approx 4$, i.e., $\alpha_K \approx 1.3\times10^{-3}$. The error introduced in measuring the area under the beta-spectrum is about 10 percent.

[21] Mayer, Moszkowski, and Nordheim, Argonne National Laboratory Report No. 4626 (1951).
[22] Mandeville, Scherb, and Keighton, Phys. Rev. **74**, 888 (1948).
[23] J. E. Hudgens, Jr., and W. S. Lyon, Phys. Rev. **75**, 206 (1949).

A comparison of the measured internal conversion coefficient with the theoretical values corresponding to different multipole transitions[1] is given in Table IV. Therefore, the 0.77-Mev gamma-ray is classified as magnetic dipole or electric quadrupole radiation, or a mixture of both.

Nb^{93} has a spin 9/2, and should, according to the shell structure model, be in a $g_{9/2}$ state. This is perhaps also the state of Nb^{95}, because adding two neutrons usually does not change the nuclear configurations.[21]

TABLE III. Results of Nb^{95}.

	Present measurement	Hudgens and Lyon
Beta-ray end-point energy	0.160±0.003 Mev	0.146 Mev
Gamma-ray energy	0.77±0.01 Mev	0.75 Mev
Total internal conversion coeff.	$(1.6\pm0.16)\times10^{-3}$	2.4×10^{-3}

The spin of Mo^{95} is known to be 5/2. Shell structure model predicts $d_{5/2}$.[21] The multipole order of the 0.77-Mev gamma-ray (M-2^1 and/or E-2^2) together with the shape of the beta-spectrum (allowed) and the ft value ($\log ft = 5$) would then be consistent with 9/2+ or 7/2+ for the excited state of Mo^{95}. The shell structure favors a $g_{7/2}$ state, which is adopted in the tentative level values shown in Fig. 8.

3. Au^{198}

The beta-spectrum and the internal conversion coefficients of 2.69-day Au^{198} have been the subject of extensive investigations. In some earlier work by Levy and Grueling,[24] several gamma-rays with energies of 0.157, 0.208, and 0.411 Mev and two beta-ray components of maximum energies 0.601 and 0.97 Mev were observed. However, the spectrometric work of Peacock and Wilkinson,[25] Siegbahn and Hedgran,[26] and the latest work of Saxon and Heller[27] show that the beta-spectrum is simple with an end-point energy of 0.97

TABLE IV. K conversion coefficient for Nb^{95}.

Experimental value×10³	Theoretical values×10³			
	M-2^1	M-2^2	E-2^1	E-2^2
1.3±0.2	1.32	3.50	0.53	1.31

±0.01 Mev followed by an internally converted gamma-ray of 0.411 Mev. These conflicting results were explained by Hill and Mihelich,[28] who showed that the additional activities observed by Levy and Grueling were due to Au^{199} formed through successive neutron capture during the pile irradiation of gold as follows:

$$Au^{197}+n\rightarrow Au^{198}, \quad Au^{198}+n\rightarrow Au^{199}.$$

[24] P. W. Levy and E. Grueling, Phys. Rev. **75**, 819 (1949).
[25] C. L. Peacock and G. Wilkinson, Phys. Rev. **74**, 297 (1948).
[26] K. Siegbahn and A. Hedgran, Phys. Rev. **75**, 523 (1949).
[27] D. Saxon and R. Heller, Phys. Rev. **75**, 909 (1949).
[28] R. D. Hill and J. W. Mihelich, Phys. Rev. **79**, 275 (1950).

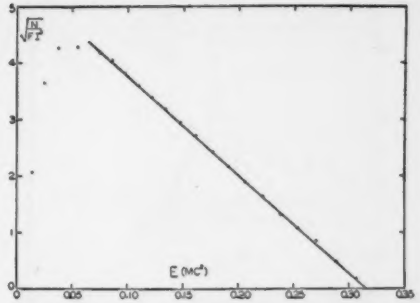

FIG. 7. The Fermi plot for the beta-spectrum of Nb^{95}.

The method used by Hill and Mihelich was to identify the photographic lines of conversion electrons taken with a spectrograph using secondary electrostatic focusing. The ratio of Au^{199} to Au^{198} was estimated to be 1:95 by comparing the intensities of the 0.157-Mev and 0.411-Mev gamma-rays; it was reduced to 0.6:100 later[29] by drastically changing the percentage of 0.157-Mev gamma-rays per beta-particle emission of Au^{199}. Here the same problem was studied by measuring simultaneously the total beta-disintegrations of both Au^{199} and Au^{198}. The result differs considerably from that of Hill and Mihelich.

Figure 9 shows the beta-spectrum of Au^{198}. The sample was obtained from Oak Ridge, where it had been irradiated for seven days with an average flux of approximately 6.5×10^{11} cm^{-2} sec^{-1}; the measurement was performed about three days after the irradiation. The spectrographic analysis of the particular piece of gold from which the sample was taken shows the presence of a small amount of Ag and very small amount of Ca, Cu, and Mg,[30] none of which should interfere with the present study.

The Fermi plot for the spectrum is shown in Fig. 10 and indicates clearly the superposition of two components. The end point of the high energy component is 0.97±0.01 Mev, while that of the low energy component is estimated from the Fermi plot as about 0.4 Mev. Besides the well-known 0.411-Mev gamma-ray, two

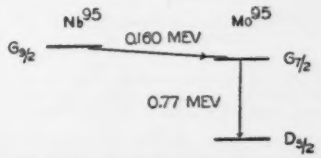

FIG. 8. The decay scheme of Nb^{95} and the suggested level values.

[29] R. D. Hill, Phys. Rev. **79**, 413 (1950).
[30] The author is indebted to Mr. J. A. Cox, Superintendent of the Radioisotope Control Department, Oak Ridge National Laboratory, for supplying this information.

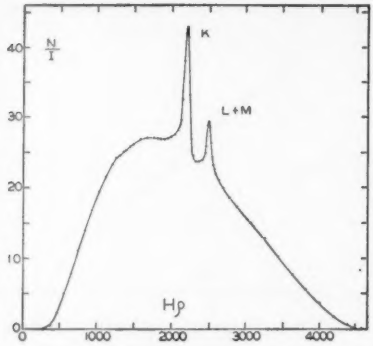

FIG. 9. The beta-spectrum of Au^{198}. Sample was obtained from Oak Ridge National Laboratory.

gamma-rays of energy 0.159 and 0.207 Mev, respectively, were also found. None of the impurities leads to the observed activities. Chemical purification was performed[31] and the activities were found to be unaffected. Therefore the activities must be due to some isotope of gold.

Figure 11 shows the beta-spectra of Au^{198} irradiated in the heavy water pile of Argonne Laboratory. In these measurements some older and therefore weaker sources were used. Hence the spectrometer was operated with lower resolution but higher transmission. Furthermore, an end-window mica counter of window thickness 1 mg/cm² was used instead of a Nylon window counter, because the supporting grid of the Nylon window counter cuts down the transmission by a factor of about one-half. Curve 1 in Fig. 11 is the spectrum of a sample irradiated for 45 hours in the pile. The measurement was done about one week after irradiation. Curve 2 corresponds to the measurement on the same sample 34 days after irradiation, with the high energy part normalized to coincide with that of the first measurement. It can be seen that the two activities have different half-lives. Assuming that the beta-spectrum of Au^{198} is simple as indicated by the dotted curve (No. 3) in the figure, the half-life of the low energy component can be estimated by comparing curves 1 and 2. It is found to be 3.2 days, which differs by about 4 percent from the accepted value of the half-life of Au^{199}, 3.3 days.

The end-point energy of the low energy component can be estimated from the Fermi plot which is shown in Fig. 12. It is 0.35±0.04 Mev. This agrees with the values for Au^{199} of 0.32 Mev by Beach, Peacock, and Wilkinson,[32] and of 0.38 Mev by Mandeville, Scherb, and Keighton.[33]

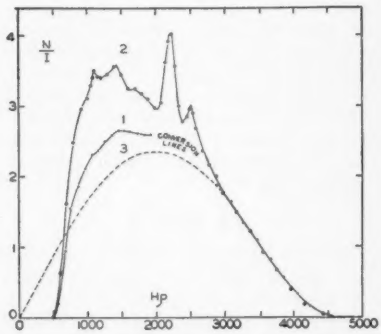

FIG. 11. The beta-spectra of Au^{198}, sample was irradiated in the heavy water pile of Argonne National Laboratory. Curves 1 and 2 are the spectra measured 7 and 34 days after irradiation, respectively. Curve 3 is the spectrum corresponding to a straight Fermi plot.

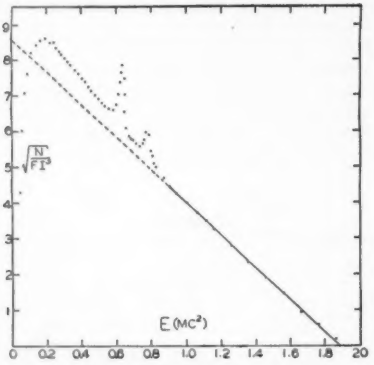

FIG. 10. The Fermi plot for the beta-spectrum of Au^{198} shown in Fig. 9.

The internal conversion peaks in curve 2 are readily identified with the energy spectrum of Au^{199} found by Beach *et al.*[32] with a thinner counter and a better resolution. The first peak can be identified with the *K* conversion line of the 0.157-Mev gamma-ray. The second peak is the *L* line corresponding to the 0.157-Mev gamma-ray, the *K* line of the 0.207-Mev gamma-ray, and the *K* line of the 0.230 gamma-ray, which are not resolved. The third peak is the *L* line of the 0.207-Mev gamma-ray. All these findings show that the extra activity is due to Au^{199}. The neutron absorption cross section of Au^{198} can be estimated from the comparison of the beta-activities of Au^{198} and Au^{199} and the neutron flux.

After making the correction for window absorption, the total amount of Au^{199} compared to Au^{198} under the curve in Fig. 9 was about 16 percent, while that under

[31] R. S. Krishnan, Proc. Cambridge Phil. Soc. **37**, 186 (1941). Thanks are due to Mr. J. B. Niday and Mrs. A. Tompkins for their help in performing the chemical process.

[32] Beach, Peacock, and Wilkinson, Phys. Rev. **76**, 1624 (1949).
[33] Mandeville, Scherb, and Keighton, Phys. Rev. **74**, 601 (1948).

curve 1 in Fig. 11 was about 11 percent and that under curve 2 was about 30 percent. The first value gives a neutron absorption cross section of Au^{198} of $\approx 8.8\times10^5$ barns, and the last two give an average result of 9.1×10^5 barns if a neutron flux is 10^{12} cm^{-2} sec^{-1} is assumed. This is much higher than the value of Hill and Mihelich, i.e., 1.6×10^4 barns. This large discrepancy might partly be due to the uncertainty in the pile neutron flux on which the calculations are based.

The K internal conversion coefficient for 0.411-Mev gamma-ray is 3.0 percent. The L and M conversion coefficients are 1.3 percent. All these values agree exactly with the results of Siegbahn and Hedgran.[32] The radiation is classified as electric quadrupole radiation. This classification is consistent with the lifetime of the isomeric state (10^{-11} sec).[34]

The multipole order of the 0.411-Mev gamma-ray, together with the fact that Hg^{198} has zero spin and presumably even parity, enable one to assign 2+ to the excited state of Hg^{198}. The Fermi plot of Au^{198} is

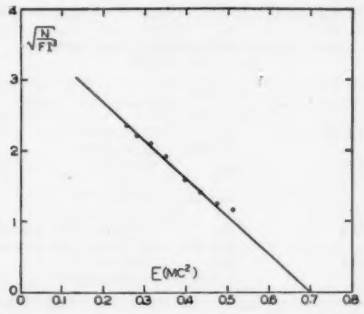

FIG. 12. The Fermi plot for the beta-spectrum of Au^{198}.

straight, which could mean that this is an allowed spectrum or a first-forbidden spectrum ($\Delta J=0$ or 1, yes) with allowed shape which happens more often for high Z isotopes. Indeed, the condition that the correction factor for forbiddenness reduces to a constant is given by Konopinski[5] as

$$Z \gg 1.6W_0^{1.5},$$

where W_0 is the maximum energy (including rest mass) in unit of mc^2 of the beta-particles. For Au^{198}, $1.6W_0^{1.5} \approx 8$, and this condition is thus fulfilled. Therefore the ground state of Au^{198} could be 1±, 2±, or 3±. The ft value ($\log ft=7.3$) tends to indicate a first-forbidden spectrum and hence a negative parity of the ground state.

The shell structure model favors a 2− state[21] for the ground state of Au^{198}. Adopting this assignment, one obtains the tentative level scheme shown in Fig. 13.

[34] R. L. Graham and R. E. Bell, Phys. Rev. **84**, 380 (1951).

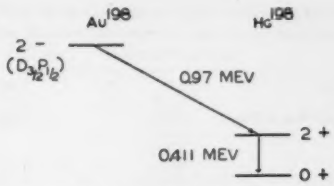

FIG. 13. The decay scheme of Au^{198} and the suggested level values.

4. Hf^{181}

The decay of Hf^{181} and the internal conversion coefficients have been investigated by Chu and Wiedenbeck[35] and lately by Hedgran and Thulin.[36] The decay scheme proposed by Chu and Wiedenbeck is shown in Fig. 14. It fits with the delayed nature of the gamma-rays[37] following the beta-decay and the cascade nature of the 0.130-Mev and the 0.471-Mev gamma-rays.[38,39]

Later, Jensen found another gamma-ray of energy 0.087 Mev.[40] This gamma-ray was identified by Cork *et al.*[41] as due to the activity of Hf^{175}. The total amount of Hf^{175} relative to the activity of Hf^{181} one month after four weeks of irradiation was determined by Hedgran and Thulin[36] as 2.1 percent. However, Cork *et al.*[41] found one other gamma-ray of energy 0.601 Mev by using a photographic registration. This was also confirmed by Burson *et al.*[42] They assigned the gamma-ray to the direct transition from the highest excited state of Ta^{181} to the ground state. Since this gamma-ray has not been reported by Chu and Wiedenbeck and Hedgran and Thulin, it is presumably of very low intensity.[43] The

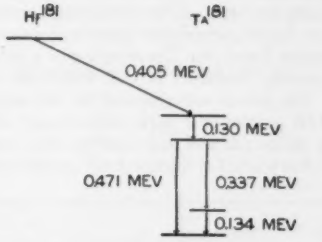

FIG. 14. The proposed decay scheme of Hf^{181} of Chu and Wiedenbeck.

[35] K. Y. Chu and M. L. Wiedenbeck, Phys. Rev. **75**, 226 (1949).
[36] A. Hedgran and S Thulin, Phys. Rev. **81**, 1072 (1951).
[37] S. De Benedetti and F. K. McGowan, Phys. Rev. **75**, 728 (1948).
[38] Mandeville, Scherb, and Keighton, Phys. Rev. **75**, 221 (1949).
[39] Bunyan, Lundby, and Walker, Proc. Phys. Soc. (London) **A62**, 253 (1949).
[40] E. N. Jensen, Phys. Rev. **76**, 958 (1949).
[41] Cork, Stoddard, Rutledge, Branyan, and Le Blanc, Phys. Rev. **78**, 299 (1951).
[42] Burson, Blair, Keller, and Wexler, Phys. Rev. **83**, 62 (1951).
[43] The branching ratio is less than 2 percent according to Mr. S. B. Burson's private communication.

TABLE V. Number of conversion electrons for Hf^{181}.

	Chu and Wiedenbeck	Hedgran and Thulin
$N_{K1}+N_{K2}$	0.78	0.32
$N_{K1}:N_{K2}$	2.5:1	2:1
$N_{L1}+N_{L2}+N_{M1}+N_{M2}$	0.514	0.36
N_{K3}	0.019	
N_{L3}	0.0053	
N_{K4}	0.021	
N_{L4}	0.0071	

proposed decay scheme seems to be well established, except that there are some small differences in the energies of gamma-rays as measured by different authors. But the problem of the internal conversion coefficients is still an open one as is shown in Table V, where N_{Ki} ($i=1, 2, 3, 4$) is the number of K conversion electrons of the ith gamma-ray emitted per second per unit beta-disintegration, and N_{Li} and N_{Mi} denote the number of L and M conversion electrons, respectively. The gamma-rays are numbered according to increasing energies. The purpose of the present measurement, which was done before the publication of Hedgran and Thulin's paper, was to measure the conversion coefficients of the gamma-rays to compare with Chu and Wiedenbeck's results. It was found that the results were in agreement with Hedgran and Thulin's and, in spite of the complications of the problem and the uncertainties of the measurements, could be taken in conjunction with the determinations of the branching ratio, the ratio of $N_{K1}:N_{K2}$ and the ratio of $N_{K2}:N_{L2}$ of the latter, to give a complete comparison with the theoretical predictions of the shell structure model and Goldhaber and Sunyar's empirical classification of nuclear isomers.[18]

The beta-spectrum of the present measurement is shown in Fig. 15, where the dotted curve corresponds to a straight Fermi plot. The sample was in the form of Hf_2O_3 powder irradiated in Oak Ridge pile for four weeks. The source was prepared by depositing very fine Hf_2O_3 powder of 2 microcurie strength on a conducting Nylon foil and then covering the source with a piece of zapon foil of thickness $\approx 5\ \mu g/cm^2$ to hold the powder in place. The size of the source was ≈ 0.5 cm in diameter and the thickness was ≈ 0.3 mg/cm^2. The energies of the gamma-rays of Hf^{181} and their internal conversion coefficients are listed in Table VI, where $N_{K1}:N_{K2}\approx 2:1$, $N_{K2}:N_{L2}\approx 8$, the branching ratio for the 4th gamma-ray ≈ 87 percent, and the activity of Hf^{181} to that of $Hf^{175}\approx 2.1$ percent just after four week irradiation, $\alpha_K\approx 40$ percent, and $\alpha_K/\alpha_L\approx 4.5$ for the 0.342-Mev gamma-ray of Hf^{175} [36,44] were used for the calculation. The errors of the internal conversion coefficients were calculated from the experimental errors of α_K', etc., which are about 10 percent. The errors of the internal conversion coefficients for the third gamma-ray could not be given because of the uncertainty of Wilkinson and Hicks' measurements.

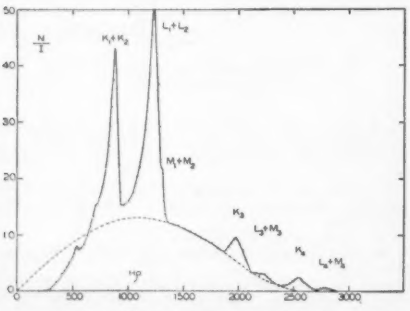

FIG. 15. The beta-spectrum of Hf^{181}.

The theoretical K-shell internal conversion coefficients for different gamma-rays for various multipole radiations from the table of Rose *et al.*[1] and the values of α_K/α_L from Goldhaber and Sunyar's empirical curves[18] are listed in Table VII.

In connection with the comparison of the experimental results with the theoretical values two remarks must be made: (1) The conversion peaks of the first two gamma-rays occur in the low energy range; considerable uncertainties could thus be involved in the corrections for the counter window absorption. (2) The theoretical values of the K-shell internal conversion coefficients for the first two gamma-rays were obtained by means of extrapolation of the curves of Rose *et al.*, and errors could thus be introduced. However, all those uncertainties do no completely obscure the nature of the gamma-rays. In fact, one can readily assign the fourth gamma-ray as an electric quadrupole radiation, both the second and the third gamma-ray as magnetic dipole radiations, and the first gamma-ray as most likely an electric quadrupole radiation. The classification of the first gamma-ray is consistent with the lifetime of the isomeric transition (22 μsec).

TABLE VI. γ-ray energies and internal conversion coefficients for Hf^{181}.

Energy of gamma-rays	Internal conversion coefficients	
0.130 Mev	K_1	0.34 ± 0.06
	L_1+M_1	0.56 ± 0.10
0.134	K_2	$3.1+2.2$ -1.1
	L_2+M_2	$0.38+0.28$ -0.16
0.340	K_3	0.13 (very poor estimation)
	L_3+M_3	0.02 (very poor estimation)
0.474	K_4	0.024 ± 0.003
	L_4+M_4	0.006 ± 0.0006

The Fermi plot of the beta spectrum is shown in Fig. 16. It is straight with an end-point energy of 0.408 ± 0.008 Mev. This straight Fermi plot could be an indication of either an allowed spectrum or a first-forbidden spectrum with a constant correction factor

[44] G. Wilkinson and H. G. Hicks, Phys. Rev. **75**, 696 (1949).

for the forbiddenness as in the case of Au^{198}. However, a first-forbidden spectrum is compatible with the nature of the first gamma-ray from the following theoretical consideration.

The spin of Hf^{177} and Hf^{179} are both 1/2. Shell structure model predicts the value $p_{1/2}$ as the state of Hf^{177}, Hf^{179}, and for Hf^{181}.[21] Because of the beta-spectrum is of an allowed shape, the highest excited is likely to be of state $3/2\pm$ or $1/2\pm$. The spin of Ta^{181} is 7/2. Shell structure model favors a $g_{7/2}$ for the ground state.[21] The multipole orders of the second, third, and fourth gamma-ray indicate the first excited state and the second excited state as 5/2+ and 3/2+, respectively. Therefore, the nature of the first gamma-ray requires 3/2+ or 1/2+ as the highest excited state. This fits with a first-forbidden spectrum and high ft value ($\log ft = 7.2$).

This case is quite interesting purely from the point of view of the shell structure model, because the states of Ta^{181} seem to cover all the term values in the sixth shell, ($g_{7/2}$, $d_{5/2}$, $d_{3/2}$, and $s_{1/2}$) except the last one ($h_{11/2}$). This is different from the scheme of Goldhaber and Sunyar.[18] They assigned the first excited state as 7/2+ and the first, third, and the fourth gamma-ray all

TABLE VII. K-shell internal conversion coefficients and K-L ratios for the γ-rays from Hf^{181}.

Energy of gamma-rays in Mev	K-shell internal conversion coefficients				α_K/α_L			
	E-2^1	E-2^2	E-2^3	M-2^1	E-2^1	E-2^2	E-2^3	M-2^1
0.130, 0.134	0.15	0.52	1.5	1.9		0.5	0.35	7.6
0.340	0.014	0.041	0.11	0.14		2.7	1.7	7.9
0.474	0.0066	0.0185	0.0475	0.060		4.3	3.0	8.0

as electric quadrupole radiations and did not mention the nature of the second one.

The author wishes to express his sincere appreciation to Professor H. L. Anderson for suggesting this problem and for his kind guidance during its progress. Thanks are also due to Mr. S. D. Bloom, Mr. S. A. Moszkowski, and Mr. D. Kahn for their friendly help.

APPENDIX

In most of the beta-ray spectrometer measurements, a single conversion line can be represented by an isosceles triangle having a width at half-maximum proportional to the momentum of the conversion electrons and a height for a source of unit strength (one particle per second) equal to the transmission of the machine t. Let p' be the momentum of the conversion electrons and w the resolution; the width of the triangle at half-maximum will be wp' if the magnetic field of the instrument is linearly proportional to the current through the coil and there is no distortion of any kind.

The shape of a single conversion line of momentum p', denoted by $K(p, p')$, is essentially the probability that an electron of momentum p' from the source appears at the slit of the detector of a beta-ray spectrometer when

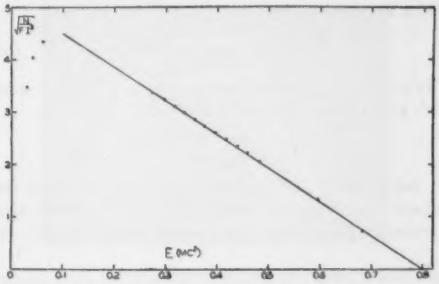

FIG. 16. The Fermi plot for the beta-spectrum of Hf^{181}.

the current through the coil is I, appropriate to the magnetic rigidity p. If $n(p')dp'$ is the number of beta-particles of momenta between p' and $p'+dp'$ emitted per second and $N_c(p)$ is the counting rate of the detector when the coil current is I, then

$$N_c(p) = \int_0^\infty K(p, p')dp'n(p').$$

In the case of $K(p, p')$ being an isosceles triangle,

$$N_c = \int_a^b tn(p')dp' \frac{wp' - (p - p')}{wp'} + \int_b^c tn(p')dp' \frac{wp' - (p' - p)}{wp'}, \quad \text{(i)}$$

where $a = p/(1+w)$, $b = p$, and $c = p/(1-w)$.

Equation (1) can be easily transformed into a differential equation. After terms containing the third or higher power of w being neglected, it reads

$$(1/wt)d^2N_c/dp^2 + 2dn/dp + pd^2n/dp^2, \quad \text{(ii)}$$

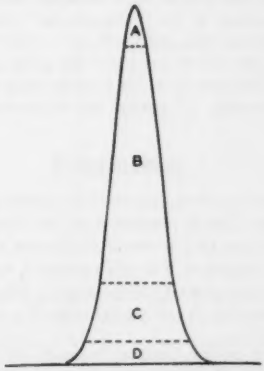

FIG. 17. A Gaussian curve, considered as a sum of an isosceles triangle and three isosceles trapezoids.

with the following solution

$$n=(1/wt)(N_e/p). \quad \text{(iii)}$$

This is Eq. (5). The correction term to N_e/p is of order w^2, which is small for $w=2$ percent.

DISCUSSION

Equation (3) can be generalized to the case that the shape of a single conversion line is symmetrical with respect to p' but other than an isosceles triangle, because it is always possible to divide a symmetrical shape into isosceles triangles so that they can be treated separately as the special case given above. For instance, a Gaussian curve can be divided into an isosceles triangle A and three isosceles trapezoids B, C, and D are illustrated in Fig. 17. An isosceles trapezoid may be regarded as the difference of two isosceles triangles whose apexes are at the position p'. Equation (3) is thus applicable to the general case, except that the width w will be an average of widths of different triangles with proper weights attached.

PHYSICAL REVIEW VOLUME 87, NUMBER 2 JULY 15, 1952

Energy Levels in C^{12}, Al^{27}, and Na^{23} Using a Scintillation Spectrometer for Heavy Particles*

H. F. STODDART AND H. E. GOVE
Laboratory for Nuclear Science and Engineering, Massachusetts Institute of Technology, Cambridge, Massachusetts

(Received March 24, 1952)

Energy levels in carbon, aluminum, and sodium have been measured using a "proportional" sodium iodide scintillation counter to determine energies of outgoing protons from inelastic proton scattering at 7.26 Mev with the following results: C^{12}: 4.45 Mev; Al^{27}: 0.84, 1.01, 2.23, 2.77, 3.03, 3.71, 4.00, 4.47, 4.60, 4.87, 5.43 Mev; Na^{23}: 2.10, 2.37, 2.69, 3.01, 3.70, 3.92, 4.45 Mev.

Factors limiting the resolution are presented, and it is found that the standard deviations of the distributions are consistent with 2.4 photoelectrons produced at the photocathode of the RCA 5819 per kev of particle energy lost.

1. INTRODUCTION

CONTINUED interest in the level structure of the nuclides has led to many recent experimental determinations of excited states. Usually the energy assignments are based on range measurements of the outgoing particles in nuclear scattering experiments or by deflection of these particles in known magnetic fields. This paper reports energies for excited states of several nuclides found by a different method which takes advantage of the "proportional" characteristics of the scintillations produced in a NaI(Tl) crystal when it is excited by protons.[1] By using a crystal of sufficient thickness all of the particle range is absorbed and, in principle, all groups can be examined simultaneously.

2. EXPERIMENTAL

The object in designing such a counter is to get as much of the light as possible from the crystal into the phototube since this is one of the factors which determines the resolution. For this purpose a simple aluminum reflector was designed as shown in Fig. 1. Because of total reflection at the crystal surface, a large part of the light comes out of the edge of the crystal, and the aluminum reflector is designed to utilize as much of this as possible. The volume of the reflector is filled with Dow-Corning DC-703 silicone oil to provide optical matching between the glass crystal holder and the glass tube face. Mineral oil, which is usually used in this application, is unsatisfactory in vacuum systems because of its high vapor pressure. The transmission of both silicone oil and mineral oil was checked and in the region of interest the silicone oil was actually found to be better.

The sodium iodide crystal was cleaved on all six sides from a larger single crystal obtained from Harshaw Chemical Company. Cleaving gives a thin flat plate with the smoothest, most uniform surface possible. The cleaving operations were carried out in a dry box. Difficulty with gamma-ray background is minimized by making the crystal thin and hence increasing the ratio of efficiency for detecting charged particles to efficiency for detecting gamma-rays.

The counter is mounted on one of the movable arms in the MIT scattering chamber.[2] No window is used between the crystal and the target, and this necessitates filling the whole chamber volume with dry nitrogen

* This work has been supported in part by the joint program of the ONR and the AEC.

[1] Taylor, Jentschke, Remley, Eby, and Kruger, Phys. Rev. **84**, 1034 (1951).

[2] Boyer, Gove, Harvey, Deutsch, and Livingston, Rev. Sci. Instr. **22**, 310 (1951).

when it is opened because of the hygroscopic nature of sodium iodide.

The photomultiplier is an RCA 5819 tube and is powered with a highly stabilized positive high voltage supply usually operated at about 600 volts. The signal is brought out of the scattering chamber through several feet of coaxial cable to an impedance matching preamplifier which also inverts the pulse. After passing through through about 50 feet more of cable the pulse is delay line clipped and amplified about 1000 times with a Brookhaven type "non-overloading" amplifier.[3] The pulse is then displayed on an oscilloscope and fed into a very stable Los Alamos single-channel analyzer.[4]

3. RESULTS

Magnesium

The simplest way to present the resulting pulse height distributions is to photograph the oscilloscope with a time exposure, thereby integrating all the pulses.[5] In each of the photographs shown in this paper

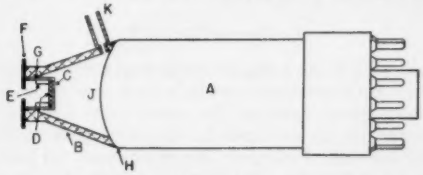

FIG. 1. Diagram of the NaI counter. The sodium iodide crystal (*D*) is held against the bottom of the glass container (*C*) by a Lucite retaining ring (*E*). The glass container is held to the aluminum reflector (*B*) by "Duco" cement (*G*), while the reflector itself is held to the tube (*A*) by "Ambroid" cement (*H*). The volume of the reflector is filled with DC-703 silicone oil (*J*) through a spout on the top (*K*). A lead defining diaphragm (*F*) is placed at the entrance to the counter.

there are a total of about 1.2×10^5 counts. Figure 2 shows proton groups emitted at about 45 degrees forward from a thin magnesium target placed in the cyclotron proton beam. Using the known level energies at 4.14 and 1.38 Mev,[6] it is found that the sodium iodide crystal has a linear response to better than 4 percent. A fainter level is seen at 5.10 Mev. From this work one cannot determine if it is from Mg^{24} or the less abundant isotopes of magnesium.

The film technique is good for locating levels but in its present application does not give accurate quantitative results for group intensity or shape. This information is better obtained from the single-channel analyzer data, which for this same magnesium reaction is shown in Fig. 3.

RESOLUTION

The discriminator run on the magnesium data does not indicate the best resolution possible with this

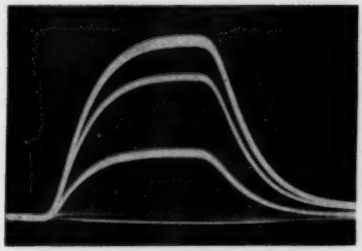

FIG. 2. Pulses resulting from magnesium bombarded by protons. The largest pulses come from the elastically scattered protons (*A*). This group appears to be broader than the others because it is considerably overexposed. The other two strong groups result from the Mg^{24} being excited to the well-known energy levels of 1.38 and 4.14 Mev. A fainter line (*D*) is seen which corresponds to a level at 5.10 Mev. Note that the oscilloscope trigger cuts off just before the thin dense base line which is artificially inserted immediately after the run.

counter. In order to separate variables affecting the resolution, such as target thickness and analyzer channel width as well as photocathode statistics, several runs were made by elastically scattering both deuterons and protons off a very thin gold leaf target with the counter at 40 degrees from the direction of the beam. Three discriminator runs were made in each case with the channel width carefully measured and the data corrected for spread due to this source.

The resulting mean standard deviation for the 14.5-Mev deuterons was 92 kev, while the proton data, at a beam energy of 7.26 Mev, gave a mean standard deviation of 74 kev. These values can then be used to compute the number n of photoelectrons released at the photocathode per kev of particle energy by using the relation

$$n=\frac{V}{s^2}\left\{1+\frac{1}{R}\left(\frac{r}{r-1}\right)\right\},$$

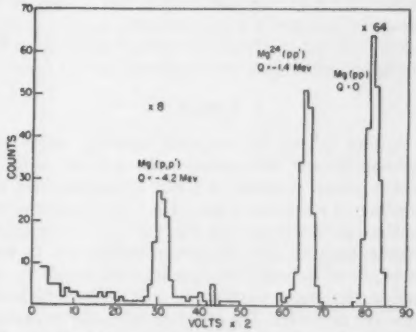

FIG. 3. Discriminator data for protons on magnesium. A single-channel analyzer was used to scan the pulses resulting from proton groups incident on the counter from magnesium bombarded with the cyclotron proton beam. Although this curve is drawn as a histogram the channel widths actually considerably overlap.

[3] W. Higinbotham and R. Chase, Rev. Sci. Instr. **23**, 34 (1952).
[4] C. W. Johnstone, Los Alamos (drawing number 4r-26323).
[5] P. Hofstadter and R. McIntyre, Phys. Rev. **80**, 631 (1950).
[6] C. E. Bradford and W. E. Bennett, Phys. Rev. **78**, 302 (1950).

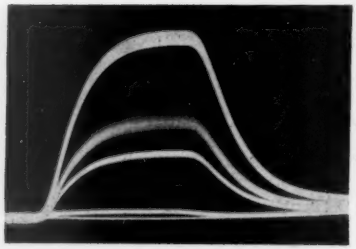

FIG. 4. Pulses resulting from carbon bombarded by protons. Group "*A*" is due to the elastic protons, "*B*" to protons elastically scattered from hydrogen impurity in the target, and "*C*" to the inelastic protons from the 4.45-Mev level in C^{12}. No other groups are seen up to very close to the base line which corresponds to about 6.5-Mev level energy. The increased density near the base line may be due to carbon recoils.

where s is the standard deviation of the data in kev, V is the particle energy in kev, R is the multiplication of the first dynode, and r is the average multiplication of all succeeding dynodes. The multiplication of the first dynode was separated from the others because it is operated at about three times higher voltage. In our case the effect of the dynodes in spreading the distribution amounts to about 20 percent.

The value of n that fits the deuteron data is 2.4 photoelectrons per kev of particle energy lost. This value leads to a somewhat smaller value of the proton standard deviation than was actually obtained, but this can be accounted for, within the errors of standard deviation, by initial spread in the cyclotron beam itself.

For the single-channel analyzer data shown in this paper the largest spread of the groups is due to the channel width which was kept rather wide to maintain high efficiency. No estimate of the resolution can be made from the photographic data since the gamma of the negatives is unknown. However, since fast (super-XX) film was used which was developed in fine-grain developer it is safe to assume that the gamma is less than one and hence the groups' widths from the microphotometer data are broadened by this factor.

Carbon

A thin (about 0.4 mg/cm²) aquadag target was bombarded with the proton beam and the resulting proton groups observed at about 45 degrees from the direction of the beam. Figure 4 is a photograph of the oscilloscope in this case and Fig. 5 is a plot of the single-channel analyzer data in a similar experiment. In both cases there are only two groups attributable to the carbon; the intense elastic group, and the inelastic group from the first level. The broad group is due to protons scattered from hydrogen contamination in the target. Part of the reason the width of this group is larger than the other two is the rapid variation of energy with angle for this process. The geometric angle of the counter then sees a greater energy distribution. However, this is not enough to account for the total width, and apparently it is necessary to include a contribution due to the multiple scattering of the particles in the target. This has the effect of adding to the geometric angle of the counter the average scattering angle.

To make a very thin carbon target a gold foil 200 μg/cm² thick was dipped into a dilute solution of polystyrene in xylene and allowed to dry. By using an energy of 4.45 Mev[6] for the first excited level of C^{13}, an energy of 7.26±0.04 Mev is found for the incoming beam. This is consistent with that obtained from the magnesium data.

Another piece of information that can be obtained from the gold-polystyrene target is the angle of the counter to the beam. This is due to the rapid shift of the energy of the hydrogen elastic group with angle. Since the protons that make up the gold elastic group have essentially the full energy of the beam while the hydrogen elastic group energy depends on the square of the cosine of the angle, we can write

$$E_H/E_B=\cos^2\theta\simeq E_H/E_G,$$

where E_H is the energy of the hydrogen elastic group, E_B is the beam energy, and E_G is the energy of the gold elastic group. Assuming the crystal to be linear with energy, we can substitute the ratio of the pulse heights for the ratio of energies. The result serves the useful purpose of checking the direction of the beam through the scattering chamber.

Aluminum

Because aluminum, which exists only as the single nuclide Al^{27}, has some uncertainties in its level structure, several photographs were made using a 1.88 mg/cm² aluminum foil target and the 7.26-Mev proton beam. The photograph obtained at a forward angle of 50 degrees (laboratory system) is reproduced in Fig. 6. This is clearly a more complicated case than magnesium or carbon. Microphotometer traces of two photographs similar to Fig. 6 but differing from each other by a

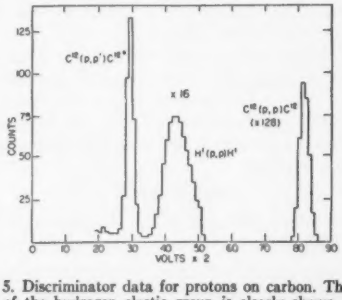

FIG. 5. Discriminator data for protons on carbon. The broad nature of the hydrogen elastic group is clearly shown. This is discussed under the carbon heading.

factor of four in exposure are shown in Fig. 7. Note the effect of nonlinear response of the film to intensity.

From the positions of the peaks and the beam energy, the level energies for aluminum are calculated and are presented in Table I. No levels are evident in the region between 1.2 and 2.0 Mev of intensity greater than 5 percent of the level at 2.23 Mev.[7] This is also true for the picture taken at a back angle of 135 degrees in the laboratory system.

This run demonstrates the limit of usefulness of this sodium iodide counter as a device for the determination of energy levels. However, when efficiency is an important factor, this technique may be more useful than the precise magnetic methods.

TABLE I. Level energies for Al^{27}. The groups can be identified on the microphotometer trace of Fig. 7 since the abscissa is calibrated in units of level energy. In each case the estimated error is ±40 kev.

Energy	Remarks	Corresponding level obtained by E. M. Reilley (private communication)
0.00	Elastic group	
0.84	Assuming only two groups	0.844
1.01		1.016
2.23		2.259
2.77		2.782
3.03		3.046
3.71		3.736
4.00		4.018
		4.115
4.47	Assuming only two groups	4.473
4.60		4.575
		4.647
4.87		4.875
		4.996
		5.107
		5.220
		5.341
5.43		5.501
		5.565
		5.620
		5.736

Sodium

An interesting target to compare with aluminum is sodium. It also exists as a single isotope, Na^{23}, and is presumably quite similar to aluminum in structure. Both nuclei have odd Z and even N, and according to current shell models the last nucleons in both cases should be in $d_{5/2}$ states.

A sodium metal target was prepared by evaporating the metal in vacuum onto a very thin collodion film. The target was transferred to the scattering chamber by keeping it under kerosene. Photographs at 90 degrees and 145 degrees from the direction of the proton beam were made, and the microphotometer traces of these negatives are shown in Fig. 8. Note the shift in energy of the groups with angle. This allows them to be identified as inelastically scattered protons from sodium.

[7] D. M. Van Patter and W. W. Buechner, Phys. Rev. **87**, 51 (1952).

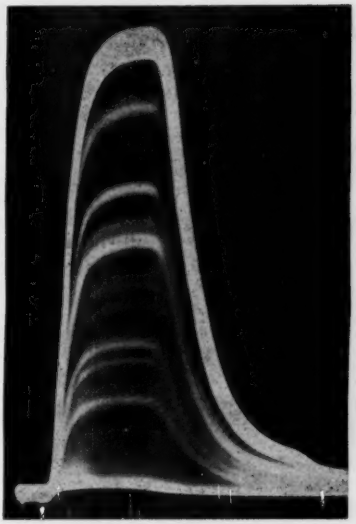

FIG. 6. Pulses resulting from aluminum bombarded with protons. Because of the large intensity, the elastically scattered proton group is considerably overexposed which causes it to appear broader than the other group.

Interference of the oxygen elastic peak with the sodium elastic peak in the 90-degree photograph makes it difficult to use this data for determining the Q values so the values in Table II are for the 145-degree photograph. Note that sodium levels e, f, g, h, and i agree numerically within the experimental error with levels in Al^{27}. The chance probability of a one-to-one correspondence, within the experimental error, between at least five levels in aluminum and sodium in the region up to 4.5 Mev is 1.2 percent. It is also interesting to

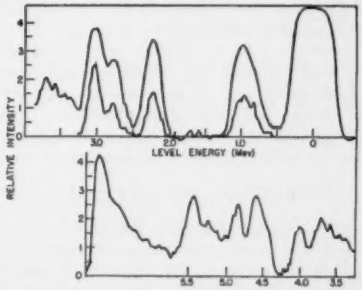

FIG. 7. Microphotometer trace of aluminum photograph. Note that the ordinate in this trace is plotted directly as level energy. This gives an idea of how well the energy levels can be determined. In this figure, as in Fig. 8, a part goes below zero relative intensity. This is due to small variations in the film backing and zero exposure density.

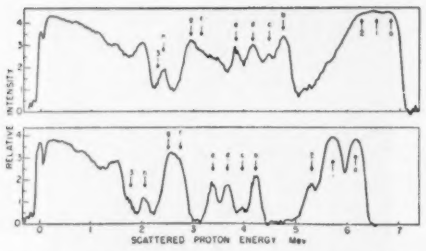

FIG. 8. Microphotometer traces of sodium photograph. Traces for two angles are included so that the effect of shift of energy with angle, which is apparent even with visual observation of the oscilloscope tube, may be recognized. Groups 1 and 2 are protons elastically scattered from oxygen and carbon, respectively. Group 3 is due to protons inelastically scattered from carbon. The groups designated by letters are described in Table II.

note that there are the same number of levels in both cases in this region.

Scintillation Counter

The sodium iodide counter offers a useful alternative to the gas proportional triple-chamber counter[2] that has proved so satisfactory in the past. No difficulty in the experiments so far attempted was experienced arising from gamma-ray or neutron backgrounds always present around the cyclotron. The distinguishing feature of the sodium iodide counter, that of detecting all particle groups simultaneously, is an advantage for the experiments described in this report, but may be a limitation when good counting statistics are desired on a weak group, since the counting rate is limited by the total counts. This feature of the counter proved to be a great value in an unexpected sense. When the oscilloscope is observed during a run, one sees a distribution just as in the photographs shown in the figures of this paper. Any difficulties due to slit scattering, beam hitting target holder, cyclotron partly on deuteron rather than molecular hydrogen resonance, etc., are immediately obvious. Also, by observing the relative positions of the groups while the counter is rotated in angle, one can decide the relative masses of the particles making up the groups.

Several experiments with both deuteron beams and proton beams are now in progress using this counter. Arrangements are being made to place a very thin gas counter in front of the sodium iodide counter, which should permit the identification of the reaction products, since for a given energy lost in the crystal there will be a characteristic pulse in coincidence from the gas counter.

We wish to thank Professor M. Deutsch and Professor M. S. Livingston for their helpful advice and to express our gratitude to the crew of the M.I.T. cyclotron for their able assistance. We should also like to express our appreciation to Professor L. H. Ahrens of the M.I.T. Geology Department for kindly allowing us the use of a microphotometer.

TABLE II. Level energies for Na^{23} compared with previously measured values. The letter designation is the same as that of Fig. 8. Levels *g* and *h* are chosen on the assumption that only two groups are present in the unresolved peak. In each case the estimated error is ±40 kev.

Level	Energy this paper	Boyer[a]	Endt *et al.*[b]	β-decay[c]
a	0.00			
b			0.43	
c	2.10±0.04 Mev	1.9	2.07	
d	2.37			
e	2.69	2.6		
f	3.01			3.03
g	3.70	3.75		
h	3.92			
i	4.45	4.45		

[a] M.I.T., Laboratory for Nuclear Science and Engineering Progress Report, July 1, 1950 (unpublished).
[b] Endt, Haffner, and Van Patter, Phys. Rev. **86**, 518 (1952).
[c] H. Brown and V. Perez-Mendez, Phys. Rev. **78**, 812 (1950).

Thermodynamic Continuity and Quantum Principles

ALFRED LANDÉ
Department of Physics, Ohio State University, Columbus, Ohio
(Received April 3, 1952)

A condensed survey is given of the results of a previous investigation on quantum concepts and principles developed from the anti-Gibbs postulate of thermodynamic continuity. The same postulate now also yields major parts of quantum statistics, such as the equality of various occupation number sets without permutation of individual particles, not however the alternative "either Bose or Fermi statistics." A distinction must be made between a coherent redistribution of particles without entropy change, and an incoherent redistribution leading to a new thermodynamic equilibrium. The latter is obtained from the former by a process of diffusion from separate level groups to a totality of levels.

I. QUANTUM PRINCIPLES OBTAINED FROM CONTINUITY

A RECENT investigation[1] demonstrated that the conceptual scheme as well as several principles of quantum theory can be derived as consequences of a fundamental *postulate of continuity* in the domain of thermodynamics: "The classical discontinuity of the diffusion entropy of two different gases gradually made alike, known as the Gibbs paradox, does not occur in reality." If one accepts this continuity principle, then the following conclusions can and must be drawn.

(1) The alternative "like or unlike" as applied to states A and B of a gas, or of the mechanical systems (particles) constituting the gas, is to be abandoned in favor of a fractional likeness between two states. The latter may be described quantitatively by an intensity factor $q(A, B)$ of mutual likeness with value between 0 and 1. The quantity q, which is symmetric in its two arguments, determines the diffusion entropy $S-S_0$ of the two gases A and B so that $S-S_0$ may have an intermediate value between zero for $q=1$ in case of like gases, and the full classical value, $2nR\ln 2$, for $q=0$ in case of n moles of gas A and n moles of a different gas B diffusing from separate volumes V into the common volume $2V$. For the entropy $S-S_0$ as a continuous function of q refer to Eq. (7) below.

(2) Among all possible states of a mechanical system (gas particle) one may pick out a certain state A_1, then another state A_2 quite unlike A_1 with $q(A_1, A_2)=0$, then a third state A_3 quite unlike A_1 and A_2, and so forth until one has a (complete) set of mutually unlike or "orthogonal" states A_k with mutual likenesses

$$q(A_k,A_{k'})=\delta_{kk'}. \qquad (1)$$

From the remaining states one now may collect another complete orthogonal set $B_1B_2\cdots$, then a set C, and so forth. This procedure is not unique, a fact known as degeneracy. The fractional likenesses $q(A_k,B_j)$ between members of different sets have values between 0 and 1. Whereas classical theory considers any state A_1 as surrounded by an indiscriminate manifold of other states all unlike A_1, the continuity principle leads to an organized arrangement of all possible states in orthogonal sets, members of different sets being linked by mutual likeness factors $0<q<1$.

(3) Likeness between two gas states is synonymous with inseparability, and unlikeness implies physical separability—by means of semipermeable diaphragms or other selective devices. Such devices play a decisive part in the definition of the diffusion entropy through a reversible process of unfusion. Any modification of the classical diffusion entropy $S-S_0$ therefore implies a modification of the classical alternative "permeable or impermeable." To be more specific, fractional likeness between states A and B will manifest itself in a fractional separability of A from B. Let us define a device permeable for particles in the state B_j and impermeable for non-B_j=orthogonal to B_j, as a B_j-selector. When this selector is confronted with particles in the state A_k, then it will pass a fraction $q=q(A_k,B_j)$ of the incident A_k gas, and will reject the remaining fraction $1-q$. A further inevitable consequence is that the passing fraction, in order to qualify for passage through the B_j-selector, must have turned from the original state A_k to B_j. Similarly, the repelled fraction $1-q$ must have turned to the state non-B_j. These transitions may be ascribed to a dynamical interaction between the particles and the selector; the latter represents an instrument of analysis, a challenge "B_j or non-B_j." The newly acquired states will persist until subjected to another perturbing analyzer, e.g., a C_m-selector. In this way the continuity postulate foreshadows the splitting effect of one state A_k into component states $B_1,B_2,\cdots$ separately collectible with fractional intensities $q(A_k,B_j)$ and quantitatively defining the q's. The sum of the intensity fractions must be unity:

$$\Sigma_j\, q(A_k,B_j)=1, \quad \text{and} \quad \Sigma_k\, q(A_k,B_j)=1, \qquad (2)$$

remembering that the q's are symmetric.

In the following we not only use the concept of a B_j-selector which passes B_j and repels non-B_j (whether coming from the right or left) but also the concept of a B-separator which projects separate components $B_1,B_2\cdots$ all to one side (working from right to left as well as from left to right; the Stern-Gerlach field is an example). In contrast to a Maxwell demon which

[1] A. Landé, Am. J. Phys. (to be published).

represents a thermodynamically objectionable one-way valve, selectors and separators are thermodynamically admissable; however, one must carefully distinguish between reversible coherent, and irreversible incoherent splitting as discussed below

(4) When the splitting effect of a gas state A_k into separately collectable components B_j is interpreted in terms of individual gas particles A_k, then $q(A_k,B_j)$ represents the statistical fraction of all incident particles A_k jumping to B_j. The same fraction $q(A_k,B_j)$ also represents the probability for a single particle irrespective of the presence of others, to carry out a transition to B_j when challenged by a B-separator. When the fractional transition probabilities are written down in the form of a matrix

$$\begin{Bmatrix} q(A_1,B_1) & q(A_1,B_2) & \cdots \\ q(A_2,B_1) & q(A_2,B_2) & \cdots \\ \cdots & \cdots & \cdots \end{Bmatrix},$$

then the rule (2) requires the sum of the elements in every row and in every column to be unity: the sum rule for the $q(A,B)$ matrix.

(5) Similar matrices may also be drawn up for $q(B,C)$ and $q(A,C)$ etc. The question now arises whether there might be a general mathematical relation between the elements of the various matrices; in particular, whether the elements of $q(A,B)$ and those of $q(B,C)$ may be determining, in a unique or multivalent way, the elements of $q(A,C)$. The problem of finding a mathematical relation between matrices in general is too vague to have a definite solution. In the present case, however, several restrictions make the relationship between the three matrices a quite definite mathematical problem. First, there is the sum rule (2) for the rows and columns which must hold not only for $q(A,B)$ and $q(B,C)$ but also, as the result of the mathematical relationship, for $q(A,C)$. Second, the relation must work also in the special case of the states A and C coinciding so that $q(A,B)$ combined with $q(B,A)$ will yield $q(A,A)$ as a unit matrix, Eq. (1). Third, the relationship is required to be self-reproducing so that it will also yield the matrix $q(A,B)$ from $q(A,C)$ and $q(B,C)$, as well as $q(B,C)$ from $q(A,B)$ and $q(A,C)$. This group requirement is not thermodynamic but represents a kind of symmetry principle: "What is good for the set A is good also for B and C."

These three requirements now restrict the relationship problem between the q-matrices so much that only one solution has ever been found—although there is as yet no proof of its uniqueness. At first sight one might think the solution to read $q(A_k,C_m) = \sum_j q(A_k,B_j)\, q(B_j,C_m)$; however, such a direct combination of the probabilities does not stand the test of the special case in the second requirement: $q(A_k,A_{k'}) = 0$ for $k \neq k'$, since $\sum_j q(A_k,B_j)\, q(B_j,A_{k'})$ is positive. The unit sum rule suggests, however, that the $q(A_k,B_j)$ be geometrically interpreted as cosine squares between "directions" A_k and B_j, with the set A representing one orthogonal axis system, and the set B another. This further suggests that the required relation be analogous to an orthogonal transformation by means of the cosine rule, $\cos(A_k,C_m) = \sum_j \cos(A_k,B_j) \cdot \cos(B_j,C_m)$ where $\cos(A_k,B_j)$ is written for $\pm[q(A_k,B_j)]^{\frac{1}{2}}$. A more general solution is then obtained when the bivalent $\pm\sqrt{q}$ are replaced by complex quantities $\psi(A_k,B_j) = \sqrt{q}\, e^{i\varphi}$, multivalent because of the arbitrary phase φ. This arbitrariness is greatly reduced, from m^2 to m arbitrary phases, by the requirement that the sum of the products of the ψ's in one row (column) with the complex conjugates of another is to be zero. The cosine relation then may be generalized to the product rule for (Hermitian) ψ's

$$\psi(A_k,C_m) = \sum_j \psi(A_k,B_j) \cdot \psi(B_j,C_m). \qquad (3)$$

This is the Born-Heisenberg-Jordan superposition rule for the complex probability amplitudes $\psi = \sqrt{q}\, e^{i\varphi}$. It is the only known mathematical solution of the relationship problem under the group restriction of self-reproduction. If any other solution could be found it would present us with a most interesting, although unrealistic, alternative to quantum mechanics. With due reservations one may say, then, that the introduction of complex probability amplitudes ψ subject to the superposition rule is inseparably linked to the admission of fractional likenesses q, which in their turn are forced on us by the anti-Gibbs postulate of thermodynamic continuity. In view of the amplitude character of the ψ's one may speak of a wave theory of matter, although Born's statistical interpretation of the ψ's as probability amplitudes is preferable and generally accepted. So far, we have recapitulated in a rather condensed fashion the results of a previous investigation.[1]

II. CONTINUITY AND QUANTUM STATISTICS

We now turn to the question as to what extent quantum statistics can be considered as a consequence of the thermodynamic principle of continuity. Classical statistics leads to the discontinuity of the Gibbs paradox, whereas quantum statistics yields the required continuity of the diffusion entropy. It therefore would not seem too surprising if one could reverse the argument and derive quantum statistics from the continuity postulate. We saw before that this postulate, via fractional intensities of mutual likeness, leads to probability amplitudes ψ subjected to superposition; this implies a "wave theory" which will also show its influence on statistics, in so far as it controls the splitting or redistribution effect of particles over the states. Indeed, the wave theory leads to a distinction between a reversible redistribution, from a state A_k in a coherent fashion through intermediate states $B_1,B_2,\cdots$ and back to A_k, symbolized by the formula

$$\psi(A_k,A_k) = \sum_j \psi(A_k,B_j)\, \psi(B_j,A_k) = 1, \qquad (3')$$

and the irreversible or incoherent redistribution with

$$\sum_j q(A_k,B_j)\, q(B_j,A_k)\neq 1, \text{ although } q(A_k,A_k)=1. \quad (3'')$$

Thermodynamic implications of both Eq. (3′) and Eq. (3″) will be considered below.

(1) Let N particles, originally in the state A_k, pass through a B-separator. The resulting distribution over the states $B_1B_2\cdots$ yields the occupation numbers $N_j=Nq_{kj}$ with dynamical certainty, both in the coherent and incoherent case, since only the intensities q_{kj} are involved. However, only in case of a coherent redistribution is this process dynamically reversible, according to Eq. (3′). The wave-dynamical certainty and reversibility of the sequence $(N,0,0,\cdots)\leftrightarrow(N_1,N_2,\cdots)$ proves that both the initial and the final distribution of the N particles are to be counted with the same statistical weight, *viz.*, unity. Now, by either starting from new original states with all N particles in one state $A_{k'}$ or $A_{k''}$ etc., or by using new separators B', or B'', etc. one may obtain other reversible sequences $(0,0,N,0,\cdots)\leftrightarrow(N_1'N_2'\cdots)$, always with wave-dynamical certainty. The final occupation number sets, $(N_1,N_2,\cdots)$ and $(N_1',N_2',\cdots)$ and so forth must, therefore, all be counted with the same statistical weight, unity. This general principle of weight counting is opposed to the classical theory with its permutation factors $N!/N_1!N_2!\cdots$.

(2) However, the discounting of permutations is only one, rather negative, feature of quantum statistics. It is important now that the transition probabilities $q(A_k,B_j)$ from the state A_k to B_j do not give preference to one individual particle over any other, i.e., the q's are symmetric with respect to the N like particles. Symmetry of $q=|\psi|^2$, however, requires ψ to be either symmetric or antisymmetric in case of two like particles, according to perturbation theory. If a third particle joins the former two, and if one *postulates* continuity of the symmetry character, then ψ will remain symmetric or antisymmetric also for more than two like particles. However, this certainly is not a result obtainable from thermodynamic considerations.

Still there is a certain gap between the proof of the weight equality of various occupation number sets $(N_1N_2\cdots)$, and the justification of the partition function $\sum_{n_1}\sum_{n_2}\cdots \exp(N_1\epsilon_1+N_2\epsilon_2+\cdots)$ which ultimately leads to the average number of particles of energy ϵ

$$\bar{n}=[(1/\zeta)e^{\epsilon/kT}\mp 1)^{-1}.$$

Indeed, it ought to be proved that *all* equivalent occupation number sets occur once within a sufficiently large time interval. Such a proof would correspond to the classical step from Liouville's weight equality of like phase volume elements to ergodicity.

In view of this gap, all one can say is that the principle of thermodynamic continuity, by virtue of reversible processes of redistribution, yields the equality of weight of various occupation number sets irrespective of permutations of individual particles. Assuming continuity of symmetry character would further leave the alternative between symmetric Bose and antisymmetric Fermi statistics. [The Nernst theorem is obtainable only from additional assumptions concerning the lack of degeneracy of the lowest energy level, as explained by Schrödinger in his "*Statistical Thermodynamics.*"]

(3) Coherent and incoherent distribution. In order to avoid a decision between the two statistics the following thermodynamic considerations deal with dilute gases in which (a) each particle has its private energy, (b) the density is so low that the question of Bose crowding together and Fermi crowding out is immaterial. This is the case when the number of particles N distributed over a group of Z levels satisfies $N\ll Z$. In this case quantum statistics yields the simple entropy formula

$$S=kN\ln(Z/N)+\text{const.} \quad (4)$$

Let N particles, all in the state A_k, be distributed over Z kinetic energy levels; the entropy according to Eq. (4) is, with omission of the additional constant,

$$S_0=kN\ln(Z/N).$$

The N particles may now be redistributed over the states $B_1,B_2,\cdots$ so that every group of $N_j=Nq_j$ particles occupies a partial volume in Z-space of $Z_j=Zq_j$ levels. This corresponds to the separate collectibility in ordinary space and represents a coherent redistribution. Indeed, the entropy

$$S'=k\sum_j N_j\ln(Z_j/N_j)$$

is identical with S_0. This distribution does not represent a thermal equilibrium, however. If we now let the various particle groups irreversibly diffuse from the separate "volumes" Z_j to the total volume of Z levels, then the final entropy is

$$S=k\sum_j N_j\ln(Z/N_j),$$

so that after this incoherent distribution the entropy increase is

$$S-S_0=-kN\sum_j q_j\ln q_j. \quad (5)$$

The q_j play the same part as the concentrations in the thermodynamics of dissociation. When a B-separator is actually applied to an A_k gas, the initial result may be a coherent redistribution; after a time, however, the distribution becomes incoherent resulting in a thermal equilibrium.

(4) Alternating application of A- and B-separators. The last example showed that application of a B-separator to a pure A_k gas increases the entropy irreversibly. Let us now consider the simple case of only two orthogonal states, A' and A'' in the set A, and similarly only B' and B'' in the set B. The mutual likeness fractions may be

$$q(A',B')=q(A'',B'')=q,$$

and

$$q(A',B'')=q(A'',B')=1-q.$$

Omitting the common factor kN as well as the additional constant one has for the original pure A' gas,

$$S_0=-1\ln 1=0.$$

Application of the B-separator splits the A' gas into a fraction q of B' and $1-q$ of B'', with resulting equilibrium entropy

$$S_1=-q\ln q-(1-q)\ln(1-q).$$

Application of an A-separator now yields

$$q_2=q^2+(1-q)^2 \text{ of } A' \text{ and } 1-q_2 \text{ of } A'',$$

with resulting entropy

$$S_2=-q_2\ln q_2-(1-q_2)\ln(1-q_2),$$

and so forth. It can be proved[2] that S_{n+1} is always larger than S_n for any given likeness fraction q between A' and B'. In the exceptional case of $q=\frac{1}{2}$, already S_1 has the value $kN\ln 2$, to be retained for all following S_n's. The value $kN\cdot\ln 2$ also is the asymptotic value of $S-S_0$ for $n\to\infty$ at any q-value under alternating application of A- and B-separators.

If the original sets A and B have a sixfold multiplicity, and the original n moles of pure A_k gas are subjected to an alternating "shake up" by B- and A-separators, the final state will be a mixture of six quite different gases, each consisting of $n/6$ moles with total entropy $kN\cdot\ln 6$. Suppose now that this gas mixture is exposed to a C-separator whose multiplicity is only five, so as to produce a mixture of five different gases $C_1\cdots C_5$. Its maximum entropy can at most be $kN\cdot\ln 5$, less than it was before. This would contradict the second law. Thermodynamic reasons thus compel us to conclude that the orthogonal sets of states A, and B, and C, and so forth of one kind of particle must all have the same multiplicity m so that all matrices $q(A,B)$, and $q(B,C)$ etc. are quadratic. In particular if the multiplicity is infinite for one set, then it must be infinite for all others. When it is m for one set, it must be m for all others. This seems to be a strange and unbelievable result. In fact, it represents a quite trivial feature of quantum theory according to the following consideration.

First, one may remember that the various sets of states A, and B, etc. represent eigenstates of observables A, and B, etc. which are mutually incompatible. (If A were compatible with B then two states A_k and B_j might actually be the same states.) In general, the number of eigenvalues of various observables of a mechanical system are unlimited and lead to quadratic infinite q-matrices. Finite matrices occur only when "the kind of particle" whose states we consider is restricted to one value of a certain observable, M (of the angular momentum, say) with m-fold degeneracy so as to allow m orthogonal values of the sub-observable $A(=M_z)$ and also m values of other sub-observables B, and C, etc. (such as $M_{z'}$ and $M_{z''}$, etc.), where all the sub-observables are compatible with K, but mutually incompatible. The thermodynamic requirement of a common multiplicity m leading to quadratic matrices $q(A_k,B_j)$ and so forth then only expresses the fact that the common multiplicity is the m-fold degeneracy of the state K_m of the particles under consideration. That finite q- and ψ-matrices must be quadratic may also be seen from the following example. Suppose A has two eigenvalues, $A_{k'}$ and $A_{k''}$, whereas B has three (or one) eigenvalues B_j. The eigenvalue equations for the latter then are

$$(B_{k'k'}-B_j)\psi_{k'j}+B_{k'k''}\psi_{k''j}=0,$$
$$B_{k''k'}\psi_{k'j}+(B_{k''k''}-B_j)\psi_{k''j}=0.$$

The determinant has only two solutions B_j, rather than three (or one), and the assumption of nonquadratic matrices ψ proves to be wrong. In the usual case of considering "one kind of particle" and its states, there is an infinite degeneracy, and each set of orthogonal states has an infinite number of members, satisfying the thermodynamic requirement.

(5) Diffusion of two partially like gases. N particles of gas A and N particles of B may diffuse from separate volumes V into the common volume $2V$. Originally the entropy is

$$S_0=2kN\ln(Z/N). \tag{6}$$

Later when N particles of B are in the same volume with N particles of A, the description in terms of orthogonal states compels us to consider the fraction q of the B gas as being in the state A, and the fraction $1-q$ in the state non-A, or orthogonal to A, or $\bar{A}$. Thus, altogether in $2V$ there are now $N(1+q)$ particles of A and $N(1-q)$ of $\bar{A}$, both groups distributed over $2Z$ levels in $2V$. The entropy now is

$$S=kN(1+q)\ln[2Z/N(1+q)]+kN(1-q)\ln[2Z/N(1-q)]. \tag{6'}$$

The diffusion entropy increase is

$$S-S_0=kN\{2\ln 2-(1+q)\ln(1+q)-(1-q)\ln(1-q)\}. \tag{7}$$

$S-S_0$ decreases monotonously from the classical value $2kN\ln 2$ valid for $q=0$ (quite unlike gases) to $S-S_0=0$ for $q=1$ (like gases diffusing). Equation (7) is the detailed expression for the continuous entropy of diffusion, $S-S_0=f(q)\,2kN\ln 2$, whose required continuity was the starting point of the derivation of quantum concepts and quantum principles from the anti-Gibbs postulate of thermodynamic continuity.

All general quantum results derived from the postulate of thermodynamic continuity are independent

[2] Clyde C. Reynolds, Masters thesis, Ohio State University (1952).

of the Planck constant. They might have been found by Gibbs through pure reasoning concerning his paradox. The constant h enters only through the special formula for the fractional likeness amplitude between q and p,

$$\psi(q,p)=\exp(2i\pi qp/h), \tag{8}$$

obtained from microphysical evidence. This ψ-function is periodic and thereby gives rise to de Broglie's $p=h/\lambda$, to the Heisenberg uncertainty relation between coordinates q and momenta p, and to the duality and complementarity of the particle theory and its wave-like formalism. Also, Eq. (8) opens the path to the dynamics of those special mechanical systems whose Hamiltonian and other observables are given as functions of the q's and p's. Those parts of quantum theory, however, which rest on the thermodynamic continuity principle are independent of microphysical experience.

PHYSICAL REVIEW VOLUME 87, NUMBER 2 JULY 15, 1952

Ionospheric Absorption by N_2 and O_2 of Certain Extreme Ultraviolet Solar Wavelengths

K. C. CLARK
University of Washington, Seattle, Washington
(Received March 24, 1952)

Measurements are reported of the coefficients of absorption by the gases N_2 and O_2 of the emission from the H Lyman series 2–7, the resonance line 584A of He I, and twenty lines of H_2 between 980A and 850A, the atomic lines likely being strong in solar radiation. For an atmosphere of constant relative composition the absorption coefficients are related to the atmospheric heights of maximum photoionization and maximum electron concentration by equations which allow for a constant temperature gradient, the inverse square decrease of gravity, and a recombination process which may vary with height. With these laboratory measurements for N_2 and O_2 and the known calculated absorption for O_2 ionosphere layer heights are computed for the simple case which assumes complete O_2 dissociation above 100 km, no N_2 dissociation, and two-body recombination. Although only the first assumption is probably secure, it appears that photoionization is capable of producing layers at heights which agree with observation.

INTRODUCTION

IONIZATION of the upper atmosphere by the absorption of solar radiation is well established as the major mechanism in the production of ionosphere layers.[1] The resulting stratified concentrations of electrons, which are observed in great detail by reflection of radio waves and designated D, E, F_1, and F_2, occur at varying heights of about 65, 100, 200, and 300 km, respectively. To study the possible photoionization processes one must correlate information on the available solar ionizing radiation, the distribution of absorbing gases, and the absorption coefficients of the gases for these wavelengths. As available radiation there very probably is, in addition to the solar blackbody continuum, an intense line emission spectrum in the extreme ultraviolet to which the resonance spectra of H and He from the vicinity of solar flares contribute strongly.[2] Below 910A the excess of radiation over that from a solar blackbody at 6000°K has been estimated by Spitzer[3] to be of the order of tenfold in order to establish a temperature of about 1500°K at the height of the F_2 layer. Hunter,[2] Sedra,[4] Tousey,[5] and others have estimated this excess to be 2 or 3 orders of magnitude. The resonance line 1216A of H has not been photographed in spectra recorded during rocket flights up to 140 km,[6,7] although from Preston's low value[8] of its absorption coefficient in N_2 ($\alpha<0.005$ cm^{-1}) one would expect considerable intensity at this height. The absorption continuum of NO, expected[9] near 1216A, may possibly account for the absence of this wavelength in ordinary spectra from rocket flights. However, the quantitative experiments of Tousey[6] using filters and thermoluminescent phosphors have detected strong radiation in the range 795A–1050A at heights between 88 and 127 km and in the band 1050A–1340A between 80 and 90 km.

Oxygen and nitrogen are major components of the upper atmosphere, the former being almost completely photodissociated[10,11] at heights greater than about 100 km. Emissions from aurorae and the airglow show the presence of molecular nitrogen and atomic oxygen.[12]

[1] D. R. Bates and H. S. W. Massey, Proc. Roy. Soc. (London) **A187**, 261 (1946).
[2] A. Hunter, Repts. Prog. Phys. (The Physical Society, London) **9**, 8 (1942).
[3] L. Spitzer, Jr., contributor, *The Atmospheres of the Earth and Planets* (University of Chicago Press, Chicago, Illinois, 1949), Chapter 7. I am indebted to Professor Spitzer for a preliminary loan of his manuscript.
[4] R. N. Sedra, Phys. Rev. **83**, 190 (1951).
[5] Tousey, Watanabe, and Purcell, Phys. Rev. **83**, 792 (1951).
[6] J. J. Hopfield and H. E. Clearman, Phys. Rev. **73**, 877 (1948).
[7] Durand, Oberley, and Tousey, Astrophys. J. **109**, 1 (1949).
[8] W. M. Preston, Phys. Rev. **57**, 887 (1940).
[9] G. L. Weissler, conversations, June, 1951.
[10] O. R. Wulf and L. S. Deming, Terr. Magn. Atmos. Elect. **43**, 283 (1938).
[11] H. E. Moses and Ta-You Wu, Phys. Rev. **83**, 109 (1951).
[12] A. B. Meinel, Repts. Prog. Phys. (The Physical Society, London) **14**, 121 (1951).

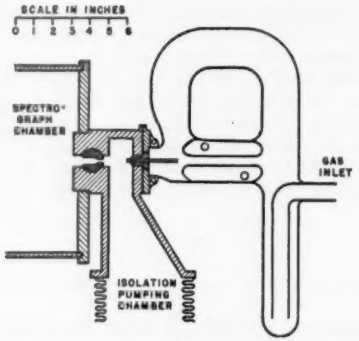

FIG. 1. Toroidal electrodeless discharge tube as mounted on vacuum spectrograph.

Also, atomic nitrogen is observed in aurorae, although the degree of nitrogen dissociation is not agreed upon.

The ionization cross section of O has been calculated by Saha and Rai[13] and by Bates.[14] Laboratory measurements of the absorption cross sections of N_2 and O_2 in the extreme ultraviolet have been made recently by Weissler[15] and earlier by Schneider,[16] both of whom used line emission sources. Qualitative absorption spectra in the extreme ultraviolet, which were made with a continuous source and used for wavelength studies, have been published by Takamine, Suga, and Tanaka,[17] and Worley[18] for N_2, by Price and Collins[19] for O_2, and by Hopfield[20] for dry air. The absorption of the H Lyman series in O_2 has been clearly photographed by Takamine and Suga,[21] who did not attempt cross-section measurements with their spark source.

The contribution reported here is a laboratory measurement of absorption coefficients of the gases N_2 and O_2 for the lines 2 to 7 of the H Lyman series, for the first line 584A of the corresponding resonance series of neutral He, and in addition for twenty lines of H_2. These measurements can be interpreted in terms of the height in the upper atmosphere at which the maximum rate of absorption occurs. The resulting layer of maximum absorption will be single for each wavelength, provided the atmosphere is considered to have constant relative composition and no density inversions. If ionization is at least a partial contributor in the absorption process, the layer of maximum ion production will coincide with that of maximum absorption. The height of maximum electron density will also depend upon how the recombination and attachment processes vary with pressure and temperature.

EQUIPMENT AND PROCEDURE

Measurements were made using a normal incidence vacuum spectrograph containing a glass grating of 15,000 lines/in. and 1-m radius. The rulings have been etched with HF to improve the intensity at short wavelengths as described by Wood and Lyman.[22] For high contrast, fine grain, and uniformity Eastman Process plates were used. These were sensitized by dipping in a 10 percent solution of Cenco pump oil in petroleum ether according to the technique of Schneider.[16] The narrow band of fluorescence permitted emulsion calibrations using 3906A from a Hg arc. Calibration exposure times were made equal to those of the vacuum spectra to avoid reciprocity failure. A slit width of 0.04 mm produced lines sufficiently broad for accurate microphotometer tracing. The absorption coefficient is obtained from the linear slope of the semilogarithmic graph of transmitted intensity *vs* density of absorbing gas in the spectrograph.

The absorbing gases N_2 and O_2 came from tank and electrolytic supplies, respectively. The O_2 was purified by passing over hot platinized asbestos, P_2O_5, solid CaOH, and solid CO_2 traps to remove H_2, H_2O, CO_2, and Hg, respectively. The N_2 was purified similarly except that the asbestos was not heated and liquid N_2 was used in the cold traps.

As a light source of steady and high intensity a toroidal electrodeless discharge tube was arranged as shown in Fig. 1 and excited by an inner coil at a frequency of 6 Mc/sec. The discharge was viewed end-on through a portion of the tube constricted to 1-cm diameter and water-cooled. An intermediate pumping chamber prevented the gas in the discharge from entering the optical slit of the spectrograph, and a suitable pressure differential was maintained by a capillary of 1-mm diameter and 30-mm length. The discharge was operated at pressures of 0.04 mm for purified H_2 and 0.08 mm for the mixture of 5 percent H_2 in He. The heating power developed in the discharge was estimated to be about 50 watts. The H_2 spectrum obtained was quite similar to that published by Jeppeson,[23] which likewise extended to about 850A. Prominent lines were used for absorption measurements.

Table I lists the resulting measurements of absorption coefficients. These values are the means of from three to five independent sets of observations, each usually covering four pressures of absorbing gas. The ranges of probable error indicated refer not only to internal consistency but to estimated errors in over-all calibrations. The line H Lyman α at 1215.7A was not studied because of its low absorption and the previous careful

[13] M. N. Saha and R. N. Rai, Proc. Natl. Inst. Sci. India **1**, 227 (1938), discussed in reference 1.
[14] D. R. Bates, Monthly Notices Roy. Astron. Soc. **100**, 25 (1939); **106**, 432, 509 (1946).
[15] Weissler, Lee, and Mohr, J. Opt. Soc. Am. **42**, 84, 200 (1952).
[16] E. G. Schneider, J. Opt. Soc. Am. **30**, 128 (1939).
[17] Takamine, Suga, and Tanaka, Sci. Papers Inst. Phys. Chem. Research (Tokyo) **34**, 854 (1938).
[18] R. E. Worley, Phys. Rev. **64**, 207 (1943).
[19] W. C. Price and G. Collins, Phys. Rev. **48**, 715 (1935).
[20] J. J. Hopfield, Astrophys. J. **104**, 208 (1946).
[21] T. Takamine and T. Suga, Sci. Papers Inst. Phys. Chem. Research (Tokyo) **29**, 213 (1936).
[22] R. W. Wood and T. Lyman, Phil. Mag. **2**, 310 (1926).
[23] C. R. Jeppeson, Phys. Rev. **44**, 165 (1933).

TABLE I. Measured absorption coefficients of N_2 and O_2 and corresponding layer heights at various temperature gradients above 120 km.

Line source	Wavelength Å	Absorp. coefficient in cm^{-1} S.T.P. N_2	O_2	O	Height in km of max absorption α=9.03°K/km	7.36	5.14	0
HLy2	1025.7	8± 3	53± 20	(calc	136	137	138	138
H_2	984.3	18 10	343 25	by	157	156	155	149
HLy3	972.6	3900 100	1350 150	Saha	400	400	346	223
HLy4	949.8	27 5	171 15	and	165	163	161	154
HLy5	937.8	100 20	113 10	Rai)	212	203	193	172
HLy6	930.8	190 30	460 20		243	228	212	181
HLy7	926.2	71 10	172 10		196	191	184	168
H_2	923.9	103 10	296 15		213	204	194	173
H_2	920.0	610 100	166 15		324	291	255	197
H_2	919.1	16 3	127 15		151	150	150	147
H_2	916.8	240 50	388 10		257	240	220	185
H_2	916.0	22 10	120 15		159	158	157	151
H_2	914.1	52 15	130 15		187	181	176	164
H_2	911.3	420 100	177 20		295	268	241	192
H_2	910.3	58 30	399 10		190	183	178	165
H_2	909.2	67 40	356 10	120	224	213	201	176
H_2	905.4	52 15	133 10	120	219	208	197	175
H_2	903.8	25 10	198 10	120	207	198	190	171
H_2	901.6	48 20	270 25	120	217	207	196	174
H_2	894.1	32 10	229 10	120	210	201	192	172
H_2	890.7	96 25	250 15	120	234	221	207	179
H_2	886.1	340 50	248 20	120	291	266	239	192
H_2	880.6	230 50	185 15	120	270	250	227	187
H_2	868.8	331 50	154 10	120	290	265	239	191
H_2	859.0	24 5	137 10	120	206	198	190	171
H_2	855.6	480 100	290 60	120	315	283	251	196
HeI	584.3	480 30	440 80	310	328	293	257	198

measurements by Preston, which Tousey[5] and others regard as the most reliable. With two exceptions the present results cannot be directly matched with those of Weissler and of Schneider, which were made using neighboring emission lines. Included in the careful measurements of Weissler[16] were the lines H Lyman β (1025.7A) and He I 584.4A. The absorption coefficients of N_2 for these lines were observed by him to be 60 cm^{-1} and 700 cm^{-1}, respectively, and for O_2 the values were 43 cm^{-1} and 550 cm^{-1}. It is seen that the agreement is quite satisfactory in the case of O_2, while the absorption by N_2 appears to be significantly greater than the values in Table I. Weissler, using 1215.13A of He II, obtained for N_2 the value of 66 cm^{-1}.

DENSITY DISTRIBUTIONS

The data for composition, pressure, and temperature of the atmosphere to 120 km are taken from the recent compilation of the National Advisory Committee for Aeronautics.[24] Below 80 km the fractions by volume of the major constituents O_2 and N_2 in dry air are taken, following Wildt,[25] to be 0.2095 and 0.7809, respectively. The region of partial O_2 dissociation in summer daylight hours is taken to lie between 80 and 100 km, the volume fraction of atomic O increasing linearly through this region from 0 to 0.346. The volume fraction of N_2 correspondingly decreases to 0.646. Above 100 km the atmosphere will be assumed to consist of N_2 and O.

If the temperature and the acceleration of gravity are considered constant, the variation of air density ρ with height h above sea level, measured relative to the value ρ_0 at h_0, follows the well-known exponential form

$$\rho/\rho_0 = \exp(-z/H_0), \tag{1}$$

where $z=h-h_0$ and the scale height $H_0=RT_0/Mg$, with R the gas constant, T_0 the temperature, M the mean molecular weight, and g the acceleration of gravity. The effect of the change in g with height can be included by using as the scale height the geometric mean of its values at h and h_0.

The temperature above 120 km, however, is undoubtedly not constant. With the exception of the low rotational temperatures observed by Vegard[26] in auroral streamers, where the excitation mechanism raises doubts,[27,28] all evidence indicates that the temperature increases rather steadily, reaching a value between 1000 and 2000°K at 300 km. If, as suggested by Bates,[29] Spitzer,[3] and Woolley,[30] this increase is described by a

[24] C. N. Warfield, Tech. Note No. 1200 (N.A.C.A., Langley Field, Virginia, 1947).
[25] R. Wildt, Revs. Modern Phys. **14**, 152 (1942).
[26] L. Vegard, contributor, *The Emission Spectra of the Night Sky and Aurorae* (The Physical Society, London, 1948), p. 82.
[27] N. C. Gerson, Repts. Prog. Phys. (The Physical Society, London) **14**, 316 (1951).
[28] L. M. Branscomb, Phys. Rev. **79**, 619 (1950).
[29] D. R. Bates, Proc. Phys. Soc. (London) **B64**, 805 (1951).
[30] R. v. d. R. Woolley, Proc. Roy. Soc. (London) **A189**, 219 (1947).

constant gradient of a°K/km, the modified density distribution above height h_0 can be simply shown[31] to be

$$\ln(\rho/\rho_0) = -(Mg_0/Ra+1)\ln(1+az/T_0), \quad (2)$$

which reduces to that of an isothermal atmosphere as a vanishes.

Allowance for the variation of g as well as the linear temperature gradient also leads to an exact expression. The substitution of $g=g_0r_0^2/r^2$ and $T=T_0(1+az)$ in the basic atmospheric equation in the form

$$-d\rho/\rho = dT/T + dz/H \quad (3)$$

gives an integrable equation. It will be convenient to use the constants

$$\beta = aH_0/T_0 \quad \text{and} \quad \gamma = r_0/(\beta r_0 - H_0). \quad (4)$$

The resulting density distribution is

$$\ln(\rho/\rho_0) = -(\gamma^2\beta+1)\ln(1+\beta z/H_0) + \beta\gamma^2\ln(1+z/r_0) + \gamma z/(r_0+z). \quad (5)$$

When the gradient $a \gg T_0/r_0$, this equation simplifies to

$$\ln(\rho/\rho_0) = -(1/\beta+1)\ln(1+\beta z/H_0) + (1/\beta)\ln(1+z/r_0) + z/\beta(r_0+z). \quad (6)$$

HEIGHT OF MAXIMUM RATE OF ABSORPTION

If the absorption coefficient of the ith component gas is given by α_i cm^{-1} for that gas at 0°C and 760-mm pressure, then the total absorption coefficient of air at height h_0 is

$$A = (\rho_0/\rho_s)(\alpha_1F_1+\alpha_2F_2+\cdots)10^5 \text{ km}^{-1}, \quad (7)$$

where the composition is given by the volume fractions F_i, and ρ_s is the density at S. T. P. of air of the same composition. The change in the intensity of incident radiation J follows Beer's law and for vertical incidence is

$$dJ = JA(\rho/\rho_0)dz. \quad (8)$$

The measured absorption coefficients can be used to compute either the height of the maximum rate of absorption or the height of maximum ion concentration. The latter computation requires certain information on the processes of electron disappearance, while the former does not. It will be seen that these heights are identical under certain commonly assumed conditions of recombination.

In obtaining the height of maximum ion concentration, one may write the standard equation for the rate of production of ion density n to include a general recombination process

$$dn/dt = (JA\rho/\rho_0) - \alpha' f\phi, \quad (9)$$

where $f=f(\rho)$, $\phi=\phi(n)$, and α' is the recombination coefficient. For the case of recombination in two-body collisions, as is commonly assumed for the F layers, $f=1$ and $\phi=n^2$. The conditions for equilibrium and for maximum ion density, respectively, are

$$dn/dt=0, \quad dn/dz=0=d\phi/dz. \quad (10)$$

Equation (9) may then be equated to zero at equilibrium and used, together with Eq. (8), to eliminate J and dJ from the differential form of Eq. (9). Since ϕ is by Eq. (10) an extreme at the height of maximum ion density, one then obtains at this height the relation

$$(\rho df/d\rho - f)d\rho/dz = A\rho^2 f/\rho_0. \quad (11)$$

If it is known or assumed how ρ and f vary with z and if A is obtained from laboratory absorption measurements, one can graphically find the height at which Eq. (11) is satisfied, which is the height of maximum ion density.

On the other hand, to find the height where the rate of absorption is a maximum, dJ/dz must be maximized. Applying the necessary condition $d^2J/dz^2=0$ to Eq. (8), one obtains at the height of this maximum

$$-d\rho/dz = A\rho^2/\rho_0, \quad (12)$$

which is identical with Eq. (11) if f is constant. This assumption of simple two-body recombination will be made in the presentation here of measured absorption coefficients, and the height of maximum ion density will therefore be identical with the height of maximum rate of absorption.

For the case of isothermal $T=T_0$ and constant $g=g_0$

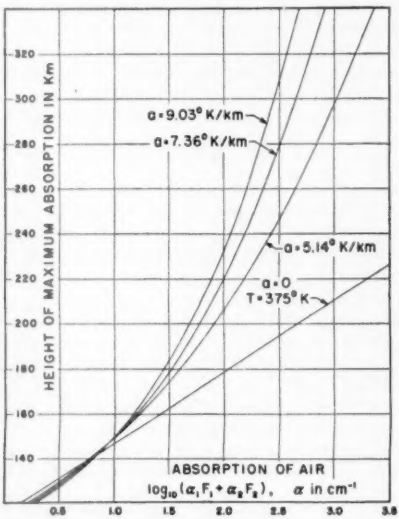

FIG. 2. Computed curves relating absorption coefficients to layer heights for inverse square gravity and various temperature gradients above 120 km.

[31] J. A. Gledhill and M. E. Szendrei, Proc. Phys. Soc. (London) **B63**, 427 (1950).

this layer height $\bar{z}$ is simply

$$\bar{z}=H_0 \ln AH_0, \tag{13}$$

and at this height the intensity is reduced from its original value by the fraction

$$J(\bar{z})/J(\infty)=e^{-1}. \tag{14}$$

The assumption of a constant temperature gradient and constant g can directly be shown[31] to produce the following modifications of Eqs. (13) and (14):

$$\ln(1+\beta\bar{z}/H_0)=\beta \ln[AH_0/(1+\beta)], \tag{15}$$

$$J(\bar{z})/J(\infty)=e^{-1-\beta}. \tag{16}$$

Nicolet[32] has given an equivalent expression for electron layer height assuming recombination by collisions of an arbitrary number of bodies and an effective recombination coefficient which has an arbitrary power dependence on density.

The concept of associating the layer of maximum absorption with a certain optical depth in the atmosphere, as indicated in Eqs. (14) and (16), becomes artificial when one allows g to vary with the inverse square law, for as Mitra[33] implies, the total mass above any height is given by a nonconvergent integral. But the treatment in Eq. (12) is still applicable, since the density function is given in Eq. (5). The equation for $\bar{z}$ becomes, in logarithmic form,

$$\ln A=\ln\left[\frac{\beta(\beta\gamma^2+1)}{H_0}\right.$$
$$\left.-\frac{\gamma}{r_0}\left(1+\frac{\beta\bar{z}}{H_0}\right)\left(\frac{r_0}{r_0+\bar{z}}\right)\left(\frac{r_0}{r_0+\bar{z}}+\beta\gamma\right)\right]$$
$$+\beta\gamma^2\ln\left(1+\frac{\beta\bar{z}}{H_0}\right)-\beta\gamma^2\ln\left(1+\frac{\bar{z}}{r_0}\right)-\frac{\gamma\bar{z}}{r_0+\bar{z}}. \tag{17}$$

INTERPRETATION OF RESULTS

Equation (17) gives the dependence of the layer height $\bar{z}$ upon A. Since the constants β, γ, H_0, and r_0 are known or estimated properties of the atmosphere and A is evaluated from absorption coefficients, the equation may be graphically solved for $\bar{z}$. Using at $H_0=120$ km the values $r_0=6490$ km, $T_0=375°$K, $M=23.94$, and $g_0=9.65\times10^{-3}$ km/sec^2 according to the N.A.C.A. tables, one computes a scale height $H_0=13.49$ km. With these values Eq. (17) is solved graphically in Fig. 2, where the right side is plotted horizontally as a function of the ordinate $\bar{z}$ for four suggested values of temperature gradient. These values of a in °K/km are 9.03 ($T=2000°$K at 300 km); 7.36 (Spitzer, 1700°K at 300 km); 5.14 (Woolley, 1300°K at 300 km); and 0 (isothermal). If g were taken to be a constant g_0, then the curve for $a=9.03$ would be lower by 10 km at 300 km. The measured absorption coefficients of N_2 and O_2 are listed by wavelength in Table I. Also, the corresponding coefficients of the continuous absorption by O as computed by Saha and Rai[13] are given. This absorption continuum is somewhat uniform between about 500A and the ionization limit at 910A because of the overlapping of the continua of excited atoms. The values $\alpha=120$ cm^{-1} above 856A and $\alpha=310$ cm^{-1} at 584A have been used.

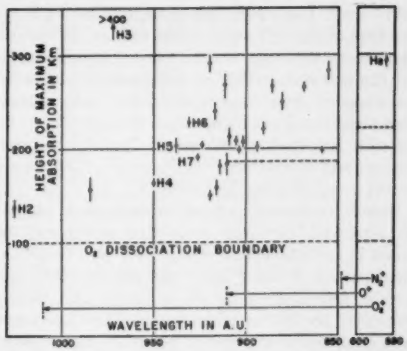

FIG. 3. Layer heights for various wavelengths, assuming $a=7.36°$K/km. Lines of H Lyman series are numbered points. Continuous absorption by O sets the lower limit shown by upper dashed line.

Assuming that N_2 and O are the sole components above 120 km, one computes $\ln A$ and from the graph of Fig. 2 finds the height of maximum rate of absorption. These heights are plotted by wavelength in Fig. 3 for the assumed value of $a=7.36°$K/km. This value of a is seen to give a maximum at 293 km for the presumably strong 584A radiation from He I, which could concurrently ionize both N_2 ($\lambda<796$) and O ($\lambda<910$). This height would agree with that of the F_2 ionosphere layer. It is seen that for this same temperature gradient no wavelength between 910A and about 500A can penetrate the continuous absorption by O at a layer height of about 190 km, regardless of N_2 transparency.

For all wavelengths measured the maximum rate of absorption occurs well above 120 km, and hence, absorption by O_2, which exists only below 100 km, need not be considered. But other wavelengths may escape the line absorption in the range $1010>\lambda>910$ and ionize O_2. Since the air density is relatively high in the dissociation region, any wavelength appreciably absorbed by O_2 would be very rapidly attenuated, and the height of maximum rate of absorption would lie close to the upper boundary of the region. This height would agree with that of the E layer. For example, if O_2 alone were the absorber, radiation for which $\alpha=120$ cm^{-1} would be reduced by $1/e$ in the first 2 km below 100 km, and only 5 km would similarly be needed if

[32] M. Nicolet, J. Atmos. Terr. Phys. **1**, 141 (1951).
[33] S. K. Mitra, *The Upper Atmosphere* (Royal Asiatic Society of Bengal, Calcutta, India, 1947), Chapter 1.

$\alpha = 17$ cm^{-1}. The strong line absorption by N_2 of those members of the H Lyman series used in the measurements seems to eliminate their role in *E* layer formation, but the necessary radiation could possibly come from the wings of these lines broadened in solar emission, from series members higher than the seventh, or from the solar blackbody continuum.[34] The observations of Tousey[5] and of Friedman[35] indicate that there may also be soft x-rays of irregular intensity.

Bates[36] has recently argued on the basis of computed and observed intensities of the first negative nitrogen bands in twilight enhancement that N_2^+ forms but a small portion of the *F* layer ions and also that the F_2 layer is derived from the F_1 through a variation with altitude of the O^+ recombination coefficient. His results raise doubt as to the importance of N_2 as an absorber even of wavelengths above its ionization limit and would indicate either or both of the following conclusions: the radiation around 584A is weak, and nitrogen in the *F* region is largely atomic. Herzberg[37] has suggested that a known predissociation of N_2 may be appreciable at these heights. The continuous absorption by N, for whose spectral head Bates has computed $\alpha = 1620$ cm^{-1}, should ideally be included in the analysis of atmospheric absorption. But as yet the degree of dissociation is not known; and hence the role of N, which may still be small, is here conveniently ignored. If the dissociation and the air density were known functions of height, then the dependence of A on z would be known. Equation (11) would be modified only by the additional term $f\alpha'\rho(dA/d\bar{z})/A$ on the right and could again be solved graphically for $\bar{z}$.

SUMMARY

Absorption coefficients of N_2 and O_2 are given for the H Lyman series to the seventh member, the principal line of the resonance series of He I, and twenty wavelengths of H_2, the atomic lines being chosen because of their probably strong contribution in solar emission. The relation of these data to ionosphere production is discussed, using an analysis for the height of maximum rate of absorption which takes into account a linear increase in atmospheric temperature with height above 120 km and the inverse square decrease of gravity. If the temperature is assumed to increase to 1700°K at 300 km, the combined absorption by N_2 and O of the principal line of He I would have a maximum at 293 km, the height of the F_2 layer. The wavelengths studied between 1010A and 910A could not penetrate N_2 to the extent necessary to ionize O_2 at the *E* layer; the source of this ionization may be broadened wings of these lines in solar emission, further lines in the H Lyman series, continuous solar radiation, or soft x-rays. Other intense solar emission than the lines studied may well contribute to the formation of other layers, in particular the F_1 layer at the height of the maximum rate of O^+ production. The location of the absorption coefficients on a height scale strongly suggests that the upper atmosphere is not isothermal. The foregoing analysis has discussed the heights of maximum production rate of ions; these are also the heights of maximum concentration of electrons in the simple case where the two-body recombination coefficient is constant and the atmosphere has constant relative composition. Under less simple conditions of electron removal these heights will, in general, fail to coincide, and this situation may exist in the upper atmosphere. In fact Bates has suggested that the F_1 and F_2 layers may be formed by the same ions and radiation and rendered separate by a marked change in recombination coefficient with height. A correct computation of electron layer height must await further knowledge of the dominant mechanism of electron removal and the variation of recombination and attachment coefficients with height.

The laboratory measurements reported here were carried out at the Lyman Laboratory of Harvard University. The writer is very grateful to Professor O. Oldenberg for his friendship, for the suggestion of this research, and for the stimulating supervision of its experiments.

[34] R. v. d. R. Woolley and C. W. Allen, Monthly Notices Roy. Astron. Soc. **108**, 292 (1948).
[35] Friedman, Lichtman, and Byram, J. Opt. Soc. Am. **41**, 292 (1951).
[36] D. R. Bates, Proc. Roy. Soc. (London) **A196**, 562 (1949).
[37] G. Herzberg, Nature **161**, 283 (1948).

The Complex Alpha-Spectra of Am^{241} and Cm^{242}

FRANK ASARO, F. L. REYNOLDS, AND I. PERLMAN
Radiation Laboratory and Department of Chemistry, University of California, Berkeley, California
(Received April 1, 1952)

The alpha-particle spectra of Am^{241} and Cm^{242} was studied in detail utilizing a 75-cm radius of curvature 60° symmetrical electromagnetic analyzer with photographic plate detection. The radioactive sources containing up to 3 $\mu g/cm^2$ of active atoms in the case of Am^{241} were prepared by vacuum sublimation. The average geometry of the spectrograph is about 4 parts in 10^5. The energy dispersion on the photographic plate is about 3.4 kev/mm for 5-Mev alpha-particles, and the width at half-maximum of these alpha-particle groups is about 7 kev. Six alpha-particle groups were found in Am^{241}, and their energies and abundances are 5.546 Mev, 0.23 percent; 5.535, 0.34 percent; 5.503, 0.21 percent; 5.476, 84.2 percent; 5.433, 13.6 percent; 5.379, 1.42 percent. In Cm^{242} two alpha-particle groups were found whose energies and abundances are 6.110 Mev, 73 percent, and 6.064, 27 percent. The alpha-decay scheme is correlated with gamma-rays and conversion electrons observed in this laboratory for both Am^{241} and Cm^{242}. The various alpha-groups are evaluated with respect to the alpha-decay systematics, and the degrees of hindrance of the various alpha-transitions are discussed with reference to normal trends in even-even nuclei. It is suggested that the totally different patterns of the spectra of the two nuclides are conditioned by the nuclear types.

INTRODUCTION

ACCORDING to simple alpha-decay theory[1,2] the predominant factor governing the decay constant is the decay energy. On this basis one might expect that alpha-transitions other than those to the ground state of the product nucleus would compete poorly with the most energetic alpha-particle so that complex spectra would be difficult to discern, particularly if the spacing between nuclear energy levels is wide. A study of the decay characteristics of the many alpha-emitters now known has shown that the even-even nuclides are in remarkable agreement with the demands of the theory while other types are not. This is not to say that the even-even nuclides show no complex structure, but where multiple alpha-groups are encountered the partial decay constants have been found to be in general agreement with expectations according to the energy for each group. The experimental manifestation of this relationship is that the ground-state transition is most abundant, whereas a transition by a lower energy alpha-group is found in lower abundance.[3,4]

There is mounting evidence, as reviewed in an earlier publication,[3] that those nuclides which have one or more unpaired nucleons depart from the regularities of the even-even type. It was found to be the rule that the alpha-decay of the odd nucleon types was hindered, in the sense that the half-life of each such nuclide was longer than predicted by the simple theory and that actually found for an even-even alpha-emitter of the same atomic number and decay energy. A further generalization was suggested that has to do with complex structure of nuclides with odd nucleons; and that is that the ground-state transition is most highly hindered, whereas one or more of the lower energy groups are present in relatively higher abundance than would be expected according to their respective energies. In fact, cases were found in which the ground-state transitions were rare, and it could be inferred that there might be instances in which the ground-state transitions have not yet been discerned. The relatively long partial half-life of the ground-state transition will in itself make complex structure more prominent. In the absence of the means of resolving alpha-groups of similar energies, the presence of abundant gamma-radiation was often the best evidence for complex alpha-decay.

The reason advanced[3] for the marked differences between the different nuclear types lay in a provision for the assembly of the components of the alpha-particle. It was suggested that the time for assembly in even-even nuclides is either negligible or nearly constant and that the theory cannot distinguish between the two. If one or two odd nucleons are present, however, it was postulated that additional time is required for the assembly of the alpha-particle for the ground-state transition, since for this transition the odd nucleon either must be a participant, or the necessary nuclear rearrangement must accompany the process in order to leave the product nucleus in its ground state.

In the absence of the means for placing this explanation upon a quantitative basis, we can examine in greater detail the complex spectra of both types of alpha-emitters with the hope that further correlations will appear which will point toward an understanding of the factors at play. For example, the odd nucleon alpha-emitters may show particular energy spacings in their complex structure and degree of hindrance in emission which can be correlated in terms of assigned states of the nucleons.

It is for these objectives in furthering alpha-decay theory, in the possibility of assigning quantum states to the nuclides as well as for the intrinsic interest in

[1] G. Gamow, Z. Physik **51**, 204 (1928); G. Gamow and C. L. Critchfield, *Theory of Atomic Nucleus and Nuclear Energy-Sources* (Oxford University Press, London, England, 1949).
[2] E. U. Condon and R. W. Gurney, Phys. Rev. **33**, 127 (1929); Nature **122**, 439 (1928).
[3] Perlman, Ghiorso, and Seaborg, Phys. Rev. **77**, 26 (1950).
[4] I. Perlman and T. J. Ypsilantis, Phys. Rev. **79**, 30 (1950).

the decay properties of heavy nuclides, that a program has been undertaken to measure complex structure of alpha-emitters. In so doing, the classical work on alpha-particle spectroscopy will be extended to the many artificially produced alpha emitters.

For the measurements, a magnetic spectrograph has been constructed, the details of which have been described elsewhere.[5] The most detailed measurements to date have been made on Am^{241} and Cm^{242} which are representatives of the odd-even and even-even nuclear types, respectively. The availability of these nuclides in sufficient quantity has dictated their early selection.

EXPERIMENTAL

The Alpha-Particle Spectrograph

The instrument used in the present measurements employs a 60° sector electromagnet, and the normal trajectory has a radius of curvature of 75 centimeters. Figure 1 is a schematic diagram of the optics of the instrument and shows the magnet, source, slit system, and detector. A more detailed description of the instrument, its power supply and operating characteristics have been published elsewhere.[6] A brief summary of the characteristics are given here: the magnet power supply is capable of maintaining the current constant to 1 part in 10,000 over at least a 24 hour period. The detection system employed consists of nuclear emulsion plates in which the alpha-particle tracks are counted using 450 power magnification. The dispersion at a given point on the detection plate varies linearly with particle energy and amounts to about 3.4 kev per millimeter at 5 Mev. The width at half-maximum for the alpha-particle peaks depends strongly upon the sample preparation and to a lesser degree upon the slit and baffle systems employed. These factors will be discussed below. The geometry factor has been varied between 10^{-6} and 10^{-4} and depends upon the slit and baffle openings.

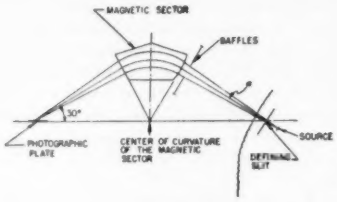

FIG. 1. Schematic diagram of the optics of the spectrograph.

Sample Preparation

In order to take advantage of the inherent high resolution of an alpha-particle spectrograph it is imperative that the sources be extremely thin. Poor samples with respect to self-absorption are manifested by a tail on the low energy side of the distribution curve, whereas the form for a thin preparation approaches a symmetrical peak. Among the natural radioactivities good samples have been prepared, when applicable, by collecting the active deposits from the emanation in the decay series.

In general, poor samples are obtained when prepared from solutions by simple evaporation of the solvents. Even when the weight of the sample corresponds only to the order of a few micrograms per square centimeter on the plate, the formation of micro crystals with high surface density effectively produces a thick sample. Impurities in the solution often produce the same results. In certain cases electrodeposition may be employed to advantage, but in general this method requires careful control of conditions which may be different for each substance. It is difficult to obtain satisfactory plates, particularly for electropositive elements such as the actinide elements in which reduction to the metal is not possible.

The most generally acceptable method employed in this laboratory for a wide variety of substances consists of vacuum sublimation. In the presently considered instances, a solution of americium or curium chloride is evaporated to dryness on a tungsten filament. Upon raising the temperature to white heat for a few seconds by passing current through the filament, the sample is vaporized onto a 2-mil platinum plate masked by another plate having a rectangular slit $1\times\frac{1}{4}$ inch which defines the sample shape. The mask and collecting plate are placed about $\frac{1}{4}$ inch above the filament. The whole system is maintained at a few microns pressure to prevent formation of tungsten oxide which, if formed, appears as a dark film on the collecting plate. Under optimum conditions the vaporized sample can contain up to 10 $\mu g/cm^2$ of active atoms and still give good resolution, but normally for high resolution the limit is about 2 $\mu g/cm^2$.

Sample Exposure and Track Detection

Referring to Fig. 1, the alpha-particle beam is defined by the slit and baffle system as indicated. With a uniform magnetic field the width (S) of the image on the photographic plate of a homogeneous beam of alpha-particles is

$$S=2(\Delta S+r_0\alpha^2+\cdots), \qquad (1)$$

where ΔS is the defining slit width, r_0 the radius of the normal trajectory and α the half-angle of emergence of the beam from the magnetic field. This formula applies to a 60° sector magnet with plane surfaces for the pole pieces, and the factor "2" arises because the photographic plate is placed at an angle of 30° with the trajectory of the alpha-particles rather than normal to it.

By proper shaping of the source side of the magnet, the second term of Eq. (1) can be made negligible with

[5] F. L. Reynolds, Rev. Sci. Instr. **22**, 749 (1951).

respect to the slit width, and this feature is indicated on the diagram by the rounded surface of the magnet. Since the magnetic field is not uniform throughout but falls off near the edges of the magnet, baffles are used as a means of confining the beam to the center. If a slit opening of 0.018 inch and a 3-inch opening between the baffles is used, the alpha-beam half-width on the photographic plate for a 6-Mev alpha-particle is 2 mm which corresponds to 8 kev.

Sample strengths were in general selected to permit exposures of 1 to 2 days. However, exposures as short as 6 minutes and as long as 16 days have been employed. The lengthy exposures were required to examine the alpha-groups present in low abundance in complex spectra. The limiting factor for long exposures is the background of the instrument. Because of the undulating character of the background it was found desirable to have the peak heights at least three times the average background for positive identification. A single field of view in the microscope encompasses $\frac{1}{4}\times\frac{1}{4}$ mm of the photographic plate, and a scan of one field width across the entire height of the plate (2 inches) gave as background about two alpha-tracks for each day exposure. On the low energy side of an alpha-peak, the apparent background could be considerably higher than this, presumably because of the low energy tailing due to absorption in the sample.

As already mentioned, the alpha-particles are determined photographically. The detecting plates used were 9×2 inch Eastman NTA plates with 25 micron thick emulsions and these were examined under a 450 power microscope with bright field illumination. The track length of a 6-Mev alpha-particle is approximately 25 microns and, because of the position of the plate as shown in Fig. 1, the track makes an angle of 30° with the plane of the emulsion. Because of the small angle of acceptance parallel to the magnetic field permitted by the gap between the pole pieces, the tracks should be nearly parallel and only these are recorded. A photograph of one graph of one field of view is shown in Fig. 2 in which are seen six acceptable alpha-tracks and two tracks which are rejected.

The particular microscope stage employed in these measurements cannot hold a 9-inch plate so each plate was cut into three parts. Before sectioning, an axial line was ruled with a razor blade along the center of the plate parallel to the long dimension. Cross lines perpendicular to the axial line were also ruled in each of the proposed sections. The distances between the intersections of the lines were measured, and after sectioning these served as indices to relate distances on the three sections.

In counting the tracks, the microscope stage was moved perpendicular to the axial line giving a scan $\frac{1}{4}$ mm wide across the width of the plate. The stage was then moved one field of view parallel to the axial line and another scan made. The count from each scan was plotted on a count *versus* distance graph as shown in Fig. 3.

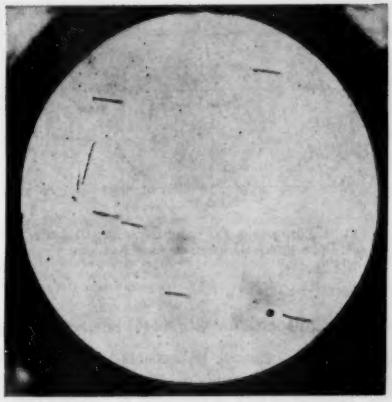

FIG. 2. Alpha-tracks in photographic emulsion.

Dispersion

The energy dispersion on the plate for a normal trajectory r_0 and energy E_0 is

$$\text{dispersion} = E_0/2r_0. \tag{2}$$

The relation of the magnetic field to E_0 and r_0 is given by Eq. (3) in which B is in gauss, r_0 in centimeters and E_0 in electron volts.

$$B = (144/r_0)E_0^{\frac{1}{2}}. \tag{3}$$

Since the position of the normal trajectory cannot be determined precisely, it is not possible to determine the value of B necessary to focus a particular alpha-particle at that point and E_0 is best eliminated between the Eqs. (2) and (3). The resulting Eq. (4) for the disper-

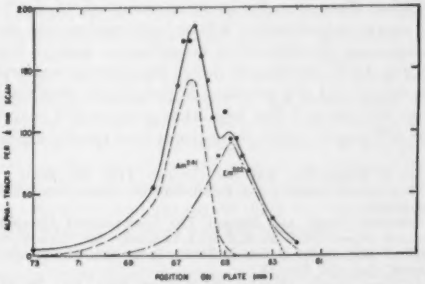

FIG. 3. Positions of Em^{222} and the principal Am^{241} alpha-group. Dispersion—3.96 kev/mm; —— spectrum as measured; — — — Em^{222} peak resolved by subtracting background and using half-width for the peak as determined on a separate measurement with the Em^{222} sample alone; — — resolved alpha-group of Am^{241}.

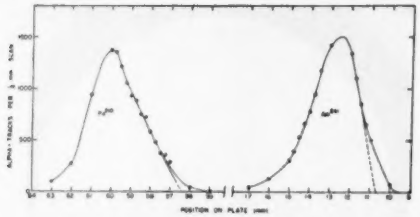

FIG. 4. Positions of Po^{210} and the principal Am^{241} alpha-group. Dispersion—3.90 kev/mm.

sion is then

$$\text{dispersion} = r_0 B^2/(2\times 144^2). \quad (4)$$

In addition, r_0 cannot be expected to be precisely equal to the nominal radius of curvature of the magnet (75 cm) because of lack of precision in construction and alignment of source and detector. An effective radius, however, can be determined by measuring distances between alpha-groups of known energy. In other words, the dispersion is obtained experimentally for the particular energy range of interest. For this purpose measurements were made of the complex spectrum of Ra^{226}, the distance between the main group of Ra^{226} and Em^{222}, and between Em^{222} and Po^{218}. The energies taken for Em^{222} and Po^{218} alpha-particles were those given by Briggs[6] (5.486 and 5.998 Mev) and for the two Ra^{226} groups, the determination by Rosenblum[7] (4.795 and 4.6105 Mev). Within the limits of experimental error (about 2 percent of the energy differences) the radius so determined was constant and indicated that the nominal 75-cm radius must be increased by 5.4 percent; that is, energy differences calculated by the use of Eq. (4) using 75-cm radius were low by this amount.

RESULTS

Am^{241} Energy Calibration

Before discussing the complex structure of Am^{241}, the energy determination will be mentioned so that the groups may be referred to according to energy. The nuclide Am^{241} was that by which the element was first identified,[8] and it is prepared in isotopically pure form from Pu^{241} decay.[9] The half-life is given as 470 years[10] and 475 years[11] which corresponds to a specific alpha-activity of 6.95×10^6 disintegrations per minute per microgram. Previous to the present studies the measurement of alpha-energy has been made with an ionization chamber coupled to a pulse-height discriminator from which the value 5.48 Mev was reported.[12] Although one could observe from the pulse-height analysis that the spectrum was not simple, it was not possible to resolve it into its components. The measurement therefore gives the energy of the principal group distorted to an unknown extent by one or more other groups.

The energy for Am^{241} was determined with the spectrograph by comparing that of the principal group with two standards, Po^{210} and Em^{222}. The other groups of Am^{241} were assigned energies by comparison with the main group.

The comparison between Am^{241} and Em^{222} is shown in Fig. 3. The plate was made by placing sources of Am^{241} and radium simultaneously in the spectrograph for an exposure of 27 hours. That the higher energy group is that of Em^{222} could be proved by comparing the observed number of tracks with that expected from the observed Po^{218} tracks caught on another part of the plate. If it was assumed that half of Po^{218} formed from Em^{222} left the source by the recoil mechanism, the observed number of tracks in the high energy component was in agreement with the expected amount from Em^{222}. The resolution of the curve in Fig. 3 was aided by a separate exposure with the radium source alone in which the width of the Em^{222} peak at half-maximum was determined. The distance between the peaks was 2.7 ± 0.3 mm which corresponds to an energy difference of 11 ± 2 kev. Taking the energy of Em^{222} as 5.486 Mev,[6] the energy of the principal group of Am^{241} becomes 5.475 ± 0.002 Mev.

Similar exposures were made with Po^{210} the results of which are shown in Fig. 4. The distance between peaks was 45.8 mm which corresponds to an energy difference of 179 ± 2 kev. From this measurement the main group of Am^{241} has an energy of 5.477 ± 0.002 Mev. The energy which we shall use is 5.476 ± 0.002 Mev. As will be described, the most energetic alpha-group is higher in energy than this group by 70 kev, therefore its energy is 5.546 Mev. The decay energy[13] of Am^{241} is accordingly 5.640 Mev.

Complex Structure of Am^{241}

There are now known to be six measurable alpha-groups of Am^{241}, three of which are of greater energy than the most prominent group. In discussing complex spectra, a system for designating the different groups is of value. That used here is directed toward visualizing the energy relations of the groups and was suggested by A. Ghiorso. In this system the group known or

[6] G. H. Briggs, Proc. Roy. Soc. (London) **A157**, 183 (1936).
[7] Rosenblum, Guillot, and Bastin-Scoffier, Compt. rend. **229**, 191 (1949).
[8] Seaborg, James, and Morgan, *The Transuranium Elements: Research Papers* (McGraw-Hill Book Company, Inc., New York, 1949), p. 1525, National Nuclear Energy Series, Plutonium Project Record, Vol. 14B, Div. IV.
[9] Ghiorso, James, Morgan, and Seaborg, Phys. Rev. **78**, 472 (1950).
[10] B. G. Harvey, Abstract of Papers, XII International Congress of Pure and Applied Chemistry (September, 1951), p. 358; Phys. Rev. **85**, 482 (1952).
[11] Cunningham, Thompson, and Lohr, unpublished data (1950).
[12] A. Ghiorso, unpublished data (1948).
[13] The term "decay energy" or "alpha-energy" refers to the disintegration energy including the recoil energy. The kinetic energy of the alpha-particle is explicitly designated "alpha-particle energy" or "particle energy."

thought to represent the ground-state transition is termed $\alpha(0)$ or, in this case, $Am^{241}(0)$. The appropriate energy in kev above the ground state is placed in parentheses for each of the other alpha-groups. Thus, the most prominent alpha-group of Am^{241} leads to a state 71 kev above the ground state and is designated $Am^{241}(71)$ or the $\alpha(71)$ group.

The complete alpha-spectrum is shown in Fig. 5. For these particular data, the source consisted of 2.9 micrograms of Am^{241} (2.0×10^7 disintegrations/minute) and the exposure was for 94 hours. Because of the disparity in abundance of the different groups, complete peaks cannot be shown to the same scale. In exposing the plate long enough to register a statistically significant number of tracks of the rare groups, too many tracks for counting were registered at the positions of the principal groups. Partial scans across the plate were made for these peaks and the results are also shown in Fig. 5. The peak widths at half-maximum are essentially the same for all peaks.

The relative abundances of the groups were obtained by counting the tracks of the two most prominent groups on a plate exposed for a shorter period of time and comparing with the rarer peaks from the long exposure. The abundances were virtually the same whether integrated numbers of tracks under the peaks or the peak heights were compared. A summary of the abundances and the corresponding partial half-lives which will be referred to later are given in Table I. The values in each case represent at least two independent measurements. The sum in abundance of the two highest energy groups is known with better precision than each group separately because of the uncertainty in resolution. For this reason they are listed both ways in Table I.

The energy range of the observed peaks was 5.38 to 5.55 Mev. Counting the plate outside of this range revealed that there can be no peak between 5.21 and 5.38 Mev of greater abundance than 0.17 percent, and from 5.55 to 5.64 Mev none in more than 0.07 percent abundance. These limits were based on the respective background counts in the regions.

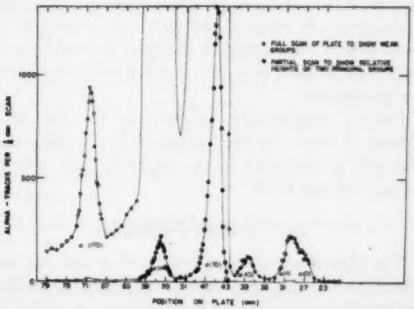

FIG. 5. Alpha-spectrum of Am^{241}.

TABLE I. Abundances of Am^{241} alpha-groups.

Alpha group[a]	Percentage abundance	Partial half-life[b] (yr)
$\alpha(0)+\alpha(11)$	0.57 ($\pm$0.06)	
$\alpha(0)$	0.23 ($\pm$0.06)	2.1×10^3
$\alpha(11)$	0.34 ($\pm$0.06)	1.4×10^3
$\alpha(43)$	0.21 ($\pm$0.02)	2.3×10^3
$\alpha(71)$	84.2 ($\pm$1.5)	564
$\alpha(114)$	13.6 ($\pm$1.4)	3500
$\alpha(170)$	1.42 ($\pm$0.15)	3.3×10^4

[a] The highest energy group, designated $\alpha(0)$, is taken to represent the ground-state transition. The parenthesis-enclosed figures used for the other groups indicate the energy levels in kilovolts above the ground state with which the alpha-groups are associated.
[b] Based on 475-year measured half-life.

Determinations of energies of the several groups were made relative to the principal alpha-group, $\alpha(71)$, which was standardized against Em^{222} and Po^{210} as already described. The actual comparisons were made by extrapolating the high energy side of each peak to the intercept after subtraction of the estimated background count and tailing from other groups. The method for obtaining the dispersion in order to translate positions on the plate to energy differences has already been described.

The results of several measurements of alpha-particle energies are summarized in Table II. The measured alpha-energy differences with their estimated limits of error are as indicated. Also shown are the selected best values and the corresponding energies of the alpha-groups based on 5.476 Mev for the most prominent group. In the last column are shown the energy levels above the ground state of Np^{237} with which each alpha-group is associated. These levels are obtained by correcting the differences of alpha-group energies for the corresponding differences in alpha-decay recoil energy. It is differences between these numbers which should correspond to gamma-ray energies.

Decay Scheme of Am^{241}

The complexity of the decay scheme of Am^{241} may be visualized readily from the number of observed levels. The precise measurement of some of the gamma-rays and L-series x-rays with a bent crystal spectrometer is covered in another paper.[14] The L x-rays arise from internal conversion processes of the gamma-rays, and they are identified by matching observed energies with those predicted for neptunium according to extrapolations of the Moseley relationship. It is presumed that other observed photons are nuclear gamma-rays, and an attempt is made to match these with energy levels deduced from the alpha-particle spectrum.

Figure 6 shows a partial decay scheme with the energy levels shown corresponding to the alpha-particle spectrum. Only a part of the measured gamma-rays have been entered because the positions of all relative to the energy levels defined by the alpha-spectrum are

[14] C. I. Browne and I. Perlman (to be published).

TABLE II. Alpha-particle energy of Am^{241} groups.

Alpha-group	Experiment number 33	48	59a*	59b*	61a	61b	Best values	Alpha-particle energies (Mev)	Energy levels above the ground state (kev)
$\alpha(0)$								5.546	0
		10.3 ±2.0	9.3 ±1.1	10.8 ±0.8	12.4 ±1.6	10.5 ±1.5	10.6 ±1.4		
$\alpha(11)$								5.535	10.8
			32.4 ±0.8	30.9 ±1.5		31.7 ±0.7	32.0 ±0.7		
$\alpha(43)$				58.6 ±1.4	59.5 ±1.3			59.0 ±1.3	5.503	43.4
			26.5 ±0.8			26.2 ±0.5			
$\alpha(71)$									5.476 ±0.002	70.8
	42.6 ±1.1		42.4 ±0.8	42.1 ±0.8	43.2 ±1.7			42.7 ±1.1	
$\alpha(114)$		95.6 ±3.6	99 +2			96.5 ±2.5	97.1 ±2.5		5.433	114.1
$\alpha(170)$									5.379	169.6

* Series *a* and *b* refer to independent counts of the alpha-tracks on the same plate.

not uniquely determined. Matching of intensities of gamma-transitions would be a valuable guide but at this time the conversion electron spectrum and abundances have not been measured. The discussion of all of the gamma-rays and their possible placement in a decay scheme will be found elsewhere,[14] but a few features of the gamma-ray spectrum are worth mentioning here.

The most abundant gamma-ray has an energy of 59.78 kev and corresponds closely with the transition from the state reached by the most abundant alpha-group, $\alpha(71)$, to the 10.8-kev level. This gamma-ray had been reported initially by Seaborg, James, and Morgan[5] with an energy of 62 kev based on absorption measurements. The conversion electron spectrum of Am^{241} has been measured by O'Kelley[15] who found L_I, L_{II}, L_{III}, M, and N lines corresponding to a gamma-ray of 59.4 kev. Conversion lines of softer gamma-rays could not be resolved from each other and from the Auger electrons.

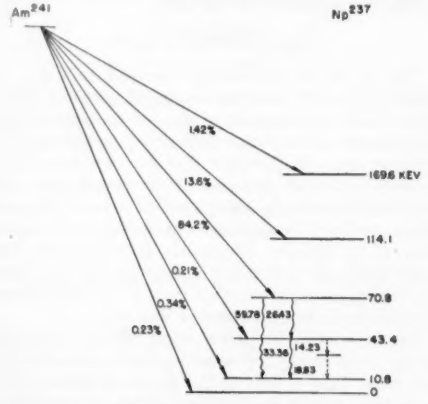

FIG. 6. Partial decay scheme for Am^{241}. Energy levels shown were obtained from alpha-spectra. Gamma-ray energies shown were obtained with a bent crystal spectrometer (see reference 14).

The gamma-ray of 59.78 kev is matched precisely by the sum of two other gamma-rays of 26.43 and 33.36 kev, and these in turn agree with differences between levels excited by $\alpha(71)$ and $\alpha(43)$, and by $\alpha(43)$ and $\alpha(11)$, respectively. It is interesting to note that no gamma-ray from a known energy level to the ground state has been observed. The de-excitation of the 10.8-kev level would not have been measured even though a significant fraction were to go by a radiative transition. Two other gamma-rays have been entered in Fig. 6 with broken lines to indicate the transitions. These same lines in conjunction with others could be given other equally good assignments and are entered as shown only to illustrate that in any case an energy level must be postulated for which there is no measured alpha-group. In view of the fact that several of the alpha-groups can barely be detected it would not be surprising if there were one or more which are in too low abundance.

Further fragmentary information on the decay scheme of Am^{241} has been obtained in this laboratory and will be discussed in the paper dealing with the gamma-ray spectrum.

Cm^{242} Energy Calibration

The highest energy group of Cm^{242} is also the most abundant and has been used in the energy determina-

[15] G. D. O'Kelley, Ph.D. thesis, University of California, 1951.

tion. This nuclide with 162.5 days half-life[16] was first prepared by alpha-particle bombardment of Pu^{239} in the cyclotron[17] but is more readily obtained in quantity by neutron irradiation of Am^{241}.[9] The best energy determination using the ionization chamber and pulse analyzer method is 6.08 Mev.[12]

In the present measurements with the alpha-particle spectrograph, Cm^{242} was compared with Po^{218} (5.998 Mev) and with the main group of Am^{241} (5.476 Mev). The method used was similar to that employed for americium (see explanation and Figs. 3 and 4). Based on the Po^{218} calibration, the energy is 6.110±0.003 Mev, and the Am^{241} comparison gave 6.112±0.010 Mev. With the limits of error as given, the close agreement is fortuitous and the value selected is that of the more accurate measurement, 6.110±0.003 Mev. Since this group is probably that of ground-state transition, the decay energy of Cm^{242} is accordingly 6.211 Mev.

Complex Structure of Cm^{242}

The spectrum of Cm^{242} in the energy range 6.0–6.1 Mev is shown in Fig. 7. Aside from the two groups

TABLE III. Energy differences and abundances of the alpha-groups of Cm^{242}.

Experiment number	Differences of alpha-particle energies	Separation between energy levels	Abundances: Low energy group (%)	Abundances: High energy group (%)
4–8	45.9±0.7	46.6±0.7	27±2[a]	73±2[a]
4–16	45.2±1.0	46.0±1.0	26.6	73.4
4–20	46.0±0.9	46.8±0.9	26	74
4–80	45.8±1.3	46.6±1.3	27	73
Averages	45.7	46.5	27	73

[a] Abundances determined by integrating alpha-track counts under peaks; others determined by comparing peak heights.

shown here none has been found between 5.5 and 6.5 Mev, but the limits of detection vary with position. These limits are best shown graphically as in Fig. 8 which illustrates the low limits of detection (<0.01 percent) on the high energy side of the main peak.

Several exposures have been made to determine the energy differences between the two alpha-groups and their relative abundances. The data are summarized in Table III. The average difference in energy is 45.7 kev which, taken with the energy of 6.110 Mev for the main group, makes the low energy group 6.064 Mev. The abundances of the two groups are 73 and 27 percent, and from the measured half-life of 162.5 days, the partial half-lives for the two groups are 222 and 602 days, respectively.

The gamma-ray corresponding to the 46.5-kev transition has been detected in low yield,[18] and low energy electrons have been found in abundance. O'Kelley[15] has measured a series of conversion lines corresponding to a gamma-ray of about 43 kev.

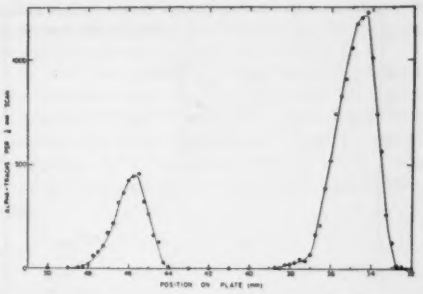

FIG. 7. Alpha-spectrum of Cm^{242}. Dispersion—4.01 kev/mm.

ALPHA-DECAY THEORY

The theory of the alpha-decay process relates the four factors: decay constant, nuclear charge, decay energy, and nuclear radius. A fifth parameter, the internal potential of the alpha-particle, is usually eliminated in the solution of the equations. Of these, only the radius cannot be determined with accuracy by measurement but can be calculated in so far as the theory is valid if the other three parameters are known. Any shortcoming of the theory in describing a particular alpha-decay process is, of course, reflected in the calculated radius. It has become a basic precept in nuclear theory that nuclear volumes are not expected to undergo wide variations from the simple addition of the number of nucleons contained. If the shapes of the nuclei, or more precisely the charge distributions, do not differ much in the limited region under considera-

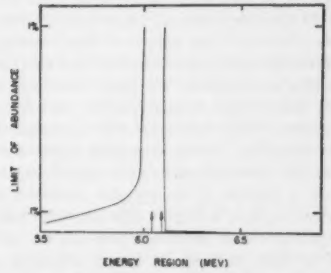

FIG. 8. Upper limit of abundance of alpha-groups of Cm^{242} as a function of energy (arrows indicate positions of known alpha-groups).

[16] Hanna, Harvey, and Moss, Phys. Rev. **78**, 617 (1950).

[17] Seaborg, James, and Ghiorso, *The Transuranium Elements: Research Papers* (McGraw-Hill Book Company, Inc., New York, 1949), p. 1554, National Nuclear Energy Series, Plutonium Project Record, Vol. 14B, Div. IV.

[18] In this laboratory, A. Ghiorso has observed this gamma-ray with a proportional counter coupled to a pulse-height analyzer and D. F. Martin has measured it with a scintillation counter spectrometer.

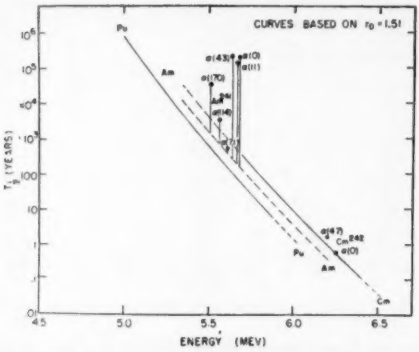

FIG. 9. Half-life energy relations of Cm^{242} and Am^{241} alpha-groups.

tion, then the radii too should vary in a regular manner. From these considerations it is seen that regularity of calculated nuclear radii may serve as a check on the alpha-decay theory. It has been found that the even-even alpha-emitters do indeed give remarkably uniform nuclear radii calculated from one-body theory.[3,4,19] The form which the expression for nuclear radius takes is simply $r = r_0 A^{\frac{1}{3}} \times 10^{-13}$ cm. The radius parameter r_0 varies somewhat with the particular theory employed. The theory followed here was developed by Preston,[20] elaborated by Kaplan,[19] and also includes a correction term for the alpha-energy pointed out by Ambrosino and Piatier.[21] This correction amounts to an addition of 40 kev in the case of curium and is the difference in binding energy of orbital electrons in curium and plutonium.[22]

There are a number of reasons for wanting a convenient method for checking alpha-decay data with the theory and since the calculations are tedious, a graphical representation has been evolved.[23,24,3] In this a family of curves are plotted which are derived from the theory applied to the even-even alpha-emitters. First, values of r_0 are obtained from values of decay energy, half-life, and charge for those even-even nuclides for which reliable data are available. The best value of r_0 is taken, and this defines the normal nuclear radius for each mass number. Using this value one calculates the half-life corresponding to the measured alpha-energy for each nuclide. For each element a smooth curve is obtained on a half-life vs energy plot as shown for plutonium and curium in Fig. 9. The curve for americium is interpolated. The measured half-life for an alpha-emitter is then entered at the appropriate energy. From the manner in which the curves were constructed it is seen that they should be the best curves drawn through the even-even nuclides.

The utility of such curves lies in the ease with which any new alpha-emitter can be tested for agreement with the theory simply by observing the departure from its curve. If a point lies above its curve, the half-life is longer than expected and the decay process is said to be hindered. Now that it is found that virtually all alpha-emitters have complex structure, these curves supplant a large number of calculations required to determine the degree of hindrance for the individual alpha-groups. Such comparisons for Am^{241} and Cm^{242} are shown in Fig. 9 and will be discussed further presently.

Another great utility of these curves is in predicting half-lives of new species being sought. It is possible to predict an alpha-energy with considerable accuracy,[3] and from this value it is simple to read from the curve the minimum alpha-decay half-life. In the case of even-even nuclides experience has shown that these half-lives are quite accurate, and for other nuclear types the actual half-lives are usually several fold greater than those read from the curves.

Returning to the curves of Fig. 9, a brief statement should be given for the choice of $r_0 = 1.51$ which was used in their construction. This has turned out to be the best value for the even-even nuclides of plutonium and curium for which data are available. The inclusion of a wider range of elements and the refinement of measurements may well necessitate revision of this value. Furthermore, although a great simplification results from the assumption of a single value of r_0 to fit all alpha-emitters in this region, this obviously cannot be rigorously correct, and as data are refined it may become advantageous to let r_0 vary slowly. If r_0 varied erratically from nuclide to nuclide, the construction of a simple family of curves such as dealt with here would not be possible, and indeed such behavior is encountered in the region of 126 neutrons.[3,4]

It is seen that the ground-state transition of Cm^{242}, $\alpha(0)$, lies on the curium curve which fact indicates its accord with other curium and plutonium nuclides. The lower energy group of Cm^{242}, $\alpha(47)$, lies above the curve in degree corresponding to a half-life ~ 1.5 times longer than expected from the theory. What selection rules are responsible for this slightly hindered decay are not yet formulated.

The disposition of the Am^{241} alpha-groups is decidedly different. Here, the three highest energy groups, designated $\alpha(0)$, $\alpha(11)$, and $\alpha(43)$, are highly hindered and have half-lives roughly 1000 times longer than the simple theory would demand. On the other hand, $\alpha(71)$ follows closely the pattern of an even-even nuclide and as a result is the most abundant alpha-group of Am^{241} even though it is only the fourth highest in energy. The two alpha-groups of still lower energy are again

[19] I. Kaplan, Phys. Rev. **81**, 962 (1951).
[20] M. A. Preston, Phys. Rev. **71**, 865 (1947).
[21] G. Ambrosino and H. Piatier, Compt. rend. **232**, 400 (1951).
[22] A further small correction for the screening effect of orbital electrons on the potential barrier has not been included and probably should be considered in further refinements.
[23] A Berthelot, J. phys. et radium VIII **3**, 52 (1942).
[24] S. Biswas, Indian J. Phys. **23**, 51 (1949).

hindered although in lesser degree than the three highest energy groups.

There is at present no quantitative explanation to account for the degrees of hindrance of the various alpha-groups. It has been pointed out,[9] and Preston[10,25] has demonstrated, that no explanation to include such high degree of hindrance as for several of the Am^{241} groups is likely to come from spin changes in the alpha-transitions. An hypothesis which we shall consider further is that the delay is involved in assembling the components of the alpha-particle and that the quantum states of the affected nucleons are involved.

This work was performed under the auspices of the United States Atomic Energy Commision. We wish to acknowledge the assistance of Mr. James Vanderveen in counting the alpha-tracks and to thank Drs. B. B. Cunningham, S. G. Thompson, and W. W. T. Crane for the preparations of Am^{241} and Cm^{242} used in these studies.

[25] M. A. Preston, Phys. Rev. **83**, 475 (1951).

PHYSICAL REVIEW VOLUME 87, NUMBER 2 JULY 15, 1952

Positron-Electron Scattering in Helium*

G. Robert Hoke†
University of North Carolina, Chapel Hill, North Carolina
(Received March 25, 1952)

Positron-electron scattering in a cloud chamber filled with helium at a pressure of 105 cm of Hg has been studied. The positron source was Na^{22}, and the primary positron energies ranged from about 20 to 600 kev. On 2420 meters of track length 1129 scattering events have been found with a fractional energy exchange between positron and electron greater than 10 percent. The frequency of scattering is in good agreement with the theory of Bhabha, but not enough events are available to discrimate between the theory with the effect of exchange taken into account and the theory without exchange (i.e., "ordinary"scattering).

I. INTRODUCTION

THIS research deals with the single scattering of positrons by electrons. The first work on this problem[1] indicated a discrepancy between theory and experiment. As this sort of discrepancy was observed in the early work on electron-electron scattering and was resolved by later more precise work, it is hoped that such may prove to be the case for positron-electron scattering.

The early results for electron-electron scattering gave cross sections greater than expected according to the relativistic theory of Möller[2] which is now accepted. The more recent work of Groetzinger *et al.*,[3] and of Page[4] is in good agreement with the theory.

Electron-electron scattering is different from positron-electron scattering in several essential ways. In the case of an electron-electron scattering process it is impossible to determine, after the collision, which was the primary electron. One cannot, therefore, separate the cases of strong energy exchange from those of weak energy exchange. It is the convention to take the electron with the lower energy as the secondary. In positron-electron scattering, on the other hand, it is easy to determine from the curvature which track in the cloud chamber is due to the positron. A second difference is that the contribution of exchange is different since the positron and electron can be created and annihilated in pairs.

In the first direct work on positron-electron scattering Ho Zah-Wei used a cloud chamber to study the positrons from Mn^{52} and F^{18}. The chamber was filled with air, a magnetic field was used, and stereoscopic photographs were made. On 395 meters of path length, 328 events were observed with an energy exchange $\epsilon = E^-/E_0^+ \geq 10$ percent, where E_0^+ and E^- are the kinetic energies of the initial positron and the secondary electron, respectively.

The result was that the frequency of single scatterings of positrons by electrons, in those cases in which the energy exchange was large, was greater than the expected frequency on the basis of the theory of Bhabha.[5] For very large energy exchanges (≥ 70 percent) the experimental frequencies were two or three times the theoretical values.

The most recent work, that of Von O. Ritter *et al.*,[6] was carried out completely independently of the present work but is similar in many ways. In their work the cloud chamber was filled with methane; the magnetic field was 300 gauss; the positron source, Cu^{64}, was outside the chamber; and on 5000 stereoscopic

* Based on a dissertation submitted in partial fulfillment of the requirements for the Ph.D. degree in the Department of Physics, University of North Carolina.

† Now with E. I. du Pont de Nemours & Company, at the Argonne National Laboratory, Chicago, Illinois.

[1] Ho Zah-Wei, Phys. Rev. **70**, 224 (1946); Compt. rend. **226**, 1083 (1948).

[2] C. Möller, Ann. Physik **14**, 531 (1932); Z. Physik **70**, 786 (1931).

[3] Groetzinger, Leder, Ribe, and Berger, Phys. Rev. **79**, 454 (1950).

[4] L. A. Page, Phys. Rev. **81**, 1062 (1951).

[5] H. J. Bhabha, Proc. Roy. Soc. (London) **A154**, 195 (1936).

[6] Von O. Ritter *et al.*, Z. Naturforsch. **6a**, 243 (1951).

photographs with 2900 meters of useful track length with primary energies between 100 and 400 kev about 821 events were found with $\epsilon \gtrsim 10$ percent. The conclusion was reached that the agreement between theory and experiment was within the experimental uncertainty.

II. THEORY

The result obtained from the calculation relating to the collision of an electron with a positron based on the Dirac theory of the positron, where the positron is considered as an unoccupied state of negative energy would be different from that which would be obtained if the calculation were done considering the positron as an independent, positively charged particle in a state of positive energy whose behavior is described by the Dirac equation. The difference would be due to the effect of exchange between the electron we observe initially and the virtual electrons in states of negative energy.

The "ordinary" scattering process is that one in which one electron in a state of positive energy goes over into a new state of positive energy, while a virtual electron in a state of negative energy jumps into the unoccupied state of negative energy which is the initial positron, leaving its state unoccupied to be observed as the new state of the positron. The effect of exchange arises because the process may take place in an alternative way; namely, the electron in a positive energy state may jump into the unoccupied state of negative energy which is the initial positron (this is annihilation), while a virtual electron in a negative energy state jumps into a state of positive energy which is then the final electron, leaving a state of negative energy unoccupied which is the final positron (this is creation of a pair).

Bhabha considered the collision of an electron with a positron including the effect of exchange and, basing his work on that of Möller, found for the effective cross section for the scattering of the positron with fractional energy exchange in the range ϵ to $\epsilon+d\epsilon$ in the system in which the electron is initially at rest (laboratory system, L)

$$dQ=\frac{2\pi e^4}{m^2c^4}\frac{\gamma}{(\gamma-1)^2\epsilon^2}F(\gamma,\epsilon)d\epsilon,$$

where

$$\begin{aligned}F(\gamma,\epsilon)=\frac{1}{\gamma(\gamma+1)}\Big[&\{1+2(\gamma-1)(1-\epsilon)\\&+(\gamma-1)^2(1-\epsilon+\tfrac{1}{2}\epsilon^2)\}\\&+\frac{(\gamma-1)^2\epsilon^2}{(\gamma+1)^2}\{3+2(\gamma-1)+(\gamma-1)^2(\tfrac{1}{2}-\epsilon+\epsilon^2)\}\\&-\frac{(\gamma-1)\epsilon}{\gamma+1}\{3+4(\gamma-1)(1-\epsilon)\\&+(\gamma-1)^2(1-\epsilon)^2\}\Big].\end{aligned}$$

Here e is the charge on the electron, m is the mass of the electron, c is the velocity of light, γ is E/mc^2, E is the total energy of the positron, ϵ is the ratio of the kinetic energy of the final electron to the kinetic energy of the initial positron in system L. The first term in square brackets is the ordinary scattering term, the second term is the one due to the annihilation of the initial pair and the simultaneous creation of a new pair, and the third term then represents the interference between the direct scattering and the latter process. By using only the first term of $F(\gamma,\epsilon)$ in the expression for dQ we obtain what may be called the differential cross section for "ordinary" scattering, dQ_o, i.e., the scattering in the absence of exchange effects.

III. APPARATUS

A cloud chamber of conventional design was used. It had an inside diameter of 8.25 in. and a depth of 4.38 in. The chamber was filled with helium at an average pressure of 104.9 cm of Hg in the expanded position. The optimum mixture of 70 percent *n*-propyl alcohol and 30 percent water was used to provide the vapor. An expansion ratio of 1.09 ± 0.005 resulted.

The chamber operated automatically on a cycle of one minute and was controlled by a simple circuit which involved only two electronic tubes. Most of the operations were controlled by relays and microswitches, operated by cams on the timing motor. A sweeping field of 600 v was provided. This sweeping field was removed at the instant of expansion and replaced when the expansion valve closed. The chamber was operated in a magnetic field produced by a pair of large Helmholtz coils giving a field of 305 ± 4 gauss.

The light source for photography consisted of two General Electric FT-127 xenon-filled arcs. They were flashed by discharging 50 mfd, charged to 2000 v, through each of them. The now conventional cylindrical lens system was used to produce a parallel beam of light of width about 4.5 cm. Stereoscopic photographs were taken on Eastman Linagraph Ortho 35-mm film. This film is particularly sensitive to the blue light of the discharge tubes and is a good compromise of speed and graininess. Several photographs of typical events may be seen in Fig. 1.

The positron source consisted of approximately 2 milli-microcuries of Na^{22},[7] which has a half-life of 2.6 years and a maximum positron energy of 0.58 Mev. The source was received as NaCl dissolved in water. The source as used was prepared by evaporating a diluted portion of the original solution on a thin collodion film held by a thin wire ring. Other collodion films were then placed above and below the first film so that none of the active material would escape into the chamber. The source was mounted at the center of the chamber and an average of 6.4 positron tracks per expansion was obtained.

[7] The Na-22 used was obtained from the AEC, Isotopes Division, Oak Ridge, Tennessee.

IV. ANALYSIS OF PICTURES

After the films were developed, they were replaced in the camera and reprojected through the same optical system with which the pictures were taken. Normally all measurements on the tracks were made on the image of the direct view of the chamber, reprojected onto a ground-glass screen. To measure the radii of curvature of the tracks a set of circles of known radius was superimposed until one was found that corresponded as closely as possible with the portion of track under consideration.

Tracks out of the plane perpendicular to the magnetic field were reprojected to this plane. The measured radii were thus caused to be about 2.2 percent large for an angle $\alpha = 10°$ between the track and the plane perpendicular to the magnetic field. It was possible to determine the angle α by a "fusion" [8] method. For long tracks it was sufficient, however, to look at the picture stereoscopically to see whether the angle α was large. Both fusion and stereoscopic viewing helped to settle questions relating to the shape and form of the tracks and to determine whether an apparent secondary started on a track.

Track lengths were measured in two ways. The higher energy tracks with a rather uniform curvature were measured by bending a flexible centimeter rule into the shape of the track. The shorter, more tortuous tracks were measured by bending a thin wire into the shape of the track and measuring its length after it was straightened out.

On every twentieth picture the curvature and length of all the tracks were recorded. From these measurements the energy spectrum of the track length available was determined. This knowledge was essential for the determination of the theoretical number of scattering events to be expected.

For every positron-electron scattering event all the available information was recorded. This included the curvature of the primary positron and the curvature and/or range of the secondary electron and positron.

In all these measurements certain criteria of track selection were imposed. These criteria were as objective as possible so that the number of decisions to be made was reduced to a minimum. The criteria were similar to those of Shearin and Pardue.[9]

A. The Range-Energy Curve for Electrons in Helium

The energies of the low energy positrons and the secondary electrons whose tracks end in the chamber were determined by the measurement of their ranges. As no published curve for range *vs* energy for electrons in helium for the energy region considered could be found, an attempt was made to determine such a curve.

[8] For a discussion of this method and other techniques see C. C. Jones and A. Ruark, Proc. Am. Phil. Soc. **82**, 253 (1940).

[9] P. E. Shearin and T. E. Pardue, Proc. Am. Phil. Soc. **85**, 243 (1942).

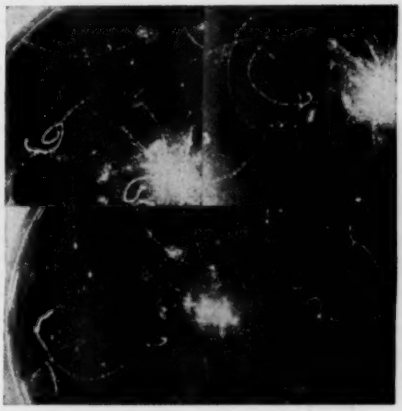

FIG. 1. Photographs of typical events. Upper left: $E_0^+ = 61$ kev, $\epsilon = 0.6$. Upper right: $E_0^+ = 82$ kev, $\epsilon = 0.6$. Lower left: $E_0^+ = 42$ kev, $\epsilon = 0.7$. Lower right: $E_0^+ = 61$ kev, $\epsilon = 0.3$.

A survey of the literature pertaining to the range-energy relation for electrons in air was made and a mean curve was drawn through what seemed the most reliable data. A similar survey of the literature was made to determine the range-energy relation for electrons in helium, but in this case less experimental data are available. The three sources of experimental data were the papers of Osgood,[10] Lehmann,[11] and O'Neill and Scott.[12] For energies between 1 and 100 kev no experimental results could be found. The values were calculated for this region by two methods. The stopping power of helium relative to air (using the above results for air), as it applies to electrons,[13,14] was used. In addition the expression of Tsien[13] for the range, involving the exponential integral, was used. Again, for helium, the best fit curve was drawn through the experimental and calculated points. In carrying through these calculations the average ionization potentials used were those given by Mano.[15]

To find the range-energy curve for the mixture in the chamber one must take into account the vapor and the residual air in the chamber. The average ionization potential and the average number of electrons per atom are then calculated. With these figures one may transpose from the range in air or helium to the range in the mixture in the chamber. It was found that in the scattering events the law of conservation of energy was well satisfied if the range-energy curve, found in the manner described above, was used.

[10] T. H. Osgood, Phys. Rev. **34**, 1234 (1929).

[11] J. F. Lehmann, Proc. Roy. Soc. (London) **A115**, 624 (1927).

[12] G. F. O'Neill and W. T. Scott, Phys. Rev. **80**, 473 (1950).

[13] San-Tsiang Tsien, Ann. phys. **19**, 327 (1944).

[14] E. J. Williams, Proc. Roy. Soc. (London) **A135**, 108 (1932).

[15] G. Mano, Ann. phys. **I**, 407 (1934).

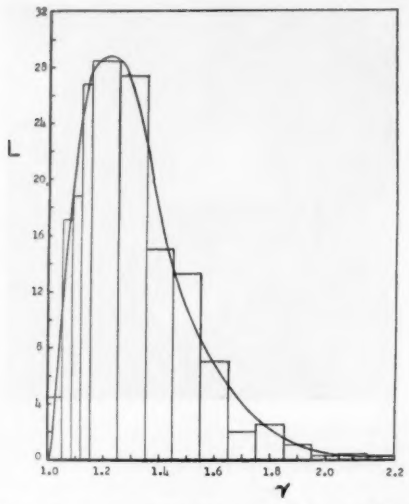

FIG. 2. Energy spectrum of the positrons used. L is track length in meters; γ is the positron energy in units of the electron rest energy. Multiply by 20.22 to find the total track length.

V. RESULTS

Several sources of error in the measurements should be mentioned. The error in the measurement of $H\rho$, including the error in H, varies from 3.5 to 5.8 percent. In addition, the error in ρ due to multiple scattering varies, according to Bethe's formulas,[16] from 4.4 to 6.8 percent. The resultant error in the energies determined by curvature measurements varies from 8.5 to 18 percent for energies between 600 and 50 kev.

The estimated error in the ranges, including error in the range-energy curve, error due to straggling, and error in the actual measurement of the ranges, varies from 12 to 14 percent. The corresponding error in the energies determined by range measurements is 6 to 7 percent.

The important thing about all these errors is not how they affect the energy value assigned to a given track, but rather how they affect the assignment of a value for the fractional energy exchange to the event in question.

A. Theoretical Number of Scattering Events

The number of events to be expected theoretically may be calculated by the theory of Bhabha discussed earlier. For the scattering of positrons by electrons the differential scattering cross section is given by dQ, which is defined as the number of collisions per second in the range ϵ to $\epsilon+d\epsilon$ per scattering center per unit current of incident particles with a given γ. But the current of incident particles with a given γ is $N_i v_i$, where N_i is the number of incident particles with a velocity v_i. Then, if n_s is the number of scattering centers (electrons) per unit volume, the probability of collision in range $d\epsilon$ for given γ is

$$N(\gamma, \epsilon)/N_i = n_s v_i \Delta l dQ.$$

But $v_i \Delta l = \Delta L$, where L is track length. Then we may write

$$N(\gamma, \epsilon) = n_s N_i(\gamma) \Delta L(\gamma) dQ = n_s(\Sigma \text{ lengths of tracks})_\gamma dQ.$$

Finally

$$N(\epsilon) = \sum_{\gamma=1}^{\gamma_{max}} N(\gamma, \epsilon).$$

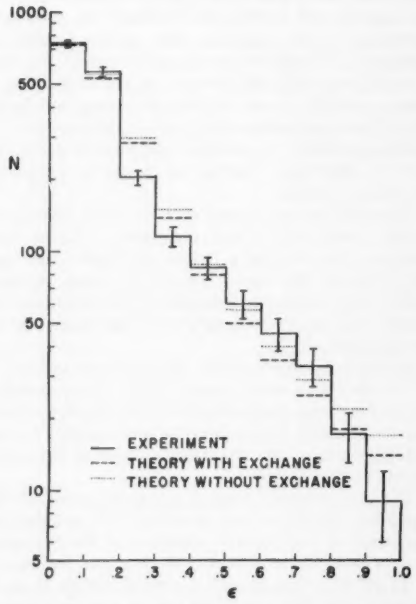

FIG. 3. The number, N, of positron-electron scattering events as a function of the fraction, ϵ, of the positron's energy that is transferred to the electron. These results are for the present experiment.

The above calculation has been carried through with γ of 1.1, 1.2, $\cdots$, 2.2, and ϵ of 0.05, 0.15, $\cdots$, 0.95. The total track length for each γ was determined by the energy spectrum measurements. These measurements were made on 219 out of the 4428 useful pictures. The results were plotted as a hodograph in Fig. 2. A smooth curve, representing the energy spectrum, was drawn through the blocks in the usual way. It should be noted that the maximum of this curve, falling at $\gamma=1.2$ which corresponds to a kinetic energy of 102 kev, is at lower energy than the maximum of the given energy spectrum for Na^{22} which is at 200 kev. This shift

[16] H. A. Bethe, Phys. Rev. **70**, 821 (1946).

toward lower energies is due to the fact that the long-range tracks pass out of the chamber or out of the illuminated region. By multiplying the values corresponding to each γ, read from the smooth curve, by the ratio of the total number of pictures to the number of spectrum pictures, namely 20.22, one finds the total track length for each γ.

B. Experimental Number of Scattering Events

After all the measurements were completed, the range and curvature measurements were converted to energy values and each scattering event classified as to primary energy, γ, and fractional energy exchange, ϵ. When more than one measurement of the energies were available, the usual practice was to average them. The results of these measurements are given in Table I along with the number of events to be expected theoretically and the sum of all events to date. These values are plotted in Figs. 3 and 4.

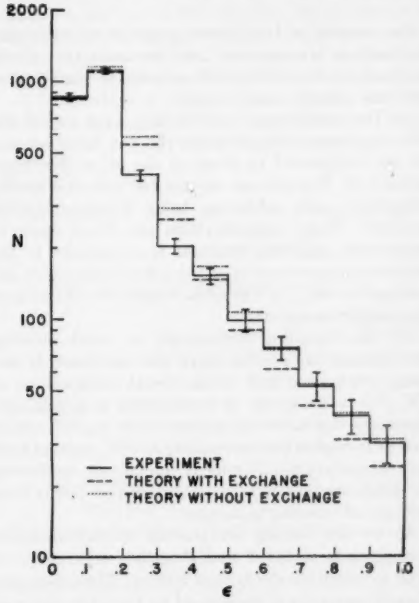

FIG. 4. The summation of the results of all experiments to date. N is the number of positron-electron scattering events, and ϵ is the fraction of the positron's energy that is transferred to the electron.

TABLE I. Comparison of the experimental number, $N_e(\epsilon)$, of positron-electron scattering events, with fractional energy exchange ϵ, with the number expected by the theory of Bhabha with exchange taken into account, $N_w(\epsilon)$, and without exchange, $N_o(\epsilon)$. 1. Present experiment. 2. Sum of results of Ho Zah-Wei, Ritter *et al.*, and present experiment.

$\epsilon =$	0 to 0.1	0.1 to 0.2	0.2 to 0.3	0.3 to 0.4	0.4 to 0.5	0.5 to 0.6	0.6 to 0.7	0.7 to 0.8	0.8 to 0.9	0.9 to 1
1. $N_e(\epsilon)$	736	562	203	115	85	60	45	33	17	9
$N_w(\epsilon)$	725	533	284	138	80	50	35	25	18	14
$N_o(\epsilon)$	738	553	299	149	88	57	40	29	22	17
2. $N_e(\epsilon)$	858	1106	402	202	152	98	75	52	39	30
$N_w(\epsilon)$	845	1097	541	261	147	89	61	43	31	24
$N_o(\epsilon)$	862	1141	581	291	167	106	74	53	40	31

VI. CONCLUSION

In Fig. 3 it is seen that the agreement between theory and the results of this experiment is not close enough to determine whether the exchange effect should be included. In Fig. 4, however, it appears that the agreement between theory and experiment is best when the exchange effect is excluded. The lack of agreement between $\epsilon=0.2$ and 0.4 is unexplained.

One factor that might be the cause of some discrepancies is the following. The number of events to be expected is very sensitive to the track length of low energy. This is the steep portion of the energy spectrum curve, Fig. 2. Thus, a small error in the low energy track length measured could shift the theoretical values considerably.

In conclusion, it may be stated that the number of positron-electron scattering events observed for positron energies up to 600 kev is in good agreement with the theory of Bhabha. The discrepancies that do exist between theory and the 1129 events of this experiment are probably statistical. Furthermore, the number of events observed is not sufficient to discriminate between the theory including exchange and the theory without exchange. Experiments involving a larger number of events and with positrons of higher energy, $\gamma=4$, or more, are necessary to determine whether the exchange theory is completely correct.

It is a pleasure to acknowledge the guidance and encouragement of Dr. Paul E. Shearin and Dr. Nathan Rosen. This problem was first brought to my attention by Dr. Herman M. Schwartz.

Antiferromagnetic Arrangements in Ferrites

Y. YAFET AND C. KITTEL
Department of Physics, University of California, Berkeley, California
(Received April 9, 1952)

The molecular field treatment of the magnetic properties of ferrites given by Néel is extended to take into account the antiferromagnetic exchange interactions within the two magnetic sublattices. On further subdividing the two lattices, we show that the ground state may, (1) have an antiparallel arrangement of the spins on the two sites; or (2) consist of a triangular arrangement of the spins on the sublattices; or (3) have antiferromagnetism in each of the two sites separately. We also show that transitions between various configurations may occur in the same substance at different temperatures, without the assumption of temperature-dependent interactions. Neutron diffraction experiments and specific heat measurements are suggested for the detection of the predicted arrangements.

I. INTRODUCTION

WE are concerned in this paper with the theory of the magnetic properties of ferrites. We demonstrate in particular the possibility that both ferromagnetic and antiferromagnetic transitions, as well as transitions to triangular arrangements of the spins, may occur at different temperatures in the same substance.

Néel[1] has given a simple model which is known to account satisfactorily for many of the magnetic properties of the ferrites. We follow, and extend as required, his model and method of calculation, based on a Weiss molecular field treatment of the exchange interactions between the several spin lattices. On the Néel theory the magnetic ions are assumed to be distributed among the tetrahedral sites A and the octahedral sites B of the spinel structure.[2] Negative (antiferromagnetic) exchange interactions exist between A and A, A and B, and B and B.

When the $A-B$ antiferromagnetic interaction is the dominant one, A and B will be magnetized in opposite directions below a transition temperature, giving rise, when the magnetizations of the A and B sites differ in magnitude, to a special case of ferromagnetism termed "ferrimagnetism." When the $A-A$ (or $B-B$) interaction is dominant, Néel found that the above transition will not take place, and he concluded that the substance remains paramagnetic down to the lowest temperatures. This conclusion is not correct, as in the presence of strong interactions some kind of ordering may be expected to occur at low temperatures. An example of this case is provided by the mixed ferrite Fe_2O_3, xNiO, $(1-x)$ZnO. Pure Ni ferrite has the inverse spinel structure, and the $A-B$ interaction is dominant. Pure Zn ferrite has the normal spinel structure; Zn^{++} being nonmagnetic, the A sites carry no magnetic moment. The $B-B$ interaction is expected then to give rise to antiferromagnetic ordering in the B lattice. As x is varied from 0 to 1, intermediate arrangements will arise.

The purpose of the present paper is to study the intermediate arrangements and the associated Curie temperatures, extending Néel's scheme. We find several quite new effects, namely, that:

(a) The ground state at 0°K may have one of the following three configurations: (1) The spins on one site are antiparallel to those on the other (ferrimagnetism). (2) The spins on one site fall into two similar sublattices, each sublattice being ferromagnetically saturated. These magnetizations are at an angle to each other, and their resultant is antiparallel to the saturation magnetization of the spins on the other site (triangular case). (3) The spins on each of the two sites have antiferromagnetism.

(b) The transition temperature at which ordering first appears on cooling down the substance is not always such as to lead to the lowest configuration at 0°K (this is in contrast to the situation in simple antiferromagnetics where the highest Curie point is always such as to lead to the lowest state at 0°K), so that even with temperature-independent interaction coefficients the substance may have several transition points from one type of ordering to another.

As we are looking for possible antiferromagnetic arrangements of the A and B lattices separately, we have to subdivide the lattices further. The subdivision actually occurring is determined by the interactions responsible for the ordering. We assume that in both A and B lattices the order is determined by the nearest-neighbor interactions. The A lattice is then subdivided into two (A', A'') face-centered cubic lattices and the B lattice into four (B_1, B_2, B_3, B_4) face-centered cubic lattices, all having the same cube edge as the spinel cell. A site from A' has four sites from A'' as nearest neighbors in the A lattice. A site from B_1 has six sites, two from each of the other three B_i's, as nearest neighbors in the B lattice. The interactions between any two B_i's are equal. In order to simplify the formalism we shall assume that only one type of magnetic ion is present. Actually, in a molecular field approximation, the more complicated case of several types of magnetic ions may be formally equivalent to our treatment.

[1] L. Néel, Ann. phys. 3, 137 (1948).
[2] For details of the crystal structure of ferrites, see E. J. W. Verwey and E. L. Heilmann, J. Chem. Phys. 15, 174 (1947).

II. GROUND STATE AT 0°K

At absolute zero all sublattices are saturated. We show in the appendix that if we neglect anisotropy, the four sublattices B_i may be lumped together to form two equivalent sublattices, B' and B''. The molecular fields acting on lattices A', A'', B', B'' may be written:

$$\mathbf{H}_{a'}=n(\alpha_1\mathbf{M}_{a'}+\alpha_2\mathbf{M}_{a''}-\mathbf{M}_{b'}-\mathbf{M}_{b''}),$$
$$\mathbf{H}_{a''}=n(\alpha_2\mathbf{M}_{a'}+\alpha_1\mathbf{M}_{a''}-\mathbf{M}_{b'}-\mathbf{M}_{b''}),$$
$$\mathbf{H}_{b'}=n(-\mathbf{M}_{a'}-\mathbf{M}_{a''}+\gamma_1\mathbf{M}_{b'}+\gamma_2\mathbf{M}_{b''}),$$
$$\mathbf{H}_{b''}=n(-\mathbf{M}_{a'}-\mathbf{M}_{a''}+\gamma_2\mathbf{M}_{b'}+\gamma_1\mathbf{M}_{b''}),$$

where α_1, α_2, γ_1, γ_2 are negative (antiferromagnetic) and $\alpha_1+\alpha_2=2\alpha$; $\gamma_1+\gamma_2=2\beta$. The interaction constants n, $n\alpha$ and $n\beta$ are defined for a mole of magnetic ions distributed on lattices A and B in the ratio $N_a/N_b=\lambda/\mu=y$, where y may vary from 0 to 1. Any magnetization configuration may be characterized by two angles ϕ and ψ as shown in Fig. 1. The energy is:

$$E=-\tfrac{1}{2}\sum\mathbf{H}_i\cdot\mathbf{M}_i$$
$$=-n[\alpha_1M_{a'}{}^2+\alpha_2\mathbf{M}_{a'}\cdot\mathbf{M}_{a''}+\gamma_1\mathbf{M}_{b'}{}^2+\gamma_2\mathbf{M}_{b'}\cdot\mathbf{M}_{b''}$$
$$-(\mathbf{M}_{a'}+\mathbf{M}_{a''})\cdot(\mathbf{M}_{b'}+\mathbf{M}_{b''})]$$
$$=-nM_{b'}{}^2[(\alpha_1-\alpha_2\cos2\varphi)y^2+(\gamma_1-\gamma_2\cos2\psi)$$
$$+4y\sin\varphi\sin\psi].$$

The values of ϕ and ψ that minimize this expression are:

1. If $\alpha_2\gamma_2>1$, $\phi=\psi=0$; the doubly antiferromagnetic configuration is the lowest for all y.

2. If $\alpha_2\gamma_2<1$, the lowest state will depend on y; the values of γ_2 and $1/\alpha_2$ determine three regions:

(a) For $0<y<|\gamma_2|$, the solution is $\phi=\frac{1}{2}\pi$, $\sin\psi=y/|\gamma_2|$.

(b) For $|\gamma_2|<y<1/|\alpha_2|$, the solution is $\phi=\psi=\frac{1}{2}\pi$.

(c) For $1/|\alpha_2|<y$, the solution is $\psi=\frac{1}{2}\pi$, $\sin\phi=1/(|\alpha_2|y)$.

In the triangular configuration (a)[3] the criterion $y<|\gamma_2|$ means that the molecular field of B'' acting on B' is larger than the field of A' (or A'') acting on B'. The equilibrium angle ψ is then such that lattice B' sees a total field (apart from its own) equal to the molecular field due to B''.

The triangular cases are in fact generalizations of Néel's solutions[4] III and IV. In case (a), the magnetization of lattice B is here $2M_{b'}\sin\psi=2Ma'/|\gamma_2|$; Néel gives $2Ma'/|\beta|$. The difference is due to the implicit assumption $\gamma_2=\beta$ made by Néel as a necessary consequence of his neglect of the antiferromagnetic arrangements: the condition for the paramagnetic state of lattice B to have as low an energy as an antiferromagnetic state is, from the expression for the energy, that no subdivision be possible such that $\gamma_2\neq\gamma_1$; then $\gamma_1=\gamma_2=\beta$ follows. Actually γ_2 has a value between β and $4\beta/3$, resulting in a smaller value for the magnetization of lattice B. Néel's interpretation for his solutions III and IV seems to be lack of saturation of lattices B and A respectively, rather than a triangular arrangement. This belief is based on his considerations on the variation of the total moment near 0°K: his graphical determination[5] of the effective field on lattice A leads to $\mathbf{H}_a\to0$ as $T\to0$°K, a clearly erroneous result, which, however, is the only one consistent with paramagnetic lack of saturation. The variation with temperature of the total moment that he deduces[6] for cases III and IV has a non-zero slope at the origin, violating the third law of thermodynamics. This is a consequence of a non-zero entropy at 0°K, also due to lack of saturation.

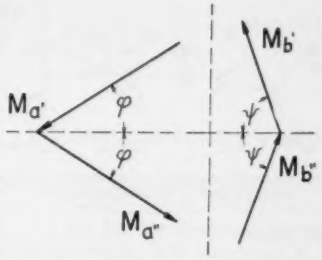

FIG. 1. Equilibrium configuration of the four sublattices.

We may notice here that it is not necessary to have two crystallographically different sites in order to have a triangular arrangement. The symmetry of a simple lattice may give rise to a triangular arrangement, as occurs in the plane triangular array which may be decomposed into three interpenetrating triangular lattices. With only nearest-neighbor antiferromagnetic interactions, the ground state has the three saturation magnetizations at 120° to each other, and is nondegenerate. Thus, the Ising model fails for this lattice.[7] The molecular field treatment gives a ratio $\theta/T_c=2$ for nearest neighbor interactions. Here θ is the constant appearing in the Curie-Weiss law $\chi=C/(T+\theta)$; T_c is the transition temperature.

III. CURIE POINTS

Let C denote the molal susceptibility. In the disordered state the magnetic moments are given by:

$$M_{a'}=\lambda CH_{a'}/2T;\quad M_{b'}=\mu CH_{b'}/2T.$$

The vanishing of the characteristic determinant of the following four homogeneous equations yields the pos-

[3] A similar consideration applies to configuration (c).
[4] L. Néel, reference 1, p. 149.
[5] L. Néel, reference 1, p. 153.
[6] L. Néel, reference 1, p. 154.
[7] G. H. Wannier, Phys. Rev. 79, 357 (1950).

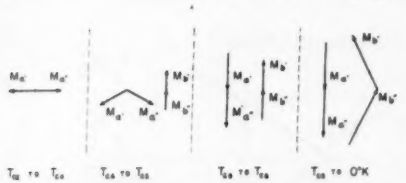

FIG. 2. A possible succession of transitions to various configurations in the same substance.

sible Curie points:

$$\alpha_1 M_{a'}+\alpha_2 M_{a''}-M_{b'}-M_{b''}=(2T/\lambda Cn)M_{a'}$$

$$\alpha_2 M_{a'}+\alpha_1 M_{a''}-M_{b'}-M_{b''}=(2T/\lambda Cn)M_{a''}$$

$$-M_{a'}-M_{a''}+\gamma_1 M_{b'}+\gamma_2 M_{b''}=(2T/\mu Cn)M_{b'}$$

$$-M_{a'}-M_{a''}+\gamma_2 M_{b'}+\gamma_1 M_{b''}=(2T/\mu Cn)M_{b''}.$$

The four solutions for T_c are:

$$T_{c1}=\tfrac{1}{2}Cn\mu(\gamma_1-\gamma_2),$$

$$T_{c2}=\tfrac{1}{2}Cn\lambda(\alpha_1-\alpha_2),$$

$$T_{c3}=\tfrac{1}{2}Cn\{\alpha\lambda+\beta\mu\pm[(\alpha\lambda-\beta\mu)^2+4\lambda\mu]^{\frac{1}{2}}\}.$$

The $-$ sign in T_{c3} gives a negative value and must be rejected. Again, we see that if $\gamma_1=\gamma_2$ and $\alpha_1=\alpha_2$, only T_{c3} is left; this is Néel's result.[8] T_{c1} and T_{c2} are the antiferromagnetic Curie points of lattices B and A, respectively. The type of ordering below these upper Curie points is ferrimagnetic for T_{c3} and antiferromagnetic in the corresponding lattice for T_{c1} or T_{c2}.

We need to determine the highest T_c among the four solutions; depending on λ/μ and the molecular field coefficients, several cases will occur.

The transition temperatures T_{c1} and T_{c2} are always positive. The criterion for a positive T_{c3}, given by Néel, is $\alpha\beta<1$. Let us introduce two numbers K and L, both between 0 and 1, such that $\alpha_2-\alpha_1=2\alpha K$ and $\gamma_2-\gamma_1=\frac{2}{3}\beta L$. From the expressions for the T_c's, the condition for T_{c3} to be the largest root may be found as follows:

(a) If $T_{c3}>T_{c2}$, then $(\lambda/\mu)<\{[1-(K+1)\alpha\beta]/[K(K+1)\alpha^2]\}$ and $[1-(K+1)\alpha\beta]>0$;

(b) If $T_{c3}>T_{c1}$, then $(\lambda/\mu)>\{L(L+3)\beta^2/3[3-(L+3)\alpha\beta]\}$ and $[3-(L+3)\alpha\beta]>0$.

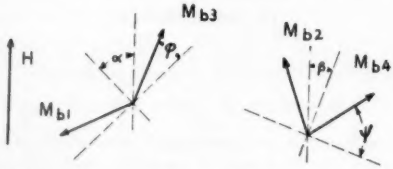

FIG. 3. Arbitrary configuration of the magnetizations on four B_i sublattices.

[8] L. Néel, reference 1, p. 145.

A value for λ/μ can satisfy these equations if:

$$\frac{L(L+3)\beta^2}{3[3-(L+3)\alpha\beta]}<\frac{1-(K+1)\alpha\beta}{K(K+1)\alpha^2}. \qquad (1)$$

This inequality reduces to $\alpha\beta<3/(K+1)(L+3)$; further, $\alpha_2=(K+1)\alpha$ and $\gamma_2=(L+3)\beta/3$ so that Eq. (1) becomes $\alpha_2\gamma_2<1$. Conversely, if $\alpha_2\gamma_2>1$, either $3-(L+3)\alpha\beta<0$, or if $3-(L+3)\alpha\beta>0$, the inequality sign in Eq. (1) has to be reversed. In either case T_{c3} is not the largest root. Thus, if the doubly antiferromagnetic arrangement is the ground state at 0°K, the upper Curie point is at either T_{c1} or T_{c2}. But if a triangular or a ferrimagnetic arrangement is the ground state, then the upper Curie point is not necessarily at T_{c3}. The possible cases are deduced from Eq. (1), whose left and right sides we designate by l and r, respectively.

(a) $\alpha_2\gamma_2<1$ with $1-(K+1)\alpha\beta>0$ and $3-(L+3)\alpha\beta>0$: then

$$T_{c3}>T_{c1} \text{ and } T_{c3}>T_{c2} \quad \text{for} \quad l<(\lambda/\mu)<r,$$
$$T_{c1}<T_{c3}<T_{c2} \quad \text{for} \quad r<(\lambda/\mu),$$
$$T_{c2}<T_{c3}<T_{c1} \quad \text{for} \quad (\lambda/\mu)<l.$$

(b) $\alpha_2\gamma_2<1$ with $1-(K+1)\alpha\beta<0$ and $3-(L+3)\alpha\beta<0$: then for all λ/μ, $T_{c3}<T_{c1}$ and $T_{c3}<T_{c2}$. There are no other possible cases when $\alpha_2\gamma_2<1$. If $\alpha_2\gamma_2=1$, then $l=r$ and at $(\lambda/\mu)=r$, we have $T_{c1}=T_{c2}=T_{c3}$.

We shall now follow the substance down to 0°K and investigate the possibilities for lower Curie points, assuming the interactions to be independent of temperature. We notice that there is no close connection between the inequalities in (a) and (b) and the inequalities defining the ground state at 0°K. We expect, therefore, several possible cases, of which we will consider the simplest case and the most complicated case. Actually, there are five cases having from one to four transition points.

When T_{c3} is the largest root and the ferrimagnetic arrangement is the ground state, then only one transition, at T_{c3}, occurs.

When T_{c2} is the largest root and the ground state is the triangular arrangement with $\phi=\frac{1}{2}\pi$ and $\sin\psi=\gamma/|\gamma_2|$, we have four transitions, indicated in Fig. 2. This case is perhaps realized in mixed Zn-Ni ferrite with $x=0.2$. The transition temperature T_{c4} is calculated as follows: the triangular case gives $\sin\phi=(M_{b'}/|\alpha_2|M_{a'})$, where $M_{a'}$ and $M_{b'}$ are now the values of the moments at a temperature $T<T_{c4}$. Eliminating $M_{a'}\sin\phi$ from the expression for $H_{b'}$, we get

$$H_{b'}=2nM_{b'}(\beta+1/|\alpha_2|).$$

The value of T_{c4} is given by using this expression in the limiting form of the Brillouin function for the magnetization:

$$M_{b'}=\mu CH_{b'}/2T,$$

whence

$$T_{c4}=\mu Cn(\beta+1/|\alpha_2|).$$

On the other hand, T_{c3} and T_{c6} may not be given in closed form. T_{c3} occurs when $(M_{a'}/M_{b'})=(1/|\alpha_2|)$ and T_{c4} when $(M_{a'}/M_{b'})=|\gamma_2|$. These conditions allow their numerical or graphical determinations.[9]

We have treated so far the case $\alpha_2\gamma_2<1$. For the case $\alpha_2\gamma_2>1$, we saw that the upper Curie point is at either T_{c1} or T_{c2}. Suppose it is at T_{c1}; then the B lattice becomes ordered first. At T_{c2}, the A lattice which still sees no field from B, also becomes ordered antiferromagnetically and no other transition occurs down to 0°K. This case is not as interesting as the preceding one.

IV. EXPERIMENTAL POSSIBILITIES

The existence of the triangular ground state may be ascertained by neutron diffraction experiments. The interaction constants n, $n\alpha$, and $n\beta$ have been determined[10] for mixed Zn-Ni ferrites, Fe_2O_3, xNiO, $(1-x)$ ×ZnO. The ratio of saturation magnetizations on lattices A and B is: $y=x/[(2-x)+0.4x]$; the value of γ_2 is in between β and $4\beta/3$. For $x=0.3$, we obtain $y\approx 0.16$ and $\gamma_2=0.14$ to 0.18. The triangular arrangement is expected to appear in this neighborhood. The angle of the two components on the B lattice will be $\approx 90°$ at $\sin\psi=(y/|\gamma_2|)=0.7$, or $x=0.2$ to 0.25.

In general, because of the smallness of β in most ferrites, the triangular case will occur for rather small values of the saturation magnetization ratio y, of the order of $|\beta|$. As the molecular field treatment of the $A-B$ and $A-A$ interactions becomes less reliable with decreasing concentrations of the magnetic ions on A, the criterion $y<|\gamma_2|$ deduced above may be only a rough estimate.

Neutron diffraction could also ascertain the existence of antiferromagnetism in pure Zn ferrite and in mixed Zn ferrites. Magnetic measurements[11] on mixed Zn-Co and Zn-Mn ferrite yield data which, extrapolated to small concentrations of Co or Mn, suggest that $T_{c3}\to 0$ for $x\sim 0.2$. For smaller x our theory predicts a doubly antiferromagnetic ground state. In this case too, the concentration of magnetic ions in lattice A is small.

The existence of the multiple Curie points should most easily be detected by heat capacity measurements. This method avoids the spurious effects in magnetic measurements caused by ferromagnetic impurities. We have estimated the discontinuities in heat capacity associated with the various types of transitions and find them to be well within the range detectable by current techniques. In antiferromagnetic transitions the contribution to the discontinuity (on the molecular field theory) due to the spin, is 2.38 k per ion. In the triangular transition occurring at T_{c4} (see Fig. 2), the ions of lattice B contribute this same amount to the discontinuity, while the ions on lattice A do not contribute because the functional dependence of $M_{a'}$ on $H_{a'}$ does not change at the transition point. On the other hand, at transformations of the types associated with T_{c3}, T_{c5} and T_{c6}, the functional dependences on $H_{a'}$ and $H_{b'}$ of both $M_{a'}$ and $M_{b'}$ change at the corresponding transformation points. The resulting discontinuities depend on the interaction parameters as well as on λ/μ; the expressions are rather complicated. As mentioned in Section III in connection with Fig. 2, mixed Zn-Ni ferrite with $x<0.3$ is a promising substance for the investigation of the multiple transitions.

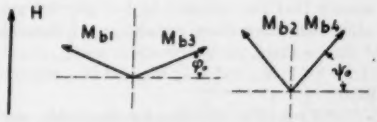

FIG. 4. Symmetrical configuration with the same energy.

This research has been assisted in part by the Office of Naval Research. One of us (Y. Y.) is a Whiting Fellow of the University of California. Mr. Harvey Kaplan has kindly checked some of the calculations.

APPENDIX

We show here that the energy of the lowest energy arrangement is the same with the B lattice subdivided into two sublattices as it is when B is subdivided into four sublattices. The effect of lattice A is equivalent to a field $\mathbf{H}$. By symmetry, $\sum \mathbf{M}_{bi}$ will be parallel to the direction of $\mathbf{H}$. Consider the general case of Fig. 3: we will show that all configurations with the same resultant moment have the same self-energy, and also the same energy in the field $\mathbf{H}$.

The self-energy is:

$$W=-\cos^2\varphi+\sin^2\varphi-\cos^2\psi+\sin^2\psi +4\sin\varphi\sin\psi\cos(\alpha+\beta),$$

where the molecular field constant $n\beta$ has been taken equal to -1. We consider now the reference state shown in Fig. 4, where $\sin\varphi_0=\sin\varphi\cos\alpha$ and $\sin\psi_0=\sin\psi\cos\beta$. We have:

$$W_0=-\cos^2\varphi_0+\sin^2\varphi_0-\cos^2\psi_0+\sin^2\psi_0+4\sin\varphi_0\sin\psi_0$$

and

$$W-W_0=2\sin^2\varphi\sin^2\alpha+2\sin^2\psi\sin^2\beta -4\sin\varphi\sin\psi\sin\alpha\sin\beta$$
$$=2(\sin\varphi\sin\alpha-\sin\psi\sin\beta)^2=0,$$

as $\sum \mathbf{M}_{bi}$ is in the direction of $\mathbf{H}$. Furthermore,

$$W_0=-2+2(\sin\varphi_0+\sin\psi_0)^2$$

is a function only of $\sin\varphi_0+\sin\psi_0$; thus, M_{b3} and M_{b4}, and also M_{b1} and M_{b2}, may be taken collinear in pairs.

This freedom in the orientations of the M_{bi}'s is a result of the equality of the interaction constants. If

[9] Néel gives a graphical method in Appendix I to his paper.
[10] L. Néel and P. Brochet, Compt. rend. **229**, 1133 (1949).
[11] C. Guillaud and H. Creveaux, Compt. rend. **230**, 1458 (1950).

we assume that the interactions 1–2 and 3–4 are $-k$, the other four interactions remaining -1, then at constant $\sin\varphi_0+\sin\psi_0$, the lowest states are:

(a) for $k<1$, M_{b1} and M_{b2}, M_{b3} and M_{b4}, respectively, collinear;

(b) for $k>1$, M_{b1} and M_{b3} (or M_{b4}), M_{b2} and M_{b4} (or M_{b3}), respectively, collinear.

Thus, if the interactions in the B lattice are such that with no applied field B is subdivided into two oppositely magnetized sublattices B' and B'', then under the influence of A there will be no tendency for B' and B'' to break into 4 (or, in general, into 2^n) sublattices, no matter what the interactions between these sublattices may be. This shows that our hypothesis about the nearest-neighbor interactions determining the ordering is not an essential one and does not affect our results.

The neglect of anisotropy is justified only as far as energy is concerned. Because of the degeneracy of the arrangements with the same total moment on the B lattice, anisotropy may lead to a configuration where the four sublattices are magnetized all in different directions.

PHYSICAL REVIEW VOLUME 87, NUMBER 2 JULY 15, 1952

Angular Correlation between Protons and Gammas in the $Li^6(d,p\gamma)Li^7$ Reaction*

W. H. Burke† and J. R. Risser
Rice Institute, Houston, Texas

(Received March 12, 1952)

The angular correlation between protons and gammas in the reaction $Li^6(d,p\gamma)Li^7$ has been experimentally determined for the purpose of obtaining information on the 480-kev excited state of Li^7. A bombarding energy of 500 kev was used, so that the Be^{8*} intermediate nucleus would be formed in the 22.5-Mev excited state reported by Whaling and Bonner. No correlation was observed within the statistical accuracy of the experiment.

INTRODUCTION

IT has long been considered that the 480-kev excited state of Li^7 is a $^2P_{\frac{1}{2}}$ state.[1] At least one shell model indicates the reasonableness of this assumption.[2] However, experimental evidence, such as the high probability of transition to this state in the $B^{10}(n,\alpha)Li^7$ reaction, has led to other hypotheses.[3] We felt it worthwhile to measure the angular correlation between protons and 480-kev gammas in the $Li^6(d,p\gamma)Li^7$ reaction in order to shed further light on the question. Any correlation would indicate a state other than $^2P_{\frac{1}{2}}$.

Presumably an angular correlation would be most pronounced if a single level in the compound nucleus is involved. Bombarding energy was chosen in relation to target thickness so that the Be^8 compound nucleus was formed with the energy of the 22.5-Mev excited state reported by Whaling and Bonner.[4]

METHOD

A Li^6SO_4 (95 percent Li^6) target was bombarded with 500-kev deuterons. Both proton and gamma-counters were of the scintillation type, using a thin anthracene layer for the protons and a large NaI crystal for the gamma-rays. The proton counter was at 90° to the deuteron beam, and the gamma-ray counter was rotated in the plane perpendicular to the beam.

NaI was used because it gives a strong photoelectric peak. By using biased trigger circuits to eliminate pulses below this peak, it was possible to eliminate most of the gamma-ray background from the accelerator while eliminating only a minor fraction of the 480-kev gamma-rays from the target. It was felt that in this manner a lower percentage of accidental coincidences (experimentally 5 to 12 percent of the true count) was achieved than would have been possible with an organic phosphor, which is faster but does not allow strong energy selection.

The biased triggered circuits were blocking oscillators. The blocking oscillator pulses fed into the coincidence circuits were the same height and shape for all sizes of triggering pulse. This made possible a direct measurement of the accidental rate by using independent sources of protons and gammas equivalent in intensity to the target. A direct measurement by this method would have been difficult or impossible if raw pulses from the amplifiers had been fed directly into the coincidence circuit, since the independent gamma-source would have necessarily had to give the same pulse-height distribution as the target.

EXPERIMENTAL EQUIPMENT

The target was made by evaporation of the Li^6 enriched lithium sulfate onto a thin polished silver disk. Its thickness was 370 micrograms/cm² or about

* Supported by ONR and AEC. This work was part of a thesis submitted to the Graduate School of Rice Institute in partial fulfillment of the requirements for the Ph.D., June, 1951. A report was presented at the Houston meeting of the American Physical Society, November, 1951.

† Now at Magnolia Petroleum Company, Field Research Laboratories, Dallas, Texas.

[1] D. R. Inglis, Phys. Rev. **50**, 783 (1936); E. Feenberg and E. Wigner, Phys. Rev. **51**, 95 (1937).

[2] M. G. Mayer, Phys. Rev. **78**, 16 (1950).

[3] D. R. Inglis, Phys. Rev. **74**, 1876 (1948); B. T. Feld, Phys. Rev. **75**, 1618 (1949).

[4] W. Whaling and T. W. Bonner, Phys. Rev. **79**, 258 (1950).

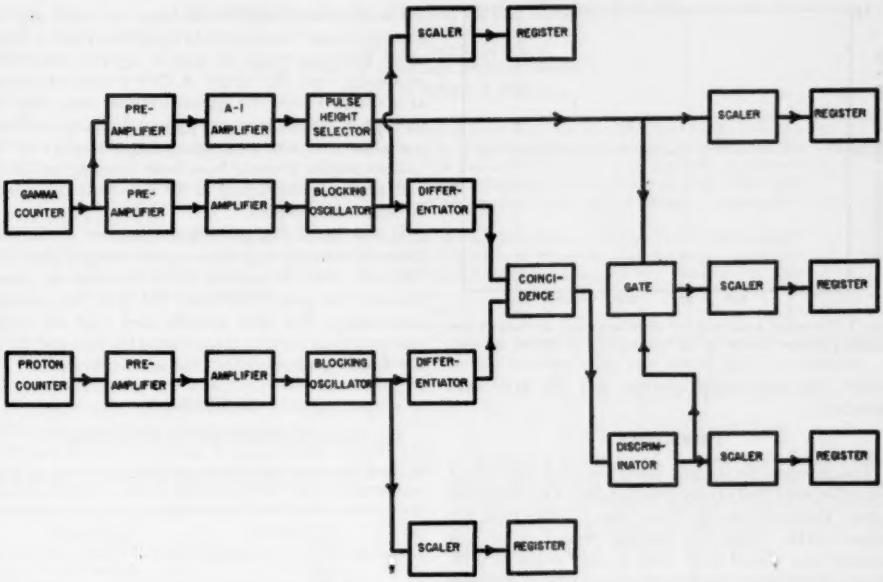

FIG. 1. Block diagram of the electronics.

250 kev for the 500-kev deuterons with which it was bombarded.

The Rice Institute Van de Graaff generator was used to accelerate the deuterons. The molecular and atomic beams were separated by the field of a small magnet and the molecular beam was eliminated by a quartz slit. Before striking the target the atomic beam had to pass through a $\frac{3}{16}$-in. diameter collimator which was 2 inches from the target. The energy of the deuterons was determined by measurement of the Van de Graaff voltage with an electrostatic voltmeter.

The target was turned so that the protons could leave it without passing through any silver, and the gamma-rays passed through a negligible thickness in going to the crystal. There were two foils between the target and the anthracene. One was a 6-cm air-equivalent foil which held the vacuum in the target chamber. Another 6-cm foil acted as a light seal for the counter. These foils eliminated protons from carbon contamination on the target, as was verified by substituting a carbon target.

The NaI crystal was a cylinder $1\frac{1}{2}$ in. in diameter by $1\frac{1}{2}$ in. high mounted in an aluminum can of $\frac{1}{8}$-in. wall. The anthracene layer used to detect the protons was about 0.1 mm thick.

Figure 1 is a block diagram of the electronics. The pulses from the photomultipliers were amplified by distributed amplifiers whose rise time was less than 0.04 μsec followed by a 0.1 μsec rise time high level stage. The proton output pulses had a rise time of 0.1 μsec. As a consequence of differentiation in the distributed amplifier the gamma-output pulses had a rise time of about 0.15 μsec. Delay line was used to compensate for the time difference.

The gamma-blocking oscillator bias was set to reject pulses below the low side of the photoelectric peak of the 480-kev gamma-rays. The proton blocking oscillator was biased to reject gamma-ray pulses and accept proton pulses. The differentiated blocking oscillator output pulses were 20 volts tall and about 0.05 μsec wide at half-height. Both height and shape were independent of the size of the input pulse. The coincidence circuit into which these pulses were fed was the two-diode type. The resolving time was somewhat dependent on the coincidence detector bias. For the bias used, it was computed from the accidental rate as 0.15 μsec.

The NaI pulses were also amplified by an Atomic Instrument Company Model 204-*B* linear amplifier and fed into a pulse-height selector which was set to pass only pulses in the 480-kev photoelectric peak. The output of the pulse-height selector was used to gate the coincidence pulses. The lower discriminator in the selector was set to reject exactly the same pulses as the gamma-blocking oscillator. The purpose of the pulse-height selector and gate was to reject coincidences due to gamma-rays of higher energy than 480 kev. Output pulses from the blocking oscillators, the coincidence

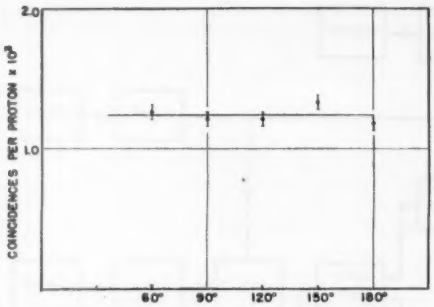

FIG. 2. Corrected total number of coincidences at each of five angular positions divided by the total number of protons counted.

circuit, the pulse-height selector, and the gate were recorded.

PROCEDURE

The gamma-counter was turned so that the axis of the cylindrical NaI crystal was parallel to the deuteron beam. The center of the crystal was 3 inches from the target center. Thus the angular resolution of this counter was about $\pm 14°$ with a solid angle of 0.19. Small variations in gamma-counting rates at different angular positions resulted from the impossibility of maintaining the target-counter distance exactly the same. The coincidence rates were corrected for this effect.

The protons had to pass through a $\frac{5}{8}$-in. diameter circular window which was 2 inches from the center of the target. All protons passing through this window hit the anthracene and were counted. The angular resolution of the protons counter was therefore about $\pm 10°$.

Observations were made with the gamma-counter at angles of 60°, 90°, 120°, 150°, and 180° to the proton counter. The final data included in the figure and table were taken in four runs over the five angles. At each angle in each run 160 coincidence counts were taken. The accidental coincidence rate varied between 5 and 12 percent of the true rate. It was measured after each run. For these measurements the proton counter was left in place counting protons from the target and the gamma-counter was moved to a position about a meter away from the target so that it counted practically no quanta from the target. A Cs^{137} source was placed at a distance from the gamma-counter such that the number of counts from the gamma-blocking oscillator was about the same as it was during the runs over the various angles. Counts from both blocking oscillators and random coincidences in the two-diode coincidence circuits were recorded.

It was found that a negligible number of the coincidences were due to gamma-rays of energy higher than 480 kev. Over 98 percent of all coincidences passed through the gate. Therefore, the gate was actually unnecessary. The data actually used were the singles and coincidence counts taken during the runs and during the direct measurements of the accidental rate.

CONCLUSION

The results are shown in Fig. 2 and Table I.

TABLE I. Corrected total number of coincidences at each of five angular positions divided by the total number of protons counted.

Angle	Coincidences per proton $\times 10^3$
60°	1.26±0.05
90°	1.21
120°	1.21
150°	1.33
180°	1.18

The statistical relative deviation of the points is 4 percent. The maximum deviation from the average is 7 percent at 150°. The 150° point is also 9 percent above the 90° point. The reasonable conclusion is that actually the distribution is isotropic and that no angular correlation exists. This is of course what would be expected if the Li^{7*} state were $^2P_{\frac{1}{2}}$, as has been frequently assumed. However, it naturally does not rule out states or combination of states yielding small asymmetries.

Thanks are due Professor T. W. Bonner for suggesting that the angular correlation from the $Li^6(d,p\gamma)Li^7$ reaction would be of interest and for subsequent helpful discussions.

Neutron-Proton Scattering in the Region 0–5 Mev

L. HULTHÉN AND S. SKAVLEM*
Royal Institute of Technology, Stockholm, Sweden
(Received January 4, 1952)

The theoretical cross section for scattering of neutrons by protons has been calculated on the basis of a pure central Yukawa potential with the same range in ^1S and ^3S states, corresponding to meson mass 200 and 300, respectively. The results indicate that the best over-all fit with most recent scattering experiments would be obtained with a meson mass of roughly 350 m_e. Allowing different ranges in singlet and triplet states and making use of the deuteron binding energy, we found a "triplet mass" of 290 and a "singlet mass" of about 380.

A further result of this work is that, at least in the case of Yukawa potential, the "effective range" approximation is prone to give the total cross section much more accurately than the singlet and triplet cross sections separately. Accordingly, this approximation ought to be handled with some care in other problems than n–p scattering.

THE present work aims at an accurate theoretical calculation of the neutron-proton scattering in the energy region up to 5 Mev where influence from P and higher states can still be neglected.[1]

We assume a pure central Yukawa potential with the same range in the ^3S as well as in the ^1S state, thus

$$\left.\begin{aligned} V_{^1S}(r)&=-Ae^{-\kappa r}/r,\\ V_{^3S}(r)&=-Be^{-\kappa r}/r,\end{aligned}\right\}\quad \kappa=\mu mc/\hbar. \tag{1}$$

To begin with we take singlet and triplet ranges equal, simply because it is a natural assumption if we want to retain the connection between meson theory and nuclear force theory.

The calculations were performed with two different values of the meson mass μm: 200 and 300 m (m=electron mass). In each case the constants A and B were determined from the singlet and triplet scattering amplitudes, a_s and a_t, respectively. For these quantities we have the well-known equations

$$\tfrac{3}{4}a_t+\tfrac{1}{4}a_s=f,\quad 3\pi a_t^2+\pi a_s^2=\sigma_0, \tag{2}$$

where σ_0 is the epithermal neutron-proton scattering cross section and f the coherent scattering amplitude. Starting from

$$\left.\begin{aligned} f&=-(3.78\pm0.03)\cdot10^{-13}\text{ cm},^2\\ \sigma_0&=(20.32\pm0.10)\cdot10^{-24}\text{ cm}^2,^3\end{aligned}\right. \tag{3}$$

and remembering that a_t must be positive (triplet interaction corresponding to a bound state), we obtain

$$\left.\begin{aligned} a_t&=(5.37\pm0.03)\cdot10^{-13}\text{ cm},\\ a_s&=(-23.67\pm0.06)\cdot10^{-13}\text{ cm}.\end{aligned}\right. \tag{4}$$

According to Blatt and Jackson[4] the effective range can be defined as a coefficient in the expansion of $k\cot\eta$ in powers of k, the reduced wave number of the neutron-proton system, η being the asymptotic phase of the singlet or triplet S wave function, thus

$$k\cot\eta=-1/a+\tfrac{1}{2}rk^2+O(k^4), \tag{5}$$

where a is the scattering amplitude. The quantity k is related to the energy E_i of the incident neutrons in the laboratory system through the following formula[5]

$$k=\left(\frac{M_pE_i}{2\hbar^2}\right)^{\frac{1}{2}}=\frac{M_pc}{\hbar}\left(\frac{E_i}{2M_pc^2}\right)^{\frac{1}{2}}, \tag{6}$$

(M_p=proton mass).

The method of calculating the effective range r_s (singlet) and r_t (triplet) when a_s and a_t are known will be outlined below. The results in the present case are given in Table I. Accepting now the effective range approximation, we get the following expression for the total cross section:

$$\sigma=\tfrac{1}{4}\sigma_s+\tfrac{3}{4}\sigma_t, \tag{7}$$

with

$$\sigma_i=\frac{4\pi a_i^2}{1+(a_i^2-a_ir_i)k^2+\frac{1}{4}a_i^2r_i^2k^4}. \tag{8}$$

TABLE I. Scattering amplitude a from (4). Calculated effective range r (Yukawa potential).

State	Meson mass assumed	$a\cdot10^{13}$ cm	$r\cdot10^{13}$ cm
Singlet	200	−23.67	4.717
Singlet	300	−23.67	3.006
Triplet	200	5.37	1.759
Triplet	300	5.37	1.599

* On leave from the University of Oslo, Oslo, Norway. Permanent address: Universitetets fysiske institutt, Blindern, Oslo, Norway.

[1] See, however, L. Hulthén and A. Pais, Physical Society of London, Cambridge Conference Report (1947), p. 177, Table II. For meson mass 200 the P states may contribute to the total cross section by 3–5 percent at 5 Mev, depending on the P interaction assumed. On the other hand, the contribution does not exceed 5 parts in a thousand for meson mass 300.

[2] Ringo, Burgy, and Hughes, Phys. Rev. **82**, 344 (1951).

[3] This figure differs slightly from the value given by E. Melkonian [Phys. Rev. **76**, 1744 (1949)] (20.36±0.10) which, according to private information kindly given by Professor Rainwater, is still the best value.

[4] J. M. Blatt and J. D. Jackson, Phys. Rev. **76**, 18 (1949).

[5] Present best values give $k^2=1.2051\cdot10^{24}\,E_i(\text{Mev})\text{ cm}^{-2}$.

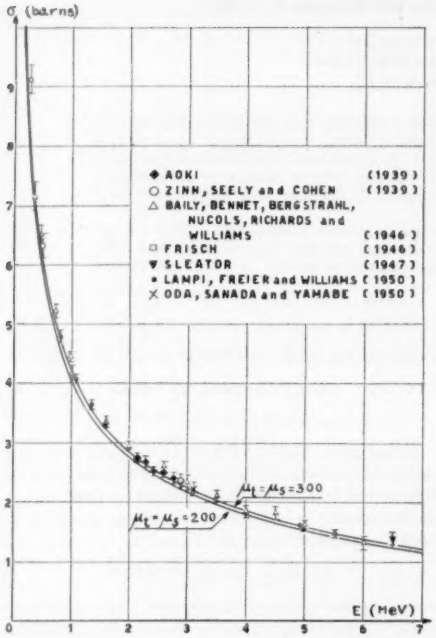
σ (barns)
◆ AOKI (1939)
○ ZINN, SEELY and COHEN (1939)
△ BAILY, BENNET, BERGSTRAHL, NUCOLS, RICHARDS and WILLIAMS (1946)
□ FRISCH (1946)
▼ SLEATOR (1947)
• LAMPI, FREIER and WILLIAMS (1950)
× ODA, SANADA and YAMABE (1950)
μt = μs = 300
μt = μs = 200
E (MeV)

FIG. 1. Neutron-proton scattering cross section based on Yukawa potential with same range in ^1S and ^3S corresponding to meson masses 200 and 300, plotted against incident neutron energy E and compared with various measurements.

The results obtained in this way are compared with experimental results[6–12] in Fig. 1.

THE MATHEMATICAL METHOD

We start by recalling the main features of the variational method as formulated in a previous paper.[13] Take the equation

$$\{d^2/dx^2+q^2+v(x)\}\phi(x)=0, \tag{9}$$

where $v(x)$ is supposed to be a short-range potential, for instance, be^{-x}/x. The boundary conditions are

$$\phi(0)=0, \quad \phi(x)\to\cot\eta\,\sin qx+\cos qx \text{ as } x\to\infty, \tag{10}$$

η being the unknown asymptotic phase. Writing $\phi(x)$ in the form

$$\phi(x)=\cot\eta\,\sin qx+\cos qx-y(x), \tag{11}$$

we have for $y(x)$ the following boundary conditions:

$$y(0)=1, \quad y(\infty)=0. \tag{12}$$

Inserting (11) into (9) we obtain

$$y''+q^2y+v(x)y=v(x)(\cos qx+\cot\eta\,\sin qx). \tag{13}$$

This is the Euler equation of the following variational problem. Require

$$J=\int_0^\infty[-y'^2+q^2y^2+v(x)\,(\cos qx-y)^2]dx \tag{14}$$

to be stationary under the accessory condition

$$N=\int_0^\infty v(x)\,\sin qx(\cos qx-y)dx=\text{const.} \tag{15}$$

If we introduce a multiplier λ, we get a variational equation

$$\delta J+2\lambda\delta N=0, \tag{16}$$

which leads to Eq. (13), with λ for $\cot\eta$. Furthermore, it is easy to show[13] that the integral in (15) can be expressed in terms of η if y is an exact solution of (13); we have

$$N=q(1-\eta_B\cot\eta), \tag{17}$$

where

$$\eta_B=\frac{1}{q}\int_0^\infty v(x)\,\sin^2qx dx, \tag{18}$$

is the eigenphase in Born's approximation. Regarding $y(x)$ as a trial function which depends linearly on a number of indeterminate parameters, we obtain from (16) and (17) a unique approximate solution, if λ is identified with $\cot\eta$. In this way we get a value for $\lambda=\cot\eta$ which is not stationary; this is however easily remedied, as will be shown presently.[14]

Define

$$\mathfrak{L}=\int_0^\infty\phi\left(\frac{d^2}{dx^2}+q^2+v(x)\right)\phi dx, \tag{19}$$

and insert here Eq. (11) for $\phi(x)$, and we obtain after partial integrations with due regard to the boundary conditions (12),

$$\mathfrak{L}=-q\lambda+q\eta_B\lambda^2+J+2\lambda N, \quad (\lambda=\cot\eta). \tag{20}$$

On an infinitesimal variation of ϕ we get from (19) after partial integrations

$$\delta\mathfrak{L}=2\int_0^\infty\delta\phi\left(\frac{d^2}{dx^2}+q^2+v(x)\right)\phi dx+q\delta\lambda. \tag{21}$$

For the exact solution of (9) the integral in (21) obviously vanishes. We now fix an approximate solution by requiring this integral to vanish for all possible $\delta\phi$, thus (compare Zeilon[15])

$$\int_0^\infty\delta\phi\left(\frac{d^2}{dx^2}+q^2+v(x)\right)\phi dx=0. \tag{22}$$

[6] H. Aoki, Proc. Phys. Math. Soc. Japan **21**, 232 (1939).
[7] Zinn, Seely, and Cohen, Phys. Rev. **56**, 260 (1939).
[8] Bailey, Bennet, Bergstrahl, Nuckols, Richards, and Williams, Phys. Rev. **70**, 583 (1946).
[9] D. H. Frisch, Phys. Rev. **70**, 589 (1946).
[10] W. Sleator, Jr., Phys. Rev. **72**, 207 (1947).
[11] Lampi, Freier, and Williams, Phys. Rev. **80**, 853 (1950).
[12] Oda, Sanada, and Yamabe, Phys. Rev. **80**, 469 (1950).
[13] L. Hulthén, Arkiv. Mat. Astron. Fysik. **A35**, No. 25, 1 (1948). See also the original paper, K. Fysiogr. Sällsk. Lund, Förh. **14**, 1 (1944).
[14] See reference 13, pp. 7–9.
[15] N. Zeilon, Lunds Univ. Årsskr. Avd. 2 (C. W. K. Gleerup, Lund, 1947), New Series, Sec. 2, Vol. 43, Nr. 10.

Then we obtain the equation

$$\delta\mathfrak{L}=q\delta\lambda, \tag{23}$$

where $\delta\mathfrak{L}$ and $\delta\lambda$ denote variations out from the approximate solution. But J and N in (20) do not depend on λ. Hence (23) can be split up in two equations; the first one is (16), the second one,

$$\partial\mathfrak{L}/\partial\lambda=q,^{16} \tag{24}$$

is easily found to be identical with (17) (with $\cot\eta=\lambda$). Thus the condition (22) is equivalent with the formalism quoted in the beginning of this section.

The λ-value obtained in this way is not stationary. However, the first-order deviation from the stationary value can be obtained from Eq. (23), letting now $\delta\mathfrak{L}$ and $\delta\lambda$ denote deviations from the exact solution of (9) and (10). Neglecting second-order terms, we have $\delta\mathfrak{L}=\mathfrak{L}$, since $\mathfrak{L}=0$ for the exact solution, and thus obtain, by using (17) and (20),

$$\delta\lambda=\mathfrak{L}/q=(J+\lambda N)/q=\Delta/q, \tag{25}$$

J, λ, and N being fixed by the approximate solution determined from (16) and (17). The improved λ-value is then

$$\lambda_0=\lambda-\Delta/q, \tag{26}$$

which is stationary because the first-order deviation has been removed, the remaining error in λ_0 being of the second order (or higher) in δy.[17]

Taking for $y(x)$ in (11) a trial function containing a number of indeterminate parameters $c_1\cdots c_n$, we get from (16) and (17)

$$\partial J/\partial c_\nu+2\lambda\partial N/\partial c_\nu=0, \quad \nu=1, 2, 3, \cdots, n, \tag{27a}$$

$$N=q(1-\eta_B) \tag{27b}$$

which determine the approximate solution. If $y(x)$ depends linearly on the parameters c_ν, Eqs. (27) are linear in the c_ν's and λ, and the solution is unique.

In the numerical calculation of Δ from (25) it is convenient to make direct use of (27). With a trial function depending linearly on the parameters c_ν, we can write

$$\left.\begin{aligned} J&=J^{(0)}+\sum_{\nu=1}^{n}\beta_\nu c_\nu+\tfrac{1}{2}\sum_{\mu,\nu=1}^{n}\alpha_{\mu\nu}c_\mu c_\nu,\\ N&=N^{(0)}+\sum_{\nu=1}^{n}\gamma_\nu c_\nu,\ \alpha_{\mu\nu}=\alpha_{\nu\mu},\end{aligned}\right\} \tag{28}$$

and Eqs. (27) become

$$\left.\begin{aligned} &\sum_{\nu=1}^{n}\alpha_{\mu\nu}c_\nu+2\lambda\gamma_\mu=-\beta_\mu, \quad \mu=1, 2, \cdots, n\\ &\sum_{\nu=1}^{n}\gamma_\nu c_\nu+q\eta_B\lambda=q-N^{(0)}.\end{aligned}\right\} \tag{29}$$

Thus the quadratic terms can be eliminated from $J+\lambda N$, the result being

$$\Delta=J+\lambda N=J^{(0)}+\lambda N^{(0)}+\tfrac{1}{2}\sum_{\nu=1}^{n}\beta_\nu c_\nu. \tag{30}$$

Turning now to the Yukawa potential $v(x)=be^{-x}/x$, we have the equation

$$(d^2/dx^2+q^2+be^{-x}/x)\phi(x)=0, \tag{31}$$

where

$$q^2=ME/\hbar^2\kappa^2=k^2/\kappa^2, \quad \kappa=\mu mc/\hbar.^{18} \tag{32}$$

$M/2$ is the reduced mass of the neutron-proton system and E the total energy in the center-of-mass system [see Eq. (6)]. μm and m are the masses of meson and electron, respectively.

Comparison with (1) gives

$$b=\begin{cases}{}^1b=MA/\kappa\hbar^2,\\ {}^3b=MB/\kappa\hbar^2,\end{cases} \quad M=\tfrac{1}{2}(M_n+M_p). \tag{33}$$

As a trial function for $y(x)$ in (11) we choose the following expression, which satisfies the boundary conditions (12)

$$y(x)=e^{-x}+(1-e^{-x})\sum_{1}^{n}c_\nu e^{-\nu x}. \tag{34}$$

Inserting this into (14), (15), and (18), putting $v(x)=be^{-x}/x$, we obtain with the notations (28)

$$\left.\begin{aligned} J^{(0)}&=-\tfrac{1}{2}(1-q^2)+b[\ln\{(4+q^2)/3\}\\ &\qquad -\tfrac{1}{4}\ln(1+4q^2)],\\ \beta_\nu&=\frac{2(1+q^2)}{(\nu+1)(\nu+2)}-b\ln\frac{(\nu+2)^2((\nu+2)^2+q^2)}{(\nu+3)^2((\nu+1)^2+q^2)},\\ \tfrac{1}{2}\alpha_{\mu\nu}&=\frac{2q^2-2\mu\nu-\mu-\nu}{(\mu+\nu)(\mu+\nu+1)(\mu+\nu+2)}\\ &\qquad +b\ln\frac{(\mu+\nu+2)^2}{(\mu+\nu+1)(\mu+\nu+3)},\\ N^{(0)}&=b(\tfrac{1}{2}\operatorname{arctg}2q-\operatorname{arctg}\tfrac{1}{2}q),\\ \gamma_\nu&=-b\left(\operatorname{arctg}\frac{q}{\nu+1}-\operatorname{arctg}\frac{q}{\nu+2}\right),\\ \eta_B&=(b/4q)\ln(1+4q^2).\end{aligned}\right\} \tag{35}$$

[16] See S. S. Huang, Phys. Rev. **76**, 1878 (1949) and L. Hulthén and P. O. Olsson, Phys. Rev. **79**, 532 (1950). The identity of (24) with (17) was first pointed out to us by Dr. P. O. Olsson and Dr. B. C. H. Nagel (unpublished manuscript). See also T. Kato, Phys. Rev. **80**, 475 (1950).

[17] See reference 13, original paper, pp. 4–6. An explicit stationary expression for λ can be obtained by putting $(20)=0$ and solving with respect to λ. We then have

$$\lambda=-\frac{1}{q\eta_B}\left(N-\frac{q}{2}-[(N-\tfrac{1}{2}q)^2-q\eta_B J]^{\frac{1}{2}}\right), \tag{20a}$$

the sign of the square root being fixed for instance by the condition that λ must approach $1/\eta_B$ (Born approximation) when the potential $v(x)$ decreases sufficiently ($N\ll q$). Requiring λ to be stationary, we obtain an equation (system) equivalent to (16), which together with (20a) determines an approximate solution. This is virtually the same method as that described in the original paper (1944).

[18] Present best values give $1/\kappa=(386.12/\mu)\cdot10^{-13}$ cm.

TABLE II. Approximate solutions of (31) from Eqs. (27a, b) and (26), with trial functions according to (11) and (34). $b=1.5$.

q	$-c_1$	$+c_2$	$-c_3$	λ	Δ/q	λ_0	$\eta=\text{arc cot}\lambda_0$
0.1	0.4752	···	···	1.02192	0.03742	0.98450	0.79321
	0.5246	0.0720	···	0.99936	0.01569	0.98367	0.79363
	0.5643	0.2076	0.1104	0.99084	0.00738	0.98346	0.79374
0.2	0.5090	···	···	0.69803	0.02616	0.67187	0.97920
	0.5731	0.0931	···	0.68249	0.01130	0.67119	0.97967
	0.6248	0.2679	0.1417	0.67655	0.00553	0.67102	0.97978
0.3	0.5596	···	···	0.66521	0.02564	0.63957	1.00179
	0.6451	0.1229	···	0.65014	0.01133	0.63881	1.00233
0.4	0.6211	···	···	0.69873	0.02786	0.67087	0.97989
	0.7313	0.1561	···	0.68242	0.01243	0.66999	0.98050
0.5	0.6880	···	···	0.75417	0.03143	0.72274	0.94497
	0.8231	0.1869	···	0.73596	0.01416	0.72180	0.94559
0.6	0.7561	···	···	0.81752	0.03600	0.78152	0.90743
	0.9147	0.2126	···	0.79689	0.01629	0.78060	0.90800
	1.0213	0.5312	0.2424	0.78919	0.00872	0.78047	0.90808
0.7	0.8220	···	···	0.88373	0.04169	0.84204	0.87094
	1.0012	0.2300	···	0.86021	0.01896	0.84125	0.87140
	1.1184	0.5529	0.2347	0.85089	0.00972	0.84117	0.87145
0.8	0.8829	···	···	0.95099	0.04878	0.90221	0.83676
	1.0783	0.2360	···	0.92419	0.02254	0.90165	0.83707
	1.1849	0.4926	0.1706	0.91418	0.01255	0.90163	0.83708
0.9	0.9357	···	···	1.01914	0.05794	0.96120	0.80518
	1.1316	0.2174	···	0.99012	0.02916	0.96096	0.80531
1.0	0.9758	···	···	1.08928	0.07057	1.01871	0.77613
	1.5606	0.5744	···	0.99261	−0.02636	1.01897	0.77600
	1.3199	0.3733	0.0447	1.03386$_8$	0.01494$_8$	1.01891$_9$	0.77602$_8$

Equations (29) are then solved for instance by Gauss' method, and the improved value of $\cot\eta$, λ_0, is obtained from (26) and (30).

Numerical results have already been given in reference 13 for $b=1.5$ and 1.6. These results are quoted in our Tables II and IV. In Tables III, V–XI, the calculations have been extended to some other b-values of immediate interest. A comparison between the results obtained with one and two parameters, respectively, gives an idea of the accuracy of the corrected phase value η.[19] Moreover, the eigenfunctions were checked by means of certain integral identities;[13,20] with two parameters the deviations were about five parts in a thousand or less. This seems satisfactory since the uncertainty in the corrected phase η is of the second order, errors of first order being removed by the procedure comprised in Eq. (26).[21]

TABLE III. Approximate solutions of (31) from Eqs. (27a, b) and (26), with trial functions according to (11) and (34). $b=1.55$.

q	$-c_1$	$+c_2$	λ	Δ/q	λ_0	$\eta=\text{arc cot}\lambda_0$
0.1	0.4988	···	0.76260	0.03754	0.72506	0.94345
	0.5478	0.0715	0.74029	0.01605	0.72424	0.94399
0.2	0.5329	···	0.56083	0.02601	0.53482	1.07968
	0.5963	0.0922	0.54553	0.01137	0.53416	1.08020
0.3	0.5839	···	0.56575	0.02530	0.54045	1.07531
	0.6680	0.1210	0.55096	0.01125	0.53971	1.07589
0.4	0.6459	···	0.61619	0.02732	0.58887	1.03860
	0.7538	0.1530	0.60028	0.01225	0.58803	1.03922
0.5	0.7134	···	0.68042	0.03064	0.64978	0.99458
	0.8454	0.1829	0.66268	0.01380	0.64888	0.99521
0.6	0.7822	···	0.74865	0.03492	0.71373	0.95091
	0.9371	0.2079	0.72854	0.01569	0.71285	0.95150

TABLE IV. Approximate solutions of (31) from Eqs. (27a, b) and (26), with trial functions according to (11) and (34). $b=1.6$.

q	$-c_1$	$+c_2$	$-c_3$	λ	Δ/q	λ_0	$\eta=\text{arc cot}\lambda_0$
0.1	0.5232	···	···	0.51566	0.03755	0.47811	1.12482
	0.5716	0.0708	···	0.49368	0.01638	0.47730	1.12547
0.2	0.5575	···	···	0.43018	0.02580	0.40438	1.18652
	0.6199	0.0908	···	0.41517	0.01143	0.40374	1.18707
0.3	0.6089	···	···	0.47103	0.02491	0.44612	1.15117
	0.6913	0.1188	···	0.45660	0.01119	0.44541	1.15176
0.4	0.6714	···	···	0.53760	0.02672	0.51088	1.09848
	0.7769	0.1498	···	0.52209	0.01202	0.51007	1.09912
0.5	0.7395	···	···	0.61023	0.02981	0.58042	1.04490
	0.8683	0.1787	···	0.59297	0.01341	0.57956	1.04554
0.6	0.8090	···	···	0.68309	0.03377	0.64932	0.99490
	0.9602	0.2032	···	0.66352	0.01504	0.64848	0.99549
	1.0671	0.5229	0.2434	0.65582	0.00746	0.64836	0.99558
0.7	0.8768	···	···	0.75451	0.03865	0.71586	0.94950
	1.0483	0.2205	···	0.73211	0.01697	0.71514	0.94998
	1.1645	0.5406	0.2326	0.72287	0.00781	0.71506	0.95004
0.8	0.9404	···	···	0.82425	0.04461	0.77964	0.90860
	1.1318	0.2316	···	0.79806	0.01893	0.77913	0.90891
0.9	0.9974	···	···	0.89286	0.05213	0.84073	0.87171
	1.2147	0.2412	···	0.86069	0.02023	0.84046	0.87187
1.0	1.0445	···	···	0.96149	0.06215	0.89934	0.83834$_3$
	1.1526	0.1060	···	0.94359	0.04423	0.89936	0.83833$_4$
	1.3101	0.2356	−0.0314$_8$	0.91648$_6$	0.01715$_6$	0.89933$_9$	0.83835$_2$

TABLE V. Approximate solutions of (31) from Eqs. (27a, b) and (26), with trial function (34) [see (11)]. $b=1.65$.

q	$-c_1$	$+c_2$	λ	Δ/q	λ_0	$\eta=\text{arc cot}\lambda_0$
0.1	···	···	···	···	···	···
	0.5637	0.0224	0.27282	0.03081	0.24200	1.33336
0.2	···	···	···	···	···	···
	0.6441	0.0891	0.29075	0.01151	0.27923	1.29850
0.3	···	···	···	···	···	···
	0.7153	0.1162	0.36653	0.01109	0.35544	1.22816
0.4	···	···	···	···	···	···
	0.8003	0.1459	0.44755	0.01182	0.43573	1.15987
0.5	···	···	···	···	···	···
	0.8915	0.1739	0.52651	0.01301	0.51350	1.09641

TABLE VI. Approximate solutions of (31), with $b=2.1$. For trial function see (11) and (34).

q	$-c_1$	$+c_2$	λ	Δ/q	λ_0	$\eta=\text{arc cot}\lambda_0$
0.1	0.8306	···	−1.49943	+0.04729	−1.54672	2.56766
	0.8666	0.0529	−1.51453	+0.03286	−1.54739	2.56786
0.2	0.8567	···	−0.63878	+0.02020	−0.65897	2.15345
	0.8941	0.0553	−0.64738	+0.01182	−0.65920	2.15361
0.3	0.9098	···	−0.30240	+0.01797	−0.32036	1.88083
	0.9592	0.0723	−0.31066	+0.00995	−0.32061	1.88105
0.4	0.9746	···	−0.10267	+0.01755	−0.12052	1.69074
	1.0372	0.0903	−0.11147	+0.00933	−0.12080	1.69101
0.5	1.0460	···	+0.03968	+0.01833	+0.02135	1.54945
	1.1218	0.1070	+0.02992	+0.00886	+0.02106	1.54974
0.6	1.1204	···	+0.15137	+0.01887	+0.13250	1.43906
	1.2102	0.1225	+0.14014	+0.00793	+0.13221	1.43935

[19] In Tables II and IV we also find some three parameter results.
[20] L. Hulthén, K. Fysiogr. Sällsk. Lund, Förh. **14**, Nr. 8 (1944).

[21] In one particular case ($\mu_t=290$) we compared the triplet effective range calculated by the variational method ($r_t=1.618$) with the value obtained from the integral formula (see reference 4)

$$\kappa\sigma_t=2\int_0^\infty\left\{\left(1-\frac{x}{\kappa a_t}\right)^2-[\phi_t^{(0)}(x)]^2\right\}dx,$$

TABLE VII. Approximate solutions of (31), $b=2.3$. For trial functions see (11), (34).

q	$-c_1$	$+c_2$	λ	Δ/q	λ_0	$\eta=\text{arc cot}\lambda_0$
0.1	0.9771	...	−2.19459	0.02503	−2.21962	2.71830
	0.9882	0.0166	−2.19932	0.02036	−2.21968	2.71831
0.2	1.0117	...	−1.00031	0.01549	−1.01580	2.36403
	1.0285	0.0253	−1.00413	0.01165	−1.01578	2.36402
0.3	1.0636	...	−0.56248	0.01317	−0.57565	2.09312
	1.0887	0.0370	−0.56657	0.00916	−0.57573	2.09318
0.4	1.1271	...	−0.31655	0.01237	−0.32892	1.88857
	1.1604	0.0484	−0.32112	0.00788	−0.32900	1.88864
0.5	1.1976	...	−0.14965	0.01174	−0.16139	1.73081
	1.2393	0.0593	−0.15491	0.00657	−0.16148	1.73089
0.6	1.2722	...	−0.02408	0.01072	−0.03480	1.60558
	1.3238	0.0708	−0.03042	0.00448	−0.03490	1.60568

TABLE VIII. Approximate solutions of (31), $b=2.4$. For trial functions see (11), (34).

q	$-c_1$	$+c_2$	λ	Δ/q	λ_0	$\eta=\text{arc cot}\lambda_0$
0.1	...	...	...	...	...	...
	1.0651	−0.0011	−2.52963	0.02098	−2.55061	2.76795
0.2	...	...	...	...	...	...
	1.1032	+0.0055	−1.17711	0.01163	−1.18874	2.44221
0.3	...	...	...	...	...	...
	1.1596	+0.0141	−0.69005	0.00871	−0.69876	2.18069
0.4	...	...	...	...	...	...
	1.2274	+0.0224	−0.42178	0.00703	−0.42881	1.97589
0.5	...	...	...	...	...	...
	1.3024	+0.0300	−0.24314	0.00531	−0.24845	1.81431

TABLE IX. Approximate solutions of (31), $b=2.5$. For trial functions see (11), (34).

q	$-c_1$	$+c_2$	λ	Δ/q	λ_0	$\eta=\text{arc cot}\lambda_0$
0.1	1.1633	...	−2.86521	0.01513	−2.88034	2.80743
	1.1484	−0.0226	−2.85907	0.02138	−2.88045	2.80744
0.2	1.1954	...	−1.35168	0.00885	−1.36053	2.50776
	1.1834	−0.0181	−1.34908	0.01148	−1.36056	2.50777
0.3	1.2440	...	−0.81369	0.00682	−0.82051	2.25792
	1.2353	−0.0129	−0.81231	0.00818	−0.82049	2.25791
0.4	1.3038	...	−0.52169	0.00540	−0.52709	2.05588
	1.2982	−0.0083	−0.52094	0.00616	−0.52710	2.05589
0.5	1.3713	...	−0.33002	0.00364	−0.33366	1.89284
	1.3688	−0.0036	−0.32971	0.00395	−0.33366	1.89284
0.6	1.4444	...	−0.19027	0.00094	−0.19121	1.75973
	1.4471	+0.0039	−0.19060	0.00061	−0.19121	1.75973

EXPANSION IN k^2. COMPARISON BETWEEN "EXACT" AND "EFFECTIVE RANGE" METHOD

Equation (35) shows that J is an even function of q (or k), whereas N and η_B are odd functions. From (27a) and (27b), which are linear in the parameters c_ν and λ, we then obtain c_ν and $k\lambda$ as even functions of k. The correction Δ in (25) is also an even function, and so becomes $k\lambda_0$. These statements are, in fact, more generally valid and agree with the theory of the "effective range" approximation.[4] For small energies we then put, as in Eq. (5),

$$q\lambda_0=-1/\kappa a+\tfrac{1}{2}\kappa r q^2, \tag{36}$$

neglecting higher powers than q^2.

where $\phi_t^{(0)}$ is the eigenfunction for zero energy. With two parameters in the trial function $\phi_t^{(0)}$ the result was $r_t=1.642$, which differs from the variational value by 1.5 percent. As a test of the accuracy of the eigenfunction, this must be considered satisfactory since the integrand contains the square of the eigenfunction. It should be remembered that the value of r_t obtained from (37) is a stationary quantity and must therefore be expected to be more accurate than a value obtained from an integral formula without stationary properties. Concerning the accuracy of the variational method see also P.-O. Löwdin and A. Sjölander, Arkiv Fysik. 3, nr. 11, pp. 155–166 (1951).

TABLE X. Approximate solutions of (31), $b=2.7$. For trial functions see (11), (34).

q	$-c_1$	$+c_2$	λ	Δ/q	λ_0	$\eta=\text{arc cot}\lambda_0$
0.1	1.3894	...	−3.55092	+0.00082	−3.55174	2.86715
	1.3374	−0.0796	−3.53039	+0.02217	−3.55256	2.86721
0.2	1.4165	...	−1.70863	−0.00036	−1.70827	2.61199
	1.3641	−0.0800	−1.69765	+0.01110	−1.70875	2.61211
0.3	1.4538	...	−1.06657	−0.00162	−1.06495	2.38764
	1.4043	−0.0815	−1.05832	+0.00690	−1.06522	2.38776
0.4	1.5109	...	−0.72613	−0.00347	−0.72266	2.19657
	1.4542	−0.0844	−0.71881	+0.00409	−0.72290	2.19673
0.5	1.5721	...	−0.50805	−0.00633	−0.50172	2.03582
	1.5127	−0.0862	−0.50097	−0.00093	−0.50190	2.03596
0.6	1.6411	...	−0.35296	−0.01081	−0.34215	1.90046
	1.5823	−0.0823	−0.34606	−0.00379	−0.34227	1.90057

TABLE XI. Approximate solutions of (31), $b=2.9$. For trial functions see (11), (34).

q^2	$-c_1$	$+c_2$	λ	Δ/q	λ_0	$\eta=\text{arc cot}\lambda_0$
0.1	1.6697	...	−4.28703	−0.01979	−4.26724	2.91140
	1.5657	−0.1617	−4.24796	+0.02285	−4.27080	2.91159
0.2	1.6877	...	−2.08825	−0.01297	−2.07528	2.69256
	1.5796	−0.1674	−2.06673	+0.01043	−2.07716	2.69291
0.3	1.7173	...	−1.33209	−0.01272	−1.31937	2.49303
	1.6026	−0.1759	−1.31541	+0.00532	−1.32072	2.49352
0.4	1.7571	...	−0.93784	−0.01472	−0.92312	2.31624
	1.6336	−0.1863	−0.92259	+0.00161	−0.92420	2.31682
0.5	1.8072	...	−0.69034	−0.01865	−0.67138	2.16206
	1.6751	−0.1920	−0.67489	−0.00262	−0.67227	2.16267
0.6	1.8681	...	−0.51744	−0.02499	−0.49245	2.02839
	1.7316	−0.1931	−0.50189	−0.00878	−0.49311	2.02892

TABLE XII. Coefficients $a_0(b)$ and $a_2(b)$, defined by (36) and (37), calculated by variational method, using trial function (34) [see (11)].

b	a_0 1 param.	a_0 2 param.	a_0 3 param.	a_2 1 param.	a_2 2 param.
1.5	0.086200	0.086135	0.086117	1.23231	1.23074
1.55	...	0.060695	...	...	1.18021
1.6	0.036537	0.036475	0.036455	1.13373	1.13227
1.65	...	0.013346	...	...	1.08670
1.7	−0.008749	−0.008807	...	1.04459	1.04328
1.75	...	−0.030086	...	...	1.00182
1.8	−0.050534	−0.050585	...	0.96330	0.96216
1.9	...	−0.089572	...	...	0.88767
2.0	...	−0.126361	...	...	0.81883
2.1	−0.161439	−0.161460	−0.161491	0.75542	0.75490
2.2	−0.195306	−0.195316	...	0.69564	0.69533
2.25	...	−0.211908	...	...	...
2.3	−0.228337	−0.228339	−0.228377	0.63985	0.63974
2.35	...	−0.244660	...	...	0.61335
2.4	−0.260915	−0.260915	...	0.58783	0.58789
2.5	−0.293412	−0.293420	−0.293465	0.53957	0.53973
2.6	−0.326209	−0.326243	...	0.49522	0.49540
2.7	−0.359706	−0.359794	−0.359846	0.45521	0.45529
2.8	−0.394343	−0.394529	...	0.42026	0.42008
2.9	−0.430625	−0.430975	−0.431033	0.39153	0.39089
3.0	−0.469138	−0.469748	...	0.37083	0.36945

TABLE XIII. Singlet, triplet, and total cross sections (σ_s, σ_t, and σ) in effective range approximation, based on Yukawa potential with range corresponding to meson mass 300 ($\mu_s=\mu_t=300$). Δ is the difference between the "exact"-value (i.e., the value obtained from an accurate phase calculation, without expansion in k^2) and the "effective range" value.

E_l (Mev)	σ_s	Δ_s	σ_t	Δ_t	σ	Δ
0.2	$27.838\cdot10^{-24}$	$0.007\cdot10^{-24}$	$3.455\cdot10^{-24}$	$0.000\cdot10^{-24}$	$9.551\cdot10^{-24}$	$0.002\cdot10^{-24}$
0.6	12.502	0.011	3.158	−0.000	5.494	0.002
1.0	8.007	0.014	2.907	−0.001	4.182	0.002
2.0	4.153	0.017	2.418	−0.004	2.852	0.001
3.0	2.763	0.021	2.063	−0.007	2.238	0.000
4.0	2.048	0.023	1.795	−0.008	1.858	−0.000
5.0	1.613	0.025	1.585	−0.009	1.592	−0.001
6.0	1.322	0.027	1.415	−0.010	1.392	−0.001

By expanding (26), (29), and (30) in powers of q, retaining terms up to q^2 in J and q^3 in N, we obtain through the procedure described in the preceding section the coefficients in (36) as functions of the binding parameter b [see (33)]:

$$-1/\kappa a=a_0(b),\quad \tfrac{1}{2}\kappa r=a_2(b). \tag{37}$$

In this way a_0 and a_2 are turned into stationary quantities. It should, however, be noted that this is true for a_2 only if the parameters c_r are computed to the order of q^2. In Table XII a_0 and a_2 are given for a succession of b values in the most interesting region.

Using the figures given for a_t and a_s in (4), interpolations in Table XII give us the quantities ${}^1b$, ${}^3b$, r_s, and r_t for different meson masses.

We are now ready to compare the results of the two methods: the "effective range" approximation and the ordinary phase method. In both cases the same trial function (34) with two parameters has been used and the resulting technical errors in the cross sections are believed to be much smaller than the differences between "exact" results and "effective range" values, except at low energies, of course. Examples are found in Tables XIII (meson mass 300), XIV (meson mass 200), and XV, which give the singlet and triplet cross sections separately as well as the total cross sections, all based on the "effective range" approximation. The quantities denoted by Δ are the differences between the σ's calculated directly (i.e., without expansion in powers of k) and the σ's in the table.

Some comments may be called for. We see that the differences in the total cross sections are small, less than one part in a thousand for meson mass 300 and 1 percent for 200. On the other hand, the differences between the singlet cross sections obtained with the two methods run up to 2 percent for meson mass 300 and 7 percent for mass 200. The differences in the triplet cross sections are smaller and have the opposite sign. This fact, in connection with the different weight factors of singlet and triplet states, makes the differences in the total cross sections so small. The conclusion is that the "effective range" approximation is very accurate in calculating the total scattering cross section, the accuracy increasing with decreasing range (i.e., increasing meson mass), as is well known. This accuracy, however, is to a certain extent fortuitous, and therefore it is well advised to use the "effective range" method, even the "shape-dependent" version, with caution in other problems than neutron-proton scattering.

TABLE XIV. Same quantities as in Table XIII, with meson mass 200 ($\mu_s=\mu_t=200$).

E_l (Mev)	σ_s	Δ_s	σ_t	Δ_t	σ	Δ
0.2	$26.694\cdot10^{-24}$	$0.018\cdot10^{-24}$	$3.461\cdot10^{-24}$	$-0.000\cdot10^{-24}$	$9.270\cdot10^{-24}$	$0.004\cdot10^{-24}$
0.6	11.693	0.036	3.175	−0.001	5.304	0.008
1.0	7.372	0.044	2.930	−0.003	4.040	0.009
2.0	3.705	0.058	2.448	−0.006	2.762	0.010
3.0	2.398	0.066	2.094	−0.009	2.170	0.010
4.0	1.733	0.071	1.824	−0.011	1.801	0.010
5.0	1.333	0.074	1.611	−0.012	1.542	0.010
6.0	1.069	0.076	1.439	−0.012	1.346	0.010

TABLE XV. Same quantities as in Table XIII, "triplet meson mass" $\mu_t=290$ and "singlet meson mass" $\mu_s=380$.

E_l	σ_s	Δ_s	σ_t	Δ_t	σ	Δ
1	$8.258\cdot10^{-24}$	$0.007\cdot10^{-24}$	$2.909\cdot10^{-24}$	$-0.001\cdot10^{-24}$	$4.246\cdot10^{-24}$	$+0.001\cdot10^{-24}$
2	4.327	0.009	2.421	−0.004	2.898	−0.001
3	2.905	0.010	2.067	−0.007	2.276	−0.003
4	2.171	0.011	1.798	−0.009	1.891	−0.004
5	1.724	0.012	1.587	−0.010	1.622	−0.004
6	1.423	0.014	1.418	−0.010	1.419	−0.004

DISCUSSION

Figure 1 shows that a meson mass 300 gives a better agreement with the experimental results than meson mass 200, but it is not possible to obtain a very good over-all fit with a meson mass between 200 and 300. A rough estimate, based on a comparison with the most recent and probably most accurate measurements, those of Lampi, Freier, and Williams,[11] indicates that a meson mass of about 350 would give the best agreement with present experimental knowledge. This value is rather far from the π-meson mass, 276 m_e, and it would of course be interesting to see what meson mass would come out if noncentral forces are taken into account with the proper distance dependence. Such calculations are in progress at this institute.

So far the calculations were based on low energy scattering data exclusively [see (3)]. Taking now the deuteron binding energy E_0 into account, we have a possibility to determine the triplet range, and thus the corresponding meson mass. With $|E_0|=2.226\pm0.003$ Mev[22] and $a_t=(5.37\pm0.03)\cdot10^{-13}$ cm [see (4)], we obtain, making use of Table I[23] in the paper of Hulthén and Laurikainen,[24] combined with Table XII above,

$$\mu_t=290\pm15. \tag{38}$$

Having thus fixed a "triplet mass," we look at Fig. 1 and find again that we should not get a very close fit with recent scattering data by assuming the same "singlet mass." In fact, to obtain a good agreement with the results of Lampi, Freier, and Williams, we must choose

$$\mu_s=380\pm50,^{25} \tag{39}$$

the cross sections being rather insensitive to variations of the singlet mass. The results obtained with $\mu_t=290$ and $\mu_s=380$ are indicated in Table XV and compared with experimental results in Fig. 2. The corresponding effective ranges are, in units of 10^{-13} cm,

$$r_t=1.62\pm0.03, \quad r_s=2.33\pm0.35. \tag{40}$$

In this connection it might be of interest to mention

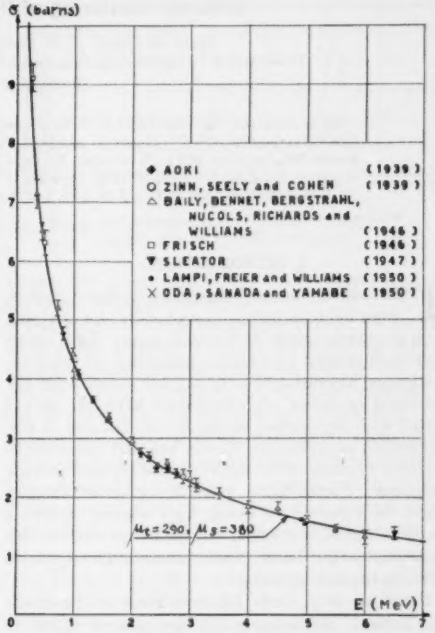

FIG. 2. Neutron-proton scattering based on Yukawa potential with "triplet mass" 290 and "singlet mass" 380 (see Fig. 1).

the results obtained by P. O. Brundell and B. Enander.[26] Using an exponential potential with the same range (real, not "effective") in singlet and triplet states and determining the parameters (range, triplet and singlet binding constants) from the low energy scattering data and the deuteron binding energy, they get a perfect agreement with the results of Lampi, Freier, and Williams. Thus in the case of an exponential potential, all the experimental data in question can be accounted for by three constants only, instead of four with other known potential forms, including Yukawa, as we have seen above.

We are indebted to Mr. V. Grinvalds and Dr. Joachim v. Schmidt for skilled numerical assistance. It is also a pleasure to thank Dr. P. O. Olsson for his kind interest and criticism.

Financial support from the Swedish Atomic Energy Committee is gratefully acknowledged.

[22] R. C. Mobley and R. A. Laubenstein, Phys. Rev. **80**, 309 (1950).

[23] With $a=ME_0/\hbar^2c^2$, we get with present best values $(-a)^{\frac{1}{2}}=89.46\gamma/\mu$.

[24] L. Hulthén and K. V. Laurikainen, Revs. Modern Phys. **23**, 1 (1951).

[25] The values (38) and (39) do not quite agree with the results of E. E. Salpeter, Phys. Rev. **82**, 60 (1951), Eqs. (12) and (14). Part of the difference is probably due to the fact that the underlying experimental data are not identical (compare Salpeter's Eqs. (5) and (6) with Eq. (3) above). A more detailed discussion of the shape-dependent effective range theory is deferred to a forthcoming paper on the photodisintegration of the deuteron by L. Hulthén and B. C. H. Nagel.

[26] P. O. Brundell and B. Enander, to be published.

Inelastic Scattering of Protons from Light Nuclei

DEAN B. COWIE, N. P. HEYDENBURG, AND G. C. PHILLIPS*
Department of Terrestrial Magnetism, Carnegie Institution of Washington, Washington, D. C.
(Received March 31, 1952)

An investigation has been made of inelastic scattering of 7.4-Mev protons at 90° from the following thin foil targets: Be, C^{12}, C^{13} (47 percent enriched), CaF_2, Ni, Al, and Na, and from the following gas targets: normal BF_3, enriched $B^{10}F_3$ (96 percent), N_2, O_2, CH_4, and Ne. The following energy levels in Mev were observed: Be^9 2.57; B^{10} 2.34; B^{11} 2.06; C^{12} 4.59; C^{13} 3.14, 4.03; N^{14} 2.35, 3.95; O^{16} none; F^{19} 1.53, 3.83; Ne 1.44, 4.36; Na^{23} 3.67; Al 1.02, 2.30, 2.89, 3.32, 4.48; Ni 1.44.

I. INTRODUCTION

THE investigation of inelastically scattered protons from light nuclei has proved useful for studying nuclear energy levels.[1,2] Although many light nuclei have been studied by inelastic scattering, no single investigation has surveyed most of these nuclei. Since the published cyclotron scattering data have not always agreed with the nuclear energy levels identified in disintegration experiments, it was believed desirable to resurvey as many of the nuclei as possible with a single technique. Furthermore, possible cyclotron energies might be expected to excite high angular momenta states in nuclei that might not appear in studies with more precise, but lower, bombarding energies available with electrostatic generators.

Consequently a study has been made of the elastic and inelastic scattering of 7.4-Mev protons at 90° to the incident beam for the stable elements through aluminum, with the exception of lithium and magnesium. In addition to the calculation of energy levels from the inelastically scattered proton groups, the relative cross sections of the groups have been determined and in the case of the gas targets, the absolute cross sections for the elastically scattered protons were obtained.

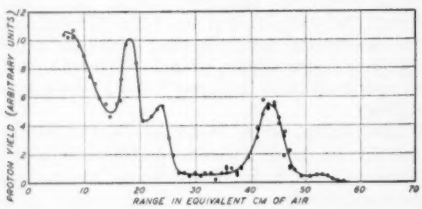

FIG. 1. Proton and deuteron groups for the reaction $Be^9(p,p)Be^{9*}$ and $Be^9(p,d)Be^8$. Ranges given in equivalent cm of air.

II. APPARATUS AND EXPERIMENTAL TECHNIQUES

The external beam of protons from the 60-inch cyclotron at this laboratory was used to bombard the targets. Passage of the beam through the fringing field of the magnet assured considerable homogeneity of the beam energy. The target was 15 feet from the point of emergence of the beam from the electrostatic beam extractor. One-inch and ¼-inch diameter collimating aperture holes were placed in the path of the beam at distances of 8.3 feet and 10 inches, respectively, from the target position. The beam passed through the target chamber and into a Faraday cage where the collected charge was measured accurately by means of a simple current integrator consisting of a "glass-mike" condenser and an electroscope. The beam current was about 0.005 microampere.

The target chamber was formed from a brass block and was sealed with rubber gaskets to the vacuum tube passing the beam and to the Faraday cage. For the gas target experiments, the chamber was sealed on beam entrance and exit sides with brass plates having, respectively, ¼- and ⅜-inch holes covered with 0.85-cm air-equivalence nickel foils. Two opposite ports at 90° to the beam direction allowed the mounting and quick removal of the thin targets supported on foils and allowed the emergence of fast particles through a nickel foil of 1.7-cm air equivalence. The particles were detected by a pair of coincidence proportional counters whose entrance port was sealed with a 1.7-cm air-equivalence nickel foil. The voltage on the counters was adjusted so that coincidences were only obtained for end-of-the-range protons. The coincidence detection was necessary because of the relatively high background near the cyclotron compared to the low counting rates for scattered protons from thin targets. Aluminum absorber foils, to measure the range of the particles, could be inserted between the 90° exit port and the counters. The foils were changed remotely by means of a wheel and selsyn system so that 24 range positions could be measured without entering the cyclotron room or interrupting the beam. The foils were weighed on a microbalance to one part in 500.

The electronic system for the counters consisted of two Los Alamos type Model 500 amplifiers of rise time 0.1 microsecond and a standard Rossi coincidence circuit

* Research Fellow, Carnegie Institution of Washington.

[1] Powell, May, Chadwick, and Pickavance, Nature **145**, 893 (1940); Heitler, May, and Powell, Proc. Roy. Soc. (London) **190**, 180 (1947); K. E. Davis and E. M. Hafner, Phys. Rev. **73**, 1473 (1948); H. W. Fulbright and R. R. Bush, Phys. Rev. **74**, 1323 (1948); H. E. Gove and J. A. Harvey, Phys. Rev. **82**, 658 (1951).

[2] Reilley, Allen, Arthur, Bender, Ely, and Hausman, Phys. Rev. **82**, 658 (1951).

with time resolution of 0.2 microsecond. The coincidences were scaled by a scale of 64 circuit and recorded.

Targets of sodium were made by evaporating in vacuum onto 0.17-cm air-equivalent nickel foils. India ink and a solution of finely divided C^{13} (47 percent) enriched carbon were painted on similar nickel foils for the normal C and C^{13} enriched targets, respectively. The aluminum and beryllium targets were thin foils of these elements. All gas targets were at a pressure of 9 inches of mercury.

The ranges, as calculated by means of the weighed aluminum absorbers, were checked by observing proton groups from the reaction $B^{10}(d,p)B^{11}$. For this experiment the apparatus was installed on the electrostatic generator and a thin target of evaporated boron (enriched to 96 percent B^{10} and supplied by the Isotopes Division AEC, Oak Ridge) was bombarded by 1-Mev deuterons. The Q-values calculated for the four longest range groups from the range data agreed with those reported by Buechner and Van Patter.[3]

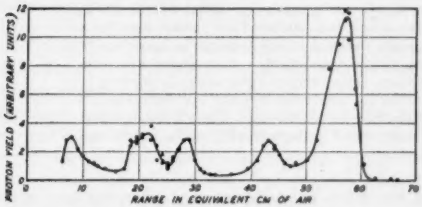

FIG. 2. Proton groups for the reaction $Al^{27}(p,p)Al^{27*}$. Ranges given in equivalent cm of air.

III. RESULTS AND CONCLUSIONS

Range curves of the charged particle groups are shown in Figs. 1, 2, and 3 for beryllium, aluminum, and neon, respectively. These curves are representative of those taken for foil and gas targets. Probable errors have not been indicated on the experimental points; however, the points of the group peaks represent several hundred counts.

The extrapolated ranges of the proton groups were measured in terms of the accurately weighed aluminum absorber foils by using an air equivalence of 1.52 mg/cm² per cm of air. The part of the range in the target gas (for gas targets only), the part in air, the part in the two nickel foils, and the average range in the counters, was added. Corrections for the variation of aluminum stopping power with range, corrections for range straggling, and angular straggling were applied and the energy of the proton groups obtained.[4]

The beam energy at the target was measured in each case by the elastically scattered groups. For the foil

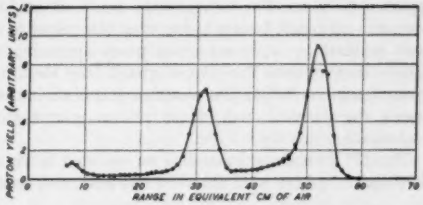

FIG. 3. Proton groups for the reaction $Ne^{20}(p,p)Ne^{20*}$. Ranges given in equivalent cm of air.

targets this energy was 7.37±0.10 Mev, while for the gas target it was 7.17±0.10 Mev.

The Q-values are presented in Table I as excited levels of the assigned nuclei. In the case of groups of uncertain origin the most reasonable reaction was tried and the Q-value calculated. The Q-values reported in the review articles by Hornyak *et al.*,[5] Alburger and Hafner,[6] and Reilley *et al.*[2] are included for comparison.

For the gas targets several integral type range curves were obtained on the elastic scattered proton groups. These data allowed the calculation of absolute cross sections for these reactions. The relative intensities of the shorter range groups were compared to the longest range group by graphical integration under the peaks of the range curves. These data are also given in Table I.

Most of the proton groups corresponded to previously

TABLE I. Summary of energy level values.

Nucleus	Target	Energy level (Mev)	Reported values (Mev)	Y_i/Y_e[a]	Cross section in barns
Be^9	Be^9 foil	2.87	2.42[b]	1.36	
B^{10}	$B^{10}F_3$ gas	0			0.44
B^{10}	$B^{10}F_3$ gas	2.34	2.14[b]		
B^{11}	normal BF_3 gas	0			0.44
B^{11}	normal BF_3 gas	2.06	2.14[b]		
C^{13}	india ink on Ni foil	4.59	4.47[b]		
C^{12}	CH_4	0			0.84
C^{13}(47%)	soot on Ni foil	3.14	3.10[b]		
		4.03	3.70[b]		
N^{14}	N_2 gas	0			0.54
N^{14}	N_2 gas	2.35	2.3[b]	0.05	0.027
N^{14}	N_2 gas	3.93	3.9[b]	0.13	0.070
O^{16}	O_2 gas	0			0.61
O^{16}	O_2 gas	no levels observed			
F^{19}	BF_3 gas	0			0.36
F^{19}	$B^{10}F_3$ and $^{11}BF_3$ gas	1.49	1.4[b]	0.30	0.11
F^{19}	$B^{10}F_3$ and BF_3 gas	3.90	not reported	0.07	0.025
Ne^{20}	neon gas	0			0.48
Ne^{20}	neon gas	1.44	1.5[b]	0.63	0.30
Ne^{20}	neon gas	4.36	4.2[b]	0.04	0.019
Na^{23}	Na on Ni foil	3.67	3.45[c]		
Al^{27}	Al foil	1.02	0.985[d]	0.13	
Al^{27}	Al foil	2.30	2.25[d]	0.11	
Al^{27}	Al foil	2.89	2.57[d]	0.11	
			3.04		
Al^{27}	Al foil	3.32	3.377[d]	0.05	
Al^{27}	Al foil	4.48	4.46[d]	0.10	
Ni	Ni foil	1.44	1.475[d]	0.12	

[a] Relative yield of inelastic to elastic scattered groups.
[b] See reference 5.
[c] See reference 6.
[d] See reference 2.

[3] W. W. Buechner and D. M. Van Patter, Phys. Rev. **79**, 240 (1950).
[4] M. S. Livingston and H. H. Bethe, Rev. Modern Phys. **9**, 245 (1937).
[5] Hornyak, Lauritsen, Morrison, and Fowler, Revs. Modern Phys. **22**, 291 (1950).
[6] D. E. Alburger and E. M. Hafner, Revs. Modern Phys. **22**, 373 (1950).

reported Q-values. For Be^9 only the one level at 2.57 Mev was observed. Levels higher than this might have been masked by a strong alpha-group appearing at ranges shorter than the proton group. The deuteron group from the $Be^9(p,d)Be^8$ reaction was observed between the inelastic and elastic proton groups with comparable intensity.

The C^{13} groups corresponding to reported levels at 3.10 and 3.70 Mev were observed but were very weak.

There were no groups in O^{16} for the energy region covered (to 4.6 Mev).

A new level at 3.90 Mev was found for fluorine in addition to the previously reported level at 1.4 Mev. This group appeared for both the BF_3 and CaF_2 targets.

Only natural neon gas was used, so the two observed levels were assigned to the most abundant isotope Ne^{20} (90 percent).

PHYSICAL REVIEW VOLUME 87, NUMBER 2 JULY 15, 1952

A Study of the Electron Traps in Zinc Sulfide Phosphor

ALAN W. SMITH* AND JOHN TURKEVICH
Frick Chemical Laboratory, Princeton University, Princeton, New Jersey
(Received March 17, 1952)

The thermoluminescence characteristics of a hexagonal zinc sulfide phosphor, copper activated, were measured as a function of the wavelength of the exciting light. The glow curve had maxima at 120, 220, and 280°K. It was found that the heights of these maxima at saturation varied with the wavelength of the exciting light, reaching the greatest values at 4270A for the 120°K maximum, 4400A for the 220°K maximum, and 4500A for the 280°K maximum. When the sample was irradiated with 4400A light for a definite time interval and then irradiated with monochromatic radiation of either shorter or longer wavelength for another time interval, it was found that the subsequently measured glow curve showed a decrease in the heights of the maxima from that with 4400A light alone. Since the glow curve can be interpreted as a process of emptying electrons from traps, the above results are interpreted to mean that light which is capable of filling the traps is also capable of stimulating electrons out of the traps. There is a long wavelength limit beyond which irradiation does not affect electrons present in traps. It is 0.7 micron for the trap represented by the 280°K maximum.

INTRODUCTION

THERMOLUMINESCENCE experiments have been used to characterize phosphors.[1-4] In these experiments a phosphor is excited with radiation for a definite period of time, the exciting light is removed, the material is heated at a constant rate, and the light output is measured as a function of the temperature of the phosphor. The glow curve so obtained is often characterized by the presence of peaks which can be interpreted in the following way: The position of the peaks on the temperature scale is a measure of the energy depth of trapped electrons in the solid, while the area under the peak often indicates the number of electrons transferred into these traps by the exciting light. It is the purpose of this investigation to study the the process of the filling and the emptying of the electron traps in a hexagonal zinc sulfide, copper activated, as a function of the wavelength of the exciting light.

EXPERIMENTAL PROCEDURE

The phosphor used in these studies was a copper-activated hexagonal zinc sulfide obtained from Leverenz of the RCA Laboratories. The phosphor was settled with ethanol in a layer about 1 mm thick on a flat-bottomed glass tube. This tube was suspended in a cavity in a copper cylinder which in turn was suspended in a Dewar flask. The phosphor could be maintained at the temperature of liquid air or heated at a rate of about 0.017°K. The temperature of the phosphor was measured by means of a chromel alumel thermocouple buried in the phosphor layer.

The phosphor was excited by monochromatic light either from a carbon arc, 100-candlepower Point-o-lite lamp or a globar. Either a Gaertner glass monochromator or a rock salt monochromator (Wadsworth mounting) was used to give monochromatic light. The current from the photomultiplier tube was amplified by means of a dc amplifier and recorded on a Brown potentiometer. No filter was used in measuring the light output of the phosphor since the emission band in the samples used was exclusively in the green region. Attempts to detect the blue band, which sometimes occurs in these phosphors, by spectral isolation with a 35D Wratten filter were unsuccessful.

RESULTS AND DISCUSSION

A typical glow curve for the phosphor sample used in these experiments is shown in Fig. 1. The important features are the three peaks at about 115°K, 225°K, and 280°K and the shoulder at about 180°K. Under

* AEC Predoctoral Fellow, 1949–50.
[1] H. W. Leverenz, *An Introduction to Luminescence of Solids* (John Wiley & Sons, Inc., New York, 1950).
[2] G. F. J. Garlick, *Luminescent Materials* (Oxford University Press, London, 1949).
[3] J. T. Randall and M. H. F. Wilkins, Proc. Roy. Soc. (London) **A184**, 365 (1945).
[4] F. Urbach, Wien. Ber. **11a**, 139, 363 (1930).

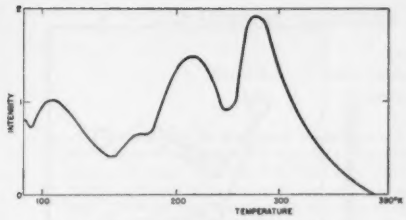

FIG. 1. Typical glow curve for ZnS:Cu.

different excitation conditions the positions of the peaks varied by as much as 20°K, but the reproducibility under the same condition was about 3°K.

The usual hexagonal form of zinc sulfide is characterized by two glow peaks, one in the region 120–160°K and the other in the region 210–240°K.[2,3] An additional peak in the region 280–320°K is found when copper is added as an activator. The glow curves obtained in this investigation is therefore very similar to that obtained by previous workers.

Urbach[4] and Randall and Wilkins[3] have worked out the relationships between the temperature of the glow peak and the energy of the corresponding electron trap. These relationships depend on whether a first- or second-order decay law is followed. In the sample studied the decay order was intermediated between first and second order. Since the variation in peak position under different excitation conditions is as great as the variation in the different formulas, the approximate Randall Wilkins formula was used: $E=T/500$, where E is the energy depth of the trap in electron volts and T is the temperature of the glow peak in degrees Kelvin. The energy depths of the traps are found to be 0.2–0.3 ev, 0.42–0.46 ev, and 0.54–0.60 ev.

The area under the glow curve is a measure of the number of electrons that left the traps by a radiative process. The number of electrons that were actually in traps may be greater than this because nonradiative transitions are possible. Since the breadth of the peaks is constant, the value of the height can be used as a measure of the area under the peaks. This can be used as an approximation to the number of electrons excited into the traps under different conditions, if one assumes the ratio of radiative to nonradiative transitions on emptying the traps is independent of the number of electrons in traps.

The effect of the wavelength of the exciting light on the position of the glow peaks on the temperature scale and their heights is given in Fig. 2. The phosphor was excited through a Gaertner monochromator with the carbon arc. The mean band width of the exciting light was 200A. The excitation time was such that a longer time of excitation made no difference in the glow curves for exciting light of wavelengths less than 5100A. For these wavelengths the time ranged from one-half to two hours. For excitation with wavelengths greater than 5100A, a four-hour exposure was used. Decreasing the intensity of the exciting light (4500A) by a factor of four only affected the glow curve slightly in the vicinity of the 120°K peak. This effect is due to thermal stimulation during excitation at 90°K competing with photostimulation. The saturation of the deeper traps is not affected by intensity of illumination in the range of light intensities used in our experiments. Thermal stimulation affects only the shallow traps, for the glow curve of a phosphor, left for two hours at liquid air temperature after irradiation, was appreciably lower only in the 120°K range. The position of the 220°K peak is definitely affected by the wavelength of light used for excitation (Fig. 2, upper section). This is interpreted to indicate that there is a number of traps associated with the 220°K peak, and these are populated in different ways depending on conditions of excitation. The dependence of the position of the 280°K peak is less marked while the position of the 120°K peak could not be measured with sufficient accuracy to determine its wavelength variation. On the other hand, the heights of the three glow peaks at saturation are markedly affected by the wavelengths of the exciting light (Fig. 2, lower section). For wavelengths greater than 5000A the heights of these glow peaks at saturation are very small. As one decreases the wavelength, the heights pass through a maximum and attain at 4000A a value two-thirds of the maximum. The peak height for the three different peaks has a slightly different wavelength dependence in that the 280°K peak has maximum height at saturation for 4500A, the 220°K peak at 4400A, and 120°K peak at 4300A. These results can be interpreted in two ways. There may be a slightly different absorp-

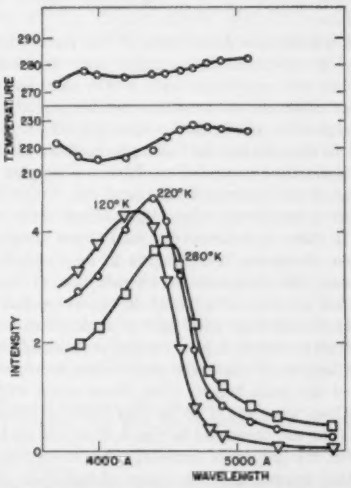

FIG. 2. Intensity and temperature of glow peaks at saturation *versus* wavelength of exciting light.

tion band associated with each peak in the glow curve, and this absorption band determines how many electrons get into the particular trap and consequently how many come out in a radiative process. The other possibility is that the exciting light both sends electrons into and spills them out of traps and that the wavelength efficiency of either or both of these processes varies from trap to trap.

To check this point the phosphor was irradiated with 4400A light until saturation, and this irradiation was followed by either a 3900A or a 4900A irradiation. As is seen from Fig. 3 re-irradiation at 3900A depresses the 280°K and 220°K peaks and leaves the height of the 120°K peak unchanged. On the other hand, if the phosphor after being saturated with 4400A light is re-irradiated with 4900A the whole glow curve drops. These experiments indicate that light can empty electrons from traps and that this process is wavelength dependent. Consequently, the variation of the "saturation" glow curve with wavelength is due to differences in the rate of filling and of emptying traps at different wavelengths.

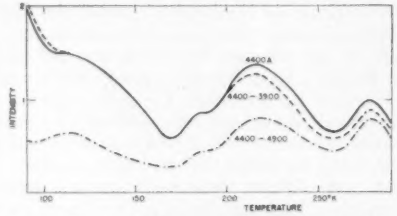

FIG. 3. Effect on the glow curve of irradiation with light of other wavelengths after 4400A light.

The wavelength dependence of the photoprocess of emptying electrons from traps was studied. The phosphor was irradiated with 4400A light for a half-hour at liquid air temperature thereby partially filling the traps with electrons. It was allowed to stand at liquid air temperature for half an hour, and a glow curve was obtained at standard conditions. This glow curve was taken as a standard curve and the results of subsequent experiments were standardized with respect to it. In these experiments designed to test the efficiency of light of various wavelengths in emptying trapped electrons, the phosphor after irradiation at liquid air for a half an hour with 4400A light was treated for an additional half-hour with light of various wavelengths from 5000 to 8000A. A glow curve was obtained and from it the heights of the three peaks were measured. The ratio of the peak heights after illumination with light of various wavelength to heights without subsequent irradiation are presented in Fig. 4. It should be pointed out that the process of removal of electrons from traps is a rate process, and the choice of half-hour time for determination of light efficiency is arbitrary. Furthermore, as one goes to longer wavelength the intensity

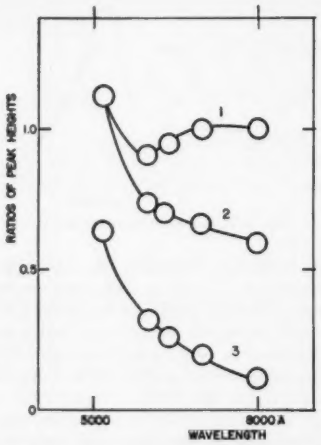

FIG. 4. Effect of subsequent radiation on glow curves of sample irradiated at 4400A. Ratios of glow peaks after second irradiation to those of a standard glow curve are plotted *versus* the wavelength of the second irradiation. Curve 1—280°K peak; curve 2—220°K peak; curve 3—120°K peak.

of the source (Point-o-light lamp with temperature 2920°K) increases so that there are more photons impinging on the solid at the longer wavelengths per unit time. Because of this the results are of qualitative nature. The 280°K peak decreases when irradiated with light of wavelength less than 7000A, and light of wavelength greater than 7000A though of greater intensity does not affect the 280°K peak. We can thus conclude that 7000A is a threshold of light energy necessary to remove electrons in the 0.6 electron volt trap. Both 220°K and 120°K peaks are diminished in height by subsequent radiation of wavelength greater than 5000A. The threshold for emptying electrons from traps by both radiative and nonradiative processes is beyond 8000A and was not determined. The threshold for emptying the traps by a radiative process (stimulation) was found to be 4 microns. The thresholds for two processes are not necessarily the same.

Mott and Gurney[8] have discussed the relation between the optical absorption spectra due to an impurity center and the thermal activation energy of an electron in a center. Defining an optical activation energy as $E_0 = h\nu$, where ν is the minimum frequency of absorption, they estimate for alkali halides that the optical activation energy is of the order of two times the thermal activation energy. This is in agreement with the results found here in that the long wavelength of light capable of stimulating electrons from the 0.6 electron volt trap is 0.7 micron (1.7 electron volts) or almost three times the thermal activation energy.

[8] N. F. Mott and R. W. Gurney, *Electronic Processes in Ionic Crystals* (Oxford University Press, London, 1940).

The Classical Equations of Motion of Point Particles. I

PETER HAVAS
Department of Physics, Lehigh University, Bethlehem, Pennsylvania
(Received August 13, 1951)

The problem of the relation of field theory and action at a distance is investigated for the neutral vector and scalar meson theories. The equations of motion of point particles with half-advanced, half-retarded interaction are found using the field theoretical methods developed for retarded interaction; they include an integral over the entire motion of the particle in analogy to an integral over the past motion in the retarded case. These are inadmissible from the point of view of action at a distance and a new set of equations is postulated. This new set is derivable from a variational principle analogous to Fokker's in electrodynamics for the symmetric case, and energy-momentum tensors guaranteeing the conservation laws can be defined. The application of the Wheeler-Feynman method to the equations of the symmetric case leads to the equations of the retarded case only for the field theoretical equations, but to slightly different ones for those of action at a distance. Some implications of these results are discussed.

I. INTRODUCTION

ONE of the the main problems of present-day theoretical physics is the satisfactory description of the behavior and interrelation of the elementary particles. While there is no doubt that such a description has ultimately to be quantum theoretical, "one ought to separate the difficulties as far as possible . . . and attack each one separately and for the purpose of this attack we may very well work with the concepts of classical mechanics in some cases."[1]

The problem of the interaction of point charges with the electromagnetic field has recently been reinvestigated extensively. The equations of motion have been studied from two different viewpoints. One is that of field theory, which considers the *total* field at all points in space to be the fundamental physical quantity and the point charges as singularities of the field.[2,3] The other is that of action at a distance, which considers only the forces exerted on a charge by *other* charges to be physically meaningful.[4–7]

In the case of electrodynamics the equations of motion for slowly moving particles were of course known experimentally to begin with. The problem was to account for the force of radiative reaction first found by Lorentz[8] and also well verified experimentally, and to avoid the appearance of infinite expressions in Lorentz's equations of motion for point charges. In the field-theoretical derivations these equations including the radiative reaction terms are obtained only if one takes the field produced by a point charge to be the retarded field; but equations of motion without these terms are obtained if one uses half the sum of retarded and advanced fields. The first attempts at a description of the motion of charged particles in terms of action at a distance were not able to obtain the radiation damping, but did succeed in showing that such a theory was entirely self-consistent. Wheeler and Feynman,[7] using half-advanced, half-retarded fields, were, however, able to obtain the damping terms by considering the field produced by all particles and imposing a condition on it. It was then pointed out[9] that the need for the exclusive use of retarded fields for the explanation of the radiative reaction arose only in the field-theoretical derivations for the one-particle problem, but that the considerations of Wheeler and Feynman on the total field due to all particles are applicable to field theory as well as to the theory of action at a distance. There too they lead to the radiative reaction terms even in the case of half-advanced, half-retarded fields. Therefore, in spite of the fundamentally different underlying physical ideas, both field theory and action at a distance, using fields symmetric in time, lead to the same equations of motion.

Much less work has been done on the problem of the motion of point particles interacting through fields other than electromagnetic. The case of nucleons interacting through a neutral vector meson field was treated by Bhabha.[10] The generalized wave fields introduced by Fierz[11] (suitable for the description of quanta of higher spin) were taken up later,[12,13] as were charged meson fields.[14] All of these papers are based on field theory and, following the method of Dirac,[2] take the conservation law for the energy-momentum tensor of the field in empty space as their starting point. Contrary to the case of electrodynamics, no experimental evidence is available on the equations of motion of

[1] P. A. M. Dirac, *The Relation of Classical to Quantum Mechanics*, Second Summer Seminar of the Canadian Mathematical Congress, 1949.
[2] P. A. M. Dirac, Proc. Roy. Soc. (London) **A167**, 148 (1938).
[3] L. Infeld and P. R. Wallace, Phys. Rev. **57**, 797 (1940).
[4] J. Frenkel, Z. Physik **32**, 518 (1925).
[5] A. D. Fokker, Z. Physik **58**, 386 (1929).
[6] J. L. Synge, Trans. Roy. Soc. Can. **34**, 1 (1940).
[7] J. A. Wheeler and R. P. Feynman, Revs. Modern Phys. **17**, 157 (1945); and **21**, 425 (1949).
[8] H. A. Lorentz, *Collected Papers* (M. Nijhoff, The Hague, 1936), Vol. II, pp. 281 and 343. Also *The Theory of Electrons* (B. G. Teubner, Leipzig, Germany, 1909), pp. 49 and 253.
[9] P. Havas, Phys. Rev. **74**, 456 (1948).
[10] H. J. Bhabha, Proc. Roy. Soc. (London) **A172**, 384 (1939).
[11] M. Fierz, Helv. Phys. Acta **12**, 3 (1939).
[12] H. J. Bhabha and Harish-Chandra, Proc. Roy. Soc. (London) **A185**, 250 (1946).
[13] Harish-Chandra, Proc. Roy. Soc. (London) **A185**, 269 (1946).
[14] M. Fierz, Helv. Phys. Acta **14**, 257 (1941); K. J. LeCouteur, Proc. Cambridge Phil. Soc. **45**, 429 (1949).

particles moving in meson and other generalized wave fields. Therefore, the problem taken up by these papers was to find equations of motion leading to conservation laws for the system of particles and field.

In all these papers the field of each particle was taken as purely retarded; the equations of motion were then found to contain radiation terms similar to the electrodynamic ones. In addition, however, there appeared terms depending on the entire previous motion of the particles.

In this paper we shall discuss the relation of the equations of motion obtained from the points of view of field theory and of the theory of action at a distance for particles interacting through neutral vector and scalar meson fields. A second paper will deal with these questions for particles interacting through charged fields.

As a preliminary step we shall obtain the field-theoretical equations of motion if the field is taken as half-retarded, half-advanced. These equations do not contain any radiation terms; however, the self-action of the particle appears explicitly as an integral over its entire motion. The question of the meaning of such terms in field theory is discussed.

Then the problem of the motion of such particles is taken up from the point of view of action at a distance. Obviously in such a theory there is no place for self-action terms of the above type and it is proposed to omit them from the postulated equations of motion. It is then shown that the remaining equations form a completely self-consistent set, are derivable from a variational principle[15] similar to the one discovered in electrodynamics by Fokker,[5] and permit the construction of an energy-momentum tensor of the "adjunct" field theory again similar to electrodynamics.[4,6,7] However, just as the postulated equations are not identical with the ones arising from field theory, so the application of the considerations of Wheeler and Feynman[7] does not furnish exactly the same equations as field theory using retarded fields only, nor does it agree with other postulated equations of action-at-a-distance theory assuming retarded interaction only.

It is noteworthy that while in electrodynamics action at a distance and a "divergence-free" field theory lead to exactly the same result if fields symmetric in time are used, we obtain slightly different sets of equations in meson theory. They are both finite and cannot be changed into each other by arbitrary omission or addition of terms without destroying their self-consistency. There is no experimental evidence on which a choice can be based, but the fact that different basic viewpoints might lead to different finite equations might have a bearing on some current quantum theoretical procedures of obtaining finite equations.

[15] For the vector meson case this variational principle has independently been suggested from different considerations by H. Kanazawa, Prog. Theoret. Phys. **5**, 1050 (1950) and H. Steinwedel, S.-B. Heidelberger Akad. Wiss., math.-naturwiss. Kl. 281 (1950).

II. THE EQUATIONS OF MOTION

We shall first outline the field-theoretical derivation of the equations of motion of a particle interacting with a neutral vector meson field or a neutral scalar meson field as first given by Bhabha[10] and Harish-Chandra,[13] respectively. With minor changes we shall follow the notation of these papers.

We consider a four-space with coordinates x_μ, Greek letters taking the values 0, 1, 2, 3, where x_0 is the time coordinate. Repetition of an index implies summation over this range. If u_μ is any vector, we shall write u for $+(u_\mu u^\mu)^{\frac{1}{2}}$. The velocity of light is taken as unity. The metric tensor $g_{\mu\nu}$ is given by

$$g_{\mu\nu}=0 \text{ if } \mu\neq\nu, \quad g_{00}=-g_{11}=-g_{22}=-g_{33}=1. \quad (1)$$

The vector meson field is assumed to be described by potentials U_μ and field strengths $G_{\mu\nu}$ which satisfy the equations[16]

$$G_{\mu\nu}=\partial U_\nu/\partial x^\mu-\partial U_\mu/x^\nu, \quad \partial G_{\mu\nu}/\partial x_\mu+\chi^2 U_\nu=4\pi j_\nu. \quad (2a)$$

Here $\chi=\mu/\hbar$, μ being the rest mass of the meson, which however does not appear explicitly in classical theory. j_ν is the mesic charge-current density, which we take for a point particle to be

$$j_\nu=g\int_{-\infty}^{\infty} v_\nu(\tau)\delta(x_0-z_0)\delta(x_1-z_1) \times\delta(x_2-z_2)\delta(x_3-z_3)d\tau, \quad (3a)$$

where z_ν are the coordinates of the particle, v_ν is its four-velocity, τ its proper time, g its "mesic charge," and δ Dirac's δ-function.

Similarly we have for the scalar meson field a scalar potential U and field strengths F_μ whose equations are

$$F_\mu=-\partial U/\partial x^\mu, \quad -\partial F_\mu/\partial x_\mu+\chi^2 U=4\pi\rho, \quad (2b)$$

with the charge density

$$\rho=g\int_{-\infty}^{\infty}\delta(x_0-z_0)\delta(x_1-z_1)\delta(x_2-z_2)\delta(x_3-z_3)d\tau. \quad (3b)$$

From (2) we get respectively,

$$\partial^2 U_\nu/\partial x_\mu\partial x^\mu+\chi^2 U_\nu=4\pi j_\nu, \quad (4a)$$

$$\partial^2 U/\partial x_\mu\partial x^\mu+\chi^2 U=4\pi\rho. \quad (4b)$$

These equations are solved with the help of a Green's function G in the form

$$U_\nu(x_\rho)=\int_{-\infty}^{\infty} j_\nu(x_\rho')G(x_\rho, x_\rho')dx_\rho', \quad (5a)$$

$$U(x_\rho)=\int_{-\infty}^{\infty}\rho(x_\rho')G(x_\rho, x_\rho')dx_\rho', \quad (5b)$$

where x_ρ' stands for all four variables and dx_ρ' for the

[16] In the following all Eqs. (a) refer to vector mesons, Eqs. (b) to scalar mesons.

product of the differentials. The Green's function corresponding to a retarded potential is given by

$$ {}_rG(x_\rho, x_\rho') = \begin{cases} 2\delta(u^2) - (\chi/u)J_1(\chi u) & u_0 \gtrless u_r \\ 0 & |u_0| < u_r, \\ 0 & u_0 < -u_r \end{cases} \quad (6) $$

and the one corresponding to an advanced potential by

$$ {}_aG(x_\rho, x_\rho') = \begin{cases} 0 & u_0 \gtrless u_r \\ 0 & |u_0| < u_r, \\ 2\delta(u^2) - (\chi/u)J_1(\chi u) & u_0 < -u_r \end{cases} \quad (7) $$

where $u_\rho = x_\rho - x_\rho'$, J_1 is the Bessel function of order 1, and

$$ u_r = \sum_1^3 (-u_k u^k)^{\frac{1}{2}}. \quad (8) $$

We note that we can also take a Green's function corresponding to a half-retarded, half-advanced potential[17]

$$ {}_sG = \tfrac{1}{2}({}_rG + {}_aG) = \begin{cases} \delta(u^2) - \tfrac{1}{2}(\chi/u)J_1(\chi u) & u_0 \gtrless u_r \\ 0 & |u_0| u_r \\ \delta(u^2) - \tfrac{1}{2}(\chi/u)J_1(\chi u) & u_0 < -u_r. \end{cases} \quad (9) $$

Introducing (6), (7), or (9) into (4a) and (4b), respectively, and using the notation

$$ s_\mu = x_\mu - z_\mu(\tau), \quad \kappa = s_\mu v^\mu, \quad (10) $$

we obtain the following expressions for the potentials

$$ {}_{\rm ret}U_\nu(x_\rho) = g\frac{v_\nu({}_r\tau)}{\kappa({}_r\tau)} - g\int_{-\infty}^{{}_r\tau} \frac{v_\nu}{s} J_1(\chi s)\,d\tau, \quad (11a) $$

$$ {}_{\rm adv}U_\nu(x_\rho) = -g\frac{v_\nu({}_a\tau)}{\kappa({}_a\tau)} - g\int_{{}_a\tau}^{\infty} \frac{v_\nu}{s} J_1(\chi s)\,d\tau, \quad (12a) $$

$$ {}_{\rm sym}U_\nu(x_\rho) = \tfrac{1}{2}g\left(\frac{v_\nu({}_r\tau)}{\kappa({}_r\tau)} - \frac{v_\nu({}_a\tau)}{\kappa({}_a\tau)}\right) - \tfrac{1}{2}g\int_{-\infty}^{\infty} \frac{v_\nu}{s} J_1(\chi s)\,d\tau + \tfrac{1}{2}g\int_{{}_r\tau}^{{}_a\tau} \frac{v_\nu}{s} J_1(\chi s)\,d\tau, \quad (13a) $$

$$ {}_{\rm ret}U(x_\rho) = g\frac{1}{\kappa({}_r\tau)} - g\int_{-\infty}^{{}_r\tau} \frac{1}{s} J_1(\chi s)\,d\tau, \quad (11b) $$

$$ {}_{\rm adv}U(x_\rho) = -g\frac{1}{\kappa({}_a\tau)} - g\int_{{}_a\tau}^{\infty} \frac{1}{s} J_1(\chi s)\,d\tau, \quad (12b) $$

$$ {}_{\rm sym}U(x_\rho) = \tfrac{1}{2}g\left(\frac{1}{\kappa({}_r\tau)} - \frac{1}{\kappa({}_a\tau)}\right) - \tfrac{1}{2}g\int_{-\infty}^{\infty} \frac{1}{s} J_1(\chi s)\,d\tau + \tfrac{1}{2}g\int_{{}_r\tau}^{{}_a\tau} \frac{1}{s} J_1(\chi s)\,d\tau. \quad (13b) $$

${}_r\tau$ and ${}_a\tau$ are the proper times of the "retarded" and "advanced" points respectively, i.e., the points on the world line such that $s_\mu s^\mu = 0$ and $s_0 > 0$ and < 0, respectively.[18]

The energy-momentum tensors of the fields are given by

$$ 4\pi T_{\mu\nu} = G_{\mu\sigma}G^\sigma{}_\nu + \tfrac{1}{4}g_{\mu\nu}G_{\sigma\rho}G^{\sigma\rho} + \chi^2 U_\mu U_\nu - \tfrac{1}{2}\chi^2 g_{\mu\nu}U_\rho U^\rho, \quad (14a) $$

$$ 4\pi T_{\mu\nu} = F_\mu F_\nu - \tfrac{1}{4}g_{\mu\nu}(F_\sigma F^\sigma - \chi^2 U^2). \quad (14b) $$

Here we have to insert the total fields and potentials, including the field of the particle itself. Following the method of Dirac,[2] Bhabha and Harish-Chandra now enclose the world line of the particle by a narrow tube, the radius of which will in the end be made to tend to zero. The equations of motion are now derived from the condition that the flow of energy and momentum out of a portion of the tube in the presence of an external field as calculated by using Eqs. (14) shall only depend on the conditions at the two ends of the tube, that is, that it shall be a perfect differential. We put

$$ G_{\mu\nu} = {}_{\rm ext}G_{\mu\nu} + {}_{\rm ret}G_{\mu\nu}, \quad (15a) $$

$$ U = {}_{\rm ext}U + {}_{\rm ret}U, \quad F_\mu = {}_{\rm ext}F_\mu + {}_{\rm ret}F_\mu, \quad (15b) $$

respectively, the subscript "ext" denoting the external field. The equations of motion obtained are then

$$ M\dot v^\mu - \tfrac{2}{3}g^2(\ddot v^\mu + v^\mu \dot v^2) - g^2\chi^2 v_\nu \int_{-\infty}^{\tau} \frac{s^\mu v^\nu(\tau') - s^\nu v^\mu(\tau')}{s^2} J_2(\chi s)\,d\tau' = g\,{}_{\rm ext}G^\mu{}_\nu v^\nu, \quad (16a) $$

$$ M\dot v^\mu - \tfrac{1}{3}g^2(\ddot v^\mu + v^\mu \dot v^2) - \tfrac{1}{2}g^2\chi^2 v^\mu + g^2\chi^2 \int_{-\infty}^{\tau} \frac{s^\mu}{s^2} J_2(\chi s)\,d\tau' + g^2\chi \frac{d}{d\tau}\left[v^\mu \int_{-\infty}^{\tau} \frac{1}{s} J_1(\chi s)\,d\tau\right] = g\,{}_{\rm ext}F^\mu + \frac{d}{d\tau}({}_{\rm ext}U v^\mu), \quad (16b), $$

where M is an arbitrary constant identified with the mass of the particle, and dots indicate differentiation with respect to τ; all field quantities are taken at the positions of the particle.

If we take instead

$$ G_{\mu\nu} = {}_{\rm ext}G_{\mu\nu} + {}_{\rm sym}G_{\mu\nu}, \quad (17a) $$

$$ U = {}_{\rm ext}U + {}_{\rm sym}U, \quad F_\mu = {}_{\rm ext}F_\mu + {}_{\rm sym}F_\mu, \quad (17b) $$

[17] This is 4π times the $\bar\Delta$-function of J. Schwinger, Phys. Rev. **75**, 651 (1949). $({}_rG - {}_aG)/4\pi$ is the well-known invariant D-function introduced by P. A. M. Dirac, Proc. Cambridge Phil. Soc. **30**, 150 (1934); see also W. Pauli, Revs. Modern Phys. **13**, 203 (1941).

[18] For a more detailed discussion of the properties of these solutions see reference 12.

a calculation exactly like the ones by Bhabha and Harish-Chandra, this leads us to

$$M\dot{v}^\mu-\tfrac{1}{2}g^2\chi^2 v_\nu\int_{-\infty}^{\infty}\frac{s^\mu v^\nu(\tau')-s^\nu v^\mu(\tau')}{s^2}J_2(\chi s)d\tau'=g_{\text{ext}}G^{\mu\nu}v^\nu, \tag{18a}$$

$$M\dot{v}^\mu+\tfrac{1}{2}g^2\chi^3\int_{-\infty}^{\infty}\frac{s^\mu}{s^2}J_2(\chi s)d\tau'+\tfrac{1}{2}g^2\chi\frac{d}{d\tau}\left[v^\mu\int_{-\infty}^{\infty}\frac{1}{s}J_1(\chi s)d\tau'\right]=g_{\text{ext}}F^{\mu\nu}+g\frac{d}{d\tau}({}_{\text{ext}}Uv^\mu). \tag{18b}$$

The expressions (15) and (17) differ only by one-half of the "radiation field" as defined in reference 12. As it was shown there to be finite on the world line of the particle, it acts just like an additional external field, so that Eqs. (18) follow from (16) without the necessity of going through any computations not treated in arriving at Eqs. (16). We only have to subtract the expressions (valid on the world line of the particle)

$$\tfrac{1}{2}({}_{\text{ret}}G_{\mu\nu}-{}_{\text{adv}}G_{\mu\nu})^0=\tfrac{2}{3}g(\ddot{v}_\mu v_\nu-v_\mu\ddot{v}_\nu)+\tfrac{1}{2}g\chi^2\left\{\int_{-\infty}^{\tau}\frac{s_\mu v_\nu(\tau')-s_\nu v_\mu(\tau')}{s^2}J_2(\chi s)d\tau'-\int_{\tau}^{\infty}\frac{s_\mu v_\nu(\tau')-s_\nu v_\mu(\tau')}{s^2}J_2(\chi s)d\tau'\right\}$$

and

$$\tfrac{1}{2}({}_{\text{ret}}U-{}_{\text{adv}}U)^0=-\tfrac{1}{2}g\chi\left\{\int_{-\infty}^{\tau}\frac{1}{s}J_1(\chi s)d\tau'-\int_{\tau}^{\infty}\frac{1}{s}J_1(\chi s)d\tau'\right\},$$

$$\tfrac{1}{2}({}_{\text{ret}}F_\mu-{}_{\text{adv}}F_\mu)^0=\tfrac{1}{3}g(\ddot{v}_\mu+v_\mu\dot{v}^2)+\tfrac{1}{2}g\chi^2 v_\mu-\tfrac{1}{2}g\chi^2\left\{\int_{-\infty}^{\tau}\frac{s_\mu}{s^2}J_2(\chi s)d\tau'-\int_{\tau}^{\infty}\frac{s_\mu}{s^2}J_2(\chi s)d\tau'\right\} \tag{19b}$$

respectively from the appropriate external fields and potentials in Eqs. (16) to arrive at Eqs. (18).

Some misunderstanding might be caused by the fact that Bhabha states that he is only considering retarded potentials "since the theory is quite symmetrical in retarded and advanced potentials." A similar statement in the original paper by Dirac[2] has been discussed previously,[9] and it was shown that the "symmetry" mentioned by Dirac (and Bhabha) is only apparent. It is due to their (formally symmetric) definition,

$$\begin{aligned}{}_{\text{ret}}G&={}_{\text{in}}G+{}_{\text{ret}}G={}_{\text{out}}G+{}_{\text{adv}}G\\&=\tfrac{1}{2}({}_{\text{in}}G+{}_{\text{out}}G)+\tfrac{1}{2}({}_{\text{ret}}G+{}_{\text{adv}}G).\end{aligned} \tag{20}$$

Clearly this is only meaningful if it is specified which of these fields is independent of the particle.[19] Once this has been done, the theory is physically no longer symmetric between retarded and advanced fields. In Eq. (15) we have identified ${}_{\text{in}}G$ with the external field; in (17) the external field would correspond to $\tfrac{1}{2}({}_{\text{in}}G+{}_{\text{out}}G)$ of Dirac and Bhabha. These different identifications must clearly lead to different equations of motion.[20]

From now on we shall assume that the external field is entirely due to other particles. Calling our particle under consideration a, we obtain finally

$$M_a\dot{v}_a^\mu-\tfrac{2}{3}g_a{}^2(\ddot{v}_a{}^\mu+v_a{}^\mu\dot{v}_a{}^2)-g_a{}^2\chi^2 v_{a\nu}\int_{-\infty}^{\tau_a}\frac{s_a{}^\mu v_a{}^\nu(\tau')-s_a{}^\nu v_a{}^\mu(\tau')}{s_a{}^2}J_2(\chi s_a)d\tau'=g_a\sum_{k\neq a}{}_{\text{ret}}G^{\mu\nu}{}^{(k)}v_a{}^\nu, \tag{21a}$$

$$\begin{aligned}M_a\dot{v}_a{}^\mu-\tfrac{1}{3}g_a{}^2(\ddot{v}_a{}^\mu+v_a{}^\mu\dot{v}_a{}^2)-\tfrac{1}{2}g_a{}^2\chi^2 v_a{}^\mu+g_a{}^2\chi^2\int_{-\infty}^{\tau_a}\frac{s_a{}^\mu}{s_a{}^2}J_2(\chi s_a)d\tau'+g_a{}^2\chi\frac{d}{d\tau_a}\left[v_a{}^\mu\int_{-\infty}^{\tau_a}\frac{1}{s_a}J_1(\chi s_a)d\tau'\right]\\=g_a\sum_{k\neq a}{}_{\text{ret}}F^{\mu(k)}+g_a\frac{d}{d\tau_a}\Big(\sum_{k\neq a}{}_{\text{ret}}U^{(k)}v_a{}^\mu\Big)\end{aligned} \tag{21b}$$

[19] This was first pointed out by T. Lewis, Phil. Mag. **36**, 533 (1945). For the subsequent discussion see P. A. M. Dirac, Phil. Mag. **39**, 31 (1948), and T. Lewis, Phil. Mag. **39**, 116 (1948).

[20] R. C. Majumdar and A. S. Apte [Phys. Rev. **74**, 538 (1948)] have used the method of reference 3 to obtain the equations of motion for neutral meson fields. Their result is in agreement with our Eqs. (16a) and (18a) except for the fact that through an oversight they inserted in the final equations of motion for the symmetric case the same integral which appears in the equations for the retarded case. Our Eqs. (16b) and (18b) however differ from their results for the scalar field, which are also in disagreement with the results of Harish-Chandra (see reference 13). This discrepancy is probably due to an uncritical application of the method of Infeld and Wallace; this question is being investigated at present by F. R. Crownfield, Jr. and the author. It was indeed found that the application of the complete method of Infeld and Wallace leads to Eqs. (16b) and (18b).

for the retarded case, and

$$M_a\dot{v}_a^\mu-\tfrac{1}{2}g_a^2\chi^2v_a{}^\mu\int_{-\infty}^{\infty}\frac{s_a{}^\mu v_a{}^\nu(\tau')-s_a{}^\nu v_a{}^\mu(\tau')}{s_a{}^2}J_2(\chi s_a)d\tau'=g_a\sum_{k\neq a}({}_{\rm ret}G^\mu{}_\nu{}^{(k)}+{}_{\rm adv}G^\mu{}_\nu{}^{(k)})v_a{}^\nu, \tag{22a}$$

$$M_a\dot{v}_a^\mu+\tfrac{1}{2}g_a^2\chi^2\int_{-\infty}^{\infty}\frac{s_a{}^\mu}{s_a{}^2}J_2(\chi s_a)d\tau'+\tfrac{1}{2}g_a^2\chi\frac{d}{d\tau_a}\Big[v_a{}^\mu\int_{-\infty}^{\infty}\frac{1}{s_a}J_1(\chi s_a)d\tau'\Big]$$
$$=g_a\sum_{k\neq a}\tfrac{1}{2}({}_{\rm ret}F^{\mu(k)}+{}_{\rm adv}F^{\mu(k)})+g_a\frac{d}{d\tau_a}\Big[\sum_{k\neq a}\tfrac{1}{2}({}_{\rm ret}U^{(k)}+{}_{\rm adv}U^{(k)})v_a{}^\mu\Big] \tag{22b}$$

for the symmetric case.

Equations (21a) and (22a) are of the same form as those of a point charge in an electromagnetic field, except for the integrals over the previous motion in the retarded case and over the entire motion in the symmetric case. Similar integrals appear in Eqs. (21b) and (22b). Physically they are due to the fact that the meson field does not necessarily propagate with the velocity of light. Therefore, the particle might "catch up" with its own field, which will act on it just like an external field. In the electromagnetic case this cannot happen, as the field propagates with the velocity of light and the particle necessarily moves with a smaller velocity.[21]

Mathematically we can raise no objection against these equations. However even from the point of view of field theory there appear to be difficulties connected with the physical interpretation. Originally fields were defined in terms of their action on test particles, i.e., fields are measured by observing the force exerted on (or motion of) some test bodies. This force depends on the charge of the test body, its position and conceivably its velocity or even acceleration, but after these quantities are specified, the force should specify the field strength uniquely. Now, however, the force depends on the previous (for the retarded case) or entire (for the symmetric case) history of the particle; two test particles will only give the same motion due to the field at a given point if they were brought to the point in the same manner. This difficulty cannot be avoided as long as we want to keep the viewpoint of field theory; as long as the total field is considered to be a basic physical quantity, its action on the particle emitting it cannot be excluded from the theory.

Clearly however such an action of a particle on itself has no meaning from the point of view of action at a distance. We propose therefore simply to omit it and to investigate if a consistent theory can be built up without it. Thus we shall postulate as the basic equations of motion

$$M_a\dot{v}_a^\mu=g_a\sum_{k\neq a}({}_{\rm ret}G^\mu{}_\nu{}^{(k)}+{}_{\rm adv}G^\mu{}_\nu{}^{(k)})v_a{}^\nu, \tag{23a}$$

$$M_a\dot{v}_a^\mu=g_a\sum_{k\neq a}\tfrac{1}{2}({}_{\rm ret}F^{\mu(k)}+{}_{\rm adv}F^{\mu(k)})$$
$$+g_a\frac{d}{d\tau_a}\Big[\sum_{k\neq a}\tfrac{1}{2}({}_{\rm ret}U^{(k)}+{}_{\rm adv}U^{(k)})v_a{}^\mu\Big] \tag{23b}$$

for the symmetric case. A possible set of equations in the retarded case would be

$$M_a\dot{v}_a^\mu-\tfrac{2}{3}g_a^2(\ddot{v}_a{}^\mu+v_a{}^\mu\dot{v}_a{}^2)=g_a\sum_{k\neq a}{}_{\rm ret}G^\mu{}_\nu{}^{(k)}v_a{}^\nu, \tag{24a}$$

$$M_a\dot{v}_a^\mu-\tfrac{1}{3}g_a^2(\ddot{v}_a{}^\mu+v_a{}^\mu\dot{v}_a{}^2)=g_a\sum_{k\neq a}{}_{\rm ret}F^{\mu(k)}$$
$$+g_a\frac{d}{d\tau_a}\Big(\sum_{k\neq a}{}_{\rm ret}U^{(k)}v_a{}^\mu\Big). \tag{24b}$$

(As the term $-\tfrac{1}{3}g_a^2\chi^2v_a{}^\mu$ of Eq. (21b) originates in the integrals of (11b) and (12b), it is omitted from (24b) together with the integrals.) Another possible set of equations would be

$$M_a\dot{v}_a^\mu=g_a\sum_{k\neq a}{}_{\rm ret}G^\mu{}_\nu{}^{(k)}v_a{}^\nu, \tag{25a}$$

$$M_a\dot{v}_a^\mu=g_a\sum_{k\neq a}{}_{\rm ret}F^{\mu(k)}+g_a\frac{d}{d\tau_a}\Big(\sum_{k\neq a}{}_{\rm ret}U^{(k)}v_a{}^\mu\Big). \tag{25b}$$

Just as in electrodynamics, the symmetric case will prove to be of more interest as it is the only one for which the equations of motion follow from a variational principle.

III. THE VARIATIONAL PRINCIPLE

The equations of motion (23a) have exactly the same form as the corresponding ones of electrodynamics. The difference in the behavior of the particles is due to the different equations for the $G_{\mu\nu}$—Eq. (2a) in the vector meson case, Maxwell's equations (which are Eqs. (2a) with $\chi=0$) in the electrodynamic case. It was first shown by Fokker[22] that both the equations of motion and the field equations of electrodynamics are a consequence of the single variational principle

$$J=\sum_i m_i\int v_i{}^\mu dv_i{}^\mu+\sum_{i<k}e_ie_k\int\int\delta(z_{i\nu}-z_{k\nu},\,z_i{}^\nu-z_k{}^\nu)$$
$$\times v_{i\mu}v_k{}^\mu d\tau_i d\tau_k=\text{extremum}, \tag{26}$$

[21] It can happen however if world lines going backward in time are admitted, as has been repeatedly suggested for a classical theory of the positron; then it represents the interaction of the electron and the positron. See P. Havas, Acta Phys. Austriaca 3, 342 (1949).

[22] See reference 5. See also the second paper of reference 7.

where the integrals are extended over the entire motion of the particles.

We propose to show similarly that both the field equations and the equations of motion of meson theory are a consequence of the variational principle

$$J=\sum_i M_i\int v_i d\tau_i+\sum_{i<k} g_i g_k\int\int {}_sG(z_i-z_k)\times v_{i\nu}v_k{}^\nu d\tau_i d\tau_k=\text{extremum} \quad (27a)$$

for the vector meson case, and

$$J=\sum_i M_i\int v_i d\tau_i-\sum_{i<k} g_i g_k\int\int {}_sG(z_i-z_k)\times v_i v_k d\tau_i d\tau_k=\text{extremum} \quad (27b)$$

for the scalar meson case. ${}_sG$ is the function defined by (9).

We introduce the abbreviations

$$U_\nu{}^{(k)}(x)=g_k\int {}_sG(s_k)v_{k\nu}d\tau_k, \quad (28a)$$

$$U^{(k)}(x)=g_k\int {}_sG(s_k)v_k d\tau_k \quad (28b)$$

with s given by (10). We also note that

$$v^2=1,\quad v_\mu v^\mu=0. \quad (29)$$

Now let the world line of particle a be altered from $z_a{}^\mu(\tau_a)$ to $z_a{}^\mu(\tau_a)+\delta z_a{}^\mu(\tau_a)$. The variation produced by this equals

$$\delta J=M_a\int\frac{v_{a\mu}\delta v_a{}^\mu}{v_a}d\tau_a+g_a\sum_{k\neq a}\int\left\{\frac{\partial U_\nu{}^{(k)}}{\partial z_a{}^\mu}v_a{}^\nu\delta z_a{}^\mu+U_\nu{}^{(k)}\frac{\partial v_a{}^\nu}{\partial v_a{}^\mu}\delta v_a{}^\mu\right\}d\tau_a, \quad (30a)$$

$$\delta J=M_a\int\frac{v_{a\mu}\delta v_a{}^\mu}{v_a}d\tau_a-g_a\sum_{k\neq a}\int\left\{\frac{\partial U^{(k)}}{\partial z_a{}^\mu}v_a\delta z_a{}^\mu+U^{(k)}\frac{v_{a\mu}\delta v_a{}^\mu}{v_a}\right\}d\tau_a \quad (30b)$$

from which we get by an integration by parts, dropping the integrated terms as the variations vanish at the limits,

$$\delta J=\int d\tau_a\delta z_a{}^\mu\left\{-M_a\frac{d}{d\tau_a}\frac{v_{a\mu}}{v_a}+g_a\sum_{k\neq a}\left(\frac{\partial U_\nu{}^{(k)}}{\partial z_a{}^\mu}-\frac{\partial U_\mu{}^{(k)}}{\partial z_a{}^\nu}\right)v_a{}^\nu\right\}, \quad (31a)$$

$$\delta J=\int d\tau_a\delta z_a{}^\mu\left\{-M_a\frac{d}{d\tau_a}\frac{v_{a\mu}}{v_a}-g_a\sum_{k\neq a}\left[\frac{\partial U^{(k)}}{\partial z_a{}^\mu}v_a-\frac{d}{d\tau_a}\left(\frac{U^{(k)}v_{a\mu}}{v_a}\right)\right]\right\}. \quad (31b)$$

This has to equal zero for arbitrary $\delta z_a{}^\mu$ and therefore, remembering (29) and using the abbreviations

$$G_{\mu\nu}{}^{(k)}(z_a)=\partial U_\nu{}^{(k)}/\partial z_a{}^\mu-\partial U_\mu{}^{(k)}/\partial z_a{}^\nu, \quad (32a)$$

$$F_\mu{}^{(k)}(z_a)=-\partial U^{(k)}/\partial z_a{}^\mu \quad (32b)$$

we obtain finally

$$M_a\dot v_a{}^\mu=g_a\sum_{k\neq a}G^\mu{}_\nu{}^{(k)}v_a{}^\nu, \quad (33a)$$

$$M_a\dot v_a{}^\mu=g_a\sum_{k\neq a}F^{\mu(k)}+g_a\frac{d}{d\tau_a}\left(\sum_{k\neq a}U^{(k)}v_a{}^\mu\right) \quad (33b)$$

which are the required equations of motion.

We still have to find the equations obeyed by the potentials and field strengths defined by Eqs. (28) and (32). Now we have[23]

$$(\partial^2/\partial x_\mu\partial x^\mu+\chi^2)\,{}_sG(s)=4\pi\delta(s_0)\delta(s_1)\delta(s_2)\delta(s_3). \quad (34)$$

Multiplying both sides by $g_k v_{k\nu}d_\nu\tau_k$ for the vector meson case, by $g_k v_k d\tau_k$ for the scalar meson case, and integrating from $-\infty$ to ∞ we obtain, using the definitions (3) and (28)

$$\partial^2 U_\nu{}^{(k)}/\partial x_\mu\partial x^\mu+\chi^2U_\nu{}^{(k)}=4\pi j_\nu{}^{(k)}, \quad (35a)$$

$$\partial^2 U^{(k)}/\partial x_\mu\partial x^\mu+\chi^2U^{(k)}=4\pi\rho^{(k)} \quad (35b)$$

which are just our Eqs. (4).

Equations (2b) follow immediately from (35b) and (32b). To obtain (2a) we calculate

$$\frac{\partial U_\mu{}^{(k)}}{\partial x_\mu}=g_k\int v_{k\mu}\frac{\partial {}_sG(s_k)}{\partial x_\mu}d\tau_k=g_k\int v_{k\mu}\frac{d\,{}_sG(s_k)}{ds_k}\frac{\partial s_k}{\partial x_\mu}d\tau_k$$

$$=-g_k\int\frac{d\,{}_sG(s_k)}{ds_k}\frac{ds_k}{d\tau_k}d\tau_k=-g_k\,{}_sG(s_k)\Big|_{-\infty}^{\infty}=0. \quad (36a)$$

Differentiating this divergence with respect to x^ν and subtracting this from (35a) we obtain (2a).

Finally we substitute our expression (9) for ${}_sG$ into Eqs. (28) and obtain immediately our expressions (13a) and (13b) for the symmetric potentials, which completes the proof that Eqs. (33) are identical with Eqs. (23).[15,24]

[23] See reference 10, Appendix, Eq. (47). This and all subsequent equations of the appendix are erroneously given without the factor 4π; however the definition of G given in the text, Eqs. (5a) and (5b) [our Eqs. (6) and (7)] is given correctly.

[24] A variational principle of the form (27a) with arbitrary G and including the term $i=k$ was used by R. P. Feynman, Phys. Rev. **74**, 939 (1948) in his investigation of electrodynamic field theory following the work of F. Bopp, Ann. Physik **42**, 573 (1943). Inclusion of this term and use of our ${}_sG$ yields (just as the use of the δ-function in electrodynamics) an infinite term. The use of a different function which avoids such a divergence would still

IV. THE ENERGY-MOMENTUM TENSOR

It has been shown by several authors in electrodynamics that there exists an energy-momentum tensor in the field theory "adjunct"[7] to the theory of action at a distance. Two different forms of this tensor have been suggested, one by Frenkel[4] and Synge,[6] the other by Wheeler and Feynman.[7] They differ only by a tensor of zero divergence and are both equally suitable for a statement of the law of conservation of energy and momentum.

We shall first show that the equations assumed for our theory of action at a distance (23) derivable from the variational principle (27) also allow the existence of the analogous energy-momentum tensors.

Detailed conservation of energy and momentum as customary in field theory requires[25] the existence of a tensor $T_{\mu\nu}$ with the properties, first

$$\frac{dP_{a\mu}}{d\tau_a}+\frac{d}{d\tau_a}\int\frac{\partial T_{\mu\nu}}{\partial x_\nu}dx^0dx^1dx^2dx^3=0, \tag{37}$$

when the integral is extended over the neighborhood of particle a and second, vanishing of the above integral if the region of integration does not include any particles; P_a is a quantity depending on the variables at the position of particle a only. From this it follows that the quantity

$$\sum_{\text{all } k} P_{k\mu}+\int T_{\mu\sigma}d\sigma^\sigma \tag{38}$$

is conserved, i.e., its value is the same for any space-like surface σ.

With the choice

$$P_{a\mu}=M_a v_{a\mu}, \tag{39a}$$

$$P_{a\mu}=M_a v_{a\mu}-g_a\sum_{k\neq a}U^{(k)}v_{a\mu}, \tag{39b}$$

we can take the energy-momentum tensor in analogy to the tensor defined by Frenkel and Synge in electrodynamics as

$$4\pi T_{\mu\nu}=\sum_{i\neq k}\{G_{\mu\sigma}{}^{(i)}G^{\sigma}{}_{\nu}{}^{(k)}+\tfrac{1}{4}g_{\mu\nu}G_{\sigma\rho}{}^{(i)}G^{\sigma\rho(k)}+\chi^2U_\mu{}^{(i)}U_\nu{}^{(k)}-\tfrac{1}{2}\chi^2g_{\mu\nu}U_\rho{}^{(i)}U^{\rho(k)}\}, \tag{40a}$$

$$4\pi T_{\mu\nu}=\sum_{i\neq k}\{F_\mu{}^{(i)}F_\nu{}^{(k)}-\tfrac{1}{2}g_{\mu\nu}(F_\sigma{}^{(i)}F^{\sigma(k)}-\chi^2U^{(i)}U^{(k)})\}. \tag{40b}$$

Here it is understood that all the fields and potentials are the symmetric ones, but now and in the following we are omitting the subscript.

We note that just as in electrodynamics, our tensor (40) is obtained from the tensor (14) of the field theory formed from the *total* field at any point by subtracting from it the tensors formed by the fields and potentials of each particle *separately*. Therefore, it cannot be formed without a knowledge of the sources of the field and does not allow such a simple interpretation as the field theoretical tensor. It is precisely the fact that the tensor of field theory can be formed from a knowledge of the total field alone regardless of its origin which suggested the acceptance of the field as the fundamental physical quantity.

On the other hand the tensor (40) avoids the infinities of field theory and equally allows an "accounting" of energy and momentum "in transit."

Just as in field theory, the energy-momentum tensor is not uniquely defined by the requirement (37). We could, for example, take instead of (40) a tensor (analogous to the "canonical" tensor defined by Wheeler and Feynman in electrodynamics) given by

$$8\pi T_{\mu\nu}=\sum_{i\neq k}\{{}_{\text{ret}}G_{\mu\sigma}{}^{(i)}\,{}_{\text{adv}}G^{\sigma}{}_{\nu}{}^{(k)}+{}_{\text{adv}}G_{\mu\sigma}{}^{(i)}\,{}_{\text{ret}}G^{\sigma}{}_{\nu}{}^{(k)}+\tfrac{1}{2}g_{\mu\nu}\,{}_{\text{ret}}G_{\sigma\rho}{}^{(i)}\,{}_{\text{adv}}G^{\sigma\rho(k)}+\chi^2\,{}_{\text{ret}}U_\mu{}^{(i)}\,{}_{\text{adv}}U_\nu{}^{(k)}+\chi^2\,{}_{\text{adv}}U_\mu{}^{(i)}\,{}_{\text{ret}}U_\nu{}^{(k)}-\chi^2g_{\mu\nu}\,{}_{\text{ret}}U_\rho{}^{(i)}\,{}_{\text{adv}}U^{\rho(k)}\}, \tag{41a}$$

$$8\pi T_{\mu\nu}=\sum_{i\neq k}\{{}_{\text{ret}}F_\mu{}^{(i)}\,{}_{\text{adv}}F_\nu{}^{(k)}+{}_{\text{adv}}F_\mu{}^{(i)}\,{}_{\text{ret}}F_\nu{}^{(k)}-g_{\mu\nu}({}_{\text{ret}}F_\sigma{}^{(i)}\,{}_{\text{adv}}F^{\sigma(k)}-\chi^2\,{}_{\text{ret}}U^{(i)}\,{}_{\text{adv}}U^{(k)})\}. \tag{41b}$$

This tensor differs from the tensor (40) (constructed from the symmetric fields and potentials) only by a tensor of the same form (40) constructed from the radiation fields and potentials defined by

$${}_{\text{rad}}G_{\mu\nu}=\tfrac{1}{2}({}_{\text{ret}}G_{\mu\nu}-{}_{\text{adv}}G_{\mu\nu}), \tag{42a}$$

$${}_{\text{rad}}U=\tfrac{1}{2}({}_{\text{ret}}U-{}_{\text{adv}}U),$$
$${}_{\text{rad}}F_\mu=\tfrac{1}{2}({}_{\text{ret}}F_\mu-{}_{\text{adv}}F_\mu). \tag{42b}$$

This difference has a zero divergence everywhere and, therefore, the two tensors (40) and (41) are equivalent for our purposes. As the calculations are slightly

---

yield finite self-action terms which are incompatible with the point of view of action at a distance, as discussed in Sec. II. In this paper we are not concerned with such possible modifications of the theory. In discussing Feynman's work, H. Steinwedel, Z. Naturforsch. **6a**, 123 (1951) suggested a variational principle for scalar fields, which differs from our Eq. (27b) by a factor of $-v_iv_k$ and inclusion of the term $i=k$ in the second integral. Omitting this term from his principle we would be led to the equations

$$M_av_a{}^\mu=-g_a\sum_{k\neq a}F^{\mu(k)},$$

which are not the same as Eqs. (23b) suggested by the field theory. This however is not a possible set of equations of motion: by multiplying both sides by $v_{a\mu}$ and using (29) we obtain

$$0=-g_a\sum_{k\neq a}F^{\mu(k)}v_{a\mu},$$

which can in general only be satisfied by $\sum_{k\neq a}F^{\mu(k)}=0$. Similarly the equations actually obtained by Steinwedel by including the term $i=k$, which contain the total field instead of the field due to the other particles only, could only be satisfied by $\sum_{\text{all } k}F^{\mu(k)}=0$.

The omission of the factor has been corrected (except for the sign) in a paper by A. Schoch and H. Steinwedel, Z. Naturforsch. **7a**, 66 (1952).

[25] See, e.g., reference 7 or 2.

simpler using (40), we shall restrict our considerations to it from now on.

We have

$$4\pi\frac{\partial T_{\mu\nu}}{\partial x_\nu}=\sum_{i\neq k}\Big\{\frac{\partial G_{\mu\sigma}{}^{(i)}}{\partial x_\nu}G^{\nu}{}_{\nu}{}^{(k)}+G_{\mu\sigma}{}^{(i)}\frac{\partial G^{\nu}{}_{\nu}{}^{(k)}}{\partial x_\nu}$$
$$+\tfrac{1}{2}\frac{\partial G_{\rho\sigma}{}^{(i)}}{\partial x^\mu}G^{\rho\sigma(k)}+\chi^2\frac{\partial U_\mu{}^{(i)}}{\partial x_\nu}U^{\nu(k)}$$
$$+\chi^2U_\mu{}^{(i)}\frac{\partial U_\nu{}^{(k)}}{\partial x_\nu}-\chi^2\frac{\partial U_\rho{}^{(i)}}{\partial x^\mu}U^{\rho(k)}\Big\}, \quad (43a)$$

$$4\pi\frac{\partial T_{\mu\nu}}{\partial x_\nu}=\sum_{i\neq k}\Big\{\frac{\partial F_\mu{}^{(i)}}{\partial x_\nu}F_\nu{}^{(k)}+F_\mu{}^{(i)}\frac{\partial F_\nu{}^{(k)}}{\partial x_\nu}$$
$$-\frac{\partial F_\sigma{}^{(i)}}{\partial x^\mu}F^{\sigma(k)}+\chi^2\frac{\partial U^{(i)}}{\partial x^\mu}U^{(k)}\Big\}. \quad (43b)$$

The first and third term of (43b) cancel. The first and third term of (43a) can be rewritten

$$\frac{1}{2}\sum_{i\neq k}\left(\frac{\partial G_{\mu\sigma}{}^{(i)}}{\partial x^\nu}+\frac{\partial G_{\nu\mu}{}^{(i)}}{\partial x^\sigma}+\frac{\partial G_{\sigma\nu}{}^{(i)}}{\partial x^\mu}\right)G^{\sigma\nu(k)},$$

and the expression in brackets equals zero from the definition of the $G_{\mu\nu}$ (2a). Using (2a) and (2b) respectively we can write the remaining terms

$$4\pi\frac{\partial T_{\mu\nu}}{\partial x_\nu}=\sum_{i\neq k}\Big\{G_{\mu\sigma}{}^{(i)}(\chi^2U^{\sigma(k)}-4\pi j^{\sigma(k)})$$
$$+\chi^2\frac{\partial U_\mu{}^{(i)}}{\partial x_\nu}U_\nu{}^{(k)}-\chi^2\left(G_{\mu\rho}{}^{(i)}+\frac{\partial U_\mu{}^{(i)}}{\partial x_\rho}\right)U^{\rho(k)}\Big\}$$
$$=-4\pi\sum_{i\neq k}G_{\mu\sigma}{}^{(i)}j^{\sigma(k)}, \quad (44a)$$

$$4\pi\frac{\partial T_{\mu\nu}}{\partial x_\nu}=\sum_{i\neq k}\{F_\mu{}^{(i)}(\chi^2U^{(k)}-4\pi\rho^{(k)})-\chi^2F_\mu{}^{(i)}U^{(k)}\}$$
$$=-4\pi\sum_{i\neq k}F_\mu{}^{(i)}\rho^{(k)}. \quad (44b)$$

Using definitions (3) and (39) and the equations of motion (23) we obtain the required relation (37).

It is noteworthy that our simple tensor (40) leads to the conservation law (37) only if the action-at-a-distance equations are used, but not if the field-theoretical equations are used. For these latter, Eq. (37) is of course guaranteed from the very method of obtaining the equations of motion both in the retarded and in the symmetric case. It is actually fulfilled if the customary tensor (14) is used, but care has to be taken in compensating infinities. It has been proved that this is always possible, and furthermore it has been shown (following the method suggested by Pryce[26] in electrodynamics) that it is always possible to modify the energy-momentum tensor in such a way that no infinities appear at all.[27] One of the modified tensors suggested[12] is constructed by subtracting from the tensor (14) formed from the total retarded field similar tensors formed from the "modified symmetric field" of each particle separately; this field is obtained by omission from the symmetric field of the integral over the entire motion of the particle. The use of this modified tensor and the equations of motion of the retarded case (21) again leads to the conservation law (37). It is easy to see that (37) also results from the use of the equations of motion of the symmetric case (22) and a tensor constructed by subtracting the same tensors formed from the modified symmetric fields as above from the tensor (14) formed from the total symmetric field. All of these modifications however require a knowledge of the sources of the field just as for the tensor (40) and are, therefore, not consistent with a purely field-theoretical interpretation.

It is also impossible to satisfy the conservation law (37) with our tensor (40) for the equations of motion (24) of the retarded case of action at a distance, or indeed apparently with any other tensor. It is, however, possible for the alternative equations (25) without any radiation terms provided we construct the tensor (40) using retarded fields and potentials only. This again is completely analogous to the results of Frenkel and Synge in electrodynamics.

V. APPLICATION OF THE WHEELER-FEYNMAN METHOD

In the theory of action at a distance in electrodynamics as developed by Wheeler and Feynman[7] the field F acting on the ath particles is assumed to be of the form

$$\sum_{k\neq a}\tfrac{1}{2}[{}_{\rm ret}F^{(k)}+{}_{\rm adv}F^{(k)}]. \quad (45)$$

This can be broken down into three parts

$$\sum_{k\neq a}{}_{\rm ret}F^{(k)}+\tfrac{1}{2}({}_{\rm ret}F^{(a)}-{}_{\rm adv}F^{(a)})$$
$$-\sum_{\rm all\ k}\tfrac{1}{2}[{}_{\rm ret}F^{(k)}-{}_{\rm adv}F^{(k)}]. \quad (46)$$

The case called "complete absorption" by these authors is characterized by

$$\sum_{\rm all\ k}[{}_{\rm ret}F^{(k)}-{}_{\rm adv}F^{(k)}]=0 \text{ (everywhere)}. \quad (47)$$

The second term of (47),

$$\tfrac{1}{2}[{}_{\rm ret}F^{(a)}-{}_{\rm adv}F^{(a)}]\equiv{}_{\rm rad}F^{(a)}, \quad (48)$$

can be shown to contribute just the force of radiative

[26] M. H. L. Pryce, Proc. Roy. Soc. (London) **A168**, 389 (1938).

[27] H. J. Bhabha and Harish-Chandra, Proc. Roy. Soc. (London) **A183**, 134 (1944); Harish-Chandra, Proc. Roy. Soc. (London) **A183**, 142 (1944).

reaction to the equations of motion. Therefore, the condition (47) added to the equations of motion using interactions symmetric in time just leads to the equations of motion including the radiative reaction and using retarded interactions only.

As discussed previously[9] the considerations of Wheeler and Feynman are applicable in field theory as well as in the theory of action at a distance and lead to identical results. This is because in electrodynamics the equations of motion assumed outright in action at a distance are the same as those obtained in field theory starting from an energy-momentum tensor constructed from fields symmetric in time. As discussed in Sec. II however, in the case of meson fields the equations of motion (22) obtained from field theory are not suitable for a theory of action at a distance, for which we chose Eqs. (23) instead. We have, therefore, to investigate separately for the two points of view, whether or not the considerations of Wheeler and Feynman can be taken over in meson theory.

The case of the field-theoretical equations can be discussed without any calculation. As pointed out in reference 9, under the so-called "complete absorption" condition (47) any results of field theory must be the same in the symmetric and in the retarded (and also advanced) case. This condition can also be written

$$\sum_{\text{all } k} {}_{\text{ret}}F^{(k)} = \sum_{\text{all } k} {}_{\text{adv}}F^{(k)} = \sum_{\text{all } k} \tfrac{1}{2}[{}_{\text{ret}}F^{(k)} + {}_{\text{adv}}F^{(k)}], \quad (49)$$

and these are the fields (due to sources) which have to be inserted into the energy-momentum tensor at the start of any field-theoretical calculation in the retarded, advanced and symmetric cases, respectively. As these are equal, it is obvious that the equations of motion must also be the same in all cases.

This argument clearly is not restricted to electrodynamics. The only change necessary is that due to the gauge invariance of electrodynamics we had to require condition (47) for the field strengths only, while now we have to assume it for the potentials already.

Therefore, the condition (47) for the potentials applied to Eqs. (22) of the symmetric case will again lead to Eqs. (21) of the retarded case of field theory.

The situation is different however for the equations of motion adopted from the point of view of action at a distance. Expression (48) is still finite on the world line of the particle and is given for the different quantities involved by Eqs. (19). Thus the considerations of Wheeler and Feynman applied to our Eqs. (23) lead to the equations of motion

$$M_a\dot{v}_a{}^\mu - \tfrac{2}{3}g_a{}^2(\ddot{v}_a{}^\mu + v_a{}^\mu\dot{v}_a{}^2) - \tfrac{1}{2}g_a{}^2\chi^2 v_{a\nu}\left\{\int_{-\infty}^{\tau_a}\frac{s_a{}^\mu v_a{}^\nu(\tau') - s_a{}^\nu v_a{}^\mu(\tau')}{s_a{}^2}J_2(\chi s_a)d\tau' - \int_{\tau_a}^{\infty}\frac{s_a{}^\mu v_a{}^\nu(\tau') - s_a{}^\nu v_a{}^\mu(\tau')}{s_a{}^2}J_2(\chi s_a)d\tau'\right\} = g_a\sum_{k\neq a}{}_{\text{ret}}G^\mu{}_\nu{}^{(k)}v_a{}^\nu, \quad (50a)$$

$$M_a\dot{v}_a{}^\mu - \tfrac{1}{3}g_a{}^2(\ddot{v}_a{}^\mu + v_a{}^\mu\dot{v}_a{}^2) - \tfrac{1}{2}g_a{}^2\chi^2 v_a{}^\mu + \tfrac{1}{2}g_a{}^2\chi^2\left\{\int_{-\infty}^{\tau_a}\frac{s_a{}^\mu}{s_a{}^2}J_2(\chi s_a)d\tau' - \int_{\tau_a}^{\infty}\frac{s_a{}^\mu}{s_a{}^2}J_2(\chi s_a)d\tau'\right\} + \tfrac{1}{2}g_a{}^2\chi\frac{d}{d\tau_a}\left\{v_a{}^\mu\left[\int_{-\infty}^{\tau_a}\frac{1}{s_a}J_1(\chi s_a)d\tau' - \int_{\tau_a}^{\infty}\frac{1}{s_a}J_1(\chi s_a)d\tau'\right]\right\} = g_a\sum_{k\neq a}{}_{\text{ret}}F^{\mu(k)} + g_a\frac{d}{d\tau_a}\Big(\sum_{k\neq a}{}_{\text{ret}}U^{(k)}v_a{}^\mu\Big). \quad (50b)$$

These equations[28] differ both from those expected from a theory of action at a distance, which should not contain any integrals over past or future motion [like our Eqs. (24) or (25)], and from Eqs. (21) obtained from field theory, which contain integrals over the past motion only. Therefore, the Wheeler-Feynman method of obtaining the equations of the retarded case from those of the symmetric one gives the correct transition only in the case of the field-theoretical equations. This however does not by itself furnish an argument in favor of the field-theoretical equations, as we do not know which equations describe the radiation damping correctly (within the framework of classical theory).

Just as in electrodynamics, the equations obtained by an application of the Wheeler-Feynman method both in field theory and in action at a distance are mathematically not completely equivalent to the original equations of the retarded case, as they are to be solved subject to the condition (48), which does not have to be imposed on the original equations.[9,29]

VI. DISCUSSION

In this paper we have been concerned with the equations of motion of point particles interacting through neutral vector and scalar meson fields, both from the point of view of field theory and from that of action at a distance. Since all our considerations lead to identical conclusions for both types of fields, we do not have to distinguish between them in the discussion.

We started our investigation by finding from the point of view of field theory the equations of motion both if the fields produced by the particles were assumed

[28] Equations (50a) have been obtained also by Kanazawa and by Steinwedel (reference 15).

[29] P. Havas, Phys. Rev. 86, 974 (1952).

to be purely retarded, and if they were taken as half-retarded, half-advanced. It was found that these Eqs. (21) and (22) contained terms depending respectively on the previous and entire motion of the particles, which are inadmissible from the point of view of action at a distance. Therefore, it was suggested that they be replaced in the theory of action at a distance by equations omitting such self-action terms, Eqs. (23) for the symmetric case and Eqs. (24) or (25) with and without radiation terms respectively for the retarded case. No such replacement is necessary in electrodynamics.

We then showed that these modified equations can be derived from a variational principle in the symmetric case, but not in the retarded one, just as in the action-at-a-distance formulation of electrodynamics; no such principle exists for the field-theoretical equations however, while the equations of the symmetric case of electrodynamic field theory do allow such a principle.

All the equations of motion except the Eqs. (24) of action at a distance including radiation terms allow the definitions of an energy-momentum tensor which permits a statement of the conservation laws for the system of particles and field without the appearance of infinite terms. However all the modified field-theoretical tensors are really inconsistent with the basic physical idea of field theory; from this point of view the original conservation law with compensating infinities appears to be preferable. No such conceptual difficulty is involved in the tensors of field theory "adjunct" to an action-at-a-distance theory, which are only introduced as auxiliary concepts for purposes of accounting.

The tensor (40) is defined in analogy to the Frenkel-Synge tensor of electrodynamics as the original field-theoretical tensor formed from the total field minus similar tensors formed from the fields of the particles separately. The use of symmetric fields allows a statement of the conservation laws for the equations of motion of the symmetric case in the theory of action at a distance; the use of retarded fields allows such a statement for the equations without radiation terms (25). No such statement appears to be possible for Eqs. (24) of this theory including radiation. Other tensors allowing conservation laws for the field-theoretical equation have been given previously for the retarded case; the methods employed there can also be used for the symmetric case.

The application of the method of Wheeler and Feynman to the equations of the symmetric case leads to the equations of the retarded case in field theory, but to a new set of equations in action at a distance.

All the discussion has been made under the assumption that the entire field is due to sources. No other assumption is possible in action at a distance theory. In field theory, on the other hand, we could have additional empty-space solutions of the field equations. The problems arising from this are the same as those of the analogous situation in electrodynamics which have been discussed elsewhere.[9]

The main difference between the results obtained here and in electrodynamics is in the question of the correct description of radiation reaction. In electrodynamics we always obtain the Lorentz-Dirac equations. They follow from the retarded case of field theory, and also from the symmetric case of either field or action-at-a-distance theory together with the Wheeler-Feynman considerations; they could also be postulated in a theory of action at a distance, as their form is consistent with the ideas of such a theory. In mesodynamics the analogous considerations do not all lead to the same equations of motion. Thus, in the retarded case of field theory and also by application of the Wheeler-Feynman method to the symmetric case of field theory we obtain Eqs. (21); the application to the symmetric case of the theory of action at a distance leads to Eqs. (50); a postulated set consistent with the ideas of action at a distance would be Eqs. (24). The fact that we obtain different equations might offer an opportunity not available in electrodynamics for a decision between the different points of view by a comparison with experiment. This however will probably only be possible after these ideas have been applied to quantum theory.[30]

The procedures of this paper are capable of generalization to other fields and interactions. A second paper dealing with charged fields is in preparation. Further generalization is in progress.

[30] The classical scattering of mesons corresponding to Eq. (50) has been calculated by C. R. Mehl and the author and will be published shortly.

Application of the Multiple Scattering Theory to Cloud-Chamber Measurements. I*

STANISLAW OLBERT
Department of Physics and Laboratory for Nuclear Science and Engineering, Massachusetts Institute of Technology, Cambridge, Massachusetts

(Received January 14, 1952)

Some questions concerning the application of the multiple scattering theory to the analysis of cloud-chamber pictures are discussed from the theoretical point of view: (a) The Molière theory of multiple scattering is modified by the consideration of the finite nuclear dimensions. It is assumed that the probability of single scattering goes abruptly to zero for angles greater than $\varphi_0=\varphi_m a/r_n$, where a is the radius of the statistical Thomas-Fermi atom, r_n the radius of the nucleus, and φ_m is the screening angle as derived by Molière. The distribution function for plural and multiple scattering is then derived for finite values of φ_0. It is shown that the cutoff affects especially the tail behavior of the distribution function as it was to be expected. While Molière's function decreases as φ^{-3} for projected angles of scattering large compared to the rms angle, the modified function decreases approximately as $(1/\varphi)$ times a Gaussian function of $(\varphi-\varphi_0)$ for angles large compared to the rms angle and the cut-off angle. (b) The distribution function for the mean value of the square angle of scattering in n plates of a multiple-plate cloud chamber is derived and compared with the normal χ^2-distribution. (c) The effect of observational errors on the distribution function for multiple scattering is estimated quantitatively and discussed in some detail for the case where the mean-square angle of real scattering is large compared to the variance of the noise level scattering.

I. INTRODUCTION

THE observation of Coulomb scattering along the tracks of charged particles in photographic emulsions has played an important role in the identification of cosmic-ray particles and in the determination of their momentum distribution.

Scattering measurements, if properly interpreted, can also be of great value in the analysis of cloud-chamber pictures. Groetzinger, Berger, and Ribe[1] have discussed, from this point of view, the scattering in the gas of a cloud chamber. In the present paper we propose to investigate some theoretical questions concerning the scattering of charged particles in their passage through the metal plates of a multiple-plate cloud chamber. In subsequent papers we shall describe the application of the scattering method to specific problems.

Coulomb scattering of charged particles in finite thicknesses of matter has been the subject of many theoretical studies. Early investigators[2] have treated the problem in the limiting case of multiple scattering, i.e., they have assumed that the particle undergoes a very large number of very small deflections in traversed layer. They have consequently obtained a Gaussian (normal) distribution for the observed angle of scattering. More recently, Snyder and Scott[3] and Molière[4] have treated the problem in a more rigorous and general manner. They have obtained solutions describing the transition from the limiting case of multiple scattering to the limiting case of single scattering through the intermediate case of plural scattering, where the observed deflection results from a small number of individual scattering events. The distribution functions found by Snyder and Scott and by Molière approach the Gaussian function at small angles, but exhibit a much longer "tail" at large angles. In our discussion we shall make use of Molière's results which are analytical in form. However, the theory of Molière (as well as that of Snyder and Scott) neglects the upper limit to the angle of single scattering determined by the finite size of atomic nuclei. Therefore, this theory overestimates the probability of deflection through large angles. In Part II of this paper we shall modify Molière's theory by taking into consideration the finite nuclear size. The other questions discussed in the present paper include, in Part III, the distribution function for the mean square values of the angles of scattering observed in n plates; in Part IV, the effect of the "noise level" scattering on the observed distribution function.

In the analysis of cloud-chamber pictures, the observed quantity is the projected angle of scattering. Therefore, we shall restrict ourselves to the discussion on the distribution of this variable. The theory may be easily modified for the case of spatial angle of scattering.

II. THE EFFECT OF THE FINITE SIZE OF NUCLEI

(a) The Probability of Single Scattering

Molière has derived the following expression for the probability that a particle suffers a deflection through a projected angle between φ' and $\varphi'+d\varphi'$ in consequence of a single collision occurring in a thickness t of the scattering material:

$$f_1(\varphi')d\varphi'=\tfrac{1}{2}Qd\varphi'/(\varphi'^2+\varphi_m^2)^2. \tag{1}$$

The symbols in Eq. (1) have the following meaning:

$$Q=4\pi\frac{Nt}{A}\left(\frac{Ze^2}{pc\beta}\right)^2, \tag{2}$$

$$\varphi_m=\frac{1.14m_ecZ^{\frac{1}{3}}}{137p}\left[1.13+3.76\left(\frac{Z}{137\beta}\right)^2\right]^{\frac{1}{2}}, \tag{3}$$

* This work was supported in part by the joint program of the ONR and AEC.

[1] Groetzinger, Berger, and Ribe, Phys. Rev. **77**, 584 (1950).

[2] For a review, see B. Rossi and K. Greisen, Revs. Modern Phys. **13**, 240 (1941).

[3] H. S. Snyder and W. T. Scott, Phys. Rev. **76**, 220 (1949).

[4] G. Molière, Z. Naturforsch. **2a**, 133 (1947); **3a**, 78 (1948).

where p = momentum of scattered particle; $c\beta$ = velocity of scattered particle; Ze = nuclear charge of scattering material; A = atomic weight of scattering material; t = thickness of scattering material in g cm^{-2}; N = Avogadro number; m_e = electron mass. The factor Q is the well-known term occurring in the Rutherford formula. The parameter φ_m is the so-called "screening" angle accounting for the shielding effect of atomic electrons. Molière obtained Eq. (3) by assuming the Thomas-Fermi model of the atom with a nucleus of vanishing radius. We shall take into account in an approximate manner the effect of the finite nuclear dimensions by assuming that the scattering probability is given by Eq. (1) for $\varphi' < \varphi_0$ and is identically zero for $\varphi' > \varphi_0$:

$$f_1(\varphi';\varphi_0)d\varphi' = \begin{cases} \frac{1}{2}Qd\varphi'/(\varphi'^2+\varphi_m^2)^{\frac{1}{2}}, & |\varphi'| < \varphi_0 \\ 0, & |\varphi'| > \varphi_0. \end{cases} \quad (4)$$

As a definition for the limiting angle φ_0 we shall use the equation

$$\varphi_0/\varphi_m = a/r_n, \quad (5)$$

where $a = 1.67\times 10^{1}r_eZ^{-\frac{1}{3}}$ represents the radius of the atom computed from the Fermi-Thomas theory, and r_n is of the order of the nuclear radius $R_n = \frac{1}{2}r_eA^{\frac{1}{3}}$ ($r_e = e^2/m_ec^2$). In the classical limit, $(Z/137\beta)^2 \gg 1$, φ_0, as defined by Eq. (5), tends to the value $2Z(r_e/r_n)(m_ec/p\beta)$, which represents the angle of deflection corresponding to a collision with impact parameter r_n. At the limit for $(Z/137\beta)^2 \ll 1$, φ_0 becomes practically equal to the value $\lambda\!\!\!^{-}/r_n$ in agreement with the results of Born's approximation.

It is convenient to use the Fourier representation for the expression (4):

$$f_1(\varphi';\varphi_0) = \frac{1}{2\pi}\int_{-\infty}^{+\infty} d\xi e^{i\xi\varphi'} g(\xi;\varphi_0), \quad (6)$$

with the Fourier transform

$$g(\xi;\varphi_0) = Q\left[\frac{1}{2}\int_{-\infty}^{+\infty}\frac{e^{-i\xi\varphi'}d\varphi'}{(\varphi'^2+\varphi_m^2)^{\frac{1}{2}}} - \int_{\varphi_0}^{+\infty}\frac{\cos(\xi\varphi')d\varphi'}{\varphi'^3}\right], \quad (7)$$

wherein we made use of the fact that $\varphi_0 \gg \varphi_m$.

The evaluation of the first integral in Eq. (7) is discussed in detail by Molière. As one may easily verify, expansion in powers of φ_m yields with sufficient accuracy

$$\frac{1}{2}Q\int_{-\infty}^{+\infty}\frac{e^{-i\xi\varphi'}d\varphi'}{(\varphi'^2+\varphi_m^2)^{\frac{1}{2}}} \approx Q\left[\frac{1}{\varphi_m^2}+\frac{\xi^2}{4}\ln\left(\frac{\gamma^2\varphi_m^2}{4e}\xi^2\right)\right],$$

where $\ln(\gamma^2/e) = 0.154\cdots$ ($\ln\gamma$ = Euler's constant).

Hence, the Fourier transform may be written as follows:

$$g(\xi;\varphi_0) = Q\left[\frac{1}{\varphi_m^2}+\frac{\xi^2}{4}\ln\left(\frac{\gamma^2\varphi_m^2}{4e}\xi^2\right) - \int_{\varphi_0}^{+\infty}\frac{\cos(\xi\varphi')d\varphi'}{\varphi'^3}\right]. \quad (8)$$

(b) The Distribution Function for Plural and Multiple Scattering

In order to derive the distribution function we follow a method analogous to that used by Molière.

Let the probability that a particle will suffer a deflection through an angle φ' and $\varphi'+d\varphi'$, as a result of one single scattering, be given by Eq. (6); then the probability that the same particle will be deflected through an angle between $\varphi^{(k)}$ and $\varphi^{(k)}+d\varphi^{(k)}$, as a result of k scattering collisions, is given by

$$f_k(\varphi^{(k)};\varphi_0)d\varphi^{(k)} = \frac{d\varphi^{(k)}e^{-g_0}}{2\pi k!}\int_{-\infty}^{+\infty} d\xi \exp(i\xi\varphi^{(k)})[g(\xi;\varphi_0)]^k, \quad (9)$$

where $g_0 \equiv g(0;\varphi_0)$. Therefore, the total probability that the particle will suffer a deflection through an angle between φ and $\varphi+d\varphi$, as a result of the accumulation of 0, 1, 2, $\cdots$, k, scattering collisions is given by the sum of Eq. (9). One thus obtains

$$f(\varphi;\varphi_0)d\varphi = \frac{d\varphi e^{-g_0}}{2\pi}\int_{-\infty}^{+\infty} d\xi e^{i\xi\varphi}e^{g(\xi;\varphi_0)}. \quad (10)$$

One may verify that the factor e^{-g_0} normalizes Eq. (10) so that

$$\int_{-\infty}^{+\infty} d\varphi f(\varphi;\varphi_0) = 1.$$

Substituting for $g(\xi;\varphi_0)$ the expression (8) and taking into account that $g_0 = Q(1/\varphi_m^2 - 1/2\varphi_0^2)$, one arrives at the following expression for the distribution function:

$$f(\varphi;\varphi_0) = \frac{1}{2\pi}\int_{-\infty}^{+\infty} d\xi e^{i\xi\varphi}\exp\left\{Q\left[\frac{\xi^2}{4}\ln\left(\frac{\gamma^2\varphi_m^2}{4e}\xi^2\right) + \frac{1}{2\varphi_0^2} - \int_{\varphi_0}^{\infty}\frac{\cos(\xi\varphi')}{\varphi'^3}d\varphi'\right]\right\}. \quad (11)$$

It now remains to evaluate the integral in Eq. (11). For this purpose it is convenient to introduce with Molière a new dimensionless parameter G, defined by the transcendental equation

$$G = -\tfrac{1}{2}\ln\left(\frac{\gamma^2}{e}\frac{\varphi_m^2}{2GQ}\right). \quad (12)$$

In addition, let us transform simultaneously the variables φ and ξ into the new variables

$$x = \varphi/(2GQ)^{\frac{1}{2}} \quad \text{and} \quad \eta = (2GQ)^{\frac{1}{2}}\xi.$$

Our new scattering variable x represents, therefore, a projected angle measured in units of the characteristic parameter $(2GQ)^{\frac{1}{2}}$. We shall denote this important quantity by $\sqrt{2}\sigma$, referring it thereby to the standard

deviation of the normal distribution. The reason for it will become evident later. After a few simple algebraic operations one then finds the following distribution function for the scattering variable x:

$$f(x;x_0)=\frac{1}{2\pi}\int_{-\infty}^{+\infty}d\eta e^{i\eta x}\exp\left[-\frac{\eta^2}{4}+\frac{1}{2G}\left(\frac{\eta^2}{4}\ln\frac{\eta^2}{4}+\frac{1}{2x_0^2}-\int_{x_0}^{\infty}\frac{\cos(\eta x')dx'}{x'^3}\right)\right], \quad (13)$$

where $x_0=\varphi_0/\sqrt{2}\sigma$.

While Eq. (11) is characterized by the three parameters Q, φ_m, and φ_0, note that Eq. (13) is characterized by the three different parameters σ, G, and x_0.

By solving numerically the transcendental Eq. (12), one finds that G may be represented with sufficient accuracy by the explicit expression[5]

$$G\simeq 5.66+1.24\log_{10}\left[\frac{Z^{4/3}A^{-1}t}{1.13\beta^2+3.76(Z/137)^2}\right], \quad (14)$$

for $t>0.1$ g cm^{-2}. Note that G depends not only on the thickness and the atomic number of the scattering material, but also on the velocity of the scattered particle. However, for heavy materials, the dependence on β is slight, e.g., one finds for $\frac{1}{4}$ inch of lead

$$G_0\simeq 6.89 \text{ for } \beta=0, \quad \text{and} \quad G_1\simeq 6.56 \text{ for } \beta=1.$$

Since, in general, G is appreciably larger than unity, we can expand the exponential in Eq. (13) in powers of $(1/2G)$ and neglect terms containing powers higher than the first. After having performed some integrations on the right-hand side of Eq. (13), we find the following approximate expression for $f(x;x_0)$:

$$f(x;x_0)=\exp(-x^2)/\sqrt{\pi}+(1/4G)[f^{(1)}(x;\infty)-\kappa(x;x_0)], \quad (15)$$

where we have used the following abbreviations:

$$f^{(1)}(x;\infty)=\frac{1}{\pi}\int_{-\infty}^{+\infty}d\eta\exp(i\eta x-\eta^2/4)\left(\frac{\eta^2}{4}\ln\frac{\eta^2}{4}\right), \quad (16)$$

$$\kappa(x;x_0)=\frac{2}{\sqrt{\pi}}\exp(-x^2)\left[\int_{x_0}^{\infty}\frac{dx'}{x'^3}\times\exp(-x'^2)\cosh(2xx')-\frac{1}{2x_0^2}\right]. \quad (16')$$

The first term in Eq. (15) is the properly normalized Gaussian. It is predominant for $x<1$, i.e., for angles smaller than $\sqrt{2}\sigma$, since the correction functions $f^{(1)}(x;\infty)$ and $\kappa(x;x_0)$ do not exceed unity, as we shall see later on.

[5] The straight-line relation between G and $\log t$ has been pointed out independently and discussed more exhaustively by W. T. Scott, Phys. Rev. **85**, 245 (1952).

One easily verifies that $f(x;x_0)$ is normalized in such a way that

$$\int_{-\infty}^{+\infty}f(x;x_0)dx=1.$$

The function $f^{(1)}(x;\infty)$, defined by Eq. (16), is the first correction function in Molière's theory. Its properties are discussed by Molière. In particular, it has the following expansions in power series:

For small arguments

$$f^{(1)}(x;\infty)=\frac{2}{\sqrt{\pi}}\exp(-x^2)\sum_{\nu=0}^{\infty}a_\nu x^{2\nu}, \quad (17)$$

where

$$a_0=\tfrac{1}{2}\Psi(\tfrac{1}{2})=0.01825; \quad \Psi(z)=\Gamma'(z+1)/\Gamma(z+1);$$

$$a_1=-1-\Psi(\tfrac{1}{2})=-1.0365;$$

$$a_\nu=\frac{\sqrt{\pi}}{2}\frac{1}{\nu(\nu-1)\Gamma(\nu+\frac{1}{2})}, \quad \nu=2,3,4,\cdots. \quad (18)$$

For large arguments

$$f^{(1)}(x;\infty)\approx 1/x^3+3/x^5+45/4x^7+\cdots. \quad (19)$$

The correction function $\kappa(x;x_0)$, defined by Eq. (16'), describes the effect of finite size of the nucleus. Note that, as x_0 approaches infinity, $\kappa(x;x_0)$ vanishes, and Eq. (15) becomes identical with the distribution function given by Molière. However, x_0 is large compared to one only for fairly thin layers of light materials. For, according to Eqs. (5), (3), and (2), x_0 is given by

$$x_0=\frac{\varphi_0}{(2GQ)^{\frac{1}{2}}}\simeq\frac{260}{Z}\left[\frac{A^{\frac{1}{2}}}{Gt}\left(1.13\beta^2+3.76\left(\frac{Z}{137}\right)^2\right)\right]^{\frac{1}{2}}. \quad (20)$$

Equation (20) shows that x_0 is of the order of one for larger values of Z and t, e.g., for $\frac{1}{4}$ inch of lead, one finds that

$$x_0\simeq 1.17(1.19+\beta^2)^{\frac{1}{2}}.$$

In the case of lead, the correction function, $\kappa(x;x_0)$, will modify the Molière distribution appreciably even for angles comparable to σ, as we shall see in the following section.

(c) The Cut-Off Correction Function

We now turn to the calculation of the cut-off correction function, $\kappa(x;x_0)$. By expanding $\cosh(2xx')$ in Eq. (16') in a power series we obtain the following representation of $\kappa(x;x_0)$:

$$\kappa(x;x_0)=\frac{2}{\sqrt{\pi}}\exp(-x^2)\sum_{\nu=0}^{\infty}b_\nu(x_0)x^{2\nu}, \quad (21)$$

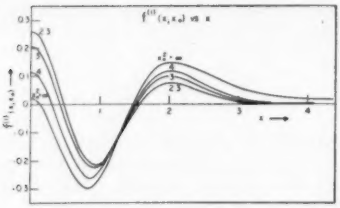

FIG. 1. $f^{(1)}(x; x_0)$ *versus* x for four values of x_0^2: $x_0^2 = \infty$; 4; 3; 2.3.

where

$$b_0(x_0) = -\frac{1}{2}\left[\frac{1-\exp(-x_0^2)}{x_0^2} - \mathrm{Ei}(-x_0^2)\right];$$
$$b_1(x_0) = -\mathrm{Ei}(-x_0^2); \tag{21'}$$
$$b_\nu(x_0) = a_\nu[1 - I(x_0^2; \nu-2)]; \quad \nu = 2, 3, 4, \cdots$$

$$-\mathrm{Ei}(-u) = \int_u^\infty e^{-t}t^{-1}dt$$

is the exponential integral; and

$$I(v; p)p! = \int_0^v e^{-t}t^p dt$$

is the incomplete gamma-function.[6]

The similarity between Eqs. (21) and (17) offers the possibility of condensing the functions $f^{(1)}(x; \infty)$ and $\kappa(x; x_0)$ into one expression. By doing so, we obtain a compact form for the distribution function:

$$f(x; x_0) = \exp(-x^2)/\sqrt{\pi} + (1/4G)f^{(1)}(x; x_0), \tag{22}$$

where now

$$f^{(1)}(x; x_0) = \frac{2}{\sqrt{\pi}}\exp(-x^2)\sum_{\nu=0}^{\infty}\alpha_\nu(x_0)x^{2\nu} \tag{23}$$

with the coefficients

$$\alpha_0(x_0) = \frac{1}{2}\left[\Psi(\tfrac{1}{2}) + \frac{1-\exp(-x_0^2)}{x_0^2} - \mathrm{Ei}(-x_0^2)\right];$$
$$\alpha_1(x_0) = \mathrm{Ei}(-x_0^2) - 1 - \Psi(\tfrac{1}{2}); \tag{23'}$$
$$\alpha_\nu(x_0) = \frac{\sqrt{\pi}}{2}\frac{I(x_0^2; \nu-2)}{\nu(\nu-1)\Gamma(\nu+\frac{1}{2})}, \quad \nu = 2, 3, 4, \cdots.$$

The power series in Eq. (23) converges for all values of x. It converges rapidly even for x larger than unity. Equation (23) may, therefore, be used conveniently for mathematical calculations.

Figure 1 shows the behavior of $f^{(1)}(x; x_0)$ for several values of the cut-off parameter x_0. The Molière correction function $f^{(1)}(x; \infty)$ has been drawn for comparison. In all cases, the two correction functions differ markedly from one another for angles appreciably greater than the cut-off angle. Indeed, as we shall prove in the Appendix, for $x \gg x_0$, our correction function becomes

$$f^{(1)}(x; x_0) \approx \frac{1}{2\sqrt{\pi}}\frac{1}{x_0^2 x}\exp[-(x-x_0)^2]$$
$$\times\left[1 + \left(x_0 + \frac{3}{2x_0}\right)\frac{1}{x} + \cdots\right]. \tag{24}$$

It thus drops to zero with increasing x much more rapidly than the Molière correction function which decreases as x^{-3} as x approaches infinity [see Eq. (19)]. Consequently, the "tail" of the distribution function is represented by the equation

$$f(x; x_0) \approx \frac{1}{\sqrt{\pi}}\left\{\exp(-x^2) + \frac{1}{8Gx_0^2 x}\exp[-(x-x_0)^2]\right.$$
$$\left.\times\left[1 + \left(x_0 + \frac{3}{2x_0}\right)\frac{1}{x} + \cdots\right]\right\}. \tag{25}$$

Among other consequences of the cutoff the following is worth mentioning: The mean-square angle of scattering is no longer infinity as in Molière's theory; for now the expression

$$\langle x^2\rangle_{su} \equiv \int_{-\infty}^{+\infty} x^2 f(x; x_0)dx \tag{26}$$

converges. Indeed, the substitution of Eqs. (22) and (23) into Eq. (26) and a straightforward integration and summation yield

$$\langle x^2\rangle_{su} = \frac{1}{2}\left(\frac{\varphi^2}{\sigma^2}\right)_{su} = \frac{1}{2}\left[1 + \frac{1}{2G}\{\ln(\gamma x_0^2) - 1 - \Psi(\tfrac{1}{2})\}\right]. \tag{27}$$

Alternately, the mean-square angle can be expressed as

$$\langle\varphi'^2\rangle_{su} \equiv \int_{-\varphi_0}^{+\varphi_0}\varphi'^2 f_1(\varphi'; \varphi_0)d\varphi', \tag{28}$$

where $f_1(\varphi'; \varphi_0)$ is the probability function of single scattering. By virtue of Eq. (4), one finds that

$$\langle\varphi'^2\rangle_{su} = Q\left[\frac{1}{2}\ln\frac{\varphi_0 + (\varphi_m^2 + \varphi_0^2)^{\frac{1}{2}}}{-\varphi_0 + (\varphi_m^2 + \varphi_0^2)^{\frac{1}{2}}} - \frac{\varphi_0}{(\varphi_m^2 + \varphi_0^2)^{\frac{1}{2}}}\right],$$

or, since $\varphi_0 \gg \varphi_m$,

$$\langle\varphi'^2\rangle_{su} \approx Q[\ln(2\varphi_0/\varphi_m) - 1]. \tag{29}$$

This is identical with Eq. (27), as one may verify by

[6] See K. Pearson, *Tables of the Incomplete Gamma-Function* (Cambridge University Press, Cambridge, 1946).

remembering that

$$\sigma^2=GQ;\quad x_0{}^2=\frac{\varphi_0{}^2}{2\sigma^2};\quad G=-\frac{1}{2}\ln\left(\frac{\gamma^2}{e}\frac{\varphi_m{}^2}{2\sigma^2}\right);$$

$$\Psi(\tfrac{1}{2})=2-\ln 4\gamma.$$

III. DISTRIBUTION OF MEAN-SQUARE ANGLE

The distribution function derived in Part II can be applied directly to the interpretation of experimental data only when the number of measured angles of scattering is very large and when all measurements refer to particles of the same kind and the same momentum. In this case a fitting of the experimental data to the theoretical distribution curve yields the value of the parameter σ and, therefore, affords a determination of the momentum of the particle. More simply, if $\varphi_1, \varphi_2, \cdots, \varphi_n$ represent the measured angles, the quantity

$$(\varphi^2)_{Av}\equiv\frac{1}{n}\sum_{i=1}^{n}\varphi_i{}^2 \tag{30}$$

may be regarded as equal to the mean-square angle, $\langle\varphi^2\rangle_{Av}$, which is related to σ by Eq. (27).

In the evaluation of cloud-chamber results, however, we are often faced with a different problem. The observed particles have, in general, different momenta and different masses, and each particle goes through a small number of plates. For each particle we may compute the value of $(\varphi^2)_{Av}$ by means of Eq. (30), but, because of the small value of n, there is no longer a definite relation between the value of $(\varphi^2)_{Av}$ and the value of σ^2 for the particle in question. From the distribution in the experimental values of $(\varphi^2)_{Av}$, we wish to derive the maximum amount of information concerning the scattering parameter σ. Clearly, for the solution of this problem, it is necessary to compute the distribution function for the quantity $(\varphi^2)_{Av}$ in the case of a homogeneous group of particles.

For simplicity, we neglect the momentum loss of the particles in the traversal of the plates and we introduce, instead of $(\varphi^2)_{Av}$, the quantity

$$\chi^2=\frac{n(\varphi^2)_{Av}}{2\sigma^2}=\sum_{i=1}^{n}x_i{}^2. \tag{31}$$

Let $F_n(\chi;x_0)d\chi$ represent the probability that χ lies between χ and $\chi+d\chi$. One may derive the mathematical expression of $F_n(\chi;x_0)$ with the following argument.

The distribution function for each of the n scattering variables x_i is known and is given by Eq. (22). Since we may consider the variables x_i as statistically independent, the probability that x_1 will lie in the interval between x_1 and x_1+dx_1, x_2 in the interval between x_2 and x_2+dx_2, etc., is given by the product of n expressions of the type of Eq. (22), *viz.*,

$$f_n(x_1,\cdots,x_n;x_0)d^nx = f(x_1;x_0)f(x_2;x_0)\cdots f(x_n;x_0)d^nx, \tag{32}$$

where d^nx stands for $dx_1dx_2\cdots dx_n$.

If one interprets the variables x_i as Cartesian coordinates in an n-dimensional space, one immediately sees from Eq. (31) that χ has a constant value over the surface of a hyper-sphere, since χ has the meaning of the radius of this hyper-sphere. Therefore, the probability $F_n(\chi;x_0)d\chi$ is given by the equation

$$F_n(\chi;x_0)d\chi=\int f(x_1;x_0)\cdots f(x_n;x_0)d^nx, \tag{33}$$

where the integration extends over the volume included between the hyper-spheres of radii χ and $\chi+d\chi$. One can easily prove that the following transformation satisfies Eq. (31):

$$\begin{aligned}
x_1&=\chi\cos\beta_1\cos\beta_2\cdots\cos\beta_{n-1},\\
x_2&=\chi\sin\beta_1\cos\beta_2\cdots\cos\beta_{n-1},\\
&\cdots\cdots\cdots\cdots\cdots\cdots\\
x_i&=\chi\sin\beta_{i-1}\cos\beta_i\cdots\cos\beta_{n-1},\\
&\cdots\cdots\cdots\cdots\cdots\cdots\\
x_n&=\chi\sin\beta_{n-1}.
\end{aligned}$$

The β_i, $(i=1,\cdots,n-1)$, are now independent variables with respect to the limits of the integral in Eq. (33). We write for the volume element

$$d^nx=dAd\chi,$$

where dA is the surface element on the n-dimensional hyper-sphere, and has the expression

$$dA=\begin{vmatrix}\partial x_1/\partial\chi & \cdots & \partial x_n/\partial\chi\\ \partial x_1/\partial\beta_1 & \cdots & \partial x_n/\partial\beta_1\\ \cdots & \cdots & \cdots\\ \partial x_1/\partial\beta_{n-1} & \cdots & \partial x_n/\partial\beta_{n-1}\end{vmatrix}d\beta_1d\beta_2\cdots d\beta_{n-1}$$

$$=\chi^{n-1}\cos\beta_2\cos^2\beta_3\cdots\cos^{n-2}\beta_{n-1}d\beta_1\cdots d\beta_{n-1}. \tag{34}$$

We can rewrite Eq. (33) as

$$F_n(\chi;x_0)d\chi = d\chi 2^n\int_0^{\pi/2}\cdots\int_0^{\pi/2}f(x_1;x_0)\cdots f(x_n;x_0)dA, \tag{35}$$

where dA is given by Eq. (34). The factor 2^n in Eq. (35) arises from the fact that the integral in Eq. (35) is extended only over the positive part (positive 2^n-ant) of our hyper-sphere. By substituting Eq. (22) for $f(x_i;x_0)$ and neglecting terms proportional to powers of $(1/2G)$ greater than the first, one obtains

$$F_n(\chi;x_0)=\left(\frac{2}{\sqrt{\pi}}\right)^n\exp(-\chi^2)$$

$$\times\int_0^{\pi/2}\cdots\int_0^{\pi/2}\left(1+\frac{1}{2G}\sum_{i=1}^{n}\sum_{\nu=0}^{\infty}\alpha_\nu(x_0)x_i{}^{2\nu}\right)dA. \tag{36}$$

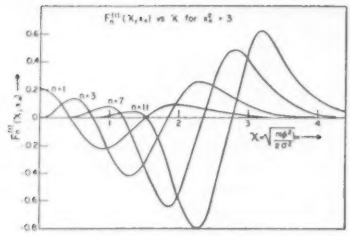

FIG. 2. $F_n^{(1)}(\chi; x_0)$ *versus* χ for $x_0^2=3$, and for four values of n: $n=1, 3, 7, 11$.

The integrals in Eq. (36) are all of the form

$$\int_A x_i^{2\mu} dA = \chi^{2\mu+n-1} \int_0^{\pi/2} \cdots \int_0^{\pi/2} \sin^{2\mu}\beta_{i-1} \cos\beta_i^{2\mu} \cdots$$

$$\times \cos^{2\mu}\beta_{n-1} \cos\beta_2 \cos^2\beta_3 \cdots \cos^{n-2}\beta_{n-1} d^{n-1}\beta.$$

This integral has the value

$$\int_A x_i^{2\mu} dA = \chi^{2\mu+n-1} \left(\frac{\sqrt{\pi}}{2}\right)^{n-1} \frac{\Gamma(\mu+\frac{1}{2})}{\Gamma(\mu+\frac{1}{2}n)}. \quad (37)$$

Note that the right-hand side of Eq. (37) is independent of the index i, so we can replace the sum over i in Eq. (36) by the factor n. By combining Eqs. (37) and (36) one thus obtains

$$F_n(\chi; x_0) = \frac{2}{\Gamma(\frac{1}{2}n)} \chi^{n-1} \exp(-\chi^2) \times \left(1+\frac{1}{2G}\sum_{\nu=0}^{\infty} \alpha_\nu^{(n)}(x_0)\chi^{2\nu}\right), \quad (38)$$

where

$$\alpha_\nu^{(n)}(x_0) = \frac{2}{\sqrt{\pi}} \frac{\Gamma(1+\frac{1}{2}n)\Gamma(\nu+\frac{1}{2})}{\Gamma(\nu+\frac{1}{2}n)} \alpha_\nu(x_0).$$

The coefficients α_ν are defined by Eqs. (23′). The series in Eq. (38) converges for all χ. Also, it can be shown that F_n is properly normalized, i.e.,

$$\int_0^\infty F_n(\chi; x_0) d\chi = 1.$$

The first term in Eq. (38) corresponds to the Gaussian approximation. It is identical with the expression known in the literature as "χ^2-distribution for n degrees of freedom." The second term represents the corrections to this normal distribution. Figure 2 shows the behavior of the correction function

$$F_n^{(1)}(\chi; x_0) = \frac{2}{\Gamma(\frac{1}{2}n)} \chi^{n-1} \exp(-\chi^2) \sum_{\nu=0}^{\infty} \alpha_\nu^{(n)}(x_0)\chi^{2\nu} \quad (39)$$

for $n=3, 7$, and 11. For the cut-off variable, x_0, we have taken $x_0^2=3$, which is a good approximate value for the $\frac{1}{4}$ inch lead plates. (A very accurate value of x_0 is not necessary since the correction functions $F_n^{(1)}$ are fairly insensitive to x_0.)

Figure 3 shows the deviation of F_n from the normal χ^2-distribution. The ordinate R_n represents the ratio

$$R_n(\chi; x_0) = \frac{[2/\Gamma(\frac{1}{2}n)]\chi^{n-1}\exp(-\chi^2)}{F_n(\chi; x_0)} = \frac{1}{1+(1/2G)\sum \alpha_\nu^{(n)}(x_0)\chi^{2\nu}} \quad (40)$$

for $2G=13.4$, $x_0^2=3$, and $n=1, 3, 7, 11$. In particular, R_1 represents the ratio of the Gaussian $\exp(-x^2)/\sqrt{\pi}$ to the distribution function $f(x; x_0)$, derived in Part II; $(F_1=2f(x; x_0))$. One sees that in all cases the deviations become significant for $\langle\varphi^2\rangle_{\text{Av}} > \sigma^2$.

To conclude the discussion on the distribution function F_n, we calculate the position of the maximum of $F_n(\chi; x_0)$. For this purpose we have to solve the equation

$$[\chi^2_{\text{most prob.}} - \tfrac{1}{2}(n-1)]\left(1+\frac{1}{2G}\sum_{\nu=0}^{\infty} \alpha_\nu^{(n)}\chi^{2\nu}_{\text{most prob.}}\right) - \frac{1}{2G}\sum_{\nu=1}^{\infty} \nu\alpha_\nu^{(n)}\chi^{2\nu}_{\text{most prob.}} = 0,$$

which follows from the differentiation of Eq. (38). By setting

$$\chi^2_{\text{most prob.}} = \tfrac{1}{2}(n-1) + \omega_n(x_0)/2G \quad (41)$$

and neglecting terms proportional to $(1/2G)^2$, we find that

$$\omega_n(x_0) = \sum_{\nu=1}^{\infty} \nu\alpha_\nu^{(n)}(x_0)\left(\frac{n-1}{2}\right)^\nu. \quad (42)$$

Table I gives the numerical values of ω_n for some values of x_0 and n. Combining Eqs. (31), (41), and (42) one thus has the following expression for the most probable value of the rms angle $\sqrt{\langle\varphi^2\rangle_{\text{Av}}}$:

$$[\langle\varphi^2\rangle_{\text{Av}}^{\frac{1}{2}}]_{\text{most prob.}} = \left(\frac{n-1}{n}\right)^{\frac{1}{2}} \sigma\left[1+\frac{1}{2G}\frac{\omega_n(x_0)}{n-1}\right]. \quad (41')$$

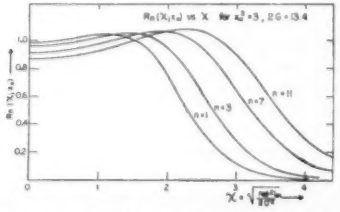

FIG. 3. $R_n(\chi; x_0)$ *versus* χ for $x_0^2=3$, $2G=13.4$, and for four values of n: $n=1, 3, 7, 11$.

IV. "NOISE LEVEL" SCATTERING[7]

We now turn our attention to a different problem that occurs in the theory of multiple scattering. Up to now, we have assumed that the projected angles of deflection corresponding to the scattering in the plates of a cloud chamber can be measured with absolute accuracy. In practice, of course, this is not the case. A cloud-chamber track consists of a discrete array of droplets whose centers do not lie exactly along the trajectory of the ionizing particle. This fact, together with the imperfection of the measuring instruments, introduce errors in the determination of the direction of the track between consecutive plates. These errors result in an apparent scattering that we may term "noise level" scattering.

Let us introduce an arbitrary line of reference, and let γ be the measured value of the angle between this line and the central line of the track. Let $\bar{\gamma}$ be the true value of this angle. The distribution of γ around $\bar{\gamma}$ may be assumed to be normal:

$$N_1(\gamma)=\frac{1}{\sigma_1(2\pi)^{\frac{1}{2}}}\exp\left[-\frac{1}{2\sigma_1^2}(\gamma-\bar{\gamma})^2\right],$$

where σ_1 is the standard deviation corresponding to the noise level scattering.

If we assume that there is no real scattering in any of n plates, the measured $(n+1)$ angles, $\gamma_0, \gamma_1, \cdots, \gamma_n$, between the line of reference and the ith section of the track will obey the $(n+1)$-dimensional normal distribution

$$N_{n+1}(\gamma_0, \cdots, \gamma_n)=\left[\frac{1}{\sigma_1(2\pi)^{\frac{1}{2}}}\right]^{n+1}\exp\left[-\frac{1}{2\sigma_1^2}\sum_{i=0}^{n}(\gamma_i-\bar{\gamma})^2\right]. \quad (43)$$

However, we are not interested in the distribution of the angles γ_i, but rather in the distribution of their consecutive differences, i.e.,

$$\Delta_i=\gamma_i-\gamma_{i-1}.$$

One may derive the n-dimensional distribution function of Δ_i from Eq. (43) by expressing the γ_i in terms of Δ_i. One finds

$$h_n(\Delta_1, \cdots, \Delta_n)=\left(\frac{1}{\sigma_1(2\pi)^{\frac{1}{2}}}\right)^n D_n^{-\frac{1}{2}}\times\exp\left[-\frac{1}{2\sigma_1^2}\sum_{i,k}^{n}a_{ik}^{-1}\Delta_i\Delta_k\right], \quad (44)$$

where a_{ik}^{-1} are the elements of the matrix reciprocal to the following matrix:

$$(a_{ik})=\begin{bmatrix} 2 & -1 & 0 & \cdot & \cdot & 0 \\ -1 & 2 & -1 & 0 & \cdot & 0 \\ 0 & -1 & 2 & -1 & \cdot & 0 \\ \cdot & \cdot & \cdot & \cdot & \cdot & \cdot \\ \cdot & \cdot & \cdot & \cdot & \cdot & \cdot \\ 0 & \cdot & \cdot & \cdot & -1 & 2 \end{bmatrix}$$

and D_n is the determinant of matrix (a_{ik}).

TABLE I. Numerical values of $\omega_n(x_0)=2G[x^2_{\text{most prob.}}-\frac{1}{2}(n-1)]$.

	$n=3$	$n=7$	$n=11$
$x_0^2=2.3$	−0.667	−0.964	−0.775
$x_0^2=3$	−0.628	−0.694	−0.190

On the other hand, if we disregard the noise level scattering, and consider only the real scattering in n plates, the n-dimensional distribution for the differences φ_i between the angular positions of consecutive segments of the track is described by Eq. (32):

$$f_n(\varphi_1, \cdots, \varphi_n; x_0)=\prod_{i=1}^{n}f(\varphi_i; x_0), \quad (45)$$

where

$$f(\varphi_i; x_0)=\frac{1}{\sigma(2\pi)^{\frac{1}{2}}}\times\exp(-\varphi_i^2/2\sigma^2)\left[1+\frac{1}{4G}\sum_{r=0}^{\infty}\alpha_r(x_0)\left(\frac{\varphi_i^2}{2\sigma^2}\right)^r\right]. \quad (45')$$

We are now in the position to write the complete distribution function for the actually observed angles:

$$\theta_i=\varphi_i+\Delta_i,$$

which include both real scattering and noise level scattering. This distribution function is given by

$$H_n(\theta_1, \cdots, \theta_n)=\int_{-\infty}^{+\infty}\cdots\int_{-\infty}^{+\infty}d^n\Delta\times\hat{f}_n(\theta_1-\Delta_1, \cdots, \theta_n-\Delta_n)h_n(\Delta_1, \cdots, \Delta_n), \quad (46)$$

where $\hat{f}_n$ is defined by Eq. (45), h_n is defined by Eq. (44) and $d^n\Delta$ stands for $d\Delta_1 d\Delta_2\cdots d\Delta_n$. One can integrate Eq. (46) without difficulty in the case where the functions $\hat{f}(\varphi_i, x_0)$ obey the normal distribution, i.e., if one neglects terms involving $(1/2G)$ in Eq. (45′). The result may be written as

$$H_n(\theta_1, \cdots, \theta_n)=\left(\frac{1}{\sigma'(2\pi)^{\frac{1}{2}}}\right)^n D_n'^{-\frac{1}{2}}\times\exp\left[-(1/2\sigma'^2)\sum_{i,k}^{n}A_{ik}^{-1}\theta_i\theta_k\right], \quad (47)$$

[7] This discussion is based in outline on the theory of noise level scattering in photographic plates developed by G. Molière [*Theorie der Streuung schneller geladener Teilchen, III*, to be published]. It is an adaptation of Molière's theory for the analysis of multiple-plate cloud-chamber pictures.

where now

$$\sigma'^2=(1+2\mu)\sigma^2; \quad \mu=\sigma_1^2/\sigma^2,$$

$$A_{ik}=(\delta_{ik}+\mu a_{ik})/(1+2\mu), \quad \delta_{ik}=\begin{cases}1 & i=k\\ 0 & i\neq k\end{cases};$$

$$D_n'=\det(A_{ik}).$$

Explicitly, one has for A_{ik}

$$(A_{ik})=\begin{bmatrix}1 & -\epsilon & 0 & 0 & \cdot & 0\\ -\epsilon & 1 & -\epsilon & 0 & \cdot & 0\\ 0 & -\epsilon & 1 & -\epsilon & \cdot & 0\\ \cdot & \cdot & \cdot & \cdot & \cdot & \cdot\\ \cdot & \cdot & \cdot & \cdot & \cdot & \cdot\\ 0 & \cdot & \cdot & \cdot & -\epsilon & 1\end{bmatrix}, \tag{48}$$

with $\epsilon=\mu/(1+2\mu)$. Furthermore, note that all parameters in Eq. (47), i.e., σ', D_n', A_{ik}, are expressed in terms of one quantity μ. If μ approaches zero, H_n approaches the distribution function $\bar{f}_n$ computed under the Gaussian approximation, i.e., the function

$$\bar{f}_n(\varphi_1, \cdots, \varphi_n)=\left(\frac{1}{\sigma(2\pi)^{\frac{1}{2}}}\right)^n \exp\left[-\frac{1}{2\sigma^2}\sum_{i=1}^{n}\varphi_i^2\right].$$

Explicit formulas for D_n' and the reciprocal matrix elements A_{ik}^{-1} may be calculated from the matrix (48). Because of its complicated character we shall omit this computation and limit ourselves to one special case

$$\mu\ll 1,$$

i.e., we assume that the noise level scattering is much smaller than the real scattering. In this case

$$\epsilon\approx\mu; \quad (A_{ik}^{-1})\approx\begin{bmatrix}1 & \mu & 0 & 0 & \cdot & 0\\ \mu & 1 & \mu & 0 & \cdot & 0\\ 0 & \mu & 1 & \mu & \cdot & 0\\ \cdot & \cdot & \cdot & \cdot & \cdot & \cdot\\ \cdot & \cdot & \cdot & \cdot & \cdot & \cdot\\ 0 & \cdot & \cdot & \cdot & \mu & 1\end{bmatrix},$$

and $D_n'\approx 1$, so that the expression in the exponent of Eq. (47) becomes simply

$$\sum_{i,k}^{n} A_{ik}^{-1}\theta_i\theta_k\approx\theta_1^2+\theta_2^2+\cdots+\theta_n^2 +2\mu(\theta_1\theta_2+\theta_2\theta_3+\cdots+\theta_{n-1}\theta_n).$$

Hence we may write for Eq. (47)

$$H_n(\theta_1, \cdots, \theta_n)\approx\left(\frac{1}{\sigma'(2\pi)^{\frac{1}{2}}}\right)^n \exp\left[-\frac{1}{2\sigma'^2}\sum_{i=1}^{n}\theta_i^2\right] \times\left[1-\frac{\mu}{\sigma'^2}(\theta_1\theta_2+\cdots+\theta_{n-1}\theta_n)\right]. \tag{49}$$

From Eq. (49) one can see that the noise level scattering has two effects. First, it increases the standard deviation from the value σ to the value

$$\sigma'\approx(1+\mu)\sigma.$$

Secondly, it introduces a statistical correlation between the consecutive angles θ_i and θ_{i+1}. The n-dimensional distribution function can no longer be expressed as a product of Gaussians, i.e., the scattering angles are no longer statistically independent. However, one may verify that the distribution function for the root-mean-square angle $(\theta^2)_{Av}^{\frac{1}{2}}$ is not affected by the correlation mentioned above. An integration of H_n, similar to that discussed in Part III, yields the following distribution for $\chi'=[n(\theta^2)_{Av}/2\sigma'^2]^{\frac{1}{2}}$:

$$F_n'(\chi'; x_0)d\chi'\approx\frac{2}{\Gamma(\frac{1}{2}n)}\chi'^{n-1}\exp(-\chi'^2) \times\left[1+\frac{1}{2G}\sum\alpha_\nu^{(n)}(x_0)\chi'^{2\nu}+\cdots\right],$$

i.e., $(\theta^2)_{Av}$ is distributed in the same manner as $(\varphi^2)_{Av}$ but has a different standard deviation. The latter fact affects the position of the maximum of the distribution in rms angle. We now have for small μ

$$[(\theta^2)_{Av}^{\frac{1}{2}}]_{\text{most prob.}}=(1+\mu)[(\varphi^2)_{Av}^{\frac{1}{2}}]_{\text{most prob.}},$$

where $[(\varphi^2)_{Av}^{\frac{1}{2}}]_{\text{most prob.}}$ is given by Eq. (41′).

The noise level scattering also modifies the expression (29), *viz.*,

$$\langle\theta^2\rangle_{Av}=(1+2\mu)Q[\ln(2\varphi_0/\varphi_m)-1].$$

The author wishes to express his gratitude to Professor B. Rossi for his great interest and active help in the preparation of this paper, and to Dr. W. T. Scott for his review and criticism of the manuscript.

APPENDIX

The representation of the correction function $f^{(1)}(x; x_0)$ in power series of x, as given by Eq. (23), is inconvenient for the study of the behavior of this function for large arguments. In order to find the asymptotic expansion of $f^{(1)}(x; x_0)$ for $x\gg 1$ we rewrite the correction function as follows:

$$f^{(1)}(x; x_0)=\frac{2}{\sqrt{\pi}}\exp(-x^2)\left[\alpha_0+\alpha_1 x^2 +\sum_{k=0}^{\infty}(-1)^k\frac{x_0^{2k-2}}{k!}w_k(z)\right], \tag{A1}$$

where $z=2xx_0$ and

$$w_k(z)=\frac{1}{2}\sum_{\nu=2}^{\infty}\frac{z^{2\nu}}{(2\nu)!(\nu-1+k)}. \tag{A2}$$

One may verify the correctness of the above expressions

by making use of the following formula:

$$I(x_0^2;\nu-2)=\frac{1}{(\nu-2)!}\sum_{k=0}^{\infty}(-1)^k\frac{x_0^{2k+2\nu-2}}{k!(\nu-1+k)}. \quad \text{(A3)}$$

By virtue of the known theorem

$$\frac{1}{(2\nu)!}=\frac{1}{2\pi i}\int_\gamma e^t t^{-2\nu-1}dt$$

(where γ represents any integration path encircling the origin once in a counter clockwise direction), we may express Eq. (A2) as follows:

$$w_k(z)=\frac{1}{2z}\frac{1}{2\pi i}\int_\gamma dt e^t\sum_{\nu=2}^{\infty}\left(\frac{z}{t}\right)^{2\nu+1}\frac{1}{k+\nu-1}. \quad \text{(A4)}$$

If we choose the integration path so that $|z/t|<1$, we may sum up the series in Eq. (A4) as

$$\sum_{\nu=2}^{\infty}\left(\frac{z}{t}\right)^{2\nu+1}\frac{1}{\nu+k-1}=-\left(\frac{z}{t}\right)^{2-2k}\left[\ln\left(1-\frac{z^2}{t^2}\right)+p_k\left(\frac{z}{t}\right)\right],$$

where

$$p_0=0;\quad p_k(\zeta)=\sum_{\mu=1}^{k}\frac{\zeta^{2\mu}}{\mu},\quad k=1,2,3,\cdots.$$

We thus obtain the following integral representation for $w_k(z)$:

$$w_k(z)=-\tfrac{1}{2}z^{2-2k}\frac{1}{2\pi i}\int_\gamma dt e^t t^{3-2k}\left[\ln\left(1-\frac{z^2}{t^2}\right)+p_k\left(\frac{z}{t}\right)\right]. \quad \text{(A5)}$$

By deforming the integration path, γ, into three parts, γ_0, γ_+, and γ_-, as indicated in Fig. 4, we may express Eq. (A5) as a sum of three contributions, $w_k^{(0)}$, $w_k^{(+)}$, and $w_k^{(-)}$, corresponding to the three paths, γ_0, γ_+, and γ_-, respectively; i.e., we put

$$w_k=w_k^{(0)}+w_k^{(+)}+w_k^{(-)}.$$

By expanding the integrand in Eq. (A5) in inverse powers of z, one finds

$$w_0^{(0)}=\tfrac{1}{2}z^2(\tfrac{3}{2}-\ln\gamma);\quad w_1^{(0)}=-\tfrac{1}{4}z^2-\ln\gamma;$$

$$w_k^{(0)}=-\left[\frac{z^2}{4k}-\frac{1}{2}\frac{1}{k-1}+z^{2-2k}\Gamma(2k-2)\right],\quad k=2,3,\cdots;$$

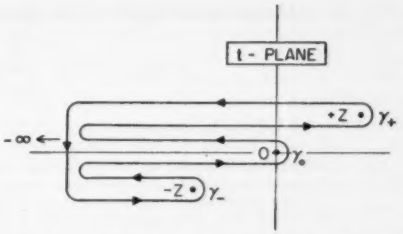

FIG. 4. Integration path γ for the integral in Eq. (A5).

and

$$w_k^{(\pm)}\approx\frac{1}{2z}\sum_{\mu=0,1,2,3,\cdots}\binom{2k-3}{\mu}\frac{\mu!}{(\mp z)^\mu},$$

$$k=0,1,2,3,4,\cdots.$$

Substituting the above expressions into Eq. (A1) and summing over k, we obtain the following semiconvergent series:

$$f^{(1)}(x;x_0)\approx\frac{2}{\sqrt{\pi}}\exp(-x^2)\left[\ln(2x_0)(2x^2-1)-\frac{1!}{(2x)^2}+\frac{3!}{(2x)^4}\mp\cdots\right]$$
$$+\frac{1}{2x\sqrt{\pi}}\left[\exp[-(x-x_0)^2]\sum_{\mu=0,1,2,\cdots}\frac{q_\mu(x_0)}{(2x)^\mu}-\exp[-(x+x_0)^2]\sum_{\mu=0,1,2,\cdots}\frac{q_\mu(x_0)}{(-2x)^\mu}\right], \quad \text{(A6)}$$

where

$$q_\mu(x_0)=(-1)^\mu\exp(x_0^2)\frac{d^\mu}{dx_0^\mu}\left(\frac{\exp(-x_0^2)}{x_0^3}\right).$$

For the case where x_0 is of the order of one, Eq. (A6) becomes for $x\gg1$

$$f^{(1)}(x;x_0)\to\frac{1}{2\sqrt{\pi}}\frac{\exp[-(x-x_0)^2]}{xx_0^3}\times\left[1+\left(x_0+\frac{3}{2x_0}\right)\frac{1}{x}+\cdots\right].$$

Mass Corrections to the Fine Structure of Hydrogen-Like Atoms

E. E. SALPETER
Laboratory of Nuclear Studies, Cornell University, Ithaca, New York
(Received March 7, 1952)

A relativistic four-dimensional wave equation, derived previously, for bound states of a two-body system is discussed further. For any "instantaneous" interaction function an exact three-dimensional equation is derived from it, similar to, but not identical with, the Breit equation. A perturbation theory is developed for a small additional non-instantaneous interaction.

Using this covariant method, corrections of relative order $\alpha(m/M)$ to the fine structure of hydrogen, due to the finite mass of the nucleus, are calculated. No terms of this order were obtained in previous approximate treatments using the Breit equation. Some of the terms obtained contain $\log\alpha$ as a factor. It is shown that these special terms can also be derived simply by means of orthodox quantum electrodynamics and perturbation theory.

These corrections to the fine structure are $+0.379$ Mc/sec for the $2s$ state of hydrogen and -0.017 Mc/sec for the $2p$ state. For hydrogen-like atoms with heavier nuclei the corrections are roughly (Z^4/A) times those for hydrogen.

I. INTRODUCTION

FOR a hydrogen-like atom with an infinitely heavy nucleus the Dirac equation gives an exact expression for the fine structure. If the infinitely heavy nucleus is assumed to have a fixed magnetic dipole moment of the Pauli type, an exact expression is also obtained from the Dirac equation for the hyperfine structure. For a nucleus of mass M, corrections arise to these expressions, due to the motion of the nucleus (apart from the fact that the reduced mass μ has to be used in the nonrelativistic approximation to the binding energy). One would expect these corrections to involve the ratio m/M, where m is the electron mass, and some power of the fine structure constant α. Since the fine structure and hyperfine structure are themselves essentially relativistic terms, corrections to these terms due to nuclear motion require a relativistic treatment for bound-states of a two-body system.

Many years ago an approximately relativistic treatment of such problems was proposed by Breit.[1] One can first solve exactly (or at least approximately to the required accuracy) the Breit equation for one electron and one nucleus using as interaction only the instantaneous Coulomb interaction. One can then allow for the effect of retardation, at least approximately, by adding to the Hamiltonian the so-called Breit interaction. This Breit interaction is equivalent to a term obtained from quantum field theory by second-order perturbation theory, due to the exchange of one transverse photon between the electron and nucleus, if the recoil energy of the electron and nucleus is neglected in the intermediate state. If we further prescribe that this Breit interaction is to be considered as a small perturbation and only its expectation value is to be evaluated, then this treatment can be carried out unambiguously. Essentially such a program was carried out very carefully for the fine structure (fs) by Breit and Brown[2] and for the hyperfine structure (hfs) by Breit, Brown, and Arfken[3] for hydrogen-like atoms. Expanding in powers of m/M they find first of all a correction factor of $(1-m/M)$ for the fs. This correction can be included in the Dirac expression for fs by replacing m by the reduced mass μ. Breit, Brown, and Arfken show that no correction terms of relative order of magnitude $\alpha(m/M)$ are obtained, neither for fs nor hfs if the aforementioned prescriptions are used.

But, as mentioned above and pointed out previously by Breit and others, a treatment involving the Breit equation and interaction is only approximately relativistic and the orders of magnitude of the errors made cannot be obtained very easily. It is the main aim of the present paper to show that corrections of relative order $\alpha(m/M)$ are obtained for the fs, if a fully relativistic treatment is used, and expressions are derived for these corrections. In the main part of the present paper we only deal with the case of hydrogen and consider the proton, which forms the nucleus, to be a point particle of the Fermi-Dirac type and neglect any internal structure of the proton (anomalous magnetic moment, mesonic charge cloud, etc.). No divergences occur in the terms treated, even for a point particle. In Sec. VII a simple, but approximate, generalization of the case of a nucleus consisting of several nucleons will be given. In a subsequent paper nuclear structure effects omitted in the present paper, as well as various corrections to the Lamb shift, will be discussed. In another paper it will be shown that corrections of the same relative order are also obtained for the hfs.

Recently a four-dimensional, fully relativistic wave equation for bound states of two Fermi-Dirac particles, with an arbitrary interaction between them, was derived from the Feynman[4] formalism by Salpeter and Bethe.[5] A rigorous derivation of this equation from quantum field-theory was given by Gell-Mann and Low.[6] The

[1] G. Breit, Phys. Rev. **34**, 553 (1929).
[2] G. Breit and G. E. Brown, Phys. Rev. **74**, 1278 (1948).
[3] Breit, Brown, and Arfken, Phys. Rev. **76**, 1299 (1949).
[4] R. P. Feynman, Phys. Rev. **76**, 749 (1949).
[5] E. E. Salpeter and H. A. Bethe, Phys. Rev. **84**, 1232 (1951), thereafter referred to as SB.
[6] M. Gell-Mann and F. Low, Phys. Rev. **84**, 350 (1951).

aim of the present paper is twofold. First, to derive a perturbation method for the solution of a general equation of this type, for which the main interaction term is instantaneous and the coupling constant small. Secondly, to use the methods developed to calculate corrections of order $\alpha(m/M)$(fs) to the expressions obtained by Breit and co-workers for the fine structure.

In Sec. II it will be shown that, if the interaction function occurring in this four-dimensional wave equation is instantaneous, an exact three-dimensional wave equation can be derived, which is similar to, but not identical with, the equivalent Breit equation. The equivalent of first-order perturbation theory for such a four-dimensional equation is also derived. In Sec. III the general theory of Sec. II is applied to the special case of the Coulomb interaction in hydrogen, where an expansion in powers of m/M can be used. In Sec. IV it is shown how the correction terms due to the exchange of transverse photons can be derived from the four-dimensional equation. Some of the correction terms of order $\alpha(m/M)$ also contain $\log\alpha$ as a factor. In Sec. V it is shown that these special terms can also be derived very simply, directly from quantum field theory, by means of orthodox (not fully relativistic) perturbation theory. In Sec. VI the exact expressions for all the correction terms of order $\alpha(m/M)$ for the fs of hydrogen (with $m \ll M$) are calculated.

II. INSTANTANEOUS INTERACTION AND PERTURBATION THEORY FOR THE FOUR-DIMENSIONAL EQUATION

A. Instantaneous Interaction

Wherever possible we shall use the same notation as used by Feynman[4] and SB,[5] and we put $\hbar=c=1$. In the Feynman formalism for two Fermi-Dirac particles of equal and opposite electric charge e two alternative expressions for the electromagnetic interaction function can be used. In momentum space these two functions are

$$G(k_\mu)=(e^2/2\pi^2)(\gamma_\mu{}^a\gamma_\mu{}^b/k_\mu{}^2) \tag{1}$$

and

$$G(k_\mu)=-(e^2/2\pi^2)\left[(\gamma_4{}^a\gamma_4{}^b/k^2)+\left(\sum_{i=1}^{2}\gamma_i{}^a\gamma_i{}^b/k_\mu{}^2\right)\right], \tag{2}$$

where γ_μ is the usual Dirac-matrix four-vector and the suffix a refers to particle a, k_μ is the four-dimensional energy-momentum transfer, and $\mathbf{k}$ denotes the three-dimensional momentum-components of this vector. k^2 denotes $|\mathbf{k}|^2$ and $k_\mu{}^2$ denotes $[k_4{}^2-|\mathbf{k}|^2]$. In (2) the first term represents exactly the Coulomb interaction, instantaneous in a particular frame of reference. In the second part of (2), which we shall call the transverse part, the sum over $i=1$ to 2 involves a summation over two mutually perpendicular directions of polarization, both perpendicular to $\mathbf{k}$.

One might be tempted to use the manifestly Lorentz-invariant form (1), in which case the elegant methods of integration used by Feynman[4] could be used without modification. If expression (1) were used in the present problem, however, the higher terms $G^{(n)}$ in the expansion for the complete interaction function $\bar{G}$, defined by SB, are fairly large and, to several orders in α, pairs of correction terms would be obtained which finally cancel each other. The similar case of a deuteron with neutral scalar mesons was discussed by SB. For this reason it is more convenient to use expression (2). The loss of relativistic elegance, entailed by this choice, is compensated by the fact that a nonrelativistic treatment, involving only the first part of (2), already furnishes a fairly good approximation.

We first discuss the solutions of a general four-dimensional wave equation of the type derived by SB, but with the complete interaction function $\bar{G}(k_\mu)$ replaced by a function $G(\mathbf{k})$, which is quite general except that it depends only on $\mathbf{k}$, the first three components of the energy-momentum transfer k_μ. The Fourier-transform of such a function $G(\mathbf{k})$ is an instantaneous potential in coordinate space. Such an interaction function is, of course, not Lorentz-invariant. After separating out the motion of the "center of mass," the equation we consider is of the form[5]

$$(\mu_a K_\mu\gamma_\mu{}^a+p_\mu\gamma_\mu{}^a-m_a)(\mu_b K_\mu\gamma_\mu{}^b-p_\mu\gamma_\mu{}^b-m_b)\psi(p_\mu) = -(2\pi i)^{-1}\int d^4k G(\mathbf{k})\psi(p_\mu+k_\mu), \tag{3}$$

where K_μ is a fixed four-vector (energy-momentum of the "center of mass"), whose spatial components are zero and whose fourth component is E. E then represents the eigenvalue of this equation. p_μ is the relative energy-momentum four-vector and $p_\mu\gamma_\mu{}^a$ and $p_\mu\gamma_\mu{}^b$ differ only by the γ-operators operating on particles a and b, respectively. The dimensionless coefficients μ_a and μ_b are

$$\mu_a=m_a/(m_a+m_b), \quad \mu_b=m_b/(m_a+m_b).$$

The wave function $\psi(p_\mu)$ is a 16-component spinor.

On multiplying Eq. (3) by $\gamma_4{}^a\gamma_4{}^b$ we obtain

$$F(p_\mu)\psi(p_\mu)=-(2\pi i)^{-1}\int d^4k G'(\mathbf{k})\psi(p_\mu+k_\mu), \tag{4}$$

where

$$F(p_\mu)\equiv[\mu_a E-H_a(\mathbf{p})+\epsilon][\mu_b E-H_b(\mathbf{p})-\epsilon],$$
$$H_a(\mathbf{p})\equiv(m_a\beta^a+\mathbf{p}\cdot\boldsymbol{\alpha}^a), \quad H_b(\mathbf{p})\equiv(m_b\beta^b-\mathbf{p}\cdot\boldsymbol{\alpha}^b),$$
$$G'(\mathbf{k})=\gamma_4{}^a\gamma_4{}^b G(\mathbf{k}), \qquad \epsilon\equiv p_4.$$

$G'(\mathbf{k})$ is completely general, except for it being independent of k_4, and may contain Dirac matrices. For our equation to represent Dirac hole theory both m_a and m_b must be considered to contain a negative imaginary infinitesimal part, according to the prescriptions of the Feynman formalism. As in SB, we

define a three-dimensional wave function $\phi(\mathbf{p})$,

$$\phi(\mathbf{p})=\int_{-\infty}^{\infty}d\epsilon\psi(\mathbf{p},\epsilon). \tag{5}$$

Since $G'(\mathbf{k})$ does not depend on $k_4\equiv\omega$ we can integrate the RHS of (4) immediately over ω, which gives

$$\Gamma(\mathbf{p})\equiv-(2\pi i)^{-1}\int d^3kG'(\mathbf{k})\phi(\mathbf{p}+\mathbf{k}). \tag{6}$$

We define the usual Casimir projection operators for the two particles

$$\begin{aligned}\Lambda_+{}^a(\mathbf{p})&=[E_a(p)+H_a(\mathbf{p})]/2E_a(p),\\ \Lambda_-{}^a(\mathbf{p})&=[E_a(p)-H_a(\mathbf{p})]/2E_a(p),\end{aligned} \tag{7}$$

where

$$E_a(p)=+(m_a{}^2+p^2)^{\frac{1}{2}},$$

with similar definitions for the particle b. We further define four wave functions

$$\begin{aligned}\psi_{++}(p_\mu)&=\Lambda_+{}^a(\mathbf{p})\Lambda_+{}^b(\mathbf{p})\psi(p_\mu),\\ \psi_{-+}(p_\mu)&=\Lambda_-{}^a(\mathbf{p})\Lambda_+{}^b(\mathbf{p})\psi(p_\mu),\text{ etc.}\end{aligned} \tag{8}$$

We can now write (4) in the form of four simultaneous equations, using Eq. (6),

$$F_{++}(\mathbf{p},\epsilon)\psi_{++}(\mathbf{p},\epsilon)=\Lambda_+{}^a(\mathbf{p})\Lambda_+{}^b(\mathbf{p})\Gamma(\mathbf{p}), \tag{9a}$$

$$F_{-+}(\mathbf{p},\epsilon)\psi_{-+}(\mathbf{p},\epsilon)=\Lambda_-{}^a(\mathbf{p})\Lambda_+{}^b(\mathbf{p})\Gamma(\mathbf{p}), \tag{9b}$$

$$F_{+-}(\mathbf{p},\epsilon)\psi_{+-}(\mathbf{p},\epsilon)=\Lambda_+{}^a(\mathbf{p})\Lambda_-{}^b(\mathbf{p})\Gamma(\mathbf{p}), \tag{9c}$$

$$F_{--}(\mathbf{p},\epsilon)\psi_{--}(\mathbf{p},\epsilon)=\Lambda_-{}^a(\mathbf{p})\Lambda_-{}^b(\mathbf{p})\Gamma(\mathbf{p}), \tag{9d}$$

where

$$\begin{aligned}F_{++}(p,\epsilon)&=[\mu_aE-E_a(p)+\epsilon+i\delta]\\ &\quad\times[\mu_bE-E_b(p)-\epsilon+i\delta],\\ F_{-+}(p,\epsilon)&=[\mu_aE+E_a(p)+\epsilon-i\delta]\\ &\quad\times[\mu_bE-E_b(p)-\epsilon+i\delta],\text{ etc.}\end{aligned} \tag{10}$$

In (10) we have written out explicitly the imaginary term coming from the imaginary negative parts of m_a and m_b, δ being an infinitesimal, real, and positive quantity.

The RHS of Eq. (9) does not depend on the variable ϵ. We can divide the four Eqs. (9) by the appropriate function $F(p,\epsilon)$, which no longer contains any Dirac operators. The only term on the RHS depending on ϵ is then $F^{-1}(p,\epsilon)$ and the four equations can then be integrated over ϵ. Using the relations

$$\begin{aligned}\int_{-\infty}^{\infty}d\epsilon(a\pm i|\delta|-\epsilon)^{-1}(b\pm i|\delta|+\epsilon)^{-1}\\ =\pm(2\pi i)(a+b)^{-1},\end{aligned} \tag{11}$$

$$\int_{-\infty}^{\infty}d\epsilon(a\pm i|\delta|-\epsilon)^{-1}(b\mp i|\delta|+\epsilon)^{-1}=0,$$

and Eq. (5), the integrated Eqs. (9) reduce to four coupled three-dimensional equations,

$$\begin{aligned}&[E-E_a(p)-E_b(p)]\phi_{++}(\mathbf{p})\\ &\quad=\Lambda_+{}^a(\mathbf{p})\Lambda_+{}^b(\mathbf{p})\int d^3kG'(\mathbf{k})\phi(\mathbf{p}+\mathbf{k}),\end{aligned} \tag{12a}$$

$$\begin{aligned}&[E+E_a(p)+E_b(p)]\phi_{--}(p)\\ &\quad=-\Lambda_-{}^a(\mathbf{p})\Lambda_-{}^b(\mathbf{p})\int d^3kG'(k)\phi(\mathbf{p}+\mathbf{k}),\end{aligned} \tag{12b}$$

$$\phi_{-+}(\mathbf{p})=\phi_{+-}(\mathbf{p})=0, \tag{12c}$$

where the three-dimensional wave functions $\phi_{++}(\mathbf{p})$, etc., are derived from $\phi(\mathbf{p})$ in a manner analogous to Eq. (8). The four coupled Eqs. (12) can now be written as one single operator equation

$$\begin{aligned}&[E-H_a(\mathbf{p})-H_b(\mathbf{p})]\phi(\mathbf{p})\\ &\quad=\{\Lambda_+{}^a(\mathbf{p})\Lambda_+{}^b(\mathbf{p})-\Lambda_-{}^a(\mathbf{p})\Lambda_-{}^b(\mathbf{p})\}\\ &\qquad\times\int d^3kG'(\mathbf{p})\phi(\mathbf{p}+\mathbf{k}),\end{aligned} \tag{13}$$

which is the main result of this section. In deriving (13) we have used the identity

$$\begin{aligned}&[\Lambda_+{}^a(\mathbf{p})\Lambda_+{}^b(\mathbf{p})+\Lambda_-{}^a(\mathbf{p})\Lambda_+{}^b(\mathbf{p})+\Lambda_+{}^a(\mathbf{p})\Lambda_-{}^b(\mathbf{p})\\ &\qquad+\Lambda_-{}^a(\mathbf{p})\Lambda_-{}^b(\mathbf{p})]=1.\end{aligned} \tag{14}$$

The dependence of $\psi(p_\mu)$ on ϵ is then determined completely and the wave function can be written in the form

$$\psi(p_\mu)=-[E-H_a(\mathbf{p})-H_b(\mathbf{p})][2\pi iF(p,\epsilon)]^{-1}\chi(\mathbf{p}), \tag{15}$$

where $\chi(\mathbf{p})$ is a 16-component spinor independent of ϵ and

$$\phi(\mathbf{p})=\{\Lambda_+{}^a(\mathbf{p})\Lambda_+{}^b(\mathbf{p})-\Lambda_-{}^a(\mathbf{p})\Lambda_-{}^b(\mathbf{p})\}\chi(\mathbf{p}). \tag{15a}$$

Using (15) and (9) we also find that

$$[E-H_a(\mathbf{p})-H_b(\mathbf{p})]\chi(\mathbf{p})=\int d^3kG'(\mathbf{k})\phi(\mathbf{p}+\mathbf{k}). \tag{15b}$$

We note that Eq. (13) is similar to the equivalent Breit equation for the present problem,

$$[E-H_a(\mathbf{p})-H_b(\mathbf{p})]\phi(\mathbf{p})=\int d^3kG'(\mathbf{k})\phi(\mathbf{p}+\mathbf{k}), \tag{16}$$

but differs from it by containing the term in curly brackets, which contains several projection operators. In the nonrelativistic limit, with both particles in positive energy states, only ϕ_{++} is important and Eqs. (13) and (16) are identical in this limit. An

approximate equation of similar form to Eq. (13) has been derived previously by Brown and Ravenhall.[7]

It is of some interest to note how the equations would be modified if single-electron theory were used instead of hole theory. In the Feynman formalism the only change would be that the energy E, instead of the masses m_a and m_b, has an infinitesimal imaginary part. This would mean that the sign multiplying $i\delta$ in all the expressions (10) for F would be the same. On integrating (9) one would then obtain exactly the Breit-equation, Eq. (16), instead of Eq. (13). In the non-relativistic limit with, say, one electron and one proton for both particles in negative energy states, only ϕ_{--} is important and the kinetic energies are negative. If the Breit equation is used, the interaction energy is also negative and no bound states are obtained, which is quite consistent with single-electron theory. However, if Eq. (13) is used, the interaction energy is now positive and bound states are obtained, with kinetic, interaction, and binding energies all equal and opposite to the equivalent quantities for a bound state for both particles in positive energy states. Such a wave function could then be said to correspond to a bound state of a positron and a negative proton. Our main conclusion is that, even if an instantaneous interaction is postulated, the Breit equation is only correct for single-electron theory but not for hole theory.

B. Perturbation Theory

The function F, defined in Eq. (4), is not only a function of the variables $(\mathbf{p}, \epsilon)$, but is also a quadratic function of the constant eigenvalue E. Thus E occurs quadratically in our fundamental equation and not linearly as in the three-dimensional Schrödinger equation. To obtain the equivalent of first-order perturbation theory for such equations we therefore have to use a slightly different method of derivation.

Equation (13) is an ordinary Schrödinger equation of Hamiltonian form. Let $\phi_n(\mathbf{p})$, E_n be the wave function and energy eigenvalue, respectively, for any stationary state of this equation. The wave function $\psi_n(p_\mu)$ is then determined explicitly by Eq. (15), where the value E_n is substituted for E both in the numerator and in the expression F_n for F. The function $\chi_n(\mathbf{p})$ is then also determined by Eq. (15b). We assume ϕ_n to be normalized in such a way that

$$\int d^3p\chi^*(\mathbf{p})\phi(\mathbf{p})=\int d^3p[\phi_{++}{}^*(\mathbf{p})\phi_{++}(\mathbf{p}) -\phi_{--}{}^*(\mathbf{p})\phi_{--}(\mathbf{p})]=1. \quad (17)$$

For simplicity we denote the integral operator involving $-(2\pi i)^{-1}G'(\mathbf{k})$ by $\mathcal{G}$. Equation (4) can then be written as

$$(F_n-\mathcal{G})\psi_n=0. \quad (18)$$

[7] G. E. Brown and D. G. Ravenhall, Proc. Roy. Soc. (London) **A208**, 552 (1951).

For any arbitrary constant value E_Δ (not necessarily equal to E_n) we can define two new functions

$$\psi_n{}^\Delta(p_\mu)=-[E_\Delta-H_a(\mathbf{p})-H_b(\mathbf{p})]\times[2\pi iF_\Delta(p,\epsilon)]^{-1}\chi_n(\mathbf{p}), \quad (19)$$

$$\bar{\psi}_n{}^\Delta(p_\mu)=-[E_\Delta-H_a(\mathbf{p})-H_b(\mathbf{p})]\times[2\pi iF_\Delta(p,\epsilon)]^{-1}\chi_n{}^*(\mathbf{p}), \quad (19a)$$

where F_Δ is the expression for F with E having the value E_Δ. Using the fact that $G'(\mathbf{k})$ does not depend on k_4 and using Eqs. (5), (11), (15b), and (19), it can be shown that

$$(F_\Delta-\mathcal{G})\psi_n{}^\Delta=-(2\pi i)^{-1}(E_\Delta-E_n)\chi_n, \quad (20)$$

$$\bar{\psi}_n{}^\Delta(F_\Delta-\mathcal{G})=-(2\pi i)^{-1}(E_\Delta-E_n)\chi_n{}^*. \quad (20a)$$

Equation (20a) is correct in the sense that the LHS and RHS yield identical expressions when they are multiplied on the right by an arbitrary function $\psi'(p_\mu)$ and are integrated over d^4p.

We next consider an equation similar to Eq. (4), but with an extra interaction function $G_\Delta'(k_\mu)$ added to $G'(\mathbf{k})$, which is considered only as a small perturbation but which may depend on k_4. Consider the particular solution $\Psi_n(p_\mu)$ of this modified equation which reduces to $\psi_n(p_\mu)$ as G_Δ' approaches zero. Let the energy eigenvalue of this state be

$$E_\Delta=E_n+\Delta E. \quad (21)$$

Denoting again the integral operator involving $-(2\pi i)^{-1}G_\Delta(k_\mu)$ by $\mathcal{G}_\Delta$ we have

$$(F_\Delta-\mathcal{G}-\mathcal{G}_\Delta)\Psi_n=0, \quad (22)$$

where E in the expression for F_Δ has the value E_Δ. It is convenient to define a new function ψ_Δ by means of

$$\psi_\Delta=\Psi_n-\psi_n{}^\Delta, \quad (23)$$

where $\psi_n{}^\Delta$ is defined as in (18). Equation (22) can then be written as

$$(F_\Delta-\mathcal{G})\psi_n{}^\Delta+(F_\Delta-\mathcal{G})\psi_\Delta=\mathcal{G}_\Delta\psi_n{}^\Delta+\mathcal{G}_\Delta\psi_\Delta. \quad (22a)$$

Since $\mathcal{G}_\Delta$ is assumed to be "small" compared with $\mathcal{G}$, ΔE will be small compared with E_n, and ψ_Δ small compared with $\psi_n{}^\Delta$, and $\psi_n{}^\Delta$ will be approximately equal to ψ_n.

Multiply Eq. (22a) on the left by $\bar{\psi}_n{}^\Delta$ and integrate over d^4p. Using (20a), the integrand of this equation becomes

$$\Delta E\chi_n{}^*(\psi_n{}^\Delta+\psi_\Delta)=-(2\pi i)\bar{\psi}_n{}^\Delta\mathcal{G}_\Delta(\psi_n{}^\Delta+\psi_\Delta). \quad (22b)$$

The first terms on both the LHS and RHS of Eq. (22b) are small quantities of the first order, the second terms of the second order. We obtain the first-order perturbation approximation $\Delta E^{(1)}$ to ΔE by omitting these two second-order terms and replacing $\psi_n{}^\Delta$ by ψ_n in the two first-order terms. Integrating this approximate form of Eq. (22b) over d^4p and using (5) and (17),

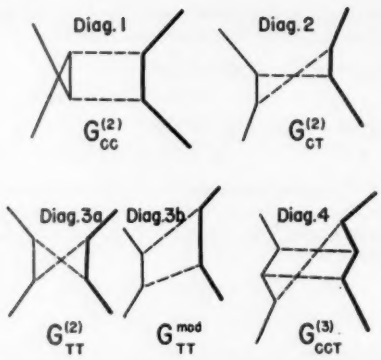

FIG. 1. Feynman diagrams corresponding to various interaction terms. Light solid lines denote electrons, heavy solid lines protons. Horizontal broken lines denote instantaneous Coulomb interactions, inclined broken lines denote transverse photons.

we obtain the desired expression for $\Delta E^{(1)}$,

$$\Delta E^{(1)}=-(2\pi i)\int d^4p\bar{\psi}_n(p_\mu)\mathcal{G}_A\psi_n(p_\mu)$$

$$=\int\int d^4p d^4k\bar{\psi}_n(p_\mu)G_A'(k_\mu)\psi_n(p_\mu+k_\mu). \quad (23a)$$

III. INSTANTANEOUS COULOMB INTERACTION

We shall now apply the general theory of the preceding section to the special case of two Fermi-Dirac particles of electric charge e and $(-e)$, respectively. We use form (2) of the electromagnetic interaction $G(k_\mu)$ and consider in this section only the effect of the first part of this interaction involving the instantaneous Coulomb interaction

$$G_C'(\mathbf{k})=-(e^2/2\pi^2k^2). \quad (24)$$

The effect of the transverse part $G_T(k_\mu)$ of the interaction will be discussed in the following three sections by means of a modified perturbation theory treatment.

The four-dimensional equation for this problem is then of the form

$$F(\mathbf{p},\epsilon)\psi(p_\mu)=-(2\pi i)^{-1}\int d^4k\{G_C'(\mathbf{p})$$

$$+G_{CC'^{(2)}}(k_\mu)+\cdots\}\psi(p_\mu+k_\mu). \quad (25)$$

As discussed by SB the kernel of this integral equation involves not only $G_C(\mathbf{k})$, but also all the expressions corresponding to higher order irreducible diagrams. Of these only one term contributes to the accuracy we require, $G_{CC'^{(2)}}$. This corresponds to diagram 1 shown in Fig. 1, i.e., a "crossed double photon" term involving two instantaneous Coulomb interactions. As discussed by SB, this term is not identically equal to zero if hole theory is used,[8] a finite contribution being obtained from intermediate states in which one of the two particles is in a negative energy state. The term is small, however, its contribution to the binding energy being of order $\alpha(\mathrm{fs})$, and it will be considered only as a perturbation, using the first-order perturbation expression (23) derived in the last section.

We therefore consider first Eq. (25) with the full kernel replaced by the first term of its expansion, $G_C(\mathbf{k})$. This function does not depend on k_4 and hence the considerations of the last section, leading to Eq. (13), apply. We therefore obtain a three-dimensional equation of type (13),

$$[E-H_a(\mathbf{p})-H_b(\mathbf{p})]\phi(\mathbf{p})$$

$$=\{\Lambda_+^a(\mathbf{p})\Lambda_+^b(\mathbf{p})-\Lambda_-^a(\mathbf{p})\Lambda_-^b(\mathbf{p})\}(-e^2/2\pi^2)$$

$$\times\int d^3kk^{-2}\phi(\mathbf{p}+\mathbf{k}). \quad (26)$$

The extreme nonrelativistic approximation to this equation is the ordinary nonrelativistic Schrödinger equation

$$[W-p^2/2\mu]\phi_0(\mathbf{p})=(-e^2/2\pi^2)\int d^3kk^{-2}\phi_0(\mathbf{p}+\mathbf{k}), \quad (27)$$

where

$$W=E-m_a-m_b,\quad \mu=m_am_b/(m_a+m_b).$$

This approximation to W, the binding energy, is of course in error by an amount of relative order α^2 (the fine-structure being missing completely). The approximate wave function $\phi_0(\mathbf{p})$ is in error by an amount of relative order $[(p+p_0)/\mu]^2$, where p_0 is the Bohr momentum

$$p_0=\alpha\mu,\quad \alpha=(e^2/\hbar c)=1/137.03,\quad \mathrm{Ry}=\alpha^2\mu/2. \quad (28)$$

$\phi_0(\mathbf{p})$ is therefore a very poor approximation for $p\gtrsim\mu$. It is useful to note that a better approximation to the wave function, $\phi_1(\mathbf{p})$, can be obtained by applying an iteration method once to (26), using $\phi_0(\mathbf{p})$ as our initial trial wave function. $\phi_1(\mathbf{p})$ is then defined by means of

$$\phi_1(\mathbf{p})=[E-H_a(\mathbf{p})-H_b(\mathbf{p})]^{-1}\{\Lambda_+^a(\mathbf{p})\Lambda_+^b(\mathbf{p})$$

$$-\Lambda_-^a(\mathbf{p})\Lambda_-^b(\mathbf{p})\}(-e^2/2\pi^2)\int d^3kk^{-2}\phi_0(\mathbf{p}+\mathbf{k}). \quad (29)$$

$\phi_1(\mathbf{p})$ is in error by only an amount of relative order $\alpha[(p+p_0)/(p+\mu)]$, i.e., an error of the same order as, or less than, α for all values of p.* This improved accuracy is due to the fact that the wave function $\phi(\mathbf{p})$ decreases more rapidly with increasing p than the potential $G_C(\mathbf{p})$. For large values of p the main contributions to the integrals in Eqs. (26) and (29) come

[8] It would be zero, however, if single electron theory were used.
* More exactly, for all $p\ll p_0$ exp (137).

then from values of $|\mathbf{p}+\mathbf{k}|$ of the order of p_0, where $\phi_0(\mathbf{p}+\mathbf{k})$ is a good approximation.

For simplicity we shall now consider the case of an electron of mass $m_a=m$ and a proton of mass $m_b=M$, where $M\gg m$. A similar treatment could, however, be given for the case of general m_a and m_b (for instance, positronium). The Breit equation Eq. (16) for a Coulomb potential is

$$[E-H_a(\mathbf{p})-H_b(\mathbf{p})]\phi(\mathbf{p}) = (-e^2/2\pi^2)\int d^3k k^{-2}\phi(\mathbf{p}+\mathbf{k}). \quad (26a)$$

In Table I we give the order of magnitude of the four components ϕ_{++}, etc., for ϕ, the solution of Eq. (26a), for $m\ll M$. Note that for $p\gtrsim p_0$ the other three components are smaller than ϕ_{++} by a factor of at least α^2. The order of magnitude of ϕ_{++} and ϕ_{--} of the solution of (26) are the same as those shown in Table I, but ϕ_{-+} and ϕ_{+-} are zero. To the required accuracy the normalization condition, Eq. (17), is fulfilled if ϕ_{++} alone is normalized to unity.

In this paper we shall neglect all terms which are of a smaller order of magnitude than $\alpha(m/M)$(fs). To this approximation the term involving $\Lambda_-{}^a\Lambda_-{}^b$ in Eq. (26) can be omitted. It is of some interest to note that the lowest order approximation to the fine structure can be obtained very simply from Eq. (26). If we were to neglect (m/M) completely and expand in powers of (p/m) and (k/m), Eq. (26) would reduce to the following approximate equation:

$$[W-p^2/2m+p^4/8m^3]\phi(\mathbf{p}) = -(e^2/2\pi^2) \times\int d^3k[1+(\boldsymbol{\sigma}\cdot\mathbf{p})(\boldsymbol{\sigma}\cdot\mathbf{k})/4m^2]k^{-2}\phi(\mathbf{p}+\mathbf{k}), \quad (26b)$$

where $\boldsymbol{\sigma}$ is the Pauli spin-operator for the electron and $\phi(\mathbf{p})$ now has only 2 spin components, instead of 16 spinor-components. The factor in square brackets on the RHS of Eq. (26a) is an approximation to $\Lambda_+{}^a$, derived in the appendix. Equation (26a) can be shown to be exactly the momentum space Fourier-transform of the approximate equation obtained for the fine structure in the usual treatment involving a Pauli reduction to the "large variables."[9]

Instead of actually evaluating the energy eigenvalues of Eq. (26), it is more convenient and instructive to evaluate merely the difference between the energies obtained by the present treatment and from the Breit equation, Eq. (26a). To the accuracy required, Eq. (26) reduces to

$$[E-E_a(p)-E_b(p)]\phi_{++}(\mathbf{p}) = (-e^2/2\pi^2)\Lambda_+{}^a(\mathbf{p})\Lambda_+{}^b(\mathbf{p})\int d^3k k^{-2} \times[\phi_{++}(\mathbf{p}+\mathbf{k})+\phi_{-+}(\mathbf{p}+\mathbf{k})], \quad (30)$$

$$[E+E_a(p)-E_b(p)]\phi_{-+}(\mathbf{p}) = (-e^2/2\pi^2)\Lambda_-{}^a(\mathbf{p})\Lambda_+{}^b(\mathbf{p})\int d^3k k^{-2} \times[\phi_{++}(\mathbf{p}+\mathbf{k})+\phi_{-+}(\mathbf{p}+\mathbf{k})], \quad (30a)$$

where the ϕ_{++}, etc., are again obtained from ϕ by multiplication with two projection operators, as in (8). To the required accuracy, the terms involving ϕ_{+-} and ϕ_{--} (negative energy states for the nucleus) can be neglected. An approximation to ϕ_{-+} in terms of ϕ_{++}, accurate to lowest order in α, can be obtained by omitting the term in $\phi_{-+}(\mathbf{p}+\mathbf{k})$ on the RHS of (30a). Using this approximation we obtain an equation involving only ϕ_{++},

$$[E-E_a(p)-E_b(p)]\phi_{++}(\mathbf{p}) = \left(\frac{-e^2}{2\pi^2}\right)\Lambda_+{}^a(\mathbf{p})\Lambda_+{}^b(\mathbf{p}) \times\int\frac{d^3k\phi_{++}(\mathbf{p}+\mathbf{k})}{k^2}+\left(\frac{e^2}{2\pi^2}\right)^2\Lambda_+{}^a(\mathbf{p})\Lambda_+{}^b(\mathbf{p}) \times\int\int\int\frac{d^3kd^3p'\Lambda_-{}^a(\mathbf{p}+\mathbf{k})\Lambda_+{}^b(\mathbf{p}+\mathbf{k})\phi_{++}(\mathbf{p}')}{k^2(\mathbf{p}'-\mathbf{p}-\mathbf{k})^2[E+E_a(\mathbf{p}+\mathbf{k})-E_b(\mathbf{p}+\mathbf{k})]}. \quad (31)$$

To this accuracy our Eq. (26) is the same as (31), except that the second term on the RHS is missing, which is of order α(fs). We shall only need to evaluate the contribution of this term to the binding energy by first-order perturbation theory.

In our treatment we have to add to the energy eigenvalue obtained from Eq. (26) the expectation value of the interaction term $G_{CC}{}^{(2)}$, using Eq. (23). In this expression two "energy"-denominators of the type $(p_a\gamma_a-m)$ occur. Instead of using the Feynman methods for evaluating such integrals we first split up this expectation value into the sum of four terms with the help of the identity (14). Each of these four terms then contains only energy-denominators which do not involve any Dirac matrices. The contribution to the energy eigenvalue is then given by the following expectation value, using Eq. (23) and the expression

TABLE I. Order of magnitude of the four components (eigenfunctions of the projection operators) of the solution ϕ of the Breit equation, Eq. (26a). $p_0=\alpha m$ is the Bohr momentum, m and M are the electron and proton mass, respectively.

	$p<p_0$	$p_0<p<m$	$m<p<M$	$p>M$
ϕ_{++}	1	$(p_0/p)^4$	$\alpha^4(m/p)^3$	$\alpha^4(m/p)^3$
ϕ_{-+}	α^3	$\alpha^3(p_0/p)$	$\alpha^4(m/p)^3$	$\alpha^4(m/p)^3$
ϕ_{+-}	$\alpha^5(m/M)^3$	$\alpha^3(p_0/p)(m/M)^3$	$\alpha^4(m/p)(m/M)^3$	$\alpha^4(m/p)^3$
ϕ_{--}	$\alpha^4(m/M)^3$	$\alpha^4(m/M)^3$	$\alpha^4(m/p)(m/M)^3$	$\alpha^4(m/p)^3$

[9] H. A. Bethe, *Handbuch der Physik* (Verlag. Julius Springer, Berlin, 1933), Vol. 24/1, p. 305.

for $G_{CC}{}^{(2)}$ defined by SB,

$$\left(\frac{e^4}{8\pi^5 i}\right)\int\int\int \frac{d^4p d^4k d^4p' \bar{\psi}(p_a)\Lambda_-{}^a(\mathbf{p}+\mathbf{k})\Lambda_+{}^b(\mathbf{p}'-\mathbf{k})\psi(p_a')}{k^2(\mathbf{p}'-\mathbf{p}-\mathbf{k})^2[\mu_a E+E_a(\mathbf{p}+\mathbf{k})+\epsilon+\omega-i\delta][\mu_b E-E_b(\mathbf{p}'-\mathbf{k})-\epsilon'+\omega+i\delta]}+\cdots, \tag{32}$$

where ϵ, ϵ', and ω stand for p_4, p_4', and k_4, respectively. The three additional terms, not written explicitly in (32) (involving $\Lambda_+{}^a\Lambda_+{}^b$, $\Lambda_+{}^a\Lambda_-{}^b$ and $\Lambda_-{}^a\Lambda_-{}^b$), do not give a contribution to the required order of accuracy.

We only require the integral (32) accurate to lowest order in α. To this accuracy $\bar{\psi}(p_a)$ and $\psi(p_a')$ can be replaced by $\bar{\psi}_{++}(p_a)$ and $\psi_{++}(p_a')$, respectively. $\psi_{++}(p_a)$ is an explicit function of $\phi_{++}(\mathbf{p})$, the solution of (26), given in (15),

$$\psi_{++}(p_a)=-[E-E_a(p)-E_b(p)]\times[2\pi i F_{++}(\mathbf{p},\epsilon)]^{-1}\phi_{++}(\mathbf{p}). \tag{15c}$$

The dependence of the integrand of (32) on ϵ, ϵ', and ω is then known explicitly and the integrals over ϵ, ϵ', and ω can be carried out. The major contributions to the integral (32) are found to come from the range of integration

$$p,\ p'\sim p_0;\quad k\sim m. \tag{33}$$

Carrying out the integrations over ϵ, ϵ', and ω and expanding the result in powers of α, (32) reduces to lowest order in α, to the expression

$$\left(\frac{e^2}{2\pi^2}\right)^2\int\int\int \frac{d^3p d^3k d^3p' \phi_{++}{}^*(\mathbf{p})\Lambda_-{}^a(\mathbf{p}+\mathbf{k})\Lambda_+{}^b(\mathbf{p}'-\mathbf{k})\phi_{++}(p')}{k^2(\mathbf{p}'-\mathbf{p}-\mathbf{k})^2[(\mu_a-\mu_b)E+E_a(\mathbf{p}+\mathbf{k})+E_b(\mathbf{p}'-\mathbf{k})]}. \tag{34}$$

The expectation value (34) in our treatment has to be compared with the equivalent term in the Breit treatment, the expectation value of the operator in the second line of (31). In the limit of (m/M) tending to zero it is found that these two terms are equal. This was to be expected, since in this limit the Breit Eq. (30) reduces exactly to the Dirac equation for a single electron, which is certainly correct if the nucleus is infinitely heavy. For a finite mass M of the nucleus, however, these two terms are not exactly equal and the energy eigenvalue obtained by the Breit treatment is in error by the difference of these two terms. We expand in powers of (m/M) and shall retain the first nonzero term in this expansion.

We call the correction to the Breit energy eigenvalue [expression (34) minus expectation value of the second term of (31)] ΔE_{CC}. The integrands are important only in the range of integration given by (33), i.e., $p,\ p'\ll k\ll M$. To lowest order in α and to the first two orders in (m/M), the projection operators $\Lambda_+{}^b$ in both expressions can be replaced by unity and $\Lambda_-{}^a(\mathbf{p}+\mathbf{k})$ by $[E_a(k)-m]/4E_a(k)$. Since only $p,\ p'\sim\alpha m$ is important, we can also replace ϕ_{++} by ϕ_0, the solution of the nonrelativistic Eq. (27). We then obtain, to the required accuracy

$$\Delta E_{CC}=-\left(\frac{e^2}{2\pi^2}\right)^2\times\int\int\int\frac{d^3p d^3k d^3p' \phi_0{}^*(\mathbf{p})[E_a(k)-m]\phi_0(\mathbf{p}')}{k^2M[E_a(k)+m]^2 4E_a(k)}.$$

This expression can now be integrated over d^3k quite easily and yields

$$\Delta E_{CC}=-(\pi/3mM)(e^2/2\pi^2)^2\left|\int d^3p\phi_0(\mathbf{p})\right|^2 =-(2\alpha^2/3mM)|\psi_0(0)|^2, \tag{35}$$

where $\psi_0(\mathbf{r})$ is the three-dimensional Fourier-transform of $\phi_0(\mathbf{p})$, i.e., the nonrelativistic Schrödinger wave function in coordinate space for a hydrogen-like atom.

The approximations for the integrands used in deriving (35) are valid only for $p,\ p'\ll m$. The correct integrand decreases more rapidly with increasing p and p' for $p,\ p'>m$ than the approximation used and the integral over p in (35) should really be extended only to $p\sim m$ and not to infinity. But since we are using the Schrödinger wave function $\phi_0(\mathbf{p})$ (and not the Dirac functions) contributions to the integral occurring in (35) for $p\gg\alpha m$ are already small and the error made in extending the integral to infinity (using $\psi_0(\mathbf{r})$ for $r=0$ instead of $r\sim m^{-1}$) is of a smaller order of magnitude than the terms considered in this paper. Throughout this paper $\psi_0(0)$ will denote the value of the nonrelativistic Schrödinger wave function (in three-dimensional coordinate space) at the origin.

For all atomic states of nonzero angular momentum, the expression (35) vanishes exactly (to this order). For an s-state with principal quantum number n, the correction ΔE_{CC}, to be added to the Breit energy eigenvalue for hydrogen, is

$$\Delta E_{CC}=-(4\alpha^3 m\ \mathrm{Ry}/3\pi n^3 M). \tag{36}$$

This term is of the order $\alpha(m/M)$(fs), but the numerical coefficient is small. In hydrogen it represents an energy-shift of only -0.037 Mc/sec for the $2s$ state.

IV. CORRECTIONS INVOLVING TRANSVERSE PHOTONS

We have so far considered only the effect of the instantaneous Coulomb interaction and must now consider the effects produced by the second part of (2), which we call $G_T(k_\mu)$ corresponding to the interchange of a transverse photon. We first discuss the method of SB as applied to this term, which involves an expansion in powers of α. Instead of (4) we have the full equation

$$F(\mathbf{p},\epsilon)\psi(p_\mu)=-(2\pi i)^{-1}\int d^4k[G_C'+G_{CC}'^{(2)}+G_T' +G_{CT}'^{(2)}+G_{TT}'^{(2)}+\cdots]_{(k_\mu)}\psi(p_\mu+k_\mu), \quad (37)$$

where

$$G_T'(k_\mu)=-(e^2/2\pi^2)\sum_{i=1}^{2}\alpha_i^a\alpha_i^b/k_\mu^2. \quad (38)$$

(α^a is the Dirac matrix for particle a.) In (37), G_{CT}' is the expression defined by SB which corresponds to a "crossed double photon" graph with one interaction given by G_C and the other by G_T (Fig. 1, diagram 2); G_{TT}' is the equivalent expression with both interactions given by G_T (Fig. 1, diagram 3a). In (37) the expressions corresponding to higher order irreducible graphs, $G_{CCT}'^{(3)}$, etc., also occur on the RHS. The terms $G_{CT}'^{(2)}$ and $G_{TT}'^{(2)}$ give energy shifts only of order $\alpha(m/M)$(fs) and it will be sufficient to evaluate these energy shifts by means of four-dimensional first-order perturbation theory, as was done for $G_{CC}'^{(2)}$. But the term G_T' is of order (m/M)(fs)$\sim\alpha^2(m/M)W$. At first sight we might expect the error involved in using first-order perturbation theory for this term to be only of order $\alpha^4(m/M)^2W$, which is negligible. But there is, in fact, an error of order $\alpha(m/M)$(fs). This is connected with the well-known fact that the expectation values of some Dirac matrices may be small, whereas the square of such a matrix is unity.

We return now to the discussion of perturbation theory given in Sec. II with the instantaneous interaction $G(\mathbf{k})$ now standing for G_C and the perturbation G_Δ for G_T. The equations up to and including (22b) are still exact. Since ΔE is only of order $\alpha^2(m/M)\mathrm{Ry}$, one finds that, to the required accuracy, the second term on the LHS of Eq. (22b) can be omitted and $\psi_n{}^\Delta$, $\bar\psi_n{}^\Delta$ replaced by ψ_n and $\bar\psi_n$, respectively. But the second term on the RHS of Eq. (22b), which was also omitted in the first-order perturbation expression, Eq. (23), gives a correction of order $\alpha(m/M)$(fs). We therefore need an approximation for ψ_Δ, accurate to lowest order in α. Using Eqs. (20) and (22b) we get an exact expression

$$F_\Delta\psi_\Delta=\mathcal{G}_\Delta\psi_n{}^\Delta+[\mathcal{G}\psi_\Delta+(2\pi i)^{-1}\Delta E\chi_n+\mathcal{G}_\Delta\psi_\Delta]. \quad (39)$$

If we were to use unmodified perturbation theory we would have to carry the first two terms in square brackets on the RHS of Eq. (39). In the present electrodynamic case, however, one gets an accurate enough approximation for ψ_Δ by omitting all the terms in square brackets and by replacing F_Δ, $\psi_n{}^\Delta$ by F_n and ψ_n, respectively, i.e.,

$$\psi_\Delta\approx F_n{}^{-1}\mathcal{G}_\Delta\psi_n. \quad (39a)$$

Making these approximations and integrating (22b) over d^4p we obtain, instead of Eq. (23),

$$\Delta E=-(2\pi i)\int d^4p\bar\psi_n[\mathcal{G}_\Delta+\mathcal{G}_\Delta F_n{}^{-1}\mathcal{G}_\Delta]\psi_n$$

$$=\int\int d^4p d^4k\bar\psi_n(p_\mu)G_\Delta'(k_\mu)\psi_n(p_\mu+k_\mu)$$

$$-(2\pi i)^{-1}\int\int\int d^4p d^4k d^4p'\bar\psi_n(p_\mu)G_\Delta'(k_\mu)$$

$$\times F_n{}^{-1}(p_\mu+k_\mu)G_\Delta'(p_\mu'-p_\mu-k_\mu)\psi_n(p_\mu'). \quad (40)$$

We note that the second term on the RHS of (40) is somewhat similar to the expectation value of $G_{TT}'^{(2)}$. In fact this term is equal to the Feynman expression for the successive interchange of two transverse photons between the two particles (denoted by $G_{TT}{}^{mod}$ in Fig. 1, diagram 3b).

In the preceding discussion we have neglected the effect of the higher order irreducible graphs, $G_{CCT}'^{(3)}$, etc. (Fig. 1, diagram 4). One might expect these terms to contribute to the energy only terms of order α^2(fs)(m/M) or smaller. However, an effect similar to, but less drastic than, the well-known "infrared catastrophe" occurs. Consider any irreducible graph corresponding to the interchange of one single transverse photon of three-dimensional momentum $\mathbf{k}$ as well as any number of instantaneous Coulomb-interactions. One finds that the contribution to the energy of such a graph, for values of $k\lesssim\alpha p_0\sim W$ is finite but of order $\alpha(m/M)$(fs), which we cannot neglect. Speaking very crudely, we might say that the exchange of a transverse photon of momentum k takes place in a time of order k^{-1} and that instantaneous Coulomb-interactions take place at time intervals of the order of W^{-1}. Hence, if $k\ll\alpha p_0$, during the "time of flight" of one such transverse photon many Coulomb-interactions take place.

It is obviously impractical to have to sum an infinite number of contributions to obtain the corrections of order α(fs). This difficulty is connected with the fact that, in the method proposed by SB, the Feynman propagators K_+, corresponding to the propagation of free particles, are used. The most elegant way to overcome this difficulty would probably be to modify the method of SB along lines developed recently by Dyson.[10] Such a treatment would be equivalent to separating the electromagnetic interaction into a "low

[10] F. J. Dyson, Phys. Rev. **82**, 428 (1951); Phys. Rev. **83**, 608, 1207 (1951); Proc. Roy. Soc. (London) **A207**, 395 (1951).

frequency" and a "high frequency" part in a Lorentz-invariant way. One would then first solve the problem, without the use of an expansion in powers of α, for the low frequency part alone. Having found the equivalent Feynman propagator functions for this problem, one would then treat the high frequency part by means of the expansion proposed by SB, which should now converge rapidly.

In the present problem, however, the difficulty arises only from very nonrelativistic frequencies or momenta, $k\sim\alpha p_0$. Hence it is permissible, and much simpler, to split the transverse photon terms G_T, etc., into two parts, for momentum transfer $k<A$ and $k>A$ (in the "center-of-mass" system defined by SB), where

$$\alpha p_0 \ll A \ll p_0. \tag{41}$$

No such separation is carried out for the instantaneous Coulomb term G_C, and Eq. (26) is first derived and solved as in the preceding section. For the low frequency part of $G_T(\mathbf{k})$, for $k<A$, we do not use the formalism of SB and of Feynman, but use "old-fashioned" quantum electrodynamics and perturbation theory. In other words, we consider the solution $\phi(\mathbf{p})$ of (26) as our unperturbed three-dimensional wave function, consider as a perturbation the usual absorption and emission operators for transverse photons of momentum less than A, and evaluate the energy eigenvalue by means of fourth-order perturbation theory. For the high frequency part of $G_T(\mathbf{k})$, $k>A$, we use the methods of SB as discussed above.

This nonrelativistic treatment for the low frequency part of the transverse interaction is not elegant, but it is very simple. Some of the correction terms of order $\alpha(m/M)$(fs) contain $\log\alpha$ as a factor and are numerically larger than the terms without this factor. If this nonrelativistic treatment is carried out for momenta k not only up to a value A satisfying (41), but up to a value of the order of magnitude of m, these terms involving $\log\alpha$ can be evaluated very simply. This calculation will be carried out in the next section. But to evaluate all the terms of order $\alpha(m/M)$(fs) in a relatively simple manner, the four-dimensional treatment discussed above seems to be advantageous.[11]

As in our treatment of the Coulomb interaction, we shall not evaluate the expressions for the energy eigenvalue explicitly but only evaluate the difference between the exact expression and that obtained by the use of the Breit equation and interaction.[2] The full Breit equation is

$$[E-H_a(\mathbf{p})-H_b(\mathbf{p})]\phi(\mathbf{p})=\frac{-e^2}{2\pi^2}\int d^3k k^{-2} \times\left[1-\sum_{i=1}^{2}\alpha_i{}^a\alpha_i{}^b\right]\phi(\mathbf{p}+\mathbf{k}). \tag{42}$$

[11] The terms evaluated in this paper are, however, being calculated by Bohr, Gourary, Kroll, and Lamb, by a different method in which only the electron (but not the proton) is treated relativistically.

This equation is first solved with the omission of the term involving $\alpha_i{}^a\alpha_i{}^b$. The resulting equation, Eq. (30), was discussed in the last section. The effect of the term involving $\alpha_i{}^a\alpha_i{}^b$ is then considered by means of first-order perturbation theory only.

V. THREE-DIMENSIONAL PERTURBATION TREATMENT

We consider $\psi_n(\mathbf{r})$, the coordinate-space wave function corresponding to the solution of (26), as our unperturbed wave function. Consider the perturbation Hamiltonian

$$H'=e\sum_{k<A}\sum_{i=1}^{2}\{\alpha_i{}^a(q_{\mathbf{k},i}{}^{op}e^{i\mathbf{k}\cdot\mathbf{r}_a}+\bar{q}_{\mathbf{k},i}{}^{op}e^{-i\mathbf{k}\cdot\mathbf{r}_a}) -\alpha_i{}^b(q_{\mathbf{k},i}{}^{op}e^{i\mathbf{k}\cdot\mathbf{r}_b}+\bar{q}_{\mathbf{k},i}{}^{op}e^{-i\mathbf{k}\cdot\mathbf{r}_b})\}, \tag{43}$$

where $q_{\mathbf{k},i}{}^{op}$ and $\bar{q}_{\mathbf{k},i}{}^{op}$ are the usual emission and absorption operators for a photon of momentum $(-\mathbf{k})$ and direction of polarization i. Their matrix-elements for transitions between states of one and no such photons are $(2\pi/k)^{\frac{1}{2}}$. The second-order perturbation energy corresponding to H' is then

$$-2\left(\frac{e}{2\pi}\right)^2\int_{k<A}d^3k \times\sum_{i=1}^{2}\sum_{m}\frac{\langle n|\alpha_i{}^a e^{i\mathbf{k}\cdot\mathbf{r}_a}|m\rangle\langle m|\alpha_i{}^b e^{-i\mathbf{k}\cdot\mathbf{r}_b}|n\rangle}{k(E_n-E_m-k)}, \tag{44}$$

where E_m and E_n are the unperturbed energy eigenvalues for the intermediate and initial atomic state, respectively. The factor 2 is due to the fact that the virtual photon can be emitted by particle a and absorbed by particle b, or vice versa.

If in the denominator of expression (44) the term (E_n-E_m) is omitted (neglect of "particle recoil"), then a sum rule can be used to eliminate the summation over the intermediate states m. The expression resulting from this omission is then identical with the equivalent Breit interaction term. We shall therefore only evaluate the difference between the exact expression (44) and the equivalent Breit term. This difference is of order $\alpha(m/M)$(fs) and we only require its value to lowest order in α and (m/M). We therefore replace $\mathbf{r}_a$ by the relative distance $\mathbf{r}$ and $\mathbf{r}_b$ by zero (a referring to the electron mass m and b to the nucleus mass M). We further make the nonrelativistic approximation of replacing the Dirac matrix $\alpha_i{}^a$ by p_i/m and $\alpha_i{}^b$ by $(-p_i/M)$ where $\mathbf{p}=-i\nabla_r$. With these approximations the energy-difference becomes

$$\Delta E_{T,A}=\left(\frac{e^2}{2\pi^2 mM}\right)\int_{k<A}d^3k \times\sum_{i=1}^{2}\sum_{m}\frac{\langle n|p_i e^{i\mathbf{k}\cdot\mathbf{r}}|m\rangle\langle m|p_i|n\rangle(E_m-E_n)}{k^2(E_m-E_n+k)}. \tag{45}$$

The Breit-interaction represents the interchange of a virtual transverse photon between the electron and nucleus. Similarly the transverse self-energy of an electron can be considered as representing the interchange of a photon between the electron and itself. The Lamb shift (in nonrelativistic approximation) is the difference between this self-energy for an electron bound in an atomic state and the equivalent expression with the term (E_m-E_n) in the energy denominator omitted. There is thus some mathematical similarity between our correction (45), and the Lamb shift. In fact, (45) is identical with the expression for the Lamb-shift derived by Bethe in Eq. (5) of the nonrelativistic calculation,[12] except for a factor two (either the electron or nucleus can emit the photon), the factor $e^{i\mathbf{k}\cdot\mathbf{r}}$ (momentum $\mathbf{k}$ is transferred from the one particle to the other) and a factor m/M (ratio of velocities of nucleus and electron). Since the upper limit A on k is by assumption much less than p_0, k is very small compared with the "average" momentum in the atomic state and the factor $e^{i\mathbf{k}\cdot\mathbf{r}}$ can be neglected. The atomic wave functions can also be replaced by the Schrödinger nonrelativistic functions. (45) is then equal to $(2m/M)$ times the equivalent Lamb-shift expression, i.e.,

$$\Delta E_{T,A}=(8\alpha^2/3mM)\ln(A/\langle E_m-E_n\rangle_{Av})|\psi_n(0)|^2. \quad (46)$$

For the $2s$ and $2p$ states $\langle E_m-E_n\rangle_{Av}$ has been evaluated accurately previously[13] and we find for the $2s$ state

$$\Delta E_{T,A}=(2\alpha^3m\ \text{Ry}/3\pi M)\ln(A/16.6_4\ \text{Ry}). \quad (46a)$$

For states with nonzero orbital angular momentum the equivalent expression is very small (+0.004 Mc/sec for $2p$).

The high frequency part, $k>A$, will be treated rigorously in the next section, but we shall now show that the parts involving $\log\alpha$ as a factor can also be obtained from our nonrelativistic approximation. Let

$$p_0\ll B\ll m, \quad (47)$$

and consider the expression (45) with A as lower limit on k and B as upper limit. The term (E_m-E_n) in the denominator is then small compared with k and can be neglected. In the numerator E_m is replaced by the unperturbed Hamiltonian H_0 operating on state m, E_n by H_0 operating on state n. A sum rule can then be used again to eliminate the summation over m. Using the fact that

$$[H_0, p_i]_-=i\partial V/\partial r_i,$$

where $V(r)=(-e^2/r)$, we find that

$$\Delta E_{T,B}=\frac{ie^2}{2\pi^2mM}\int_A^B d^3kk^{-3}\sum_{i=1}^{3}\langle n|\,p_ie^{i\mathbf{k}\cdot\mathbf{r}}(\partial V/\partial r_i)\,|n\rangle. \quad (48)$$

For the $2s$-state an evaluation of (48), again using the nonrelativistic Schrödinger wave functions, gives, to lowest order in α and m/M, an expression independent of B

$$\Delta E_{T,B}=(2\alpha^3m\ \text{Ry}/3\pi M)\{\ln(p_0/A)+(25/12)\}. \quad (48a)$$

The upper limit in the logarithmic factor is of the order of the Bohr momentum p_0, and not of m as for the Lamb-shift. This is due to the factor $e^{i\mathbf{k}\cdot\mathbf{r}}$ which decreases the contribution from $k\gg p_0$.

For the $2s$ state of hydrogen the sum of (46a) and (48a) is

$$\Delta E_{CT}=(2\alpha^3m\ \text{Ry}/3\pi M)\{\ln(p_0/16.6_4\ \text{Ry})+(25/12)\}$$
$$=+0.721\ \text{Mc/sec}. \quad (49)$$

For states other than s states the equivalent expression is again small. For the $2p$ state one finds

$$\Delta E_{T,B}=-(\alpha^3m\ \text{Ry}/18\pi M)=-0.012\ \text{Mc/sec}, \quad (49a)$$

and ΔE_{CT} is thus -0.008 Mc/sec for the $2p$ state.

Equation (46) is the only term coming from $k<A$ of order $\alpha(m/M)$(fs). But there is another term, coming from values of k between p_0 and m, which will be treated rigorously in the next section, for which we can derive a simple approximation by means of the nonrelativistic treatment of this section. Consider the fourth-order perturbation energy due to the perturbation H', Eq. (43). This contains a term corresponding to the following process: One of the two particles emits a virtual transverse photon of momentum $\mathbf{k}$ and makes a transition to a negative-energy state. The same particle then emits another transverse photon of momentum $(\mathbf{q}-\mathbf{k})$ and returns to a positive-energy state. The second particle then absorbs either photon and makes a transition to a negative-energy state. Finally the second particle absorbs the remaining photon and the atom returns to the initial state.

The only contributions to order $\alpha(m/M)\log(\alpha)$(fs) to this term come from values of the momenta p, q, and k satisfying $p_0\ll k\ll m$ and $p\sim q\sim p_0$. Consequently $(\mathbf{q}-\mathbf{k})$ can be approximated by $(-\mathbf{k})$. For these values of k, the three energy denominators (E_n-energy of each of the three intermediate states) can be approximated by $(-2m)$, $(-k-|\mathbf{q}-\mathbf{k}|)$, and $(-2M)$, respectively. With these approximations sum rules can be applied to eliminate the summations over the three intermediate states. We then obtain the following approximation to the fourth-order perturbation energy,

$$\Delta E_{TT}\approx-\frac{e^4}{64\pi^4mM}\int_{p_0}^{m}d^3kk^{-3}\int d^3q$$
$$\times\sum_{i=1}^{3}\sum_{j=1}^{3}\langle n|\,\alpha_i^a\alpha_j^a(\alpha_i^b\alpha_j^b+\alpha_j^b\alpha_i^b)e^{i\mathbf{q}\cdot\mathbf{r}}\,|n\rangle. \quad (50)$$

Using the fact that

$$\int d^3qe^{i\mathbf{q}\cdot\mathbf{r}}=(2\pi)^3\delta^{(3)}(\mathbf{r}),$$

[12] H. A. Bethe, Phys. Rev. **72**, 339 (1947).
[13] Bethe, Brown, and Stehn, Phys. Rev. **77**, 370 (1950).

Eq. (50) reduces to

$$\Delta E_{TT}\approx-(2\alpha^3/mM)\ln(m/p_0)|\psi_n(0)|^2, \quad (50a)$$

or, very roughly, $(-3/4)$ times (46). The equivalent expressions for states with nonzero orbital angular momentum are again very small.

VI. FOUR-DIMENSIONAL TREATMENT OF "TRANSVERSE" TERMS

We now evaluate rigorously the terms of order $\alpha(m/M)$(fs), which involve the exchange of at least one transverse photon between the electron and the proton in hydrogen. As discussed in Sec. IV, we use Eq. (37), with all integrations over photon momenta extended from A, Eq. (41), to infinity. We consider the four-dimensional solutions $\psi_n(p_\mu)$, corresponding to the solutions of (26) as our unperturbed solutions and use the modified perturbation theory derived in Sec. IV. Since we have already dealt with the low frequency part $k<A$, in the preceding section, we can neglect the higher order terms which are not explicitly written in (37). Using (37) and (40), we then get the following contribution to the energy eigenvalue

$$\Delta E_n=\int\int d^4p\,d^4k\bar{\psi}_n(p_\mu)[G_T'+G_{CT}'^{(2)}+G_{TT}'^{(2)}+G_{TT}'^{mod}](k_\mu)\psi_n(p_\mu+k_\mu), \quad (51)$$

where G_{TT}^{mod} is the additional term, corresponding to the second term on the RHS of (40), resulting from our modification of first-order perturbation theory. It will be convenient to consider together the first two and the last two of the four terms in expression (51).

A. "Main Term"

Let us consider the first term of the RHS of Eq. (51). Using the identity (14), we can write

$$\psi(p_\mu)=\psi_{++}+\psi_{-+}+\psi_{+-}+\psi_{--},$$

and a similar relation for $\bar{\psi}(p_\mu)$. By means of these relations the desired term, involving G_T', can be split up into 16 terms. Of these 16 terms, only the one involving both ψ_{++} and $\bar{\psi}_{++}$ is found to contribute to the order of accuracy we are considering. By means of (15) and (19a) we can express ψ_{++} and $\bar{\psi}_{++}$ in terms of the solution of (26). The dependence of the integrand in (51) on $\epsilon=p_4$ and $\epsilon'\equiv(p_4+k_4)$ is then known explicitly and the integrals over these two variables can be carried out. The first term of (51) can then be written as

$$\frac{e^2}{2\pi^2}\int\int d^3p\,d^3p'\phi_{++}^*(\mathbf{p})\mathfrak{F}(\mathbf{p},\mathbf{p}')\sum_{i=1}^{2}\alpha_i^a\alpha_i^b\phi_{++}(\mathbf{p}'), \quad (52)$$

where

$$\mathfrak{F}(\mathbf{p},\mathbf{p}')=\int\int\frac{d\epsilon d\epsilon'[E-E_a(p)-E_b(p)][E-E_a(p')-E_b(p')]}{(2\pi i)^2F_{++}(\mathbf{p},\epsilon)F_{++}(\mathbf{p}',\epsilon')[k^2-|\epsilon'-\epsilon|^2-i\Delta]};$$
$$\mathbf{k}\equiv\mathbf{p}'-\mathbf{p}.$$

According to the Feynman prescription we have inserted a negative infinitesimal imaginary mass, $(-i\Delta)$, for the photon into the expression for $\mathfrak{F}(\mathbf{p},\mathbf{p}')$. The integrals in this expression can be evaluated exactly and give

$$\mathfrak{F}(\mathbf{p},\mathbf{p}')=\Big\{[k^2-|E_b(p)-E_b(p')|^2]^{-1}+\frac{[E-E_a(p)-E_b(p)]}{2k[k+E_a(p)+E_b(p')-E][k-E_b(p)+E_b(p')]}+\frac{[E-E_a(p')-E_b(p')]}{2k[k+E_a(p')+E_b(p)-E][k-E_b(p')+E_b(p)]}\Big\}. \quad (53)$$

In the Breit treatment one obtains an expression identical with (52), except that $\mathfrak{F}(\mathbf{p},\mathbf{p}')$ is replaced by k^{-2} and $\phi_{++}(\mathbf{p})$ by the equivalent solution of the Breit-equation for a Coulomb interaction. To the required order, the first term of (53) substituted into (52) gives the same contribution to the energy as the Breit-term.

Consider now the expression obtained by substituting the third term of (53) into Eq. (52). One finds that approximations, accurate to lowest order in α, are required for $\phi_{++}^*(\mathbf{p})$ in the range $p\gtrsim p_0$. We shall therefore approximate $\phi_{++}^*(\mathbf{p})$ by the nonrelativistic Schrödinger function $\phi_0^*(\mathbf{p})$ Eq. (27). For $\phi_{++}(\mathbf{p}')$ it is convenient to use the iterated wave function ϕ_{1++} defined in (29) which is a good approximation even for $p'\sim m$. Making these substitutions and changing the variables of integration, this contribution to the energy becomes

$$-(e^2/2\pi^2)^2\int\int d^3p\,d^3p'\phi_0^*(\mathbf{p})\mathfrak{H}_1(\mathbf{p},\mathbf{p}')\phi_0(\mathbf{p}'), \quad (54)$$

where $\mathfrak{H}_1(\mathbf{p},\mathbf{p}')$ is an operator involving an integral over k. The integrand involves the denominator of the third term of (53). Now $k>A\gg$Ry and only values of $k\ll m$ are found to contribute to the required order. The denominator of the third term of (53) can thus be approximated by $(2k^3)$. This gives

$$\mathfrak{H}_1(\mathbf{p},\mathbf{p}')=\int d^3k\sum_{i=1}^{2}\alpha_i^a\alpha_i^b\Lambda_+^a(\mathbf{p}+\mathbf{k})\times\Lambda_+^b(\mathbf{p}+\mathbf{k})(2k^3)^{-1}(\mathbf{p}'-\mathbf{p}-\mathbf{k})^{-2}. \quad (55)$$

We consider next one part of the second term on the RHS of (51). This expression is the equivalent of (32), but with a transverse photon of momentum $\mathbf{k}$ instead

of the Coulomb interaction with a momentum transfer $\mathbf{k}$, i.e.,

$$-\left(\frac{e^4}{8\pi^3 i}\right)\int\int\int \frac{d^4p d^4k d^4p' \sum_{i=1}^{2} \bar{\psi}(p_\mu)\alpha_i{}^a\Lambda_+{}^a(\mathbf{p}+\mathbf{k})\Lambda_+{}^b(\mathbf{p}'-\mathbf{k})\alpha_i{}^b\psi(p_\mu')}{(k^2-\omega^2-i\Delta)(\mathbf{p}'-\mathbf{p}-\mathbf{k})^2[\mu_a E-E_a(\mathbf{p}+\mathbf{k})+\epsilon+\omega+i\delta][\mu_b E-E_b(\mathbf{p}'-\mathbf{k})-\epsilon'+\omega+i\delta]}+\cdots. \quad (56)$$

In (56) the three other terms (involving $\Lambda_+\Lambda_-$, $\Lambda_-\Lambda_+$, and $\Lambda_-\Lambda_-$), which are not written explicitly, are found not to contribute to the required order. In this approximation it is further found that $\bar{\psi}(p_\mu)$ and $\psi(p_\mu')$ can be replaced by $\bar{\psi}_{++}(p_\mu)$ and $\psi_{++}(p_\mu')$, respectively. These two functions can then be expressed in terms of $\phi_{++}{}^*(p_\mu)$ and $\phi_{++}(p_\mu')$, respectively, using (15), (15c), and (19a). The dependence of the integrand of (56) on $\epsilon \equiv p_4$, $\omega \equiv k_4$, and $\epsilon' \equiv p_4'$ is then known explicitly and the integrations over these three variables can be carried out. One then finds that the integrand contributes to the required order only for

$$p,\ p' \sim p_0;\quad A \gtrsim k \gtrsim p_0. \quad (57)$$

One can then further replace $\phi_{++}{}^*$ and ϕ_{++} by the nonrelativistic Schrödinger wave functions, $\phi_0{}^*$ and ϕ_0, respectively. To the required order in α and (m/M), (56) then reduces to an expression of the form (54), with $\mathfrak{H}_1$ replaced by $\mathfrak{H}_2$,

$$\mathfrak{H}_2(\mathbf{p},\mathbf{p}') = -\int d^3k \sum_{i=1}^{2} \alpha_i{}^a\Lambda_+{}^a(\mathbf{p}+\mathbf{k}) \times\Lambda_+{}^b(\mathbf{p}'-\mathbf{k})\alpha_i{}^b(2k^3)^{-1}(\mathbf{p}'-\mathbf{p}-\mathbf{k})^{-2}. \quad (58)$$

We have so far considered only the third term of (53) and one-half of the term involving $G_{CT}{}^{(2)}$. In these two expressions $\alpha_i{}^a$ occurs to the left of $\Lambda_+{}^a$. The second term of (53) gives an expression equivalent to (54), with $\mathfrak{H}_1$ replaced by a rather similar operator $\mathfrak{H}_3$, in which $\alpha_i{}^a$ occurs to the right of $\Lambda_+{}^a$. Similarly the second half of $G_{CT}{}^{(2)}$ (corresponding to an interchange of the order of the Coulomb and transverse interaction) gives another expression, with $\mathfrak{H}_2$ replaced by another operator $\mathfrak{H}_4$ ($\alpha_i{}^a$ again to the right of $\Lambda_+{}^a$). The sum of these four operators is

$$\int d^3k(2k^3)^{-1}(\mathbf{p}'-\mathbf{p}-\mathbf{k})^{-2}\sum_{i=1}^{2}\{[\alpha_i{}^a\Lambda_+{}^a(\mathbf{p}+\mathbf{k}) - \Lambda_+{}^a(\mathbf{p}'-\mathbf{k})\alpha_i{}^a][\alpha_i{}^b\Lambda_+{}^b(\mathbf{p}+\mathbf{k}) - \Lambda_+{}^b(\mathbf{p}'-\mathbf{k})\alpha_i{}^b]\}. \quad (59)$$

We finally substitute (59) into Eq. (54). For the range of values given by (57), the term in curly brackets in (59) can be approximated by $[-(p_i'-p_i)^2/mM]$. We then get the following contribution to the energy

$$\Delta E_{T,B} = \frac{e^4}{4\pi^4 mM}\int\int\int d^3p d^3k d^3p' \phi_0{}^*(\mathbf{p}) \times\left[\sum_{i=1}^{2}(p_i'-p_i)^2(\mathbf{p}'-\mathbf{p}-\mathbf{k})^{-2}\right](2k^{-3})\phi_0(\mathbf{p}'). \quad (60)$$

The integration over k in (60) extends from A to infinity. Values of $k \gtrsim B$, Eq. (47), do not contribute to the order required. Using the properties of the nonrelativistic Schrödinger equation for the hydrogen atom, it can then easily be shown that the expression (60) is identical with (48), the equivalent expression obtained from the three-dimensional treatment.

To (60) we now have to add the contributions from $k<A$, Eq. (46). The sum of these terms, ΔE_{CT}, is then correctly given to order $\alpha(m/M)$(fs), by the expressions derived in the last section. For s states the coefficient of the term in $\log\alpha$ in this expression can also be obtained very simply, directly from (60). For $k \ll p_0$, the term in square brackets in (60) reduces to 2/3. (60) then reduces to

$$\Delta E_{CT} \sim (e^4/3\pi^2 mM)\left|\int d^3p\phi_0(\mathbf{p})\right|^2\int dk k^{-1} = (8\alpha^2/3mM)|\psi_n(0)|^2\int dk k^{-1}. \quad (61)$$

The integral over k goes from $k \sim \alpha p_0$ to $k \sim p_0$ and is thus of the order of magnitude of $\ln\alpha^{-1}$. (61) is identical with the part of the correct expression which involves $\ln\alpha^{-1}$.

B. "Transverse Double-Photon" Term

We finally have to consider the last two terms of (51), represented in Fig. 1, diagrams 3a and 3b, corresponding to the interchange of two transverse photons, "crossed" for $G_{TT}{}^{(2)}$ and "successively" for $G_{TT}{}^{mod4}$. For an exact evaluation of these terms the elegant methods of integration of Feynman are probably most suitable. But these terms are themselves of order $\alpha(m/M)$(fs), so for the purposes of this paper we only need to evaluate them to lowest order in α and (m/M). For this purpose it is most convenient to use the same method we employed for the treatment of $G_{CC}{}^{(2)}$ and $G_{CT}{}^{(2)}$.

As in the previous treatment one finds that one can approximate the four-dimensional wave functions ψ by ψ_{++}. These functions are again expressed in terms of ϕ_{++} and the nonrelativistic approximation ϕ_0 used for these three-dimensional functions. Each term is then again split into four terms, using the identity (14). Of these terms only those involving $\Lambda_-{}^a\Lambda_-{}^b$ and $\Lambda_+{}^a\Lambda_-{}^b$ are found to contribute to the required order. This is due to the fact that two Dirac matrices for the proton occur, one on either side of Λ^b. To illustrate the method, we write out explicitly one of these terms, corresponding

to $G_{TT}{}^{mod}$ and $\Lambda_-{}^a\Lambda_-{}^b$. This term substituted into (51) gives

$$-\left(\frac{e^4}{8\pi^3 i}\right)\int\int\int \frac{d^4p d^4k d^4p' \sum_{i=1}^{2}\sum_{j=1}^{2}\bar{\psi}(p_\mu)\alpha_i{}^a\alpha_i{}^b\Lambda_-{}^a(\mathbf{p}+\mathbf{k})\Lambda_-{}^b(\mathbf{p}+\mathbf{k})\alpha_j{}^a\alpha_j{}^b\psi(p_\mu)}{(k^2-\omega^2-i\delta)(k'^2-|\epsilon'-\epsilon-\omega|^2-i\delta)[\mu_a E+E_a(\mathbf{p}+\mathbf{k})+\epsilon+\omega-i\delta][\mu_b E+E_b(\mathbf{p}+\mathbf{k})-\epsilon-\omega-i\delta]}, \tag{62}$$

where

$$\mathbf{k}'\equiv\mathbf{p}'-\mathbf{p}-\mathbf{k}.$$

Expressing $\psi(p_\mu)$ in terms of $\phi_0(\mathbf{p})$ as explained above, and integrating over ϵ, ω and ϵ', (62) reduces to

$$-(e^2/2\pi^2)^2\int\int d^3p d^3p'\phi_0{}^*(\mathbf{p})\mathfrak{P}_1(\mathbf{p},\mathbf{p}')\phi_0(\mathbf{p}'), \tag{63}$$

where

$$\mathfrak{P}_1(\mathbf{p},\mathbf{p}')=\int d^3k\alpha_i{}^a\alpha_i{}^b\Lambda_-{}^a(\mathbf{p}+\mathbf{k})\times\Lambda_-{}^b(\mathbf{p}+\mathbf{k})\alpha_j{}^a\alpha_j{}^b\mathfrak{R}(\mathbf{p},\mathbf{p}';\mathbf{k})$$

and $\mathfrak{R}$ is a function not involving Dirac operators. If $p_0\ll B\ll m$, then $\mathfrak{R}$ is found to be to the required order,

$$\mathfrak{R}(\mathbf{p},\mathbf{p}';\mathbf{k})=\begin{cases}[8mMkk'(|k|+|k'|)]^{-1} & \text{for } k<B\\ [m+2k+E_a(k)]\{8Mk^3[m+k+E_a(k)]^2\}^{-1} & \text{for } k>B.\end{cases} \tag{64}$$

From $G_{TT}{}^{(2)}$ a similar term to (63) is obtained, with $\mathfrak{P}_1$ replaced by another function $\mathfrak{P}_2$, depending on the same function $\mathfrak{R}$, Eq. (64), but containing different Dirac operators. To the required order we can make the following substitution:

$$\sum_{i=1}^{2}\sum_{j=1}^{2}(1/2)[\alpha_i{}^a\Lambda_-{}^a(\mathbf{p}+\mathbf{k})\alpha_j{}^a+\alpha_j{}^a\Lambda_-{}^a(\mathbf{p}'-\mathbf{k})\alpha_i{}^a]\times[\alpha_i{}^b\Lambda_-{}^b(\mathbf{p}+\mathbf{k})\alpha_j{}^b+\alpha_j{}^b\Lambda_-{}^b(\mathbf{p}'-\mathbf{k})\alpha_i{}^b]\rightarrow 2[1+\cos^2\theta][m+E_a(k)]/2E_a(k), \tag{65}$$

where θ is the angle between $\mathbf{k}$ and $\mathbf{k}'$. Equation (65) is derived in the appendix. Using (64) and (65), the sum $\Delta E_{TT}{}^-$ of (63) and the equivalent term involving $\mathfrak{P}_2$ can then be evaluated for any particular atomic state.

The approximation (50a) for this term, derived previously from the three-dimensional treatment, can also be obtained quite simply from our present method. For $p_0\ll k\ll m$, we also have $\mathbf{k}\approx -k'$ and hence $\cos\theta\approx 1$. $\mathfrak{R}(\mathbf{p},\mathbf{p}';\mathbf{k})$ can then be approximated by $[16mMk^3]^{-1}$ and the expression (65) by a factor 4. Integrating from $k\sim p_0$ to $k\sim m$, the approximation for $\Delta E_{TT}{}^-$ becomes

$$\Delta E_{TT}{}^-\sim -(e^4/4\pi^3 mM)\ln(m/p_0)\left|\int d^3p\phi_0(\mathbf{p})\right|^2,$$

which is identical with (50a).

The exact evaluation of $\Delta E_{TT}{}^-$ can be carried out for any particular atomic state, using (63), (64), and (65). The integration over k is carried from zero to infinity. No divergences are encountered and the range $k<A$ does not contribute to the required order. The results for the $2s$ and $2p$ states of hydrogen are

$$2s:\Delta E_{TT}{}^-=-(\alpha^5 m\ \mathrm{Ry}/2\pi M)\{\ln(2\alpha^{-1})-(5/4)-0.411\}=-0.438\ \mathrm{Mc/sec}. \tag{66}$$

$$2p:\Delta E_{TT}{}^-=-(\alpha^5 m\ \mathrm{Ry}/24\pi M)=-0.009\ \mathrm{Mc/sec}. \tag{66a}$$

The term (-0.411) in Eq. (66) is a numerical approximation to a rather tedious integral.

We finally have to consider $\Delta E_{TT}{}^+$, the term equivalent to $\Delta E_{TT}{}^-$ but with the projection operators $\Lambda_-{}^a\Lambda_-{}^b$ replaced by $\Lambda_+{}^a\Lambda_-{}^b$. This term can be evaluated in a completely analogous (but simpler) manner to $\Delta E_{TT}{}^-$. The result for any state of hydrogen is

$$\Delta E_{TT}{}^+=+(2\alpha^2/mM)\{\ln 2+\tfrac{1}{2}\}|\psi_n(0)|^2, \tag{67}$$

which gives $+0.132$ Mc/sec for the $2s$ state and zero for the $2p$ state.

The terms ΔE_{CC}, $\Delta E_{T.B}$, $\Delta E_{TT}{}^-$, and $\Delta E_{TT}{}^+$ for any atomic state can be written as the expectation values for the particular state of "correction potential" operators (same operators for all atomic states). For ΔE_{CC} and $\Delta E_{TT}{}^+$ these operators are (apart from numerical factors not involving $\log\alpha$), when written in configuration space, $(\alpha^2/mM)\delta^{(3)}(\mathbf{r})$. The operators for $\Delta E_{T.B}$ and $\Delta E_{TT}{}^-$ are, for $r\neq 0$, simple multiples of (α^2/mMr^3) and thus give finite (but small) contributions also for states of nonzero orbital angular momentum. These two operators are highly singular at the origin, but can be expressed in terms of a limiting procedure

$$\mathrm{Op}=\left(\frac{\alpha^2}{mM}\right)\mathrm{Lt}_{\eta\to 0}\left\{[a\ln\alpha+4\pi b\ln\eta]\delta^{(3)}(\mathbf{r})+\frac{b}{(r+\eta)^3}\right\}, \tag{68}$$

where a and b are numerical constants of the order of magnitude of unity.

The total correction of order $\alpha(m/M)(\mathrm{fs})$ to the fine structure of hydrogen, ΔE, is then the sum of the four terms ΔE_{CC}, ΔE_{CT}, $\Delta E_{TT}{}^-$, and $\Delta E_{TT}{}^+$. For the $2s$

state Eqs. (36), (49), (66), and (67) give

$$\Delta E=+\left(\frac{\alpha^2\mathrm{Ry}}{3\pi}\right)\left(\frac{m}{M}\right)\left\{2\left[\ln\left(\frac{\alpha^{-1}}{8.32}\right)+\left(\frac{11}{6}\right)\right]-\left(\frac{3}{2}\right)\left[\ln(\alpha^{-3})-\frac{7}{4}-0.41_1\right]\right\}. \quad (69)$$

In (69) the first term in square brackets is due to $(\Delta E_{CC}+\Delta E_{CT})$, the second to $(\Delta E_{TT}^{-}+\Delta E_{TT}^{+})$.

The numerical values for the $2s$ and $2p$ states of hydrogen are

$$2s:\Delta E=+0.379\ \mathrm{Mc/sec}. \quad (70)$$

$$2p:\Delta E=-0.017\ \mathrm{Mc/sec}. \quad (70a)$$

VII. GENERALIZATION TO COMPLEX NUCLEI

In this paper we have shown that there are corrections, ΔE, to the fine structure (fs) of hydrogen of order $\alpha(m/M)$(fs), due to the finite mass of the nucleus. These corrections were calculated on the assumption that the nucleus (proton) is a single Fermi-Dirac particle of electric charge $(+e)$, and structure effects, like the anomalous magnetic moment, meson cloud, etc. for the nucleus were neglected.

Let us again neglect specifically mesonic and structure effects and consider the protons and neutrons in a nucleus as Fermi-Dirac particles of charge $(+e)$ and zero, respectively, with a phenomenological potential between them. We can then generalize the treatment of this paper to any hydrogen-like atom. The correction term ΔE arises from the interchange of photons or Coulomb interactions, involving momentum transfers $k\gtrsim m$. These momentum transfers are very small compared with the momentum distributions of the nucleons in a nucleus (photon wavelengths large compared with nuclear radius) and are also small compared with the binding energies of the nucleons in a nucleus. The terms ΔE_{CC} and ΔE_{CT} involve only positive-energy intermediate states for the nucleus and are thus completely nonrelativistic as regards the nucleus. For these terms then any nucleus should behave as a single particle of charge $+Ze$ and mass $M=AM_p$ (at least approximately), where M_p is the proton mass and Z, A are the atomic charge and weight, respectively. We can then use the formulas derived in this paper, substituting Ze for e and the total mass of the nucleus for M.

We shall now show, in somewhat greater detail, that the same results apply[14] for the terms ΔE_{TT}^{-} and ΔE_{TT}^{+}. This fact is not quite obvious, since for these terms the Dirac operators $e\boldsymbol{\alpha}$ induce transitions to negative-energy states of the nucleons. Thus the energy changes in the virtual transitions are of order $2M_p$, which is large compared with the potentials between the nucleons. The protons are coupled singly to the radiation field and one might at first sight expect the protons to make transitions to negative-energy states independently of each other, instead of the nucleus acting as a whole. This problem is similar to the nonrelativistic limit of the nucleonic Compton effect for a complex nucleus. In the Compton effect a low momentum photon is absorbed by one of the protons in the nucleus and another photon is emitted; in the present effect two (virtual) photons are emitted (or absorbed) by protons in the nucleus.

Let us consider, for example, the part of the terms ΔE_{TT} corresponding to two photons of momentum k and k', respectively, being emitted successively by a complex nucleus of atomic number and weight Z and A, respectively. We use the three-dimensional perturbation treatment of Sec. V and consider only the factor in the matrix element corresponding to the emission of the two photons by the nucleus. Before both emissions the nucleus is in its ground state (with all nucleons in positive-energy states) of total energy E_0. After the emission of the first photon the nucleus can be in any "excited" state, including those in which some nucleons are in negative-energy states. Let the energy of this intermediate state of the nucleus be E_n. After the emission of both photons, the nucleus (but not the atom) must have returned to its ground-state. In the energy-denominator for the first intermediate state we can neglect the atomic binding energy and we also neglect the effect of retardation. The part of the matrix element which we consider is then

$$\sum_n\sum_{z,z'}\langle 0|\alpha_i^z|n\rangle\langle n|\alpha_j^{z'}|0\rangle/(E_0-E_n-k), \quad (71)$$

where α_i^z is the Dirac matrix in the direction of polarization i, for the zth proton. z and z' are both summed from unity to Z. We shall neglect nuclear exchange forces throughout.

We first consider the states n for which one of the protons is in a negative-energy state. Now $k\gtrsim m\ll M_p$ and we can therefore approximate the energy denominator (E_0-E_n-k) of (71) by $(+2M_p)$. We can then use a sum rule to eliminate the summation over n, which gives

$$\sum_{z,z'}\langle 0|\alpha_i^z\alpha_j^{z'}|0\rangle/2M_p. \quad (71a)$$

In nonrelativistic approximation this term becomes

$$(Z\cos\theta/2M_p), \quad (72)$$

(where θ is the angle between the two directions of polarization) which is just Z times the equivalent term for a single free proton.

However, for a complex nucleus, positive-energy intermediate states n give contributions to (71) of the same order of magnitude as (71a). For these states we replace α_i^z by the nonrelativistic approximation (p_i^z/M_p), where p_i^z is the component of the momentum of the zth proton in the i-direction, and $\alpha_j^{z'}$ by $(p_j^{z'}/M)$. Now E_n, even for the lowest excited state, is larger than E_0 by a few Mev for most nuclei. On the other hand $k\gtrsim m\approx 0.5$ Mev, and we therefore get a fair (but

[14] This fact was first pointed out to the author by Dr. N. Kroll.

not excellent) approximation by omitting k in the energy denominator of (71) for these terms as well. With these approximations we get a term, in addition to (71a),

$$\sum_n \sum_{s,s'} \langle 0|\, p_i{}^s \,|n\rangle\langle n|\, p_j{}^{s'} \,|0\rangle / M_p{}^2 (E_0 - E_n). \quad (71b)$$

(71b) can be written in the form

$$(-\cos\theta/2M_p)\textstyle\sum_n f_{0n}, \quad (72)$$

where f_{0n} is the oscillator strength for a dipole transition. Neglecting exchange forces, the sum $\sum_n f_{0n}$ is equal to $[(A-Z)Z/A]$.[15] The sum of (71a) and (71b) is then

$$\frac{\cos\theta}{2M_p}\left[Z - \frac{(A-Z)Z}{A}\right] = \frac{\cos\theta}{2M_p}\left(\frac{Z^2}{A}\right). \quad (73)$$

Expression (73) thus shows that, even for the terms ΔE_{TT}, the expression for a single proton has to be multiplied by (Z^2/A), apart from inserting the appropriate value for $|\psi(0)|^2$. In other words, the factor (e^2/M_p) has to be replaced by $(Ze)^2/(AM_p)$, which means using the results of the present paper for a single-particle nucleus of charge (Ze) and mass (AM_p). For deuterium the total effect is then half as big as for hydrogen. For a general nucleus the effect is slightly less than (Z^2/A) times that for hydrogen, since the logarithmic factors in ΔE_{CT} and $\Delta E_{TT}{}^-$ decrease slightly with increasing Z.

Various approximations have been made in the derivation of the result of this section. The neglect of retardation introduces at most a fractional error of the order of the ratio of (wavelength of the virtual photons) to (radius of the nucleus), which is less than 1/50 (for $k \gtrsim m$). Neglecting k compared with $(E_0 - E_n)$ for negative-energy intermediate states gives a fractional error of about $(m/2M_p)$ or less, which is negligible. Neglecting $k/(E_0 - E_n)$ for positive-energy intermediate states of the nucleus introduces larger errors, however. For deuterium, for instance, the smallest value possible for $(E_0 - E_n)$ is only 2.3 Mev, the deuteron binding energy. By analogy with the photodisintegration of the deuteron one might expect the "average" value of $(E_0 - E_n)$ to be about twice this amount or about 5 Mev. For ΔE_{CT}, $k \gtrsim p_0 \ll m$ and the error is negligible. For ΔE_{TT} the term involving the logarithmic factor comes from $k \ll m$ and the error is again very small. But ΔE_{CC} and some of the parts of ΔE_{TT}, not involving a logarithmic factor, come from values of k of the order of $m \sim 0.5$ Mev. Because of the partial cancellation of ΔE_{CT} and ΔE_{TT} these terms, coming from $k \sim m$, are almost as large as the total result ΔE. The error in the total result ΔE for deuterium might thus be as large as (0.5 Mev/5 Mev) or 10 percent. The effect of nuclear exchange forces has not been investigated yet, but is probably small.

[15] J. S. Levinger and H. A. Bethe, Phys. Rev. **78**, 115 (1950).

The mass corrections to fine structure, calculated in this paper, are different for the $2s$ and $2p$ states and hence have to be considered in an analysis of the Lamb shift experiment. However, there are also mass corrections to the theoretical results for the Lamb shift itself, which are of the same order of magnitude as the corrections calculated in this paper. There are also other corrections to the fine structure and to the Lamb shift due to the finite size of complex nuclei and even due to the internal structure of nucleons. In a subsequent paper all these corrections of relevance to the Lamb shift will be discussed.

The Breit treatment has previously[16] been applied to the fine structure of positronium to lowest order and correction terms of relative order α could be calculated in a manner analogous to that for hydrogen.[2,3] The errors of order α(fs) inherent in such a Breit-treatment could then be evaluated for positronium using the methods described in the present paper.

The work of the present paper also shows that no correction terms of order $\alpha(\text{hfs}) \sim \alpha(m/M)(\text{fs})$ occur for the hyperfine structure (i.e., terms involving the nuclear spin operator) of atoms. If the expansions in powers of (m/M) of this paper are carried one power further, corrections to the hyperfine structure do occur, however. These corrections are of order $\alpha(m/M)\log(M/m)(\text{hfs})$ and will be discussed in a later paper.

I am greatly indebted to Professor H. A. Bethe for many suggestions and comments throughout this work. I also wish to thank Professors F. J. Dyson, R. Karplus, and N. Kroll for helpful discussions and Dr. M. Baranger for checking the calculations of this paper.

APPENDIX

In the present paper we have dealt with wave functions in momentum space, $\psi(\mathbf{p}, \epsilon)$ and $\phi(\mathbf{p})$, which are 16-component spinors with 4 indices for particle a and 4 for particle b. The formulas we derive in this appendix are the same for $\psi(\mathbf{p}, \epsilon)$ and $\phi(\mathbf{p})$ and, for simplicity, we discuss only $\phi(\mathbf{p})$. We have defined the usual Casimir projection operators,

$$\Lambda_\pm(\mathbf{p}) = [E(p) \pm H(\mathbf{p})]/2E(p); \quad E(p) = (m^2 + p^2)^{\frac{1}{2}}, \quad H(\mathbf{p}) = m\beta + \boldsymbol{\alpha}\cdot\mathbf{p}, \quad (A1)$$

separately for particles a and b.[17] Any wave function $\phi(\mathbf{p})$ can then be written as the sum of 16 eigenfunctions of the operator $H^a(\mathbf{p})H^b(\mathbf{p})$. These 16 functions split into 4 sets of 4 degenerate functions (2 spin states for each of the two particles),

$$\phi_{\pm\pm}(\mathbf{p}) = \Lambda_\pm{}^a(\mathbf{p})\Lambda_\pm{}^b(\mathbf{p})\phi(\mathbf{p}). \quad (A2)$$

Each of these 16 functions is then the product of two 4-component spinors, one for each of the two particles.

We shall now derive some approximate expressions, used in the text, for the matrix elements of certain operators involving the various Dirac matrices for both particles. These matrix elements are only required between wave functions of the type $\phi_{++}(\mathbf{p})$ and $\phi_{++}(\mathbf{p}')$, where $p,\ p' \ll m_a,\ m_b$. Since the Dirac matrices for particle a commute with those for particle b, and since the wave

[16] R. A. Ferrell, Phys. Rev. **84**, 858 (1951); J. Pirenne, Arch. Sci. **28**, 233 (1946); **29**, 121, 207 and 265 (1947); V. B. Berestetsky, J. Exptl. Theoret. Phys. (USSR) **19**, 1130 (1949).

[17] In the text of the paper we have denoted $(m\beta - \alpha\cdot\mathbf{p})$ by $H(\mathbf{p})$ for particle b.

functions are products of the two 4-component spinors, these matrix elements are the product of two individual matrix elements (one for each particle). We therefore only evaluate the matrix elements of operators for one single Fermi-Dirac particle between wave functions consisting of a single 4-component spinor.

We define again

$$\phi_{\pm}(\mathbf{p})=\Lambda_{\pm}(\mathbf{p})\phi(\mathbf{p}), \tag{A3}$$

and consider only matrix elements involving ϕ_+. $\phi_+(\mathbf{p})$ can further be written as a two by one matrix, $[\phi_+^+, \phi_+^-]$ where both ϕ_+^+ and ϕ_+^- are 2-component spin functions of the Pauli-type. In this notation

$$\alpha=\sigma\begin{pmatrix}0 & 1\\ 1 & 0\end{pmatrix}, \quad \beta=\begin{pmatrix}1 & 0\\ 0 & -1\end{pmatrix}, \tag{A4}$$

and

$$\phi_+^-(\mathbf{p})=(\boldsymbol{\sigma}\cdot\mathbf{p})[m+E(p)]^{-1}\phi_+^+(\mathbf{p}), \tag{A5}$$

where $\boldsymbol{\sigma}$ is the Pauli spin-vector.

We first discuss the derivation of Eq. (26a) from (26), where Λ_+^b has already been replaced by unity and Λ_-^b by zero. By means of Eq. (A5), $\phi_+(\mathbf{p})$ is explicitly given in terms of $\phi_+^+(\mathbf{p})$. We therefore want to derive from Eq. (26) an equation which only involves $\phi_+^+(\mathbf{p})$ and $\phi_+^+(\mathbf{p}+\mathbf{k})$. Using Eqs. (A1), (A4), and (A5), one finds the exact relation

$$[\Lambda_+(\mathbf{p})\phi_+(\mathbf{p}+\mathbf{k})]^+ = \left\{1+\frac{(\boldsymbol{\sigma}\cdot\mathbf{p})(\boldsymbol{\sigma}\cdot\mathbf{k})+[E(p)-E(\mathbf{p}+\mathbf{k})][E(p)-m]}{2E(p)[E(\mathbf{p}+\mathbf{k})+m]}\right\}\phi_+^+(\mathbf{p}+\mathbf{k}). \tag{A6}$$

In nonrelativistic approximation ($p, k\ll m$), the factor in curly brackets in Eq. (A6) reduces to the factor in square brackets on the RHS of Eq. (26a). Using this approximation for (A6), we obtain Eq. (26a) from (26), where ϕ in Eq. (26a) really stands for ϕ_+^+.

We further require the matrix elements of various Dirac operators O between wave functions $\phi_+(\mathbf{p})$ and $\phi_+(\mathbf{p}')$, to lowest order in an expansion in powers of p/m and p'/m. The matrix element of O is then equal to the matrix element of the operator $\Lambda_+(\mathbf{p})O$. Using Eqs. (A1), (A4), and (A5), we can then express the quantity $[\Lambda_+(\mathbf{p})O\phi_+(\mathbf{p}')]^+$ in the form $U\phi_+^+(\mathbf{p}')$, where U is an operator involving only the Pauli spin-matrix $\boldsymbol{\sigma}$, but no Dirac operators. To the required accuracy, the Dirac operator O can then be replaced by the Pauli operator U.

We merely write down the operator U corresponding to several operators O, to lowest order in p/m and p'/m and for a general value of k.

$$O=\Lambda_-(\mathbf{p}+\mathbf{k}); \quad U=[E(k)-m]/4E(k). \tag{A7}$$

$$O=\alpha_i\alpha_j; \quad U=\sigma_i\sigma_j. \tag{A8}$$

$$O=\alpha_i\Lambda_-(\mathbf{p}+\mathbf{k})\alpha_j; \quad U=\sigma_i\sigma_j[E(k)+m]/2E(k). \tag{A9}$$

$$O=\alpha_i\Lambda_+(\mathbf{p}+\mathbf{k})\alpha_j; \quad U=\sigma_i\sigma_j[E(k)-m]/2E(k). \tag{A10}$$

For $p, p', k\ll m$ we also find, to lowest order in p/m, p'/m, and k/m

$$O=\alpha_i\Lambda_+(\mathbf{p}+\mathbf{k}); \quad U=\{2p_i+k_i+i[\mathbf{k}\times\boldsymbol{\sigma}]_i\}/2m. \tag{A11}$$

$$O=\Lambda_+(\mathbf{p}'-\mathbf{k})\alpha_j; \quad U=\{2p_j'-k_j+i[\mathbf{k}\times\boldsymbol{\sigma}]_j\}/2m. \tag{A12}$$

In deriving the above equations of this appendix, use has been made of the commutation relations of the Pauli matrices,

$$\boldsymbol{\sigma}\times\boldsymbol{\sigma}=2i\boldsymbol{\sigma}.$$

In deriving the expression used in Eq. (60) of the text from Eqs. (A11) and (A12), use has been made of the fact that the direction of polarization j is perpendicular to the momentum of the photon $\mathbf{k}$, so that k_j is zero. In deriving Eq. (65) from Eq. (A9), use has been made of the anti-commutation relations of the Pauli matrices,

$$\sigma_i^2=1, \quad [\sigma_i\sigma_j+\sigma_j\sigma_i]=0, \tag{A13}$$

where i and j are two directions perpendicular to each other.

Decay of a Neutral Scalar Heavy Meson

H. P. NOYES
Department of Physics, University of Rochester, Rochester, New York
(Received April 7, 1952)

The decay of a neutral scalar heavy meson into two pseudoscalar π-mesons is renormalized by the introduction of a contact interaction $\chi\Phi_s\varphi_{ps}^*\varphi_{ps}(x)$, where the finite part of χ is an empirical constant chosen to fit the observed lifetime for this decay. This interaction contributes to the decay into two γ-rays in order $G_sg_{ps}^3e$, and all contributions to this order have been calculated. The total fifth-order contribution is negative relative to the third-order matrix element. Consequently, for a particular relationship between the heavy and light meson coupling constants, the 2γ-decay lifetime will be e^4/g^4 slower than the 2π-decay lifetime. Hence, heavy scalar mesons strongly enough coupled to nucleons to be produced copiously at high energies could be sufficiently stable to be observed experimentally; in particular the V_2^0 particle may be of this type.

INTRODUCTION

THIS paper is an investigation into the stability of neutral, scalar, heavy mesons against decay into two pseudoscalar π-mesons or two γ-rays, undertaken in order to discover if it is possible to explain any of the recently discovered unstable particles in such terms. Experimentally, the Manchester group finds two groups of neutral V-particles which they interpret according to the decay schemes $V_1^0\rightarrow p+\pi^-$ and $V_2^0\rightarrow\pi^++\pi^-$,[1] although not all workers in this field agree with their analysis.[2] Accepting their analysis for the moment the V_1^0 must have half-integral spin and will not be discussed here. Further, since decay into two scalar particles is strictly forbidden by parity for a pseudoscalar particle (and decay into three pseudoscalar particles for a scalar particle),[3] pseudoscalar heavy mesons such as the rarely observed $\tau^\pm\rightarrow\pi^\pm+\pi^++\pi^-$[4] will only be briefly considered at this time. Although numerical results will be quoted only for the V_2^0 mass and lifetime, the results can readily be extended to other unstable particles with the same decay scheme such as the ζ^0 meson[5] which are not yet easily studied by present techniques.

The difficulty in explaining any heavy particle energetically capable of decaying into π-mesons, which is coupled strongly enough to nucleons to be produced in large numbers, is that according to present field theories it would be expected to undergo such possible decays through virtual nucleon states in an unobservably short time. This problem has been previously investigated by Van Wyk using perturbation theory and by several Japanese authors using the Tomonaga-Schwinger formalism.[6] Most of the heavy boson decay schemes turn out to be divergent, making the interpretation of these results uncertain. The Japanese obtained finite answers by the use of Pauli regulators but found that in many cases the regulated results could not be made unambiguous. This is in accord with Matthews' result[7] that in fact no unambiguous prescription exists for theories that cannot be renormalized to all orders. However, the work of Salam[8] has shown that scalar and pseudoscalar meson theories without derivative couplings can be renormalized by the introduction of direct interaction terms into the Lagrangian. This means that in these cases finite and unambiguous results should be obtainable, and because of the possible importance of heavy mesons in the nuclear force problem, it seemed worthwhile to reinvestigate these cases in detail.

The lowest order process by which a scalar meson can decay into two π-mesons is logarithmically divergent but can be renormalized by the introduction of an (infinite) contact interaction between the heavy and light meson fields of the form $\chi\Phi_s\varphi_{ps}^*\varphi_{ps}(x)$ (Φ_s = heavy meson field; $\varphi_{ps}=\pi$-meson field). Since this interaction can contain a finite part, we obtain the uninformative result that any desired lifetime will be given by a correct choice of this constant. However, this interaction has further observable consequences that must be in agreement with experiment. A necessary but not sufficient condition is that the heavy neutral particle must also be sufficiently stable against decay into two γ-rays. This process is convergent to lowest order (Ge^2) and the only divergence (outside of the usual charge and mass divergences) that occurs in next order (Gg^2e^2) is precisely that divergence which is removed by the infinite part of the contact interaction term introduced to renormalize the 2π-decay. It might

[1] Armenteros, Barker, Butler, and Cachon, Phil. Mag. **42**, 1113 (1951).
[2] Proceedings of the Rochester Conference on Meson Physics (1951).
[3] In the center-of-mass system, decay into three or fewer spin zero particles depends at most on two vectors. Since no invariant pseudoscalar can be constructed from less than three vectors, the matrix element must be a scalar, and there can be no parity change.
[4] Fowler, Menon, Powell, and Rochat, Phil. Mag. **42**, 1040 (1951), see also for references.
[5] Danysz, Lock, and Yekutieli, Nature **169**, 364 (1952).
[6] C. B. Van Wyk, Proc. Phys. Soc. (London) **A62**, 697 (1949); S. Ozaki, Prog. Theoret. Phys. **5**, 373 (1950); Fukuda, Hayakawa, and Miyamoto, Prog. Theoret. Phys. **5**, 352 (1950); Sasaki, Oneda, and Ozaki, Prog. Theoret. Phys. **5**, 25 (1950).
[7] P. T. Matthews, Phys. Rev. **81**, 936 (1951).
[8] A. Salam, Phys. Rev. **82**, 217 (1951); see also J. C. Ward, Phys. Rev. **79**, 406 (1950) and F. Rohrlich, Phys. Rev. **80**, 666 (1950).

be argued that since it is necessary to introduce a direct interaction term in the case of the 2π-decay, it is unreasonable not to introduce a second direct interaction term in this case, even though it is not needed for the purposes of renormalization. However, the analogous interaction term in this case, $\chi'\Phi A_\mu A_\nu(x)$, is not gauge invariant, while the gauge invariant interaction $\chi''\Phi F_{\mu\nu}F_{\mu\nu}(x)$, because it involves derivatives, would be likely to introduce nonrenormalizable infinities in higher orders. This situation exists in spinor electrodynamics, where it is also possible to introduce direct interaction terms; here the empirical result is that the correct value for the Lamb shift, anomalous magnetic moment, etc., are obtained without such terms. Further, they would again be likely to cause divergences not removable by present techniques. Granted then that the interaction with the electromagnetic field should not contain direct interaction terms, the constant that occurs in the 2π decay is also the only unknown in the two process (to order Gg^2e^2), and it is no longer trivial to ask whether it is possible to pick this interaction in such a way as to make both decay lifetimes of the right order of magnitude.

The result of the calculation is that for the value of the interaction constant which renders the decay lifetime into two π-mesons long enough to fit the experimental facts, the particle can also be made sufficiently stable against decay into two γ-rays by postulating (in principle) a precisely determinable relationship between the coupling constants of the heavy and light mesons to nucleons. This demonstration has in fact been carried out to order Gg^2e^2 in the usual S matrix expansion in the coupling constants. However, provided only that this expansion converges, it can be argued that there will be a relationship between the coupling constants for which this stability exists even if all orders in the expansion are included. Thus, contrary to expectation, the instability of neutral, scalar, heavy mesons due to transitions through virtual nucleon states can be reduced sufficiently to make their lifetime as long as that of the observed V_2^0 particles.

DECAY INTO TWO PSEUDOSCALAR MESONS

The Feynman diagrams for the decay of a scalar, neutral meson into two pseudoscalar charged π-mesons are given in Fig. 1. After taking the spur the matrix element for this process is

$$\int d^3q d^3k_1 d^3k_2 (2\pi)^4 \delta(q+k_1-k_2) \times \Phi(q)\varphi^*(k_1)\varphi(k_2)\frac{i(G_p+G_n)g^2}{(2\pi)^4}\int d^4l \times \frac{4iM(k_1k_2-l^2-M^2)}{[(l-k_1)^2+M^2][l^2+M^2][(l+k_2)^2+M^2]}, \quad (1)$$

where k_1 and k_2 are the four-momenta of the final π-

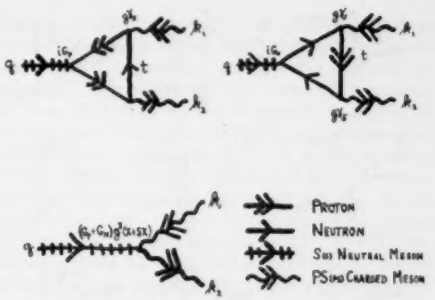

FIG. 1. Decay of a neutral scalar meson into two charged pseudoscalar mesons.

mesons, k_1-k_2 the four-momentum of the heavy meson, and hence $(k_1-k_2)^2=-K^2=k_1^2+k_2^2-2k_1k_2$; $2k_1k_2=K^2-2\mu^2$ (K=heavy meson mass, $\mu=\pi$-meson mass $=276m_e$, M=nucleon mass; for general notation see Appendix I). The l^2 term gives a logarithmic divergence, so that it is necessary to assume that the Lagrangian also contains a contact interaction of the form:

$$-(G_p+G_n)g^2(\chi+\delta\chi)\int d^4x\Phi\varphi^*\varphi(x), \quad (2)$$

where

$$\delta\chi=4iM(2\pi)^{-4}\int d^4l/(l^2+M^2)^3. \quad (3)$$

Adding the lowest order diagram due to this term and using the identity[9]

$$\int\frac{d^4l}{(2\pi)^4}\left\{\frac{1}{[l^2+M^2]^2}-\frac{1}{[l^2+M^2+C]^2}\right\}=\frac{\pi^2 i}{(2\pi)^4}\log\left(1+\frac{C}{M^2}\right), \quad (4)$$

the renormalized matrix element after integration over t becomes

$$iA\left\{\frac{(2\pi)^2M}{K^2}\chi-\frac{M^2}{K^2}\int_0^1 dx\log\left[1-\frac{K^2x(1-x)}{M^2}\right]-\left(\tfrac{1}{2}-\frac{\mu^2}{K^2}\right)\int_0^1 xdx\int_0^1 dy\frac{1}{D}\right\}, \quad (5)$$

where

$$A=\frac{(G_p+G_n)g^2K^2}{(2\pi)^2M}\int d^3qd^3k_1d^3k_2\Phi(q)\varphi^*(k_1)\times\varphi(k_2)(2\pi)^4\delta(q+k_1-k_2), \quad (6)$$

and

$$D=1-x^2y(1-y)K^2/M^2-x(1-x)\mu^2/M^2.$$

If the finite interaction constant χ were zero, this would

[9] R. Karplus and N. M. Kroll, Phys. Rev. 77, 536 (1950).

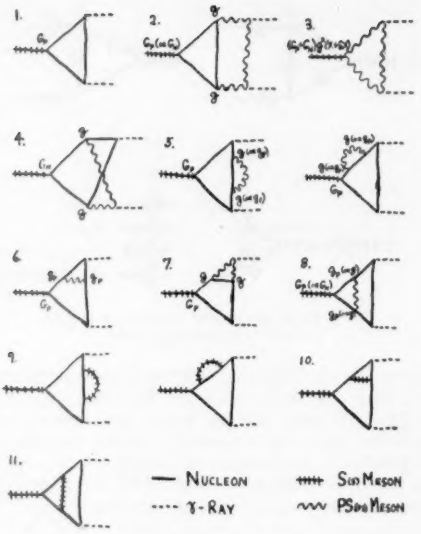

FIG. 2. Decay of a neutral scalar meson into two γ-rays to order $G_p^2e^2$ and G^2e^2.

give a decay probability of

$$\tau^{-1}\approx\frac{(G_p+G_n)^2g^4K}{(4\pi)^3}\left(1-\frac{4\mu^2}{K^2}\right)^{\frac{1}{2}}\left[\frac{(\frac{1}{6}-\mu^2/K^2)K}{8\pi M}\right]^2 \quad (7)$$

to the lowest order in an expansion in powers of K^2/M^2. It is interesting to note that this vanishes for $K=\mu\sqrt{6}=678m_e$, which number is only changed by about one electron mass if higher terms in the K^2/M^2 expansion are included. So that this particular renormalization prescription, if it could be justified on other grounds, would predict a unique stable mass for the heavy scalar meson. For the observed V_2^0 mass of about $800m_e$ the lifetime would be approximately $[(4\pi)^3/(G_p+G_n)^2g^4]\times3.2\times10^{-15}$ second, so that in order to obtain the observed lifetime of about 10^{-10} second, the finite part of the interaction constant must be chosen to be

$$\frac{\chi}{K}=\frac{K}{(2\pi)^2M}\left\{\frac{M^2}{K^2}\int_0^1 dx\,\log\left(1-\frac{x(1-x)K^2}{M^2}\right)+\left(\frac{1}{2}-\frac{\mu^2}{K^2}\right)\int_0^1 xdx\int_0^1 dy\frac{1}{D}\right\}\pm1.6\times10^{-4}. \quad (8)$$

This choice of χ affects the 2γ-decay, as will be discussed in the next section.

DECAY INTO TWO γ-RAYS

This process has already been investigated by Steinberger and by Fukada and Miyamoto,[10] who, after dropping nongauge-invariant terms, obtain for the lowest order matrix element

$$-iB\int_0^1 xdx\int_0^1 dy\frac{1-4x^2y(1-y)}{1-x^2y(1-y)K^2/M^2}, \quad (9)$$

where

$$B=G_pe^2K^2/(2\pi)^2M\int d^3qd^3k_1d^3k_2(2\pi)^4\delta(q+k_1+k_2)\times\Phi(q)A_\mu(k_1)A_\nu(k_2)(\delta_{\mu\nu}+2k_{1\nu}k_{2\mu}/K^2). \quad (10)$$

This term gives a decay probability of about

$$\tau^{-1}\approx G_p^2e^4K/(4\pi)^3(K/6\pi M)^2\approx2.8\times10^{16}(G_p^2/4\pi)\text{sec}^{-1} \quad \text{for} \quad K=800m_e,$$

which would be much too great for the scalar meson to exist long enough to be observed as a V_2^0 particle. (Schwinger also obtains this result by a different method.[11]) However, the interaction constant χ, which it was found necessary to introduce in order to give the observed lifetime for the decay into two π-mesons, contributes to this process in order Gg^2e^2 and because $g^2/(4\pi)$ is not small can significantly alter this conclusion. The Feynman diagrams to this order are given in Fig. 2. Number 1 is the lowest order diagram already discussed. Number 2 contains a logarithmic divergence that is canceled by the $\delta\chi$ term from number 3. Both of these matrix elements are complex due to the occurrence of two real π-mesons as an intermediate state in addition to the virtual states that do not conserve energy (Dyson's "displaced poles").[12] But χ has been picked to cancel the contribution from this part of the diagram when the two π-mesons are real. Consequently, it is to be expected that for this choice of χ the imaginary part contributed to the matrix element by diagrams 2 and 3 will cancel identically. Unfortunately, it has not proved feasible to evaluate exactly the fivefold integrals that are left after combining denominators by Feynman's famous formula and carrying out the four-dimensional integrations over intermediate momenta. However, the first term in an expansion of these integrals in powers of K^2/M^2 has been obtained, and to this order the expected cancellation of the imaginary parts does occur. The exact integrals for all the diagrams in Fig. 2 are given in Appendix II, and the approximations introduced to obtain the values given below are discussed there. It should be noted that although K^2/M^2 is about 0.2, the expansions actually involve $x(1-x)K^2/M^2$ with $0\leq x\leq1$, so that the error made by dropping these terms is probably less than 5 percent, which is more than adequate for the purposes of this paper. Neglecting terms of order K^2/M^2, the total contribution from diagrams 2 and 3 is $[-iB(1+G_n/G_p)g^2/(4\pi)^2](-2/9)$. Diagram 4 is irreducible and

[10] J. Steinberger, Phys. Rev. **76**, 1180 (1949); H. Fukada and Y. Miyamoto, Prog. Theoret. Phys. **4**, 347, 392 (1949).

[11] J. Schwinger, Phys. Rev. **82**, 664 (1951).

[12] F. J. Dyson, Phys. Rev. **82**, 428, 438 (1951), and lectures at Birmingham.

finite and gives a contribution $[-iBG_n g^2/G_p(4\pi)^2] \times(7/36)$. Diagrams 5 are obtained by self-energy insertions in 1. They therefore contain linear divergences which are canceled in the usual way by mass renormalization; the finite contribution is $[-iB(g^2+g_p^2)/(4\pi)^2](-0.0209)$. Diagrams 6, 7, and 8 are vertex insertions containing logarithmic divergences which are removed by using Dyson's prescription of replacing γ_μ by $\bar{\Gamma}_\mu$ and 1 by $\bar{1}$ in the original integral for diagram 1. They give rise, respectively, to the finite contributions

$$[-iBg_p^2/(4\pi)^2](-0.360); [-iBg^2/(4\pi)^2](0.242);$$

$$\text{and } [-iB(g_p^2+G_nG_p^{-1}g^2)/(4\pi)^2](-0.452).$$

Diagrams 9, 10, and 11 are the corresponding self-energy and vertex insertions due to neutral, scalar mesons in virtual states; they are functions of the heavy meson mass, even using the above-mentioned expansion, and have been evaluated for $K=800\ m_\sigma$ giving a total finite contribution of $[-iB\bar{G}_p^2/(4\pi)^2](-3.290)$.

Charged heavy mesons have not been included as their introduction would require an additional contact interaction $(\chi'+\delta\chi')\Phi_0\Phi^*\Phi(x)$, where χ' is a new empirical constant that would require the calculation of a third distinct process for evaluation. The diagrams contributed by charged heavy mesons to the 2γ-decay of the neutral heavy meson are given in Fig. 3. The neglect of these diagrams does not, however, alter the argument below, as they will contribute simply an additional term proportional to $-iBG^2/(4\pi)^2$ which merely increases the complexity of the relationship between coupling constants of heavy and light mesons for which cancellation occurs.

Collecting all the above contributions, the real part of the matrix element for decay into two γ-rays is

$$-iB\left\{\tfrac{1}{3}-\frac{g^2}{(4\pi)^2}\left[0.833\frac{g_p^2}{g^2}+0.672\frac{G_n}{G_p}-0.193\right]-3.290\frac{G_p^2}{(4\pi)^2}\right\} \quad (11)$$

and clearly can be zero for certain values of the coupling constants. In particular, for $g^2=g_p^2=g_n^2$ and $G_p=G_n$, this relationship is $g^2/4\pi+2.5G_p^2/4\pi=3.08$, which is clearly compatible with the usually assumed values for these constants. There is in addition a small imaginary term, corresponding to the interaction that allows a lifetime of about 10^{-10} second for the 2π-decay, but this clearly gives a lifetime for 2γ-decay approximately $g^4/e^4\cong 2\times 10^4$ longer. Therefore, for that value of χ which gives a reasonable lifetime for the 2π-decay, the probability of decay into two γ-rays is sufficiently small to insure that only the former process will be observed.

The extension of this calculation to higher order terms in the S matrix cannot be expected to alter this conclusion. As χ is evaluated as a power series in the coupling constants, the coefficients of the higher order terms can be chosen to keep the 2π-decay lifetime of the same order of magnitude. But since the identical diagrams will occur as the only real intermediate states in the 2γ-decay (neglecting higher terms in e), this choice will also insure that there will be negligible higher order contributions to the imaginary part of the 2γ-decay matrix element. Therefore, provided only the series converges sufficiently not to change the sign of the higher order terms relative to the third-order matrix element, there will still exist some (in principle) precisely determinable relationship between the heavy and light meson coupling constants for which the heavy neutral scalar meson will be more stable against decay into two γ-rays than into two pseudoscalar π-mesons.

FURTHER CONSIDERATIONS

It has already been pointed out that the inclusion of charged heavy scalar mesons will not alter this conclusion, although a new empirical constant enters the theory. Further, if empirical evidence should be obtained that the charged V particle decays into a charged and a neutral π-meson, the above calculation can be readily extended to this case, most of the integrals being the same as have already been evaluated.

The problem of whether the neutral scalar heavy meson is also sufficiently stable against other modes of decay is more serious. Decay into two γ-rays and a π-meson was found by Van Wyk and S. Power[13] to be of the order of $10^{-11}/G^2g^2$ seconds, which is compatible with the above relationship between the coupling constants, but might require rather too small a G to be reconciled with the copious production of V_2^0 particles. *A priori*, the decay into two π-mesons and a γ-ray would be expected to have a still shorter lifetime, and this process is now be inginvestigated.* Pais[14] has

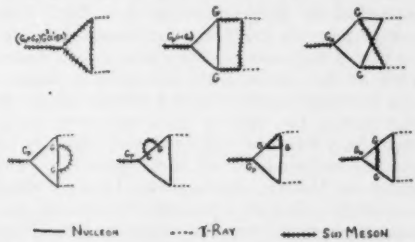

FIG. 3. Contributions of charged scalar mesons to the decay of a neutral scalar meson into two γ-rays in order G^2e^2.

[13] C. B. Van Wyk, Proc. Phys. Soc. (London) **A63**, 350 (1950); S. Power, Phys. Rev. **76**, 865 (1949).

* *Note added in proof:*—For $K=850m_\sigma$ R. S. Grover finds $\tau^{-1}=(G_p+G_n)^2g^4(2\pi)^{-3}\times 4.6\times 10^{17}$ sec^{-1} for decay into two charged mesons and a γ-ray and $G_p^2g^4\ (2\pi)^{-3}\times 1.8\times 10^{18}$ sec^{-1} for decay into two π^0 mesons and a γ-ray. The former process can be forbidden by taking $G_p=-G_n$, but the latter makes the neutral scalar particle too unstable to be observed unless a cancellation similar to that discussed in this paper occurs when Gg^3e terms are included.

[14] A. Pais, Phys. Rev. **86**, 663 (1952); see also reference 2.

shown that this lifetime for the decay of a pseudoscalar heavy meson is of the order of $10^{-17}/G^2g^4$, but the contact interaction introduced to renormalize the 2π-decay contributes in the scalar case and could conceivably alter this situation in the right direction.

The extension of this approach to pseudoscalar heavy mesons does not look hopeful, unless one follows Pais in postulating a strong interaction allowing the heavy particles to be produced in pairs and a weak interaction governing their subsequent decay. In the first place the neutral particle would presumably decay into two γ-rays in a time shorter than the lifetime of the neutral π-meson or into a γ-ray and two π-mesons, as already indicated, but this may be actually the case, since there is at present no evidence for the existence of such neutral particles with long lifetimes. However, the relatively stable charged τ-meson that decays into three π-mesons has been seen. This decay in itself offers no problem, as it is renormalizable and hence can have the observed lifetime; the finite part of the renormalization interaction contributes to the $(\pi+2\gamma)$ decay in much the same way as the scalar renormalization contributes to the 2γ-decay, so this situation could well reproduce the features already discussed. But this interaction does not contribute to the $(2\pi+\gamma)$ decay in sufficiently low order to make calculation feasible, and since Pais' result for the lowest order matrix element gives such a short lifetime, it may well prove impossible to achieve sufficient stability against this decay. A detailed investigation of this case would be required in order to determine if any new features enter which could alter this conclusion.

CONCLUSION

The decay of a neutral scalar particle strongly coupled to nucleons into two pseudoscalar π-mesons can be renormalized by the introduction of a direct interaction between the heavy and light meson fields, the finite part of which can be chosen to given any desired lifetime for this process. If the interaction is chosen to fit the observed lifetime of the V_2^0 particle, the neutral scalar particle can also be made sufficiently stable against decay into two γ-rays to insure that only the decay into two π-mesons will occur appreciably. This stability can, however, only be achieved if one is willing to accept (in principle) a precisely determinable relationship between the coupling constants of heavy and light mesons to nucleons. The present estimates of the values for these coupling constants are compatible with this relationship. Therefore, the possibility that there can exist scalar mesons strongly enough coupled to nucleons to affect the nuclear force problem cannot be ignored. The approach used in this paper is likely to prove inadequate to explain the τ-meson.

The author wishes to thank the State Department Board of Foreign Scholarships for a grant under the Fulbright Act and the Department of Mathematical Physics at the University of Birmingham, England, for its hospitality during the course of the first part of this research. The author is grateful for illuminating discussions with F. J. Dyson and R. H. Dalitz, and to A. Pais for the opportunity of seeing his paper prior to publication. Above all, the advice and encouragement of R. E. Peierls have made possible the successful completion of this work.

APPENDIX I. NOTATION

$$lx=l_\mu x_\mu=\mathbf{l}\cdot\mathbf{x}-l_0x_0;\ \boldsymbol{\gamma}=-i\beta\boldsymbol{\alpha};\ \gamma_4=\beta;\ \gamma_5=\gamma_1\gamma_1\gamma_3\gamma_4;$$

$$l=l_\mu\gamma_\mu;\ \bar{\psi}=i\psi^*\gamma_4.$$

$$\text{Lagrangian density}=-\tfrac{1}{2}[(\partial\Phi/\partial x_\mu)^2+K^2\Phi^2]$$

$$-\tfrac{1}{2}[(\partial\varphi_0/\partial x_\mu)^2+\mu^2\varphi_0^2]-\tfrac{1}{2}[(\partial\varphi^*/\partial x_\mu-ieA_\mu\varphi^*)$$

$$\times(\partial\varphi/\partial x_\mu+ieA_\mu\varphi)+\mu^2\varphi^*\varphi]+i\bar{\psi}_p[\gamma_\mu(\partial/\partial x_\mu$$

$$+ieA_\mu)+M]\psi_p+i\bar{\psi}_n[\gamma_\mu\partial/\partial x_\mu+M]\psi_n-iG_p\bar{\psi}_p\psi_p\Phi$$

$$-iG_n\bar{\psi}_n\psi_n\Phi-g_p\bar{\psi}_p\gamma_5\psi_p\varphi_0-g_n\bar{\psi}_n\gamma_5\psi_n\varphi_0$$

$$-g[\bar{\psi}_p\gamma_5\psi_n\varphi+\bar{\psi}_n\gamma_5\psi_p\varphi^*],$$

where $\psi_{p(n)}$ = proton (neutron) wave function, mass M; Φ = scalar neutral meson wave function, mass K; φ = charged pseudoscalar meson wave function, mass μ; φ_0 = neutral pseudoscalar meson wave function, mass μ; and A_μ = electromagnetic potential function.

Propagation of a fermion

$$\psi(x)\bar{\psi}(y)=-i\int\frac{d^4l}{(2\pi)^4}\frac{e^{il(x-y)}}{l-iM}.$$

Propagation of a boson

$$\varphi(x)\varphi^*(y)=i\int\frac{d^4l}{(2\pi)^4}\frac{e^{il(x-y)}}{l^2+\mu^2}.$$

Transformation to momentum space

$$\Phi(x)=\int d^3q e^{iqx}\Phi(q).$$

APPENDIX II. CALCULATION OF MATRIX ELEMENTS

The gauge invariant contribution from diagram 2 is

$$S_2=-iB\frac{(1+G_n/G_p)g^2}{(4\pi)^2}\left\{\bar{I}_2+\frac{2i(1+J\mu^2/K^2)M^2}{\pi^2K^2}\right.$$

$$\left.\times\int d^4l\frac{1}{[(l-k_1)^2+M^2][(l+k_2)^2+M^2]}\right\},\quad(12)$$

where

$$\bar{I}_2=2\int_0^1 xdx\int_0^1 dy\int_0^1 du\int_0^1 dv\int_0^1 w(1-w)dw \times\left\{\frac{a+b-8ab}{D}-\frac{K^2}{M^2}abx(1-x)\frac{1-a-b+2ab}{D^2}\right\}$$

$$a=wvy+(1-w)u;\ b=wv(1-y)+(1-w)(1-u);$$
$$D=wv+(1-wv)x(1-x)\mu^2/M^2 -wvxy(1-y)K^2/M^2-abx(1-x)K^2/M^2; \tag{13}$$

$$J=2\int_0^{\frac{1}{2}}dx\frac{\log|K^2(x^2-x_0^2)/\mu^2|}{\frac{1}{4}-x^2}-2\pi i\log\frac{1+2x_0}{1-2x_0};$$

$$x_0^2=\tfrac{1}{4}-\frac{\mu^2}{K^2}.$$

To order K^2/M^2, D may be written as

$$D_0=wv+x(1-x)\left[1-u(1-u)(1-w)^2\frac{K^2}{\mu^2}\right]\frac{\mu^2}{M^2}, \tag{14}$$

where the second term must be retained because of the pole that gives the imaginary contribution to the matrix element; in this expansion higher powers of K^2/M^2 will then have integrals of the same form as coefficients. By using care to drop all higher order terms during the integration and some algebraic manipulation $\bar{I}_2$ can be reduced to the form

$$\bar{I}_2=-2/9+(\tfrac{1}{2}-\mu^2/K^2)(1+J\mu^2/K^2). \tag{15}$$

The contribution from diagram 3 is

$$S_3=\frac{iB(1+G_n/G_p)g^2}{(4\pi)^2}(\chi+\delta\chi)\frac{(4\pi)^2M}{2K^2}\left(1+J\frac{\mu^2}{K^2}\right). \tag{16}$$

Using the value of $\delta\chi$ already assumed and the identity (4) gives for the total contribution due to both diagrams

$$S_2+S_3=\frac{iB(1+G_n/G_p)g^2}{(4\pi)^2}\left\{-\bar{I}_2+\frac{(4\pi)^2M}{2K^2}\left[\chi-\frac{4M}{(4\pi)^2} \times\int_0^1 dx\log\left(1-\frac{x(1-x)K^2}{M^2}\right)\right]\left(1+J\frac{\mu^2}{K^2}\right)\right\}. \tag{17}$$

But to order K^2/M^2,

$$\chi-4M\int_0^1 dx[\log(1-x(1-x)K^2/M^2)]/(4\pi)^2$$

is by Eq. (8), simply $2K^2(\frac{1}{2}-\mu^2/K^2)/(4\pi)^2M$, so that not only the divergent terms, but also the imaginary parts of these two diagrams cancel identically.

Diagram 4 is irreducible, and after dropping non-gauge-invariant terms, leads to the integral

$$S_4=\frac{-2iB(G_n/G_p)g^2}{(4\pi)^2}\int_0^1 du\int_0^1 dv\int_0^1 w(1-w)dw \times\int_0^1 x^2dx\int_0^1 dy\left\{\frac{1-16abw+14aw-12awv}{w(1-w)D_1} -\frac{K^2}{M^2}ab\frac{1-b+2aw+(8b-4)awv}{D_1^2}+\frac{2xy(v-1)b}{D_2} +\frac{2xyv(b-1)}{D_3}\right\}, \tag{18}$$

where $a=xy(v-u)$; $b=x(1-vy)$ and

$$D_i=xy-wv(1-v)K^2/M^2+(1-xy)w(1-w)\mu^2/M^2 -bw(1-w)[a\delta_{1i}+xy(v-1)\delta_{2i}+xyv\delta_{3i}]K^2/M^2,$$
$$i=1,2,3.$$

Diagrams 5 are obtained by replacing $1/(t-iM)$ by

$$\frac{(g^2+g_p^2)}{(4\pi)^2}\int_0^1 dx\int_0^1 dy\left\{\frac{x(1-x)[-iMtx+(1-x)t^2+M^2]}{\Lambda_0^2+yx(1-x)[t^2+M^2]} -\frac{2M^2x^2(1-x)}{\Lambda_0^2}\right\}\frac{1}{t-iM}, \tag{19}$$

where

$$\Lambda_0^2=x^2M^2+(1-x)\mu^2=M^2\lambda_0^2,$$

in diagram 1 [plus corresponding insertions for $1/(t-k_1-iM)$ and $1/(t+k_2-iM)$] giving

$$S_5=\frac{iB(g^2+g_p^2)}{(4\pi)^2}\int_0^1 x(1-x)dx\int_0^1 dy\int_0^1 udu\int_0^1 dv \times\left\{-\frac{6x}{\lambda_0^2}\frac{[1-4u^2v(1-v)]}{[1-u^2v(1-v)K^2/M^2]}+x\left[\frac{2u-1}{D_1} -\frac{1-3u+2u^2+2uv(1-u)}{D_2}-\frac{1-u-2uv(1-u)}{D_3}\right] +(1-x)\left[\frac{1-4u^2v(1-v)}{D_1}+\frac{1-4u(1-u)(1-v)}{D_2} +\frac{1-4u(1-u)v}{D_3}\right]+2yx(1-x)(1-u) \times\int_0^1 dw\left[(1-4u^2v(1-v))\left(\frac{1}{D_1^2}+\frac{1}{D_2^2}+\frac{1}{D_3^2}\right) -4u(1-u)w\left(\frac{1-v}{D_2^2}+\frac{v}{D_3^2}\right)\right]\right\},$$

where

$$D_i = yx(1-x)+(1-u)\lambda_0^2 - yx(1-x)u[uv(1-v)\delta_{1i} + (1-u)(1-v)\delta_{2i} + (1-u)v\delta_{3i}]K^2/M^2;\ i=1,2,3$$

$$D_i = yx(1-x)+w(1-u)\lambda_0^2 - yx(1-x)u[uv(1-v)\delta_{4i} + (1-v)(uv+w-uw)\delta_{5i} + v(u-uv+w-uw)\delta_{6i}]\ K^2/M^2;\ i=4,5,6.$$

To order K^2/M^2 this leads to the integral

$$S_5 = -\frac{iB(g^2+g_p^2)}{(4\pi)^2}\int_0^1 dx F_0(x) = -\frac{iB(g^2+g_p^2)}{(4\pi)^2}(-0.0209), \quad (20)$$

where

$$F_0 = x(f_1+f_2-2f_3)+(1-x)(7f_0/3-5f_1+6f_2-10f_3/3) - 4\alpha^2 x(g_0-2g_1+g_2)-5\alpha x/3,$$

$$\alpha = \frac{x(1-x)}{\lambda_0^2};\quad f_n = \int_0^1 dw w^n \log\frac{w+\alpha}{w};\quad g_n = \int_0^1 dw w^n \log\frac{w+\alpha}{\alpha}.$$

This and the following integrals were evaluated numerically.

Similarly, the replacement of γ_μ by

$$\frac{g_p^2}{(4\pi)^2}\int_0^1 xdx\int_0^1 dy \times\left\{\frac{[(1-x)t-(1-xy)k_1-iM]\gamma_\mu[(x-1)t-xyk_1+iM]}{\Lambda_0^2+x(1-x)[(t-yk_1)^2+M^2]} - \frac{x^2M^2}{\Lambda_0^2}\gamma_\mu - \gamma_\mu\int_0^1 dz\frac{x(1-x)[(t-yk_1)^2+M^2]}{\Lambda_0^2+zx(1-x)[(t-yk_1)^2+M^2]}\right\} \quad (21)$$

or

$$\frac{-2g^2}{(4\pi)^2}\int_0^1 xdx\int_0^1 dy\left\{\frac{-(1-x)t_\mu(xt-xyk_1-iM)}{\Omega_0^2+x(1-x)[(t-yk_1)^2+M^2]} + \frac{(1-x)^2M^2}{\Omega_0^2}\gamma_\mu - \gamma_\mu\int_0^1 dz \times\frac{x(1-x)[(t-yk_1)^2+M^2]}{\Omega_0^2+zx(1-x)[(t-yk_1)^2+M^2]}\right. \quad (22)$$

(where $\Omega_0^2=(1-x)^2M^2+x\mu^2$) leads (including a similar substitution for γ_ν) to the contributions

$$\frac{2iBg_p^2}{(4\pi)^2}\int_0^1 xdx\left(F_1-F_2-\frac{x^2}{3\lambda_0^2}\right) = -\frac{iBg_p^2}{(4\pi)^2}(-0.360) \quad (23)$$

and

$$\frac{-2iBg^2}{(4\pi)^2}\int_0^1 dx\left(\alpha F_3-(1-x)F_2+\frac{2\alpha x}{3}\right) = \frac{-iBg^2}{(4\pi)^2}(0.242), \quad (24)$$

where

$$F_1 = \frac{x^2}{\lambda_0^2}\left[\left(\frac{4}{3}\alpha+\frac{1}{2}\alpha^2-\alpha^2-\frac{2}{3}\alpha^4\right)\log\frac{1+\alpha}{\alpha}-\frac{11}{12}-\frac{7}{9}\alpha + \frac{2}{3}\alpha^2+\frac{2}{3}\alpha^3\right]+\frac{x^2}{2\lambda_0^2}\log\frac{1+\alpha}{\alpha}-\frac{1}{2}\alpha(1+\alpha-\alpha^2-\alpha^3) \times\log\frac{1+\alpha}{\alpha}-\alpha\left(-\frac{7}{12}+\frac{1}{4}\alpha+\frac{1}{2}\alpha^2\right);$$

$$F_2 = \left(\frac{1}{3}+\frac{2}{3}\alpha+\frac{1}{2}\alpha^2+\frac{1}{3}\alpha^3+\frac{1}{6}\alpha^4\right)\log\frac{1+\alpha}{\alpha} + \frac{1}{3}\log\alpha-\frac{7}{18}\alpha-\frac{1}{4}\alpha^2-\frac{1}{6}\alpha^3;$$

$$F_3 = \frac{5}{9}+\frac{19}{36}x+\left(\frac{37}{24}-\frac{35}{72}x\right)\alpha+\left(\frac{11}{12}-\frac{9}{4}x\right)\alpha^2-\frac{4}{3}x\alpha^3 - \left[\frac{1}{6}+\frac{1}{3}x+\left(\frac{5}{4}+\frac{5}{12}x\right)\alpha+\left(2-\frac{3}{2}x\right)\alpha^2 + \left(\frac{11}{12}-\frac{35}{12}x\right)\alpha^3-\frac{4}{3}x\alpha^4\right]\log\frac{1+\alpha}{\alpha}.$$

The replacement of 1 (i.e., the absorption of a scalar meson) by

$$\frac{(g_p^2+G_nG_p^{-1}g^2)}{(4\pi)^2}\int_0^1 xdx\int_0^1 dy\left\{\frac{(1-x)M^2}{\Lambda_0^2}-2\int_0^1 dz\frac{x(1-x)[(t-yk_1+(1-y)k_2)^2+M^2]-K^2xy(1-y)}{\Lambda_0^2-K^2xy(1-y)+zx(1-x)[(t-yk_1+(1-y)k_2)^2+M^2]} + \frac{(x-1)(tk_1-k_2t+k_1k_2)+iM[2(x-1)t+(1-2xy)k_1-(1-2x+2xy)k_2]+(1-x)t^2+(x-1)M^2+(1-x)\mu^2}{\Lambda_0^2-K^2xy(1-y)+x(1-x)[(t-yk_1+(1-y)k_2)^2+M^2]}\right\} \quad (25)$$

gives ultimately

$$\frac{-2iB(g_p^2+G_nG_p^{-1}g^2)}{(4\pi)^2}\int_0^1 dx\left(\frac{x^2F_4}{\lambda_0^2}-\frac{1}{6}\frac{\alpha\mu^2}{M^2}-xF_5\right) = \frac{-iB(g_p^2+G_nG_p^{-1}g^2)}{(4\pi)^2}(-0.452), \quad (26)$$

where

$$F_4=\frac{1}{6}\left(\frac{1}{6}-\frac{1}{2}\alpha+\alpha^2+\alpha^2(1+\alpha)\log\frac{1+\alpha}{\alpha}\right);$$

$$F_5=\alpha\left(1+\frac{7}{6}\alpha+\frac{2}{3}\alpha^2+\frac{1}{6}\alpha^3\right)\log\frac{1+\alpha}{\alpha}$$

$$+\frac{1}{3}\log(1+\alpha)-\alpha\left(\frac{10}{9}+\frac{7}{12}\alpha+\frac{1}{6}\alpha^2\right).$$

All of the above results were checked by an independent substitution of auxiliary Feynman variables, leading not only to the same numerical results, but also (after considerable algebra) to the same algebraic form for F_0 to F_5. Hence, the fact that the total fifth-order contribution from virtual π-mesons is negative relative to the third-order term is quite certain. The entirely analogous results obtained for the heavy meson insertions were not checked as carefully, since they only affect the numerical constants in the relationship between the coupling constants and not the fact that cancellation can occur.

PHYSICAL REVIEW VOLUME 87, NUMBER 2 JULY 15, 1952

The Ratio of Soft and Hard Particles in Air Showers*

KURT SITTE
Department of Physics, Syracuse University, Syracuse, New York
(Received March 12, 1952)

While the density spectrum of air showers is well established for energies above 10^{13} ev, doubt has recently been cast upon the customary procedure of identifying the energy spectrum of the shower-initiating particles calculated from this density distribution with the primary cosmic-ray spectrum. These two distributions would differ if the mechanism of energy transfer to the electron component itself varied with energy. As a result, one would then expect to find a variation with energy also in the amount and composition of the penetrating component of extensive showers. Previous investigations of penetrating particles in air showers do not extend below 10^{13} ev because of the bias imposed, in the case of low density showers, by the addition of a shielded tray. An experiment was therefore carried out at Mt. Evans, Colorado, altitude 4300 m, and at Echo Lake, Colorado, altitude 3260 m, in order to compare the penetrating components of showers in the 10^{13}-ev region and in the 10^{14}-ev region at a similar stage of their cascade development. The relative abundance of penetrating particles was $(2.06\pm0.11)\times10^{-2}$ at Mt. Evans, and $(1.20\pm0.11)\times10^{-2}$ at Echo Lake, and the fraction of N-particles among the penetrating component was (62 ± 7) percent for the lower, and (38 ± 6) percent for the higher shower energies. The ratio of μ-mesons to electrons was the same for both energy ranges. The results are therefore consistent with the assumption that the development of the large mixed cascades in air is based on the same processes for all energies above 10^{13} ev, demanding only a slight increase in the multiplicity of meson production with increasing primary energy.

I. INTRODUCTION

THE study of extensive air showers is certainly the most obvious, and hitherto probably the most successful, method of research in the high energy region of cosmic radiation. Unfortunately, though, the results of such a study yield only very indirect evidence on the nature of the primary interactions, since in these experiments a great many steps intervene between the initial acts and the final recording of the fully-grown shower. Thus, for instance, one can hardly expect from an observation on the intensity of the N-component in these showers, to obtain a unique answer as to the multiplicity of the primary nuclear collision. Or, to choose a simpler example, the old idea of deriving the energy spectrum of the primary cosmic radiation from the density spectrum of air showers (e.g., Heisenberg,[1] Hilberry[2]) is correct only if over the entire range of energies considered, the fraction of the primary energy which goes into the electronic component remains constant.

This latter assumption is certainly subject to serious doubt. Recent advances have shown the processes involved to be very complex, and to include the production of a considerable variety of different fundamental particles. It would seem quite likely that the composition of the shower secondaries produced in the initial collision varies with the energy of the primary. As the contribution to the electron cascade differs for the various components originated in the first interaction, a variation with energy of their relative abundance would, or could, also lead to an energy dependence of the abundance of electrons. The power law for the shower energies derived from the density spectrum of the air shower electrons would then no longer be applicable to the primary cosmic radiation.

The density spectrum of air showers has been thoroughly investigated. In particular, in the experi-

* Supported in part by the AEC.
[1] W. Heisenberg, *Cosmic Radiation* (Dover Publications, New York, 1946), Chap. I.
[2] N. Hilberry, Phys. Rev. **60**, 1 (1941).

ments of Cocconi and Tongiorgi,[3] and of Cocconi, Tongiorgi, and Greisen,[4] the area of the counter trays was varied between 9 cm² and 1560 cm², corresponding to a variation in the energies of the recorded showers from about 10^{13} ev to about 10^{15} ev. The result was that over this entire range the well-known power law for the differential density spectrum,

$$s(\Delta)d\Delta = A\Delta^{-\gamma}d\Delta, \qquad (1)$$

holds with a $\gamma \approx 2.5$, the exponent varying only slightly both with the density and with the altitude. Their results thus check very well with those obtained in the region of higher energies (e.g., Williams[5]), and with different arrangements (e.g., Singer[6]), and it has been shown by Rossi[7] that all these data, as well as the older ones of Hilberry[2] and the flux measurements of various authors at different latitudes, are well represented by a primary spectrum $s(E)dE = dE/(E+E_0)^{2.75}$, with $E_0 = 5.3$ Bev.

On the other hand, there is serious doubt as to the possible validity of so steep a power spectrum for the primary cosmic-ray particles in the region of 10^{12} ev to 10^{13} ev. It has been pointed out by Schein and Lord[8] that the absolute frequency of extremely energetic nuclear events observed in emulsions is inconsistent with so large an exponent. Similarly, the experiments of the Rochester group[9] yield a lower exponent at least for heavy primaries and for energies per nucleon up to about 4×10^{10} ev. Thus, it would appear that either the primary spectrum undergoes a marked change in the region around 10^{12} ev to 10^{13} ev, or that the balance of the electron-initiating processes changes in that same region, leading in some way to a decreasing fractional transfer of the primary energy to the electron component.

Although the detailed features of the development of the mixed cascades are still not fully understood, a criterion concerning their possible variation with energy can be found in the study of the energy dependence of the ratio of intensities of the soft and the hard shower component. For high energies, this ratio is well known and appears to be remarkably independent of the shower energy;[4] but as it will be shown in the following section, these measurements do not cover the same range as the investigations of the electron density spectrum, and do not extend to energies below 10^{13} ev. It was, therefore, decided to examine this point by measuring the relative abundance of penetrating particles in low energy air showers, and to compare it with values at somewhat higher shower energies.

[3] G. Cocconi and V. C. Tongiorgi, Phys. Rev. **75**, 1058 (1949).
[4] Cocconi, Tongiorgi, and Greisen, Phys. Rev. **75**, 1063 (1949).
[5] R. W. Williams, Phys. Rev. **74**, 1689 (1948).
[6] S. F. Singer, Phys. Rev. **81**, 579 (1951).
[7] B. Rossi, Princeton Conference on High Energy Nuclear Interactions, November, 1950.
[8] M. Schein and J. J. Lord, Phys. Rev. **83**, 198 (1951).
[9] Kaplon, Peters, and Ritson, Phys. Rev. **85**, 900 (1952). I am indebted to Professor B. Peters for kindly communicating these results before publication.

II. OUTLINE OF THE METHOD

Let us begin with noting two basic facts that will be of importance for the ensuing discussion:

(1) Any shower arrangement consisting of three or more coincidence counters can be used for the partially selective recording of showers of a given density.

This can be easily shown to hold for all possible counter arrangements, even if the area of the counters applied is not uniform. (More accurately, the condition reads $\Sigma_i n_i > \gamma$, where n_i stands for the number of coincidence counters of the ith type, and γ is again the exponent of the differential density spectrum, assumed to be constant.)[10]

(2) Any shower arrangement which is triggered by showers of a given density Δ will detect mostly events whose *cores* strike nearby, and hence will detect showers with cores of this particular average density. (It is assumed that the triggering arrangement consists of a number of counters, or trays of counters, not too widely separated, a certain coincidence of which will define the "shower" event.)

This point has been discussed at length by various authors (e.g., Ise and Fretter,[11] Singer[6]). It will, therefore, suffice to summarize the results of calculations analogous to theirs, but for a 4-tray arrangement of the kind described below. Using the Bethe approximation[12] for the density distribution in the immediate neighborhood of the shower axis,

$$\Phi(r/r_1) = (C/r_1^2)(r/r_1)^{-1}(1+4r/r_1)\exp[-4(r/r_1)^{\frac{1}{2}}] \qquad (2)$$

(r_1 stands for the usual characteristic shower length of the Molière theory[13]), and successive Molière approximations at larger distances,[13,14] one finds that 50 percent of all recorded showers will strike within a radius R of about $0.04r_1 \approx 4$ m from the center of the arrangement. The absolute value of this "half-width" is, of course, somewhat dependent on the approximation applied, but its accuracy is of no particular importance for the argument.

In relating the density, Δ, selected by a counter arrangement to the total particle number, and hence to the energy, of the showers recorded, one may again choose the median as the suitable representative, and, therefore, $N = \Delta/\Phi(R/r_1) \approx \Delta\times1.19\times10^3$ particles.

A proper arrangement of at least three counters or groups of counters in coincidence can, therefore, be made to select air showers of any required initial energy. The value of the energy is determined by adjusting the size, S, of the counters. For the arrangement

[10] Assume, for instance, that coincidences are formed if of each group or tray, n_i out of N_i counters of area S_i are struck ($i=1, 2\cdots m$). The contribution R to the recorded rate due to showers of the density interval $(\Delta, d\Delta)$ is then

$$Rd\Delta = A\Delta^{-\gamma}d\Delta\sum_{i=1}^{m}\binom{N_i}{n_i}(1-e^{-\Delta S_i})^{n_i}e^{-(N_i-n_i)\Delta S_i},$$

and for constant γ, the condition for the existence of a maximum becomes in view of the monotony character of the functions involved, $(dR/d\Delta)_{\Delta=0} > 0$, which can be reduced to

$$\sum_{i=1}^{m} n_i - \gamma > 0.$$

[11] J. Ise, Jr., and W. B. Fretter, Phys. Rev. **76**, 932 (1949).
[12] H. A. Bethe, Phys. Rev. **59**, 684 (1941).
[13] G. Molière, Nature **30**, 87 (1942); *Cosmic Radiation*, edited by W. Heisenberg (Dover Publications, New York, 1946), Chap. 3.
[14] The numerical values are taken from computations of the density distribution of shower electrons by F. E. Froehlich [Atomic Energy Commission Report NYO-796 (1951)].

discussed below, the relative contributions of showers of various size are shown as a function of NS in Fig. 1.

To return now to the main problem: It has been pointed out that in some of the earlier experiments[3,4] air showers of energies around 10^{13} ev have been preferentially recorded. With the same counter sets the relative abundance of hard shower particles was then measured in the usual way, that is, by adding a further shielded counter tray. However, it should be emphasized that in such an experiment, the addition of the shielded tray acts as a strong bias in favor of the detection of showers of higher density, in particular where $\beta S' \ll S$ (β = relative abundance of hard particles, S' = area of the shielded tray, S = area of the unshielded air shower trays). Take, for instance, the arrangement of Cocconi, Tongiorgi, and Greisen: Threefold coincidences of air shower counters were demanded, so that the contribution of showers of density Δ to the recorded events was

$$R(\Delta) = A(1-e^{-\Delta S})^3 \Delta^{-\gamma}, \tag{3}$$

while in the case of hard showers the corresponding rate R_h was

$$R_h(\Delta) = A(1-e^{-\Delta S})^3(1-e^{-\beta\Delta S'})\Delta^{-\gamma}. \tag{4}$$

The maximum contributions to these rates are from showers with densities satisfying $(dR/d\Delta)=0$, which gives

$$e^{-\Delta S}(3\Delta S+\gamma)-\gamma=0: \Delta S = 0.35 \tag{5}$$

in the first, and from $(dR_h/d\Delta)=0$,

$$e^{-\Delta S}(3\Delta S+\gamma)+e^{-\beta\Delta S'}(\beta\Delta S'+\gamma) - e^{-\Delta(S+\beta S')}(3\Delta S+\beta\Delta S'+\gamma)=0 \tag{6}$$

in the second case. For low density showers one has $\beta S' \ll S$, and (6) can be simplified by expansion of the exponential terms, relying on the fact that only regions where $\Delta S \sim 1$, and hence $\beta\Delta S' \ll 1$, will appreciably contribute. As a lower limit, one finds thus the approximate solution

$$e^{-\Delta S}(3\Delta S+\gamma)-(\gamma-1)=0: \Delta S = 1.25, \tag{7}$$

which shows that the maximum contribution comes now from considerably denser showers. The same fact is still more drastically exhibited by a comparison of the average densities of the showers recorded with the two arrangements. For air showers, one has (writing $\Delta S = z$)

$$\langle z_a\rangle = \frac{\int_0^\infty (1-e^{-z})^3 z^{-(\gamma-1)}dz}{\int_0^\infty (1-e^{-z})^3 z^{-\gamma}dz} = \frac{(-\gamma+1)!\sum_{n=0}^{3}(-1)^n\binom{3}{n}n^{\gamma-2}}{(-\gamma)!\sum_{n=0}^{3}(-1)^n\binom{3}{n}n^{\gamma-1}}, \tag{8}$$

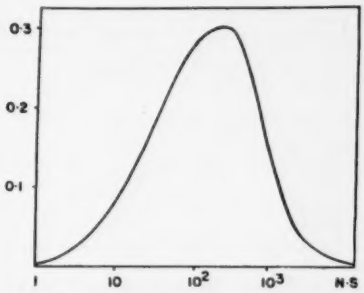

FIG. 1. Contribution to coincidences of 3 out of 4 counters, of showers of various total numbers N of electrons striking at all distances from the center of the arrangement (S in m², R in arbitrary units).

while the average density of the hard showers is (with $\beta S'/S = \alpha$)

$$\langle z_h\rangle = \frac{\int_0^\infty (1-e^{-z})^3(1-e^{-\alpha z})z^{-(\gamma-1)}dz}{\int_0^\infty (1-e^{-z})^3(1-e^{-\alpha z})z^{-\gamma}dz} = \frac{(-\gamma+1)!\sum_{n=0}^{3}(-1)^n\binom{3}{n}\{n^{\gamma-2}-(n+\alpha)^{\gamma-2}\}}{(-\gamma)!\sum_{n=0}^{3}(-1)^n\binom{3}{n}\{n^{\gamma-1}-(n+\alpha)^{\gamma-1}\}}. \tag{9}$$

For showers of low density, one has usually $\alpha \ll 1$, and the ratio of the average densities of the two types of recorded showers becomes

$$\frac{\langle z_h\rangle}{\langle z_a\rangle} = \frac{\sum_{n=1}^{3}(-1)^n\binom{3}{n}n^{\gamma-1}}{\sum_{n=1}^{3}(-1)^n\binom{3}{n}n^{\gamma-2}} \cdot \frac{[\alpha^{\gamma-2}+(\gamma-2)\sum_{n=1}^{3}(-1)^n\binom{3}{n}n^{\gamma-2}]}{[\alpha^{\gamma-2}+(\gamma-1)\sum_{n=1}^{3}(-1)^n\binom{3}{n}n^{\gamma-2}]}. \tag{10}$$

In most experiments α is of the order 10^{-2}, so that $\langle z_h\rangle/\langle z_a\rangle \sim 10$. Even in the experiment of Cocconi, Tongiorgi, and Greisen,[4] where the area of the shielded tray S' was exceptionally large, the ratio (10) is still about 5. Of course, the discrepancy between the two average densities becomes still more pronounced if showers containing more than one hard particle incident from the air are recorded.

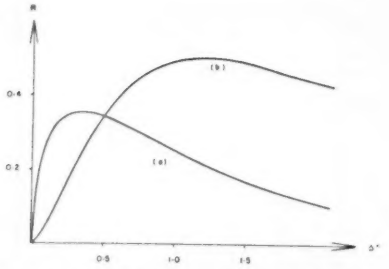

FIG. 2. Contribution to the recorded shower rates as a function of the particle density: (a) triple coincidences of unshielded counters; (b) the same with additional shielded counters ($\beta S'/S = 0.04$).

The situation is somewhat, but not radically, improved if the contributions of the denser showers are cut down by an anticoincidence arrangement demanding, for instance, that exactly n out of N counters be struck. Thus, triple coincidences in anticoincidence with a fourth counter shift the maximum contribution to the recorded rate, computed as in (5), to $\Delta S = 0.19$, and for hard showers to $\Delta S = 0.61$. While the ratio of these figures differs only little from the one obtained above for pure coincidences, the results for the average densities recorded become much better; instead of a factor 5–10, one finds a factor 2–3 between the two averages. The conditions are illustrated in Fig. 2, where the relative contributions to the counting rate of showers of various densities are plotted for a triple-coincidence experiment, and in Fig. 3, where the contributions are shown for triple coincidences in anticoincidence with a fourth counter of equal size. In both cases, a value of $\alpha = 0.04$ has been chosen, corresponding closely to the conditions and the results of the Cocconi-Tongiorgi-Greisen experiment.[4]

Thus, it appears that the range of densities over which the ratio of penetrating particles to electrons has been observed is actually considerably smaller than it has been tacitly assumed. In particular, the investigations do not reach down to the region below 10^{13} ev. It seemed, therefore, worthwhile to carry out an experiment properly designed to fill this gap.

III. THE EXPERIMENTAL ARRANGEMENT

An arrangement suitable for the determination of the relative abundance β of penetrating particles in air showers must satisfy the following conditions:

(1) Its counter area should yield maximum contributions from showers with less than 10^4 particles (at the cascade maximum);

(2) in order to minimize possible errors due to a variation of γ with the density Δ, it should be triggered only by showers over a comparatively narrow density range;

(3) "soft" air showers and air showers containing penetrating particles that are recorded should have on the average equal densities.

To satisfy (1) it becomes advantageous to run the experiment at an altitude as close as possible to the cascade maximum. Of the two convenient locations, Echo Lake and Mt. Evans, the latter was chosen; its atmospheric depth, taken for an average shower origin at one interaction mean free path in air from the top of the atmosphere, is 510 g/cm² or about 14 cascade units, which is only slightly past the maximum for a 10^{13} ev shower.

At 14 cascade units, a shower of 10^{13}-ev initial energy contains about 4.9×10^9 electrons;[15] its detection would thus require a counter arrangement set to select densities of about 3–4 particles/m². This would not be too difficult and has actually been achieved in several experiments (Broadbent and Jánossy,[16] McCusker and Millar[17]), but a most inconveniently large counter area would be required to select the corresponding hard showers. The condition was therefore relaxed and the arrangement set for shower densities of about 10 particles/m².

Condition (2) is sufficiently satisfied by an anticoincidence arrangement triggered if any three out of four counters are struck. Condition (3), however, demands the use of different sets of unshielded counters for the detection of "soft" and of "hard" air showers. The suitable counter sizes can now be determined.

As the maximum contribution to the registered air showers comes from a density $(\Delta S) = 0.19$, a counter area of 155 cm² (two standard 1-in.×12-in. counters in parallel) for the unshielded trays will select densities of about 12 particles/m², or shower energies around 2.5

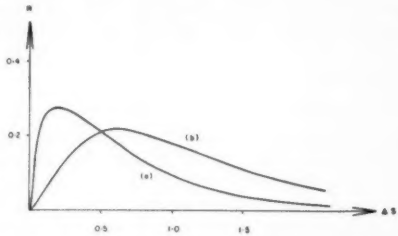

FIG. 3. Contribution to the recorded shower rates as a function of the particle density: (a) coincidences of three out of four unshielded counters; (b) the same with additional shielded counters ($\beta S'/S = 0.04$).

[15] For the determination of the total number of shower electrons, the "Tables of cascade functions" by Leonie Jánossy and H. Messel [Proc. Roy. Irish Acad. **A54**, 217 (1951)] have been used, and corrections have been made both for the ionization loss—following the procedure of these authors—and for the extension of the electron spectrum down to about one-tenth of the critical energy in air, in order to include all shower electrons capable of penetrating the counter walls.

[16] D. Broadbent and L. Jánossy, Proc. Roy. Soc. (London) **A190**, 497 (1947).

[17] C. B. A. McCusker and D. D. Millar, Proc. Phys. Soc. (London) **A64**, 915 (1951).

$\times 10^{13}$ ev. At least a considerable fraction of the recorded events belongs, therefore, to the energy region between 10^{12} ev and 10^{13} ev at which this study was aimed.

The shielded tray consisted of eight counters 1 in. $\times$20 in. As it was also desired to get some evidence on the nature of the penetrating particle, these counters were separated from each other by $\frac{1}{2}$-in. lead strips, so that most of the events in which more than one shielded counter was struck can be attributed to either a local penetrating shower, or more than one incident penetrating particle. The shielding consisted of 8 in. of lead on top of the tray, and an equal amount on all sides, so that undoubtedly even the long-range soft γ-radiation, the importance of which was pointed out by Greisen,[18] is practically eliminated.

One can now evaluate the area S of an unshielded air shower tray which in coincidence with the shielded tray of area $S'=1030$ cm^2 will record showers of the same average density as the tray of area $S_0=155$ cm^2 used to select the 2.5×10^{13}-ev air showers. At Mt. Evans, the fraction β is approximately 0.02; this leads to a ratio $S/S_0=6$. Therefore, the large air shower trays were made up of three counters 2 in.$\times$24 in. in parallel, giving $S=930$ cm^2. Again coincidences of three such groups in anticoincidence with the fourth defined the recorded events. A schematic diagram of the arrangement is shown in Fig. 4.

In view of the high individual counting rates, great care had to be taken to isolate the counters in the trays from each other by feeding the pulses through a diode mixing circuit onto the grid of the output cathode follower, all these units being mounted in the counter trays. The pulses from the air shower trays were then clipped to equal size, and fed into an integrating circuit and to the discriminators which selected the desired multiplicities. The anticoincidences were formed in standard Rossi circuits. In the shielded tray, the individual counter pulses were clipped and fed through isolating diodes to the integrating circuit and the output cathode follower. Discriminators set to pass single or double pulses then selected the events which, together with the triple coincidences of the unshielded trays, defined the "hard" air showers.

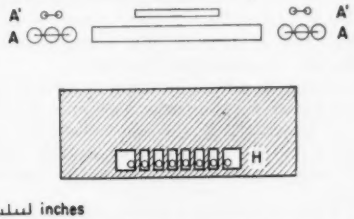

FIG. 4. Schematic diagram of the experimental arrangement (Mt. Evans experiment). A: four unshielded trays, 930 cm^2; A': four unshielded trays, 155 cm^2; H: shielded tray, 1030 cm^2.

[18] K. I. Greisen, Phys. Rev. **75**, 1071 (1949).

TABLE I. Number and rate of recorded "soft" showers A_3 and A_3', and of "hard" showers with one, or more than one, penetrating particle (A_3+H^1), (A_3+H^2), at Mt. Evans. The hard-shower rates are corrected for chance coincidences. Area of unshielded counters: 155 cm^2 and 930 cm^2; area of shielded counters: 1030 cm^2.

Event	Number of showers	Time (min)	Rate (min^{-1})
(A_3')	1867	3959	0.472 ± 0.011
(A_3)	26,278	3739	7.03 ± 0.04
(A_3+H^1)	429	4061	$0.0971\pm0.004_7$
(A_3+H^2)	189	4061	$0.0466\pm0.003_4$

Four kinds of showers were registered:

(1) three out of the four groups of area S_0 struck: "A_3'-showers";
(2) three out of the four groups of area S struck: "A_3-showers";
(3) A_3-showers with at least one hard particle on S': (A_3+H^1)-showers;
(4) A_3-showers with at least two hard particles on S': (A_3+H^2)-showers

(a subscript n denotes exactly n counters or groups of counters struck, a superscript n or more). The ratio of the rates A_3'/A_3 serves as a check on the exponent γ, the ratio $(A_3+H^2)/(A_3+H^1)$ is a measure of the fraction of N-particles among the penetrating air shower particles.

As a check on its performance, it was decided to operate the arrangement also at Echo Lake, and in a density range where previous results permit a comparison. For this purpose, it is advantageous to select showers which are in the same stage of cascade development at Echo Lake, as the 2.5×10^{13}-ev showers are at Mt. Evans. As the altitude difference between the two stations corresponds to about 2.5 cascade units in air, the Echo Lake showers should have about 12-times higher initial energies than the ones recorded at Mt. Evans. Under the conditions of this experiment, the detection of such showers would require counter areas of about 13 cm^2, and counters of this small size were not available. But with counters of 39 cm^2 ($\frac{1}{2}$ in.$\times$6 in.), the maximum contribution comes from showers of initial energy around 1.2×10^{14} ev, and the bias in favor of high densities for the hard-shower set is still rather small: It raises the most efficiently registered shower energies to about 2×10^{14} ev. As in this region there is ample experimental evidence on both the exponent of the power law of the density distribution,[2,5,6,11] and the relative abundance of penetrating particles[4,16,17] it was not deemed necessary for the present study to extend the operations at Echo Lake beyond a redetermination of β as a comparison and control run.

IV. RESULTS AND DISCUSSION

A summary of the results of the Mt. Evans run is given in Table I. As in the following only relative

TABLE II. Number and rate of "soft" showers A_3, and of "hard" showers with one, or more than one, penetrating particle (A_3+H^1), (A_3+H^2), at Echo Lake. The hard-shower rates are corrected for chance coincidences. Area of unshielded counters: 39 cm²; of shielded counters: 1030 cm².

Event	Number of showers	Time (min)	Rate (hr^{-1})
(A_3)	604	17,462	2.08 ±0.09
(A_3+H^1)	293	12,877	1.37 ±0.08
(A_3+H^2)	93	11,080	0.504±0.052

values are of importance, no corrections have been applied for the inefficiency of the counters and for the barometric effect. The correction for random coincidences turns out to be negligible for all but the $(A_3'+H^1)$-events.

The observed ratio of the air shower rates with different counter areas, A_3'/A_3, yields for the exponent of the power law $\gamma=2.51\pm0.02$, in good agreement with earlier observations at the same altitude (e.g., Treat and Greisen[19]). Using this value, one can then determine the relative abundance β of the penetrating particles in the air showers. As $\alpha=\beta S'/S\ll1$, one has for the ratio of the rates of "hard" showers N_h and of "soft" showers N_s,

$$\frac{N_h}{N_s}=-(\gamma-1)\alpha\sum_{n=0}^{3}(-1)^n\binom{3}{n}(n+1)^{\gamma-2}\Big/\sum_{n=0}^{3}(-1)^n\binom{3}{n}(n+1)^{\gamma-1}. \quad (11)$$

From the observed rates, one thus obtains $\beta=(2.06\pm0.11)\times10^{-2}$, or one penetrating particle to 49 electrons.

The showers (A_3+H^2) are mainly due to three kinds of events: (1) "hard" showers in which the penetrating particle is accompanied by a knock-on electron discharging the second counter of the H-tray; (2) "hard" showers with two random incident penetrating particles, and (3) "hard" showers in which the penetrating particle belongs to the N-component and has initiated a local shower in the 8-in. lead absorber on top of the shielded tray. The knock-on contribution was determined by taking the rates (H^1) and (H^2) separately; the first is the total flux of penetrating particles through the tray, the second essentially the flux of mesons accompanied by knock-on electrons, if corrections are applied for the chance coincidences of single mesons. The result of this test run shows that, on the average, 2.1 percent of the mesons give rise to recorded knock-on events. As the energy spectrum of the mesons in air showers is probably not much different from that of single mesons, the ratio of H^2/H^1 can also be used for an estimate of the knock-on accompaniment of the single hard particles in the shower.

[19] J. E. Treat and K. Greisen, Phys. Rev. **74**, 414 (1948).

The correction for random pairs of incident particles follows the established procedure (e.g., Auger and Daudin,[20] Broadbent and Jánossy[21]). The calculation indicates a contribution of 2.8 percent of the rate (A_3+H^1), so that the total correction for non-nucleonic events amounts to 4.9 percent. The observed fraction of 47 percent has therefore to be reduced to 42 percent. On the other hand, an appreciable fraction of the N-particles will not contribute to the (A_3+H^2) showers, either because they failed to interact in the lead absorber (about 25 percent of all particles for a mean free path of 160 g/cm²), or because the local showers are absorbed or not dense enough to strike two counters. If previous hodoscope experiments are used as a guide,[22] this latter fraction may be estimated as about 20 percent. Thus the recorded nucleonic events derive from only 60 percent of all N-particles, and if a neutron/proton ratio of 0.8 is assumed (Walker,[23] Greisen *et al.*[24]), the true fraction of the N-component among the penetrating particles is (62±7) percent. The error stated includes only the statistical deviation. This rather large value is in good agreement with the data of Greisen, Walker, and Walker,[24] observed at the same altitude. However, in view of the many differences between their experiment and the present one in the location of the shower cores and in the shower energies involved, this agreement may well be fortuitous. A comparison with the data taken with the same equipment at Echo Lake promises more reliable conclusions.

The data of the Echo Lake run are summarized in Table II. For the evaluation of β, the value of $\gamma=1.44$ is taken from the results of Cocconi and Tongiorgi,[3] and as for the Mt. Evans experiment, corrections have again been made only for random coincidences. Obviously the approximation (11) is not applicable, and the determination of β has to be done by the usual graphical method. The result is $\beta=(1.20\pm0.11)\times10^{-2}$, in satisfactory agreement with earlier measurements.[4]

In the analysis of the hard component, both corrections for random pairs and knock-ons are again substantial, and reduce the rate of (A_3+H^2) events initiated by the N-component to 24.5 percent of the (A_3+H^1)-rate. After correcting for undetected N-particles in the same way as before, one thus finds a fraction of (38±6) percent for the N-component in the penetrating shower radiation (the errors shown again include only the statistical deviation).

In comparing the two fractions, a possible different attenuation of the two components must be taken in account. Unfortunately, the theory of nuclear cascades is not yet in a state to permit accurate numerical predictions, as some of the fundamental constants are

[20] P. Auger and J. Daudin, J. phys. et rad. **6**, 233 (1945).
[21] D. Broadbent and L. Jánossy, Proc. Roy. Soc. (London) **A192**, 364 (1948).
[22] K. Sitte, Phys. Rev. **78**, 721 (1950).
[23] W. D. Walker, Phys. Rev. **77**, 686 (1950).
[24] Greisen, Walker, and Walker, Phys. Rev. **80**, 535 and 546 (1950).

still only approximately known. But it is certainly safe to conclude from the results of Messel[25] that the nucleonic component in showers of 10^{13} ev to 10^{14} ev initial energy does not decrease greatly between atmospheric depths of 600 g/cm² and 700 g/cm² where it is still close to its maximum development. For higher energies it may even increase, a fact which is borne out by the results of McCusker[26] who, working at sea level and hence in the average with more energetic showers, still finds about 30 percent N-particles in his penetrating radiation.

The attenuation of the meson component in the showers is probably not much different from that of single mesons, which according to Rossi's data[27] decrease by about a factor 0.8 between the two levels. If, as it is likely, the attenuation of the N-component is somewhat larger than that of the μ-mesons, the discrepancy between the values derived above is not completely removed: Even if the attenuation for the shower particles were the same as for single nucleons, a (62 ± 7) percent fraction at Mt. Evans would still yield a (50 ± 6) percent N-component at Echo Lake, but this last assumption is certainly an overestimate of the absorption of the shower nucleons.

It should also be noticed that, while possible systematic errors in the estimates of production and detection probabilities of the local showers may have falsified the absolute values given to the N-component above, such an error would change the data obtained at the two stations in the same direction. Thus, one is led to the conclusions that the ratio of N-particles to μ-mesons within the same shower does not change very much between atmospheric depths of 600 g/cm² and 700 g/cm², and that the observed difference in the composition of the showers of about 10^{13} ev and 10^{14} ev initial energy, though possibly exaggerating the true conditions, is nevertheless of significance.

On the other hand, it is interesting to note that the ratio of μ-mesons to electrons, if taken at the same stage of the electron cascade development—slightly past the cascade maximum—is practically identical for the two types of showers recorded in this experiment: 0.78 percent, or one in 128 particles, for the lower shower energies, and 0.74 percent, or one in 135 particles, for the higher shower energies. It is plausible that such a comparison should be made at the same stage of the cascade development, and preferably at the cascade maximum. Only then the electron shower will be truly representative of the fraction of the primary energy transferred to the electron component.

The results indicate, therefore, that the ratio of charged and neutral mesons—if the latter, in accordance with the current simple picture, are considered as the producers of the bulk of the electron component—does not undergo an appreciable change for collisions over an energy range from 10^{12} ev to 10^{14} ev. If other processes are involved as well, their relative frequencies must also have about reached an equilibrium state. The considerable decrease in the N-component can be understood as caused by a slight increase in the multiplicities of meson production with increasing energy, provided that even for the 10^{14}-ev showers the bulk of the π-mesons originated in the initial collision decays before undergoing a nuclear collision, or that at least the distribution of the energy contained in the charged-meson component, among its two successors (electrons and nucleons), does not change much between primary energies of 10^{12} ev and 10^{14} ev.

The experiment was carried out at the facilities of the Inter-University High Altitude Laboratory, and the author wishes to express his thanks to Professor Byron Cohn and Professor Mario Iona, Jr., of the University of Denver. In running the experiment, the author was assisted by Dr. E. M. Harth, Mr. H. L. Kåsnitz, and Mr. F. E. Froehlich.

[25] H. Messel, Phys. Rev. **83**, 21 (1951).
[26] C. B. A. McCusker, Proc. Phys. Soc. (London) **A63**, 1240 (1950).
[27] B. Rossi, Revs. Modern Phys. **20**, 537 (1948).

Nuclear Reactions of Iron with 340-Mev Protons*

G. RUDSTAM,† P. C. STEVENSON, AND R. L. FOLGER‡
Radiation Laboratory and Department of Chemistry, University of California, Berkeley, California
(Received April 1, 1952)

Natural iron has been bombarded with the full energy proton beam of the Berkeley 184-inch synchrocyclotron, and a number of radioactive spallation products have been isolated and identified and their formation cross sections measured against that of the reaction $Al^{27}(p, 3pn)Na^{24}$. A simple mechanism has been postulated to account for the observed product yields. A new isotope of chromium, assigned to mass 48, has been observed and partially characterized.

I. INTRODUCTION

A SERIES of bombardments of iron with 340-Mev protons has been carried out in the circulating beam of the Berkeley 184-inch cyclotron with the purpose of studying the cross section for formation of the various spallation or fission products. It has been found possible to isolate a number of radioactive product nuclides by standard radiochemical techniques using inert carriers and to identify the nuclides so obtained by observing their half-lives and radiation characteristics. Both absorption measurements and low resolution magnetic beta-spectrometer measurements were used where appropriate to differentiate between isotopes of the same element with similar half-lives.

A mechanism of spallation has been postulated which contains the basic assumption that the probability of emitting a proton from a highly excited nucleus of low atomic number (i.e., less than 30) is approximately equal to the probability of emitting a neutron from the same nucleus under the same conditions. From the postulated mechanism it can be deduced that the spallation products for a given nuclide can be divided into groups *a priori*, the yields of the products in any given group falling on a smooth curve when plotted against mass number. Five such groups were predicted for the spallation products of iron, considering only the abundant isotope Fe^{56}. Experimental results show satisfactory agreement with the hypothesis.

II. EXPERIMENTAL TECHNIQUES

A. Target Makeup

Two types of targets were used which may be referred to for convenience as "thin" and "thick." Each thin target consisted of a single iron foil approximately ten one-thousandths of an inch in thickness through which the beam passed perpendicular to the plane of the foil. On either side of the target foil were "guard foils" of 0.001-inch thick aluminum, and outside and parallel to these were foils of 0.0005-inch thick aluminum (see Fig. 1) used to monitor the total beam through the target by use of the $Al^{27}(p, 3pn)Na^{24}$ reaction as described by Stevenson and Folger.[1] Energy degradation of a 340-Mev proton beam in passing through such a foil is negligible.

Each thick target consisted of a stack of from four to six 0.01-inch iron foils, the dimensions of the stack being about $1\frac{3}{4}\times\frac{1}{2}$ inches, the beam passing through the stack parallel to the $\frac{1}{2}$-inch dimension. The energy degradation undergone by a 340-Mev proton beam in $\frac{1}{2}$ inch of iron is calculated to be about 20 Mev.[2] The beam in this case was monitored by observing the yield of Fe^{52}, previously calibrated against the $Al^{27}(p, 3pn)Na^{24}$ reaction in thin target bombardments.

The iron used was of high purity. A spectrographic analysis performed by Conway and Moore of this laboratory showed very slight amounts of a small number of impurities. These impurities are tabulated in Table I.

Seven bombardments were made. Table II lists the data pertinent to each bombardment.

B. Chemical Separations

Usually 10 mg of each element to be isolated was added as carrier to the dissolving medium prior to addition of the target. The chemical methods used in the bombardments consisted of specific or group precipitations or solvent extractions for each element sought, combined with precipitations of unwanted elements (added as carriers) by reagents not precipitating the desired elements (so-called "scavenge" precipitations). The precise combinations of extractions, specific precipitations, and scavenges used varied depending on which combinations of elements were to be isolated. However, the more important steps in the isolation and purification of the different elements are given below. The percentage recovery of the activities formed was determined gravimetrically by weighing the recovered carrier, complete exchange being assumed. The target was dissolved in approximately 12 N HCl (bombardments *FeP*1 to *FeP*5) or in approximately 3 N HNO_3 (bombardments *FeP*6 and *FeP*7).

* This work was performed under the auspices of the AEC.
† Now at the Gustaf Werner Institute for Nuclear Chemistry, University of Uppsala, Uppsala, Sweden.
‡ Now at E. I. du Pont de Nemours and Company, Oak Ridge, Tennessee.

[1] P. C. Stevenson and R. L. Folger (unpublished work).
[2] Aron, Hoffman, and Williams, AEC Unclassified Document No. 663 (May 28, 1951).

1. Cobalt

Cobalt was precipitated from ammoniacal solution with hydrogen sulfide gas. The sulfide was dissolved in hydrochloric acid containing potassium chlorate, and cobalt was then precipitated by the use of potassium hydroxide. This precipitate was dissolved in acetic acid, and potassium nitrite was added to precipitate $K_3Co(NO_2)_6 \cdot H_2O$. This precipitate was washed, dried at 110°C on an aluminum dish, and weighed. In bombardments *FeP*1 and *FeP*2 an extraction of cobalt-thiocyanate complex into ethyl acetate was used as an additional purification step.

2. Iron

The principal step in the iron isolation was the extraction of ferric chloride from 7.5 *N* HCl into isopropyl ether. The extraction is specific for iron in this region of the periodic table. The ether layer was washed three times with 7.5 *N* HCl, then iron was re-extracted into water and ferric hydroxide precipitated by the addition of ammonium hydroxide. This precipitate was dissolved in 7.5 *N* HCl and the cycle repeated. The final ferric hydroxide precipitate was washed, dried, and ignited on a platinum dish to Fe_2O_3 and weighed. In bombardment *FeP*2 ferric-thiocyanate complex was also extracted into ethyl acetate and re-extracted into aqueous ammonia. In bombardments *FeP*1 and *FeP*2 iron was precipitated as ferric phosphate from dilute hydrochloric acid, washed, dried, and weighed as $FePO_4 \cdot H_2O$.

TABLE I. Spectrographic analysis of target iron.

Impurity	Amount, parts per million by weight
As	Not detected (<100)
Co	60
Mn	Not detected (<100)
Ni	150
Cu	<50

3. Manganese

Manganese was precipitated as manganese dioxide by potassium chlorate from a fuming nitric acid solution. The precipitate was dissolved in hydrochloric acid containing hydrogen peroxide. Tartaric acid and small amounts of chromium, titanium, and vanadium were added and manganous sulfide was then precipitated from alkaline solution. The sulfide was dissolved in concentrated nitric acid and manganese dioxide was brought down from fuming nitric acid solution as before. The whole cycle was repeated once. The MnO_2 precipitate was then dried at 110°C and weighed.

4. Chromium

In bombardment *FeP*3 chromium was separated as the iodate from 1 *N* HCl (after removing titanium and iron). The iodate was destroyed by reduction with sulfur dioxide, and chromium was precipitated as the hydroxide. The hydroxide was oxidized to chromate with basic peroxide solution, and the chromium was extracted as perchromic acid from dilute perchloric acid into amyl acetate. The amyl acetate layer was washed and chromium was re-extracted into aqueous ammonia. The perchromic acid extraction was repeated. Finally, chromium was precipitated from acetic acid solution as $BaCrO_4$, washed, dried at 110°C, and weighed.

In bombardment *FeP*5 chromium was first brought down as barium chromate, then extracted into amyl acetate from a perchloric acid solution containing hydrogen peroxide. In bombardment *FeP*2 chromium was oxidized with potassium bromate in perchloric acid and then extracted into ether after cooling and addition of hydrogen peroxide.

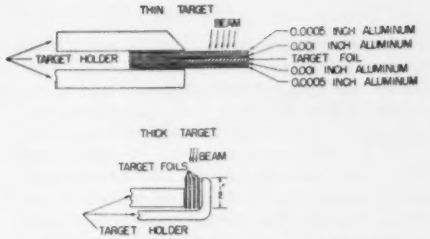

FIG. 1. Assembly of the two types of targets used.

5. Vanadium

Vanadium was separated as sulfide from ammoniacal solution. The sulfide was dissolved in concentrated nitric acid, scavenged with manganese dioxide, precipitated with potassium chlorate and fuming nitric acid and then with yttrium hydroxide in ammoniacal solution. Vanadium sulfide was again precipitated. The sulfide was dissolved and the solution was buffered with sodium acetate-acetic acid. Chromium was then added to act as holdback and vanadium was oxidized by hydrogen peroxide. Lead vanadate was precipitated. The precipitate was dissolved in 2 *N* HNO_3, and lead was removed as the sulfide. The solution was then buffered with sodium acetate-acetic acid and oxidized and $Pb(VO_3)_2$ was again brought down. This was washed, dried at 100°C, and weighed.

TABLE II. Summary of bombardments.

Bombardment No.	Duration of bombardment (min)	Type of target	Elements isolated
*FeP*1	20	Thin	Fe, Co
*FeP*2	46	Thin	Fe, Co, Cr
*FeP*3	46	Thin	Fe, Co, Cr, Mn, V
*FeP*4	17	Thick	Fe, Mn, Ca, Ti, Sc
*FeP*5	109	Thick	Fe, Co, Cr, Mn, Na, S, P, Ca
*FeP*6	65	Thin	Fe, V, Sc, K, Si, Cl
*FeP*7	55	Thin	Fe, Ti, K, Cl, Si, Cr

6. Titanium

For the separation of titanium the precipitation of titanium iodate from 6 *N* HNO_3 was used. The precipitate was dissolved in hydrochloric acid containing sodium sulfite. Titanium was then precipitated as hydroxide with ammonia. The hydroxide was dissolved in 0.5 *N* HNO_3 and scavenged with yttrium oxalate. Tartaric acid was added and the solution made ammoniacal to be scavenged with iron and manganese sulfides. The supernatant from the last scavenge was made 1 *N* in hydrochloric acid, and titanium was precipitated with cupferron. The precipitate was then metathesized to $TiO_2 \cdot H_2O$ with ammonium hydroxide. The hydrous oxide was dissolved in hydrochloric acid and the iodate precipitated. The iodate was dissolved in hydrochloric acid and sodium sulfite. Finally, titanium was precipitated as hydroxide with ammonia, washed, ignited to TiO_2, and weighed.

7. Scandium

Scandium was separated by precipitation with oxalic acid from 0.5 *N* HNO_3. The precipitate was dissolved in concentrated nitric acid; manganese carrier and fuming nitric acid were then added. Potassium chlorate was added to precipitate manganese dioxide and to destroy the oxalate. Scandium was precipitated as the hydroxide by adding ammonia gas to the supernatant. After two more oxalate-hydroxide cycles the scandium hydroxide was washed, ignited to Sc_2O_3 on a platinum dish, and weighed.

8. Calcium

Calcium was precipitated as calcium oxalate with oxalic acid (bombardment *FeP*4) or as calcium carbonate from alkaline solution. The calcium precipitates were dissolved in nitric acid (plus potassium chlorate in bombardment *FeP*4). The solution was made alkaline with ammonium hydroxide and scavenged with yttrium and titanium hydroxides, then with manganese dioxide (precipitated by hydrogen peroxide), and finally with cobalt sulfide. The supernatant was acidified with acetic acid, and calcium was precipitated with oxalic acid. The cycle was repeated twice. Finally, the calcium oxalate precipitate was washed, dried at 110°C, and weighed as $CaC_2O_4 \cdot H_2O$.

9. Potassium

After the precipitation of most elements with ammonium hydroxide, potassium was left in solution. This supernatant was made about 0.1 *N* in acid, phosphate ion added, and then ferric ion in excess to bring down ferric phosphate. The solution was then made alkaline with ammonium hydroxide and scavenged twice with iron and titanium hydroxides, then twice with chromium sulfide and with calcium carbonate or calcium oxalate. The solution was then acidified with hydrochloric acid and evaporated to dryness in a porcelain casserole. The ammonium salts were removed by fuming over a Meker burner. The residue was dissolved in water. Perchloric acid was added, the solution was heated to fuming, then cooled in an icebath, and absolute alcohol was added to precipitate potassium perchlorate. This was carefully washed with absolute alcohol to remove ammonium perchlorate and recrystallized twice from perchloric acid. The precipitate was washed with alcohol, dried at 110°C, and weighed as $KClO_4$.

10. Chlorine

When chlorine was to be isolated, the carrier was added as solid, freshly prepared silver chloride, and the target was dissolved in dilute (~3 *N*) nitric acid. The exchange between chloride ion in the silver chloride precipitate and the radioactive chloride ion in the solution is supposed to be rapid and complete.[3] After the target had completely dissolved, the silver chloride precipitate was separated. Silver chloride was then dissolved in 5 *N* NH_4OH and scavenged with ferric hydroxide. Potassium iodide was then added to precipitate silver iodide, and after centrifuging, an excess of silver nitrate was added to remove iodide. The supernatant was acidified with nitric acid to precipitate silver chloride and the precipitate was washed, dried at 110°C, and weighed.

11. Sulfur

The sulfur carrier was added in the form of $SO_4^{=}$, and the target was dissolved in concentrated hydrochloric and nitric acids. Barium sulfate was precipitated from 1 *N* HCl. This was converted to barium carbonate by boiling with 50 percent aqueous potassium carbonate solution for about 1 hour. The precipitate was discarded, and the supernatant was made 1 *N* in hydrochloric acid. Barium sulfate was precipitated by the addition of barium chloride solution. The procedure was repeated twice. Finally, the barium sulfate precipitate was washed, dried at 110°C, and weighed as $BaSO_4$.

12. Phosphorus

Phosphorus was added as PO_4^{-3}, and the target was dissolved in hydrochloric and nitric acids. Phosphorus was then isolated by precipitation as ammonium phosphomolybdate from 1 *N* HNO_3. The precipitate was dissolved in ammonium hydroxide, vanadium holdback agent was added, and magnesium ammonium phosphate was precipitated by the addition of magnesia mixture. The precipitate was dissolved in 1 *N* HNO_3 and the cycle was repeated. Finally, phosphorus was precipitated as magnesium ammonium phosphate. This was washed, ignited on a platinum dish, and weighed as $Mg_2P_2O_7$.

[3] A. S. Newton, thesis, University of Michigan, Ann Arbor, Michigan (June, 1941), University Microfilm Service.

13. Silicon

Silicon carrier was added as $(NH_4)_2SiF_6$. After the target had dissolved, silica was brought down by the addition of boric acid and digestion with hot concentrated sulfuric acid. The silica was carefully washed with warm diluted sulfuric acid, then it was dissolved in potassium hydroxide. The solution was scavenged with titanium hydroxide. Holdback agents of iron, cobalt, chromium, vanadium, and yttrium were added, and the mixture was acidified with hydrochloric acid. Silica was precipitated by digestion. The cycle was repeated. The precipitate was then washed, ignited on a platinum dish, and weighed as SiO_2.

14. Sodium

In the procedure sodium was left in ammoniacal solution. This solution was scavenged twice with iron and titanium hydroxides, with cobalt sulfide, and with calcium oxalate. The supernatant was acidified with hydrochloric acid and evaporated to dryness in a porcelain casserole. Ammonium salts were removed by fuming over a Meker burner. The residue was taken up in water, filtered, and zinc uranyl acetate was added to the cooled supernatant. The sodium zinc uranyl acetate precipitate was dissolved in alcohol saturated with hydrogen chloride gas and cooled. Sodium chloride precipitated. The precipitate was dissolved in a small amount of water, potassium holdback agent was added, and sodium zinc uranyl acetate was reprecipitated. The cycle was repeated once more. Finally, sodium chloride was washed with alcohol-hydrochloric acid, dried at 110°C, and weighed.

C. Counting Techniques

The purified counting samples were transferred to weighed aluminum or platinum dishes and spread as uniformly as possible over the total area of the dish (~5 cm²). After suitable drying, the dishes were weighed again and the sample weight obtained by difference. The samples were then fixed in position on the dishes by evaporating dilute solutions of collodion or zapon on them, and the dishes were fastened to cardboard holders with Scotch tape, as shown in the diagram (Fig. 2). These holders were designed to fit in any one of five standard positions beneath the window of a chlorine-quenched Amperex Geiger-Müller tube. The position selected for counting a given sample was as far from the counter window as convenient, the criterion being the desirability of securing a sufficiently large number of counts in a short counting time to give good statistical reliability to the calculated counting rate. Absorption curves were taken with the absorber as close as possible to the counter window and the sample as far away as possible in order to minimize scattering of radiation into the counter by the absorber.[4]

[4] R. C. Gibbs, Chairman, Division of Mathematical and Physical Sciences, National Research Council, Nuclear Science Series, Preliminary Report No. 8, "Conference on Absolute β-Counting," Papers 1 and 3 (October, 1950).

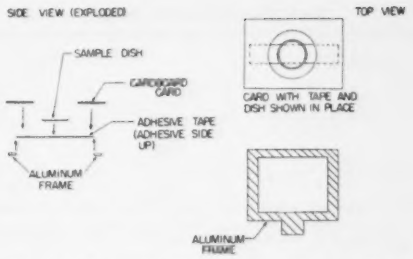

FIG. 2. Method used for mounting samples for counting.

The observed counting rates were subjected to the following corrections:

1. A correction for counts lost due to dead time of the counter tube (so-called coincidence correction).
2. A correction for background activity.
3. A geometric correction to the position in which the monitor sample was counted. This was determined empirically in each case.
4. A correction for air and window absorption, determined by back-extrapolation of the observed aluminum absorption curve.
5. A correction for backscattering from the sample dish. The figures used for beta-energies greater than 0.6 Mev were 1/1.22 for aluminum dishes and 1/1.75 for platinum dishes, calculated from the saturation backscattering data of Burtt.[6] For beta-energies less than 0.6 Mev the backscattering was calculated from the data of Yaffe and Justus.[6]
6. A factor for self-scattering and absorption by the sample material itself, estimated from the work of Malatesta.[7]
7. A factor for relative counting efficiency in the case of x-ray or gamma-activities. "Counting efficiency" is defined as the number of counts registered by the counter per particle (or photon) passing through the tube window.
8. A factor to correct for the decay of the sample from the time of the end of the bombardment to the time of initial measurement of the activity.

III. RESULTS

A. New Chromium Isotope

In the chromium decay curves a new activity was found after subtraction of the activity due to 26.5-day Cr^{51}. This half-life was found to be 19 hours, 24 hours, and 23 hours in bombardments *FeP2*, *FeP3*, and *FeP5*. Owing to a very poor chemical yield in bombardment *FeP2*, however, the last two figures should be more accurate. Since the electrons from Cr^{51} can easily be blocked by a thin aluminum absorber (~30 mg/cm²), the growth and the decay of an isotope of a half-life of 16 days could be observed. In bombardment *FeP5* two sets of absorption measurements were made, one after about 15 hours and the other several days after the bombardment. These measurements showed the growth of an activity with beta-radiation of about 0.7 Mev maximum energy. Furthermore, part of the purified chromium fraction from bombardment *FeP5*

[6] B. P. Burtt, Nucleonics **5**, 32 (1949).
[6] L. Yaffe and K. M. Justus, J. Chem. Soc. (London) S341 (1949), Part V.
[7] L. Malatesta, private communication.

TABLE III. Yield of cobalt isotopes.

Reported in literature[a]			Experimental results		
Mass No.	$T_{\frac{1}{2}}$	Radiation	Bomb. No.	$T_{\frac{1}{2}}$	Yield, mb (1 mb $=10^{-27}$ cm^2)
55	18.2 hr	β^+, γ	*FeP1*	18.3 hr	0.42
			FeP2	18.1 hr	0.14
			FeP3	17.6 hr	0.53
			FeP5	17.6 hr	0.53
56	72 days	β^+, γ, *EC*	*FeP3*	78 days	0.21
			FeP5	72 days	0.26

[a] Any previously reported data on half-lives or radiation characteristics is taken from G. T. Seaborg and I. Perlman, Revs. Modern Phys. **20**, 585 (1948).

was left to decay for two weeks in the presence of inactive vanadium carrier. The vanadium was then separated chemically. This vanadium sample showed an activity with a half-life of 16.2 days and an energy of 0.78 Mev (determined from aluminum absorption measurements). The chromium isotope can from these experiments be assigned the mass number 48. Furthermore, the counting efficiency of the isotope was determined from the counting rate of its daughter to be about 4 percent which indicates that it decays mainly by electron capture.

TABLE IV. Yield of iron isotopes.

Reported in literature			Experimental results		
Mass No.	$T_{\frac{1}{2}}$	Radiation	Bomb. No.	$T_{\frac{1}{2}}$	Yield, mb
52	7.8 hr	β^+	*FeP1*	8.1 hr	0.55
			FeP2	8.3 hr	0.56
			FeP3	8.3 hr	0.66
			FeP4	8.4 hr	···
			FeP5	8.3 hr	···
			FeP6	8.3 hr	0.71
			FeP7	8.6 hr	0.67

B. Spallation Yields

1. Cobalt

It was assumed in determining the yield of Co^{56} that all long-lived activity was to be attributed to Co^{56} (see Table III). Co^{58} can only be formed from Fe^{57} and Fe^{58}, and these isotopes are in low abundance in natural iron (together 2.5 percent). This yield of Co^{58} is not corrected for any branching decay by electron capture.

TABLE V. Yield of manganese isotopes.

Reported in literature			Experimental results		
Mass No.	$T_{\frac{1}{2}}$	Radiation	Bomb. No.	$T_{\frac{1}{2}}$	Yield, mb
51	46 min	β^+	*FeP3*	46.8 min	4.09
			FeP4	42.7 min	3.95
52	5.8 days	β^+(35%), *EC*, γ	*FeP3*	5.8 days	14.5
			FeP4	5.8 days	11.0
			FeP5	5.7 days	13.1
54	310 days	β^+, *EC*, γ	*FeP3*		12.1
			FeP4		11.8
56	2.59 hr	β^-, γ	*FeP4*	2.72 hr	0.56
			FeP4	2.43 hr	0.61

2. Iron

In bombardments *FeP4* and *FeP5*, Fe^{52} was used as a monitor (see Table IV). The counting efficiency of the isotope was determined by observation of the growth of Mn^{52} and by chemical separation of Mn^{52}. The counting efficiency was thus determined to be 1.72 for the equilibrium mixture. For Fe^{52} only, it is 0.70 which indicates that the parent isotope decays to the extent of about 30 percent by orbital electron capture.

TABLE VI. Yield of chromium isotopes.

Reported in literature			Experimental results		
Mass No.	$T_{\frac{1}{2}}$	Radiation	Bomb. No.	$T_{\frac{1}{2}}$	Yield, mb
48	(Previously unreported)		*FeP2*	19 hr	0.73
			FeP3	24 hr	0.91
			FeP5	23 hr	0.75
49	41.9 min	β^+, γ	*FeP2*	41 min	4.9
			FeP3	40 min	6.1
			FeP7	43 min	3.5
51	26.5 days	*EC*, γ, e^-	*FeP2*	(21 days)	53
			FeP3	27 days	38
			FeP5	28 days	33

3. Manganese

In the determination of the yield of Mn^{54} it was assumed that all the activity in the manganese fractions after the decay of Mn^{52} consisted of Mn^{54} (see Table V). The samples were observed for too short a time for a determination of the half-life. The figures for the yield are therefore uncertain. The counting efficiency of Mn^{54} was assumed to be 10 percent (from Miller's data).[8]

4. Chromium

For Cr^{51} a counting efficiency of 3 percent has been assumed (see Table VI). This figure is very uncertain, and the yield may be in error by a factor of two.

TABLE VII. Yield of vanadium isotopes.

Reported in literature			Experimental results		
Mass No.	$T_{\frac{1}{2}}$	Radiation	Bomb. No.	$T_{\frac{1}{2}}$	Yield, mb
47	33 min	β^+	*FeP3*	35 min	2.42
48	16 days	β^+(58%), *EC*, γ	*FeP3*	16.0 days	9.6
			FeP6	16.1 days	11.0
49	600 days	*EC*, γ	*FeP3*	···	31

5. Vanadium

The yield for V^{49} is only approximate since it was assumed that all activity after subtraction of 16-day V^{48} consisted of V^{49} (see Table VII). The counting efficiency for V^{49} is assumed to be 1 percent. (Decays solely by orbital electron capture.)

6. Titanium

No long-lived titanium isotope was found (see Table VIII).

[8] D. R. Miller, AEC Declassified Document No. 2193 (August 6, 1948).

7. Scandium

The yield of Sc^{44m} was determined by counting through 222 mg/cm² aluminum absorber to block the radiations from Sc^{47} and Sc^{48} (see Table IX). It was assumed that the decay by orbital electron capture of Sc^{44} is negligible. The yield of Sc^{46} is not corrected for possible decay by orbital electron capture. Sc^{43} and Sc^{44} could not be separated in either bombardment nor could Sc^{47} and Sc^{48} in bombardment *FeP*6. Owing to the difficulty in separating Sc^{47} and Sc^{48} in bombardment *FeP*4 the figures for the yields are uncertain. Sc^{49} could not be detected.

TABLE VIII. Yield of titanium isotopes.

Reported in literature			Experimental results		
Mass No.	$T_{\frac{1}{2}}$	Radiation	Bomb. No.	$T_{\frac{1}{2}}$	Yield, mb
45	3.08 hr	β^+, γ	*FeP*4	3.13 hr	3.31
			*FeP*7	3.07 hr	4.05

8. Calcium

In *FeP*4 the decay of the calcium sample was observed for three months (see Table X). The decay follows a 152-day line fairly well. The absorption measurements made about two and one-half months after the bombardment (*FeP*5) indicated a β^- energy of 0.3 Mev and no gamma-radiation.

9. Potassium

The reason for the large difference in the yield determinations in the two bombardments may be due to occlusion of perchloric acid by the precipitate in bombardment *FeP*6 (see Table XI). The higher figures for yield are therefore believed to be the more reliable.

TABLE IX. Yield of scandium isotopes.

Reported in literature			Experimental results		
Mass No.	$T_{\frac{1}{2}}$	Radiation	Bomb. No.	$T_{\frac{1}{2}}$	Yield, mb
43 and 44	both 3.92 hr	β^+, γ, (*EC*)	*FeP*4	4.1 hr	4.43
			*FeP*6	4.0 hr	4.14
44	2.44 days	e^-, γ	*FeP*4	2.61 days	2.61
			*FeP*6	2.48 days	2.59
46	85 days	β^-, γ, *EC*	*FeP*4	84 days	3.27
			*FeP*6		3.14
47	3.4 days	β^-	*FeP*4	3.5 days	0.84
48	44 hr	β^-	*FeP*4	44 hr	0.45

10. Chlorine

The Cl^{34} and Cl^{38} activities were resolved by the use of a recording magnetic beta-spectrometer (see Table XII). The half-lives are obtained by the analysis of the data from this instrument, and they are not very accurate.

TABLE X. Yield of calcium isotopes.

Reported in literature			Experimental results		
Mass No.	$T_{\frac{1}{2}}$	Radiation	Bomb. No.	$T_{\frac{1}{2}}$	Yield, mb
45	152 days	β^-	*FeP*4	(152 days)	0.54
			*FeP*5	(152 days)	0.58
47	5.8 days	β^-, γ	*FeP*4	5.6 days	0.007
			*FeP*5	5.5 days	0.006

11. Sulfur

The sulfur decay was observed for about two months and showed a half-life fairly close to the reported one (see Table XIII). Aluminum absorption measurements showed a β^- energy of 0.15 Mev.

TABLE XI. Yield of potassium isotopes.

Reported in literature			Experimental results		
Mass No.	$T_{\frac{1}{2}}$	Radiation	Bomb. No.	$T_{\frac{1}{2}}$	Yield, mb
42	12.4 hr	β^-, γ	*FeP*6	12 hr	0.26
			*FeP*7	12 hr	1.15
43	22.4 hr	β^-, γ	*FeP*6	22 hr	0.12
			*FeP*7	21 hr	0.72

TABLE XII. Yield of chlorine isotopes.

Reported in literature			Experimental results		
Mass No.	$T_{\frac{1}{2}}$	Radiation	Bomb. No.	$T_{\frac{1}{2}}$	Yield, mb
34	33 min	β^+, γ	*FeP*6	36 min	0.08
			*FeP*7	27 min	0.14
38	38 min	β^-, γ	*FeP*6	45 min	0.13
			*FeP*7	37 min	0.20
39	55 min	β^-	*FeP*6	55 min	0.05
			*FeP*7	58 min	0.04

TABLE XIII. Yield of sulfur isotopes.

Reported in literature			Experimental results		
Mass No.	$T_{\frac{1}{2}}$	Radiation	Bomb. No.	$T_{\frac{1}{2}}$	Yield, mb
35	87 days	β^-	*FeP*5	80 days	0.23

12. Phosphorus

TABLE XIV. Yield of phosphorus isotopes.

Reported in literature			Experimental results		
Mass No.	$T_{\frac{1}{2}}$	Radiation	Bomb. No.	$T_{\frac{1}{2}}$	Yield, mb
32	14.3 days	β^-	*FeP*5	15.0 days	0.044

13. Silicon

The half-life reported in literature seems to be too long. Both silicon samples were followed for a period of eight to ten half-lives, and both showed single com-

ponent decay with a half-life of 157 minutes (see Table XV).

14. Sodium

The yield of Na^{22} is uncertain because the decay was not followed long enough to establish the identity of the isotope with certainty (see Table XVI).

IV. DISCUSSION

A cursory examination of the data presented in Table XVII seems to show no obvious systematic trend in the yields except that, as would be expected from previous work,[9–13] the nuclides formed in high yield are those which have atomic numbers only slightly below that of iron. The converse is not necessarily true, e.g., compare Cr^{48}, 0.80 mb, with Sc^{44m}, 2.60 mb. It is, however, possible to correlate the various yields somewhat more closely. To a first approximation natural iron can be considered to consist entirely of the isotope Fe^{56} (91.6 percent).[14] At the bombarding energies under consideration the formation of a compound nucleus is believed to be unlikely. Transmission of excitation energy from the bombarding particle to the target nucleus is believed to take place by single nucleon-nucleon collisions within the nucleus,[15] the more energetic of the nucleons involved escaping from the nucleus. This will leave either Fe^{56} or Co^{56} in a highly excited state. Let us assume that these two species are formed in approximately equal abundance. Let us further assume either that protons and neutrons "boil off" with equal probability or that the most likely mode of dissipation of excitation energy is by emission of alpha-particles or deuterons with neutrons and protons boiling off with equal low probability. It can be seen that the most likely nuclide of a given mass to be formed by such a process must lie on a line represented on a plot of Z *versus* $(A-Z)$ with a 45° (positive) slope passing through Co^{57}. Such nuclides are those such that $Z=27-X$, $A=57-2X$, where $X=0, 1, 2$, etc. This simple picture would, of course, have to be modified for heavier nuclides, where the neutrons outnumber the protons appreciably. Some effects due to nuclear shell structure might also be observed.

Figure 3 represents a portion of the "Chart of the Nuclides" in which the ordinate represents the atomic number (Z) and the abscissa, the number of neutrons ($A-Z$) of the nuclides shown. The nuclides predicted by this simple picture to be formed in high yield are then those lying along the diagonal line marked "I" in

TABLE XV. Yield of silicon isotopes.

Reported in literature			Experimental results		
Mass No.	$T_{\frac{1}{2}}$	Radiation	Bomb. No.	$T_{\frac{1}{2}}$	Yield, mb
31	170 min	β^-	*FeP6*	157 min	0.12
			FeP7	157 min	0.125

TABLE XVI. Yield of sodium isotopes.

Reported in literature			Experimental results		
Mass No.	$T_{\frac{1}{2}}$	Radiation	Bomb. No.	$T_{\frac{1}{2}}$	Yield, mb
24	14.9 hr	β^-, γ	*FeP5*	15.1 hr	0.026
22	2.6 hr	β^+, γ	*FeP5*	···	0.021

TABLE XVII. Summary of the yields observed.

Isotope	Yield (mb)	Remarks
Co^{55}	0.49	
Co^{56}	0.24	No correction for orbital electron capture
Fe^{52}	0.68	
Mn^{51}	4.0	
Mn^{52}	12.9	
Mn^{54}	12	10 percent counting efficiency.[a]
Mn^{56}	0.59	
Cr^{48}	0.80	
Cr^{49}	4.8	
Cr^{51}	41	3 percent counting efficiency.[b]
V^{47}	2.4	
V^{48}	10.3	
V^{49}	31	1 percent counting efficiency assumed.
Ti^{48}	3.7	
Sc^{44m}	2.60	
Sc^{46}	3.20	No correction for orbital electron capture.
Sc^{47}	0.84	Uncertain.
Sc^{48}	0.45	
Ca^{45}	0.56	
Ca^{47}	0.007	
K^{42}	0.7	
K^{43}	0.4	
Cl^{34}	0.11	
Cl^{38}	0.17	
Cl^{39}	0.045	
S^{35}	0.23	
P^{32}	0.044	
Si^{31}	0.12	
Na^{24}	0.026	
Na^{22}	0.0?	Approximate.

[a] See reference 8.
[b] R. E. Batzel (private communication).

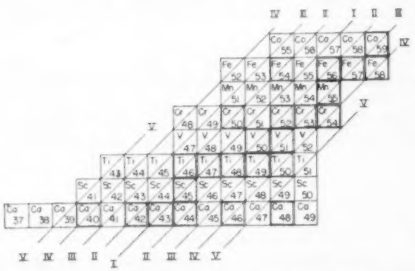

FIG. 3. Systematic grouping of nuclides formed by spallation of Fe^{56}.

[9] R. E. Batzel, Phys. Rev. **79**, 528 (1950).
[10] H. H. Hopkins, Phys. Rev. **77**, 717 (1950).
[11] M. Lindner and I. Perlman, Phys. Rev. **78**, 499 (1950).
[12] N. A. Bonner and W. C. Orr, Phys. Rev. **76**, 140 (1949).
[13] Batzel, Miller, and Seaborg, Phys. Rev. **84**, 671 (1951).
[14] J. R. White and A. E. Cameron, Phys. Rev. **74**, 991 (1948).
[15] R. Serber, Phys. Rev. **72**, 1114 (1947).

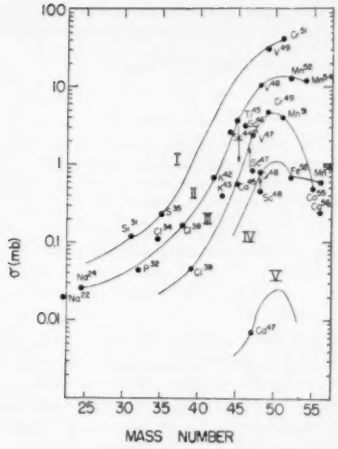

FIG. 4. Cross section for formation of various spallation products of natural iron as a function of mass number.

the figure; those next most probable by this model lie on the two lines marked "II," and so on. A tabulation of the expected nuclides is given in Table XVIII.

If one plots formation cross section *versus* mass number, it is apparent that all the nuclides of a given group (see Table XVII) fall on the same smooth curve with almost no exceptions and furthermore, that the curves so obtained are quite closely parallel on a semilogarithmic plot, as shown in Fig. 4. Since the curves are parallel on a semilogarithmic plot, the ratio of expected yields for two isobars on different curves is approximately constant. This fact enables us to draw from Fig. 4 an approximate distribution curve (Fig. 5) for the yields of various isobars of any given mass.

A few isotopes do not fall on their proper curves, e.g., for curve II, Sc^{46} is a little low. However, the counting efficiency of this isotope was not corrected for electron capture. Such a correction should indicate a higher value for the yield. Sc^{47} belonging to curve III is also low. This yield is very uncertain, however.

The yield of Ti^{45} belonging to curve III is very high. This can be partially accounted for by considering that Fe^{54} is in a rather high abundance (5.9 percent) in natural iron. With help of the distribution curve from Fig. 5 the contribution to the yields from Fe^{54} has been estimated. It comes out to be 45 percent of the total yield for the isotopes Mn^{51}, Cr^{49}, V^{47}, Ti^{45} but only 6 percent for Mn^{52}, V^{48}, Sc^{44m}. If the yields are corrected for this and also for the estimated contribution from Fe^{57} and Fe^{58}, Ti^{46} falls below curve II even if it still seems to be high.

The picture given above indicates why Fe^{52} is in

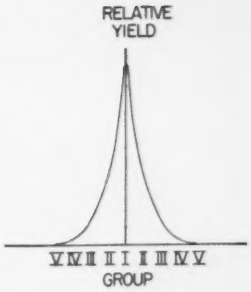

FIG. 5. The distribution of various nuclides of given mass according to the systematic method of grouping products.

such low yield. It also explains why Sc^{49} (57 minute) could not be detected. It belongs to "curve" V and its yield is probably a factor of 100 lower than the yield of Sc^{44} (3.9 hour). It will therefore be completely masked by the latter isotope. Ti^{51} also belongs to "curve" V. It could not be detected.

The yields of nuclides of mass 55 and above are not regular in this system. However, it is expected that these yields are low, since the nucleus is excited to a degree such that at least two or three nucleons may be expected to boil out. In this case the rarer, heavy isotopes of iron are expected to exert a disproportionately large effect of a magnitude which is difficult to estimate.

TABLE XVIII. A systematic grouping of measurable product nuclides.

Group	Probability	Nuclides
I	Highest	Co^{57}, Cr^{51}, V^{49}, S^{35}, Si^{31}
II	Next highest	Co^{56}, Mn^{54}, Mn^{52}, V^{48}, Sc^{46}, Sc^{44}, K^{42}, Cl^{38}, P^{32}, Na^{24}
III	Third highest	Co^{55}, Mn^{51}, Cr^{49}, V^{47}, Ti^{45}, Sc^{47}, Ca^{45} K^{43}, Cl^{39}
IV	Fourth highest	Mn^{56}, Fe^{52}, Cr^{48}, Cl^{34}, Na^{22}
V	Fifth highest	Ca^{47}

From Fig. 4 the total reaction cross section of natural iron for high energy protons is estimated to be 340 mb.

We wish to express our thanks to Professor G. T. Seaborg for his interest and helpful advice, to S. Castner for his assistance in compiling the references and reading proof, and to J. Vale, L. Hauser, and the crew of the Berkeley 184-inch cyclotron for their helpful cooperation. One of us (G.R.) wishes to express his gratitude to the Swedish Atomic Energy Commission for the fellowship under which his portion of this research was carried out. Another of us (P.C.S.) wishes to express his gratitude for the Atomic Energy Commission Postdoctoral Fellowship in the Physical Sciences under which the major part of his portion of this research was carried out.

The Inelastic Scattering of Neutrons*

WALTER HAUSER† AND HERMAN FESHBACH
Physics Department and Laboratory of Nuclear Science, Massachusetts Institute of Technology, Cambridge 39, Massachusetts

(Received March 27, 1952)

The total cross section and the differential cross section for the inelastic scattering of neutrons are considered. It is assumed that the compound nucleus is sufficiently excited so that the statistical model may be applied. If the statistical model may be applied as well to the residual nucleus, it is shown that the angular distribution of the inelastically scattered neutrons is isotropic. If only a few levels of the target nucleus can be excited, the angular distribution is anisotropic. Tables are provided which permit the calculation of the angular distribution if the incident and emergent neutron angular momenta are less than or equal to $3\hbar$. Examples of the evaluation of total cross sections are given, providing examples of the sensitivity of the results to the quantum numbers of the excited state.

I. INTRODUCTION

THE inelastic scattering of neutrons is of interest not only for the theory of the passage of neutrons through matter but also because of the light it casts upon the properties of the target nucleus. For moderate neutron energies in which only a few levels are excited, the total cross section as well as the energy and angle distribution of the emergent neutrons is sensitive to the energy, angular momentum, and parity differences which exist between the ground state of the target nucleus and the states excited. When the neutron energy is sufficiently high, the measurements are no longer as sensitive to detailed properties of the excited states. It will be shown that the angular distribution of the emergent neutrons is then isotropic. However, the energy distribution is dependent strongly upon the density of energy levels of the target nucleus as a function of the energy of excitation.

In this paper, which may be regarded as a sequel to one of Wolfenstein's[1] on the same subject, the analysis required for the prediction of the relevant experimental quantities is performed. The discussion divides the inelastic processes into two categories according to the validity of the statistical model for the compound and residual nucleus. In category I we place those situations for which the statistical model may only be applied to the compound nucleus but not to the residual nucleus. This will occur whenever the neutron energy is so small that only a few levels can be excited and whenever the target nucleus is a middleweight or heavy nucleus, for then the density of levels in the compound nucleus is sufficiently great. In category II, we assume that the neutron energy is so large that many levels of the target nucleus are excited so that the statistical theory applies to both the compound and residual nuclei. The angular distribution of neutrons in category I is generally anisotropic. Tables are provided which permit a prediction of this distribution when the orbital angular momenta of the incident or emergent neutrons is less than or equal to $3\hbar$. For neutrons in category II, we give a proof of the isotropy of the inelastically scattered neutrons. The familiar dependence of the energy distribution on level density may then be obtained.

Our emphasis is on neutrons. However, the discussion is applicable with only minor changes for protons or alpha-particles either incident or emerging.

II. GENERAL CONSIDERATIONS

The general formulas upon which our discussion will be based have been given by Wolfenstein.[1] We shall restate them here for the purposes of fixing our notation and reviewing the simplifications which follow from the application of the statistical model to the compound nucleus.

Notation.—Let the target nucleus have a spin of i (in units of $\hbar$), the residual nucleus a spin of i', the initial and final orbital neutron angular momentum by l and l', respectively, the corresponding initial and final energies E and E'. The spin of a level in the compound nucleus will be denoted by J. It is convenient to combine the neutron spin and the spin of the nucleus to form the channel spin j_i and j_i' for the initial and final states:

$$j_{1,2}=i\pm\tfrac{1}{2}, \quad j'_{1,2}=i'\pm\tfrac{1}{2}.$$

The spin of the compound nucleus J is formed by combining l and j or l' and j'. We shall drop the subscript on j and j' employing the subscript only when it is necessary to sum over initial and final states. For a given J the values of l and l' which may contribute to a reaction are given by

$$|J-j|\leq l\leq(J+j), \quad |J-j'|\leq l'\leq(J+j').$$

The z axis will be taken along the direction of incident neutron so that the z component of its orbital angular momentum will be zero. The z component associated with the initial channel spin is m and is equal to the z component of J. The z component of the angular momentum of the emergent neutron is m' so that the corresponding quantity for the final channel spin j' is $m-m'$.

* Research sponsored by Nuclear Development Associates under contract At(30-1)-862B. This paper is based on AEC Report NYO 636.

† Now at Physics Department, Boston University, Boston, Massachusetts.

[1] L. Wolfenstein, Phys. Rev. **82**, 690 (1951).

Parity must, of course, be preserved. Changes in parity will be carried by the neutron orbital angular momenta, even l and l' corresponding to no change in parity whereas odd l and l' introducing a parity change.

Simplifications following from the statistical model.— We assume that, at the excitation energy of the compound nucleus, there are many energy levels of all types. More precisely, the energy resolution of the incident beam is broad enough so that many levels of the compound nucleus are excited. The corresponding wave functions are assumed to have a random phase so that when phase averages are performed all interference terms will vanish. From the concept of the compound nucleus, it follows that it is then possible to divide the inelastic scattering process into two parts comprising (1) the formation of the compound nucleus and (2) the decay of the compound nucleus by particle emission. For the energy region under consideration we shall neglect the competition arising from gamma-ray emission and, except for the lightest nuclei, from charged particle emission. In a paper submitted for publication Margolis will consider the effects of gamma-ray competition.

Application of the statistical model permits us, therefore, to neglect the interference among the various l's which contribute to the formation of the compound nucleus as well as the interference among the l''s which are involved in the decay of the compound nucleus. Hence we may write

$$\sigma(i|i')=\sum_{l,l'}\sigma(l,i|l',i'), \tag{1}$$

where

$$\sigma(l,i|l',i')=(1/2(2i+1))\sum_{\alpha,\beta}\sigma(l,j_\alpha|l',j_\beta'). \tag{2}$$

Here $\sigma(l,i|l',i')$ is the cross section for the process involving the indicated initial and final values of the neutron orbital angular momenta and spins of the target nucleus. On the other hand, $\sigma(l,j_\alpha|l',j_\beta')$ is the cross section for the process involving an initial and final channel spin j_α and j'_β, respectively.

A certain fraction of the neutrons with orbital angular momentum l which strike the nucleus, "stick," and form a compound nucleus. The cross section for this process is denoted $\sigma_c{}^{(l)}$. It is often expressed in terms of the penetrabilities $T_l(E)$ as follows:

$$\sigma_c{}^{(l)}=(2l+1)\pi\lambda^2T_l(E). \tag{3}$$

The cross section for the formation of the compound nucleus of spin J by "l" neutrons will be given by $\sigma_c{}^{(l)}$ multiplied by the probability that the incident neutron and target nucleus form a system of spin J. This probability is equal to the square of the Clebsch-Gordan coefficient $|(lj;0m|lj;Jm)|^2$ so that the cross section in question is

$$\sigma_c{}^{(l)}|(lj;0m|lj;Jm)|^2 =(2l+1)\pi\lambda^2T_l(E)|(lj;0m|lj;Jm)|^2. \tag{4}$$

To obtain the cross section for a particular inelastic process we must multiply (4) by the relative probability of that process. This may be obtained from (4) through the use of the reciprocity theorem.[2] The cross section $\sigma(l,j|l',j'|\vartheta)$ for the production of neutrons of energy E' of angular momentum l', channel spin j' and moving in a direction ϑ turns out to be

$$\sigma(l,j|l',j'|\vartheta) =\pi\lambda^2(2l+1)T_l(E)\sum_J\frac{A_J(l,j|l',j'|\vartheta)}{1+\sum_{p,q,r}{}' T_p(E_q')/T_{l'}(E')}. \tag{5}$$

The r index refers to possible channel spins, p to possible final neutron angular momenta, E_q' to possible final neutron energies. The prime on the summation indicates that the term for which $p=l'$, $E_q'=E'$, and $j_r'=j'$ is omitted. The factor A_J is defined as

$$A_J(l,j|l',j'|\vartheta)=\sum_{m,m'}|(lj;0m|lj;Jm)|^2 \times|(l',j';m',m-m'|l'j';Jm)|^2|Y_{l'm'}(\vartheta,\varphi)|^2. \tag{6}$$

There is no dependence on φ in (7) because of the absolute value sign on $Y_{l',m'}$. Note that Eq. (6) refers to the excitation of a single level of energy E'.

The cross section $\sigma(l,j|l',j')$ may be obtained by integration and the sum rule

$$\sum_m|(lj;0m|lj;Jm)|^2=(2J+1)/(2l+1). \tag{7}$$

Hence

$$\sigma(l,j|l',j') =\pi\lambda^2T_l(E)\sum_J\left[(2J+1)\Big/\left(1+\sum_{p,q,r}{}'\frac{T_p(E_q')}{T_{l'}(E')}\right)\right], \tag{8}$$

a familiar expression.[2] At this point the sum of $\sigma(l,j|l',j')$ over j, j', l, and l' may be readily indicated obtaining $\sigma(i|i')$:

$$\sigma(i|i')=\frac{\pi\lambda^2}{2(2i+1)}\sum_l T_l(E) \times\sum_J\frac{\epsilon_{j,l'}{}^J(2J+1)}{1+\sum_{l'',j'',q}{}'\epsilon_{j'',l''}{}^JT_{l''}(E_q')/\sum_{l',j'}\epsilon_{j',l'}{}^JT_{l'}(E')}, \tag{9}$$

where

$$\epsilon_{j,l'}{}^J=\begin{cases}2 \text{ if both } j_1 \text{ and } j_2\\ 1 \text{ if } j_1 \text{ or } j_2, \text{ not both}\\ 0 \text{ if neither } j_1 \text{ nor } j_2\end{cases}$$

$$\text{satisfy } |J-l|\leq j_i\leq(J+l). \tag{10}$$

The prime in the sum (9) requires the omission of those terms in the sum for which $E_q'=E'$, $l'=l''$, and j'' equal to either value of j'. The sum over l' is meant to include all values of the angular momentum of the

[2] J. Blatt and V. F. Weisskopf, forthcoming book on nuclear theory.

TABLE I. Values of initial and final angular momenta and of the spin of the compound nucleus, entering into calculation of $\sigma(i|i')$ for the transition $0^+ \rightarrow 1^+$.

J	l	$\epsilon_{j,l}{}^J$	l'	$\epsilon_{j',l'}{}^J$
$(1/2)^+$	0	1	0	1
			2	1
$(1/2)^-$	1	1	1	2
$(3/2)^-$	1	1	1	2
			3	1
$(3/2)^+$	2	1	0	1
			2	2
$(5/2)^+$	2	1	2	2
$(5/2)^-$	3	1	1	1
			3	2
$(7/2)^-$	3	1	3	2

emergent neutrons which can lead to the particular excited state being considered.

In these expressions the properties of the compound nucleus enters only in J and T_l. For J we make the statistical assumption that all J's consistent with the conservation of angular momentum enters into the sum. The penetrabilities T_l have been computed on the bases of the schematic theory for nuclear cross section and will be given in a paper in preparation.[3] The properties of the residual nucleus occurs through the quantities E_q' and j', and of course the parity. It should be borne in mind that the penetrabilities as given by the schematic theory are averages over resonances. For a given level in the residual nucleus there can be strong fluctuations from the average.

Although (7) and (8) have been primarily developed for application to inelastic neutron scattering, it is clear that they may be employed to deal with inelastic scattering of other particles and for nuclear reactions provided, of course, that the assumptions underlying their derivation holds. The main change occurs in the factor common to both (7) and (8),

$$T_l(E)T_{l'}(E')/\sum_{p,q,r} T_p(E_q').$$

For $T_l(E)$ and $T_{l'}(E')$ we must insert the penetrabilities of the incident and emergent particles. In the denominator we must insert the penetrabilities for those particles which are readily emitted by the compound nucleus. These particles are usually neutrons. Application to reactions involving charged particles will be presented in another paper.

III. INELASTIC SCATTERING WITH EXCITATION OF FEW LEVELS

We first consider the integrated cross section, $\sigma(i|i')$ as given by Eq. (9). We shall be interested here in showing the sensitivity of $\sigma(i|i')$ to the quantum numbers of the excited levels.

Sufficiently close to threshold the energy dependence of $\sigma(i|i')$ is given by $T_0(E)$, since it is always possible for l' to equal zero and since $T_0(E)$ approaches zero less rapidly than $T_{l'}(E')$, $l' \neq 0$, as may be seen from the limiting form

$$T_{l'}(E') \underset{E'\rightarrow 0}{\longrightarrow} [(l'-1)!/(2l'-1)!]^2 \times [x'X_0/(X_0{}^2+l'^2)](2x')^{2l'}, \quad (11)$$

where $x'=k'R$, $k'=$ wave number of emergent neutron, R, the nuclear radius, and X_0 is a constant defined by Feshbach and Weisskopf.[4] Hence $T_{l'}(E')$ goes to zero like $E'^{(l'+\frac{1}{2})}$. The additional angular momentum l required to make the transition from i to i' possible is furnished by the incident neutron. In general, the term $T_0(E)$ will not dominate the series for $\sigma(i|i')$ for long. This is true even when $|i-i'|$ is small. As $|i-i'|$ increases and the energy of the excited level decreases, the energy region in which the $l'=0$ term is dominant becomes smaller and smaller. As a consequence, the shape of the total cross section curve as a function of energy may be quite sensitive to $|i-i'|$.

The results obtained for a typical example will now be exhibited. The cross section $\sigma(i|i')$ was first calculated for the case of a single excited level 0.5 Mev above the ground state, the latter having a spin $i=0$. Four assignments for the angular momentum and parity of the excited state were investigated: 0^+, 0^-, 1^+, 1^-, where the numeral indicates the value of i, $+$ means same parity as that of the ground state, and $-$ means opposite parity. Angular momenta up to 3 were considered. In Table I we list the values of l, l', J, $\epsilon_{j,l}{}^J$, $\epsilon_{j',l'}{}^J$ for one case, 1^+. The final expression for the cross section is

$$\sigma(i|i') = (\pi\lambda^2/2)\left\{\frac{2T_0(E)}{1+[T_0(E')/\{T_0(E')+T_2(E')\}]}\right.$$
$$+T_1(E)\left[\frac{2}{1+[T_1(E)/2T_1(E')]}\right.$$
$$\left.+\frac{4}{1+[T_1(E)/\{2T_1(E')+T_3(E')\}]}\right]$$
$$+T_2(E)\left[\frac{4}{1+[T_2(E)/\{T_0(E')+2T_2(E')\}]}\right.$$
$$\left.+\frac{6}{1+[T_2(E)/2T_2(E')]}\right]$$
$$+T_3(E)\left[\frac{6}{1+[T_3(E)/\{T_1(E')+2T_3(E')\}]}\right.$$
$$\left.\left.+\frac{8}{1+[T_3(E)/2T_3(E')]}\right]\right\}.$$

The resulting values of $\sigma(i|i')/(\pi\lambda^2/2)$ for a nucleus of radius 8×10^{-13} cm are plotted in Fig. 1. We see that $\sigma(i|i')$ is quite sensitive in magnitude though not in

[3] Feshbach, Shapiro, and Weisskopf, to be published.

[4] H. Feshbach and V. F. Weisskopf, Phys. Rev. **76**, 1550 (1949).

shape (for the $|i-i'|$ is small) to the value of i' but not nearly as sensitive to the parity. On the same figures we have given the predicted $\sigma(i|i')$ for $i'=3$, with a change in parity. We note the characteristic change in shape. In this case the $l'=0$ term dominates for $E'\lesssim 20$ kev while for the cases where $|i-i'|$ is small the $l'=0$ term is dominant up to E' equal to 200 kev. The sensitivity of the shape of $\sigma(i|i')$ to $|i-i'|$ was first noted by Ebel.[5] We again remark that the above calculations are based on averages as given by the schematic theory. Note also that gamma-ray competition may be important for some of the terms in $\sigma(i/i')$ close to threshold.

Angular distribution.—Returning to Eq. (6) we see that the dependence of the cross section on angle enters through the factor

$$A_J(l,\,j|l',\,j'|\vartheta)=\sum_{m,\,m'}|(lj;\,0m|lj;\,Jm)|^2 \times|(l'j';\,m',\,m-m'|l'j';\,Jm)|^2|Y_{l'm'}(\vartheta,\,\varphi)|^2. \quad (12)$$

Most of this section will be concerned with the evaluation of this sum. Our results will maintain a separation of the quantum numbers of the initial and final state permitting the rapid evaluation for various assumptions for these numbers. We therefore expand the sum in (5) over m in a power series in m

$$\sum|(l'j';\,m',\,m-m'|l'j';\,Jm)|^2|Y_{l'm'}(\vartheta,\,\varphi)|^2 = \sum_{n=0}^{l'} m^{2n}F_n(J|l',\,j'|\vartheta), \quad (13)$$

where the function F_n is the coefficient of m^{2n}. Letting

$$s_n(l,\,j|J)=\sum_{m=0}^{j} m^{2n}|(lj;\,0m|lj;\,Jm)|^2, \quad (14)$$

A_J is written as follows:

$$A_J(l,\,j|l',\,j'|\vartheta)=\sum_{n=0}^{l'} s_n(l,\,j|J)F_n(J|l',\,j'|\vartheta). \quad (15)$$

The s_n terms contain the dependence on the initial quantum numbers l and j only, while F_n contains the dependence on the quantum numbers of the final state. The functions s_n are given in Table II for arbitrary j and J for $1\leq l\leq 3$. The functions F_n are given in Table III for arbitrary J with $1\leq l'\leq 2$. The values of F_n at

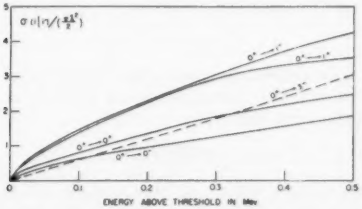

FIG. 1. Total cross section for the inelastic scattering of neutrons by a target nucleus of zero spin. The results for four different possibilities for the spin and parity of the level excited are given, the energy of the excited level being taken as 0.5 Mev above the ground state.

[5] A. Ebel, Massachusetts Institute of Technology thesis (unpublished).

TABLE II. The factors s_n in Eq. (15). The symbol C.F. stands for common factor. For example, $s_1(2,\,j|j+2)$ is $[(2j+5)/5]\times[j(j+3)/7]$.

J \ n	C.F.	0	$s_n(1,\,j\|J)$ 1	2
$j+1$	$\frac{2j+3}{3}$	1	$\frac{j(j+2)}{5}$	$\frac{(j)(j+2)(3j^2+6j-2)}{35}$
j	$\frac{2j+1}{3}$	1	$\frac{3j^2+3j-1}{5}$	$\frac{3j^4+6j^3-3j+1}{7}$
$j-1$	$\frac{2j-1}{3}$	1	$\frac{(j+1)(j-1)}{5}$	$\frac{(j+1)(j-1)(3j^2-5)}{35}$

J \ n	C.F.	0	$s_n(2,\,j\|J)$ 1	2
$j+2$	$\frac{2j+5}{5}$	1	$\frac{j(j+3)}{7}$	$\frac{j(j+3)(j^2+3j-1)}{21}$
$j+1$	$\frac{2j+3}{5}$	1	$\frac{3j^2+6j-2}{7}$	$\frac{5j^4+20j^3+10j^2-20j+6}{21}$
j	$\frac{2j+1}{5}$	1	$\frac{11j^2+11j-15}{21}$	$\frac{9j^4+18j^3-16j^2-25j+21}{21}$
$j-1$	$\frac{2j-1}{5}$	1	$\frac{3j^2-5}{7}$	$\frac{5j^4-20j^2+21}{21}$
$j-2$	$\frac{2j-3}{5}$	1	$\frac{(j-2)(j+1)}{7}$	$\frac{(j+1)(j-2)(j^2-j-3)}{21}$

J \ n	C.F.	0	$s_n(3,\,j\|J)$ 1	2
$j+3$	$\frac{2j+7}{7}$	1	$\frac{j(j+4)}{9}$	$\frac{j(j+4)(3j^2+12j-4)}{99}$
$j+2$	$\frac{2j+5}{7}$	1	$\frac{j^2+3j-1}{3}$	$\frac{5j^4+30j^3+30j^2-45j+13}{33}$
$j+1$	$\frac{2j+3}{7}$	1	$\frac{7j^2+14j-15}{15}$	$\frac{53j^4+212j^3-30j^2-484j+315}{165}$
j	$\frac{2j+1}{7}$	1	$\frac{23j^2+23j-66}{45}$	$\frac{39j^4+78j^3-190j^2-229j+366}{99}$
$j-1$	$\frac{2j-1}{7}$	1	$\frac{7j^2-22}{15}$	$\frac{53j^4-348j^2+610}{165}$
$j-2$	$\frac{2j-3}{7}$	1	$\frac{j^2-j-3}{3}$	$\frac{5j^4-10j^3-30j^2+35j+63}{33}$
$j-3$	$\frac{2j-5}{7}$	1	$\frac{(j+1)(j-3)}{9}$	$\frac{(j+1)(j-3)(3j^2-6j-13)}{99}$

TABLE III. The factors F_n in Eq. (15). The symbol C.F. stands for common factor. For example, $F_0(j'+1|1, j'|\vartheta)$ is $[1/(2j'+1)] \times[j'|Y_{11}|^2+(j'+1)|Y_{10}|^2]$ while $F_1(j'+1|1, j'|\vartheta)$ is $-(3/4\pi)[(1/(2j'+1)(j'+1)]P_1$. The functions $|Y_{lm}|^2$ and P_l are the square of the absolute value of the normalized spherical harmonics and the Legendre polynomials of order l, respectively. $|Y_{11}|^2$ equals $(3/8\pi)\sin^2\vartheta$; $|Y_{10}|^2$ is $(3/4\pi)\cos^2\vartheta$.

$J\searrow n$ Angular dependence	C.F.	$F_n(J\|1, j'\|\vartheta)$ 0 $\|Y_{11}\|^2$	$\|Y_{10}\|^2$	1 P_1
$j'+1$	$\frac{1}{(2j'+1)}$	j'	$j'+1$	$-\frac{3}{4\pi}\frac{1}{(j'+1)}$
j'	1	1	0	$\frac{3}{4\pi}\frac{1}{j'(j'+1)}$
$j'-1$	$\frac{1}{(2j'+1)}$	$j'+1$	j'	$-\frac{3}{4\pi}\frac{1}{j'}$

$J\searrow n$ Angular dependence	C.F.	$F_n(J\|2, j'\|\theta)$ 0 $\|Y_{21}\|^2$	$\|Y_{20}\|^2$	1 $(15/8\pi)P_2$	$(15/8\pi)P_1$	2 $(15/8\pi)P_2$
$j'+2$	$\frac{1}{(2j'+1)(2j'+3)}$	$\frac{j'(j'-1)}{2}$	$2j'(j'+2)$	$\frac{3(j'+2)(j'+1)}{2}$	$-\frac{4(j'+1)(2j'+1)}{7(j'+1)(j'+2)}$	$-\frac{6j'^2+30j'+31}{7(j'+1)(j'+2)}$	$\frac{1}{(j'+1)(j'+2)}$
$j'+1$	$\frac{1}{2j'+1}$	$j'-1$	$j'+2$	0	$\frac{2(j')(j'-4)}{7j'(j'+1)(j'+2)}$	$\frac{2(6j'^2+18j'+7)}{7j'(j'+1)(j'+2)}$	$-\frac{2}{j'(j'+1)(j'+2)}$
j'	$\frac{1}{(2j'-1)(2j'+3)}$	$3(j'-1)(j'+2)$	3	$(j')(j'+1)$	$\frac{2(4j'^2+4j'-15)}{7j'(j'+1)}$	$-\frac{6(6j'^2+6j'-5)}{7(j')(j'+1)}$	$\frac{6}{j'(j'+1)}$
$j'-1$	$\frac{1}{2j'+1}$	$j'+2$	$j'-1$	0	$\frac{2(j'+1)(j'+5)}{7j'(j'+1)(j'-1)}$	$\frac{2(6j'^2-6j'-5)}{7j'(j'+1)(j'-1)}$	$-\frac{2}{j'(j'+1)(j'-1)}$
$j'-2$	$\frac{1}{(2j'-1)(2j'+1)}$	$\frac{(j'+1)(j'+2)}{2}$	$2(j'^2-1)$	$\frac{3}{2}j'(j'-1)$	$-\frac{4j'(2j'+1)}{7j'(j'-1)}$	$-\frac{6j'^2-18j'+7}{7j'(j'-1)}$	$\frac{1}{j'(j'-1)}$

0° and 90° are contained in Tables IV and V. For l' equal to 0, A_J equals $(2J+1)/[4\pi(2l+1)]$, independent of ϑ. For $l=0$, $A_J=(2J+1)/[4\pi(2l'+1)]$. The case $l'=3$ may be included by employing the symmetry of our results between initial and final states, which we shall now discuss.

Following Blatt and Biedenharn,[6] it is possible to show that

$$A_J(l, j|l', j'|\vartheta) = \frac{(2l'+1)(2J+1)^2}{4\pi} |\sum_L (2L+1)V(lJL; 000)W(JJl; Lj) \cdot V(l'l'L; 000)W(JJl'l'; Lj')P_L(\cos\vartheta)|.$$

The coefficients V and W have been defined by Racah.[7] Blatt and Biedenharn introduce the coefficients $Z(a\,b\,c\,d; e\,f)$, which they have tabulated and in terms of which A_J takes on a particularly simple appearance as follows:

$$A_J(l, j|l', j'|\vartheta) = \frac{1}{4\pi(2l+1)} |\sum_L Z(lJlJ; jL)Z(l'Jl'J; j'L)P_L(\cos\vartheta)|. \quad (16)$$

From the general properties of V and W or of Z we may conclude that the summation index L takes on only even values and that

$$L \leq \min(2l, 2l', 2J),$$

an observation which has been made by several authors.[8,9] Hence if l or l' are zero or if J is either zero or $\frac{1}{2}$, A_J will be independent of ϑ. The fact that L is even is of course obvious from the definition of A_J. The symmetry between initial and final states may now be

[6] J. Blatt and L. C. Biedenharn, Phys. Rev. **86**, 399 (1952).
[7] G. Racah, Phys. Rev. **61**, 186 (1942).
[8] C. N. Yang, Phys. Rev. **74**, 764 (1948).
[9] E. Eisner and R. G. Sachs, Phys. Rev. **72**, 680 (1947); L. Wolfenstein and R. G. Sachs, Phys. Rev. **73**, 528 (1948).

TABLE IV. $F_n(J|l'j'|0)$.

$J\backslash n$	C.F.	$F_n(J\|1, j'\|0)$ 0	1
$j'+1$	$\frac{3}{4\pi}\frac{1}{2j'+1}$	$j'+1$	$-\frac{1}{(j'+1)}$
j'	$\frac{3}{4\pi}$	0	$\frac{1}{j'(j'+1)}$
$j'-1$	$\frac{3}{4\pi}\frac{1}{2j'+1}$	j'	$-\frac{1}{j'}$

$J\backslash n$	C.F.	$F_n(J\|2, j'\|0)$ 0	1	2
$j'+2$	$\frac{15}{8\pi}\frac{1}{(2j'+1)(2j'+3)}$	$(j'+2)(j'+1)$	$-\frac{(2j'^2+6j'+5)}{(j'+1)(j'+2)}$	$\frac{1}{(j'+1)(j'+2)}$
$j'+1$	$\frac{15}{4\pi}\frac{1}{(j')(j'+1)(j'+2)(2j'+1)}$	0	$(j'+1)^2$	-1
j	$\frac{5}{4\pi}\frac{1}{(2j'-1)(2j'+3)}$	$(j')(j'+1)$	-6	$\frac{9}{j'(j'+1)}$
$j'-1$	$\frac{15}{4\pi}\frac{1}{j'(j'+1)(j'-1)(2j'+1)}$	0	j'^2	-1
$j'-2$	$\frac{15}{8\pi}\frac{1}{(2j'+1)(2j'-1)}$	$(j')(j'-1)$	$-\frac{(2j'^2-2j'+1)}{j'(j'-1)}$	$\frac{1}{j'(j'-1)}$

stated:

$$A_J(l, j|l'j'|\vartheta)=[(2l'+1)/(2l+1)]A_J(l'j'|lj|\vartheta). \quad (17)$$

Because of the length of these calculations it was important to make a number of checks which were obtained from the following relations:

$$\int F_n(J|l', j'|\vartheta)d\Omega=\delta_{n0}. \quad (18)$$

$\sum_{j'}(2j'+1)F_n(J|l', j'|\vartheta)$ is independent of ϑ. (19)

$$\sum_n m^{2n}F_n(J|l', j'|0) =[(2l'+1)/4\pi]|(l'j'; 0m|l'j'; Jm)|^2. \quad (20)$$

$$\sum_J s_n(l, j|J)=\sum_m m^{2n}. \quad (21)$$

An example of the calculation of A_J will now be given in order to make the use of the tables clear. We take $A_1(1\frac{1}{2}|1\frac{1}{2}|\vartheta)$ and therefore require $F_0(\frac{3}{2}|1\frac{1}{2}|\vartheta)$ and $F_1(\frac{3}{2}|1\frac{1}{2}|\vartheta)$, where $J=j'+1$, $(2j'+1)=2$. Then

$$F_0(\tfrac{3}{2}|1\tfrac{1}{2}|\vartheta)=\tfrac{1}{2}[\tfrac{1}{2}|Y_{11}|^2+\tfrac{2}{3}|Y_{10}|^2],$$
$$F_1(\tfrac{3}{2}|1\tfrac{1}{2}|\vartheta)=\tfrac{1}{2}[(-3/4\pi)\cdot\tfrac{2}{3}]P_2.$$

The values of s_n, $J=j+1$, are

$$s_0(1\tfrac{1}{2}|\tfrac{3}{2})=4/3, \quad s_1(1\tfrac{1}{2}|\tfrac{3}{2})=\tfrac{1}{3}.$$

Hence

$$A_1(1\tfrac{1}{2}|1\tfrac{1}{2}|\vartheta)=(1/4\pi)[\tfrac{1}{2}\sin^2\vartheta+3\cos^2\vartheta-\tfrac{1}{2}P_2(\cos\vartheta)].$$

Once A_J is available, sufficient data is available for the calculation of the angular distribution. We note that as a consequence of the statistical assumption for the compound nucleus that the predicted distributions are symmetrical about 90°. If either $l=0$ neutrons incoming or $l'=0$ neutrons outgoing or if the compound nuclear states with $J=\frac{1}{2}$ form the most important components of cross section, then the distribution will be isotropic. This will generally be the case near threshold for then only $l'=0$ neutrons have appreciable transmission factors. We can be certain of large anisotropy in the angular distribution only if the spin change between the initial and final levels is large as would occur in the excitation of isomeric levels. For smaller spin changes the anisotropy will be correspondingly smaller. In Fig. 2 we give an angular distribution in which a target nucleus $i=0$ is struck by neutrons having 1-Mev energy. These excite a level at 0.5 Mev with $i=1$ and opposite in parity to the ground state. These angular distributions are essentially average results since fluctuations away from the schematic theory will affect them considerably. For this reason it is important to employ the parameters R and X_0 which best fit the

TABLE V. $F_n(J|l'j'|\pi/2)$.

$J \diagdown n$	$F_n(J\|1, j'\|\pi/2)$ C.F.	0	1
$j'+1$	$\frac{3}{8\pi}\frac{1}{2j'+1}$	j'	$\frac{1}{j'+1}$
j'	$\frac{3}{8\pi}$	1	$-\frac{1}{j'(j'+1)}$
$j'-1$	$\frac{3}{8\pi}\frac{1}{2j'+1}$	$j'+1$	$\frac{1}{j'}$

$J \diagdown n$	$F_n(J\|2, j'\|\pi/2)$ C.F.	0	1	2
$j'+2$	$\frac{15}{64\pi}\frac{1}{(2j'+1)(2j'+3)}$	$3j'^2+5j'+4$	$\frac{2j'^2-6j'-11}{(j'+1)(j'+2)}$	$\frac{3}{(j'+1)(j'+2)}$
$j'+1$	$\frac{15}{32\pi}\frac{1}{2j'+1}$	$j'-1$	$\frac{2j'^2+10j'+3}{j'(j'+1)(j'+2)}$	$\frac{-3}{j'(j'+1)(j'+2)}$
j'	$\frac{15}{32\pi}\frac{1}{(2j'-1)(2j'+3)}$	$\frac{(11j'^2+11j'-18)}{3}$	$\frac{-5(2j'^2+2j'-3)}{j'(j'+1)}$	$\frac{9}{j'(j'+1)}$
$j'-1$	$\frac{15}{32\pi}\frac{1}{2j'+1}$	$j'+2$	$\frac{2j'^2-6j'-5}{j'(j'+1)(j'-1)}$	$\frac{-3}{j'(j'+1)(j'-1)}$
$j'-2$	$\frac{15}{64\pi}\frac{1}{(2j'-1)(2j'+1)}$	$3j'^2+j'+2$	$\frac{2j'^2+10j'-3}{(j'-1)(j')}$	$\frac{3}{(j')(j'-1)}$

total cross-section data, though this will not take care of fluctuations from level to level.

IV. INELASTIC SCATTERING WHEN THE DENSITY OF LEVELS IN THE RESIDUAL NUCLEUS IS HIGH

In this section the statistical hypothesis will be assumed for the residual as well as compound nucleus. Nuclear levels of all types are then so dense that they may be considered to form a continuous distribution. It is expected that this description will be valid for the heavier nuclei or for the middle-weight nuclei if the incident neutron energy is sufficiently great.

Let then the number of levels having an energy between $(E-E')$ (this is just the excitation energy) and $(E-E')+d(E-E')$ be

$$n(E-E')d(E-E') \approx [(2j'+1)/D_R(E-E')]d(E-E'), \quad (22)$$

where $D_R(E-E')$ is the distance between levels in the residual nucleus. The factor $(2j'+1)$ implies that there are $(2j'+1)^2$ levels at the energy $(E-E')$ with channel spin j'. One factor of $(2j'+1)$ is already contained in the sum over m' in Eqs. (6) and (7). We now pause to justify this factor, which was also assumed by Wolfenstein.[1]

The motion of any ensemble of particles may be broken up into three parts: motion of the center of mass, rotation about the center of mass, and "vibration" relative to the center of mass. The rotation about the center of mass is just that of a rigid body[10] and carries the angular momentum of the system. The specification of this angular momentum requires three quantum numbers; the total angular momentum j', the projection of the angular momentum along both the figure axis of the system, and an arbitrary z axis which in the present problem is taken to be the direction of the incident particle. Hence a state of a given angular momentum has a $(2j'+1)^2$ degeneracy, since each of the projections has $(2j'+1)$ possibilities.

Level density formula (22) leads rigorously to the conclusion that the angular distribution of the emergent neutrons is isotropic. This may be seen as follows.[11] The final l' is formed by adding j' to a fixed J. In order for l' to have all possible orientations it is necessary for the possible directions of j' to cover the complete sphere with j' as radius. Since every vector j' corresponds to a state of the final system with a given value of j', the

[10] E. Kemble, *Fundamental Principles of Quantum Mechanics* (McGraw-Hill Book Company, Inc., New York, 1937).

[11] We are indebted to V. F. Weisskopf for this discussion.

number of these states is quadratic in j'. A proof of the angular isotropy has been given by Wolfenstein[1] but his proof is not as complete as the one that follows.

We now insert expression (22) into the general formula (7). We shall obtain the energy distribution of the emergent neutrons as well as the isotropic angular distribution. The cross section $\sigma(E|E',\vartheta)$ for inelastic scattering with the emergent neutron having an energy between E' and $E'+dE'$ and a direction ϑ in solid angle $d\Omega$ is

$$\sigma(E|E',\vartheta)dE'd\Omega$$

$$=\frac{\pi\lambda^2}{2(2i+1)}\sum_{l,l',J,j}(2l+1)T_l(E)T_{l'}(E')\times\sum_{j'J}\frac{(2j'+1)A_J(l,j|l',j'|\vartheta)}{\sum_{pqr}T_p(E_{q'})}\frac{dE'd\Omega}{D_r(E-E')}.$$

The sum[12] over j' may be performed through the use of a relation due to Racah:[7]

$$\frac{|(lj;m_l,mj|lj;J,m_l+m_j)|^2}{2J+1}=\frac{|(lj;m_l,-(m_l+m_j)|lJ;j,-m_j)|^2}{2j+1}. \quad (23)$$

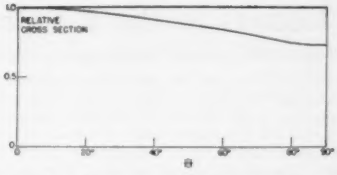

FIG. 2. Angular distribution of inelastically scattered neutrons by a target nucleus of zero spin. The excited level is assumed to have a spin of one opposite parity and an excitation energy of 0.5 Mev, while the incident neutrons have an energy of 1.0 Mev.

Therefore

$$\sum_{j'}(2j'+1)A_J(l,j|l',j'|\vartheta)=\sum_{j',m,m'}(2j'+1)|(lj;0m|lj;Jm)|^2\times|(l'j';Jm|l'j';m',m-m')|^2|Y_{l'm'}|^2$$
$$=(2J+1)\sum_{m,m'}|(lj;0m|lj;Jm)|^2|Y_{l'm'}|^2\times\sum_{j'}|(l'J;m',-m|l'J;j',m'-m)|^2$$
$$=(2J+1)\sum_{m,m'}|(lj;0m|lj;Jm)|^2|Y_{l'm'}|^2.$$

Hence

$$\sum_{j'}(2j'+1)A_J(l,j|l',j'|\vartheta)=(2J+1)^2(2l'+1)/[4\pi(2l+1)], \quad (24)$$

demonstrating the isotropy of the angular distribution which follows from the statistical assumption and energy level density (22).

The energy distribution of the emergent neutrons may be readily obtained since in virtue of (24) the sums over j and J may be performed. We find that

$$\sigma(E|E')=\int\sigma(E|E',\vartheta)d\Omega=\pi\lambda^2\frac{(\sum_l(2l+1)T_l(E))(\sum_{l'}(2l'+1)T_{l'}(E'))D_R^{-1}(E-E')}{\sum_{l''}(2l''+1)\int_0^E T_{l''}(E'')D_R^{-1}(E-E'')dE''}. \quad (25)$$

Since the cross section for the formation of the compound nucleus is

$$\sigma_c(E)=\pi\lambda^2\sum_l(2l+1)T_l(E),$$

we may rewrite (25) as

$$\sigma(E|E')=\sigma_c(E)\frac{E'\sigma_c(E')D_R^{-1}(E-E')}{\int_0^E E''\sigma_c(E'')D_R^{-1}(E-E'')dE''}. \quad (26)$$

The cross section σ_c as calculated by the schematic theory for nuclear cross sections are given in reference (3). Formula (26) has been discussed in many places in the literature.[2]

We are greatly indebted to Professor V. F. Weisskopf for many helpful discussions. We would also like to thank Dr. H. Goldstein for this thorough criticism of the manuscript.

[12] We are indebted to M. Gell-Mann for suggesting the use of Eq. (23).

Letters to the Editor

PUBLICATION of brief reports of important discoveries in physics may be secured by addressing them to this department. The closing date for this department is five weeks prior to the date of issue. No proof will be sent to the authors. The Board of Editors does not hold itself responsible for the opinions expressed by the correspondents. Communications should not exceed 600 words in length and should be submitted in duplicate.

The Fine Structure of Resonance Absorption of Mn^{++} in a Rhombic Crystalline Field

HIROO KUMAGAI, KAZUO ÔNO, IZUO HAYASHI, AND KENJIRÔ KAMBE*
Institute of Science and Technology, University of Tokyo, Tokyo, Japan
(Received March 17, 1952)

THE microwave resonance absorption of diluted salts of Mn^{++} shows fine and hyperfine structures, and the theory and experiment agree very well where the crystalline field is axially symmetric as is the case of diluted $MnSiF_6 \cdot 6H_2O$ in the paper of Bleaney and Ingram,[1] to which we shall refer as B−I. But in the case of diluted $Mn(NH_4)_2(SO_4)_2 \cdot 6H_2O$, where the crystalline field is rhombic, the analysis of the fine structure is not easy since two nonequivalent ions are located in a unit cell. For this case, theoretical calculations are given in B−I, but only up to the first order of perturbation for the rhombic part of the crystalline field.

We have recently found by paramagnetic resonance that the diluted salt of $Mn(CH_3COO)_2 \cdot 3H_2O$ (monoclinic, $a:b:c = 1.5565:1:1.8431$, $\beta = 105°34'$)[2] contains one ion in a unit cell and that the crystalline field is rhombic. The fine and hyperfine structures of the resonance lines of this salt are easily determined for comparison with theory.

One of us (K.K.) has calculated the fine structure up to the second order of perturbation by the Hamiltonian

$$\mathcal{H} = g\beta \mathbf{H} \mathbf{S} + D\{S_z^2 - \tfrac{1}{3}S(S+1)\} + E(S_x^2 - S_y^2), \qquad (1)$$

where the notations are the same as in B−I. Our results were, when the static magnetic field is in the z-direction,

$$\begin{aligned} M = \pm 5/2 \leftrightarrow \pm 3/2: &\quad H(\pm 5/2, \pm 3/2) = H_0 \mp 4D + 4E^2/H_0, \\ M = \pm 3/2 \leftrightarrow \pm 1/2: &\quad H(\pm 3/2, \pm 1/2) = H_0 \mp 2D - 5E^2/H_0, \\ M = \quad 1/2 \leftrightarrow -1/2: &\quad H(\quad 1/2, -1/2) = H_0 \qquad -8E^2/H_0, \end{aligned} \qquad (2)$$

and in the xy plane,

$$\begin{aligned} H(\pm 5/2, \pm 3/2) &= H_0 \pm 2(D - 3E\cos 2\theta) \\ &\quad + \{(D + E\cos 2\theta)^2 - 32E^2 \sin^2 2\theta\}/H_0, \\ H(\pm 3/2, \pm 1/2) &= H_0 \pm (D - 3E\cos 2\theta) \\ &\quad - \{(5/4)(D + E\cos 2\theta)^2 - 4E^2 \sin^2 2\theta\}/H_0, \\ H(1/2, -1/2) &= H_0 - \{2(D + E\cos 2\theta)^2 - 16E^2 \sin^2 2\theta\}/H_0, \end{aligned} \qquad (3)$$

where $H_0 = h\nu/g\beta$, θ is the angle between static field and x axis, D and E are the symbols in Eq. (1) divided by $g\beta$, and $H(5/2, 3/2)$ etc., express the positions of the centers of the six hyperfine structure lines, respectively. An expression for $H(1/2, -1/2)$ in the z direction is also given in B−I, and it agrees with ours.

In Table I, the successive separations of the experimental fine structure lines are given for the z, x, and y orientations, and the bisector of the xy axes. In the crystal the z and x axes of the crystalline field are the c and b axes of the crystal symmetry. From these data and other experiments in the xy-plane we determined $D = 252$ gauss and $E = 27$ gauss. The successive separations, calculated up to second-order terms, using these values of D and E, are given in Table I. The agreement between experiment and theory is quite satisfactory. The small differences may be explained by taking into account the effect of the crystalline field of another symmetry which we have neglected.

TABLE I. Successive separations of the fine structure lines for $Mn(CH_3COO)_2 \cdot 3H_2O$.

	z-direction					
	obs.(gauss)	cal.	obs.-cal.			
$H(5/2, 3/2) > \Delta H_1$	514	508	+6			
$H(3/2, 1/2) > \Delta H_2$	496	507	−11			
$H(1/2, -1/2) > \Delta H_3$	501	505	−6			
$H(-1/2, -3/2) > \Delta H_4$	512	504	+8			
$H(-3/2, -5/2)$						

	x-direction		y-direction		bisector of the xy axes	
	obs.(cal.)	obs.-cal.	obs.(cal.)	obs.-cal.	obs.(cal.)	obs.-cal.
ΔH_1	229(223)	+6	381(365)	+16	274(286)	−12
ΔH_2	187(190)	−3	337(344)	−7	271(264)	+7
ΔH_3	151(156)	−5	312(322)	−10	248(242)	+6
ΔH_4	127(123)	+4	317(301)	+16	208(220)	−8

By using Eqs. (2) and (3) and the above-determined values of D and E, we can compute H_0 from the experimental values of $H(1/2, -1/2)$. The g-values computed from this H_0 are isotropic and nearly the same as for the fluosilicate.[1]

The salt is diluted with Zn ions. The microwave wavelength is 3.0 cm and the measurements are all at room temperature. The magnetic field is modulated by a small amount with 2.5 kc, and the crystal detector output is amplified and detected by a phase sensitive detector. The magnetic field is calibrated carefully by proton resonance.

A more detailed report will appear in J. Phys. Soc. Japan.

* University of Electro-communications, Tokyo, Japan.
[1] B. Bleany and D. J. E. Ingram, Proc. Roy. Soc. (London) **205**, 336 (1951).
[2] P. Groth, *Chemische Crystallographie* (W. Engelmann, Leipzig, 1910), 3 teil, p. 68.

The Lowest Excitation Level of Hg^{196}

P. STAEHELIN
Swiss Federal Institute of Technology, Zürich, Switzerland
(Received May 26, 1952)

A SYSTEMATICAL discussion of the lowest excitation levels in even-even nuclei has shown that the position of these levels depends in a regular manner on the number of protons and neutrons, and that this regularity demonstrates a clear connection with shell structure.[1]

Only a few cases seemed to form exceptions from the regular behavior. The most striking one was Hg^{196}. For this nucleus, which contains 80 protons and 116 neutrons, a lowest level of 175 kev was recently reported,[2] while an energy of about 400 kev is to be expected.

This discrepancy induced us to examine the 5.6-day Au^{196}, which decays into Pt^{196} and Hg^{196}. We used for our measurements an electron-electron-coincidence spectrometer with 1.5 percent resolution. The experimental technique is described in a paper by Humbel *et al.*[3] The radioactive gold was produced at Amsterdam by bombarding platinum with deuterons.

Although we carefully searched for the conversion lines of a 175-kev transition, we could not detect any indication of such a line. Unfortunately a possible K-conversion line coincides energetically with a much stronger M-conversion line of the long lived Au^{196}. So a separttion would be rather difficult. However, we certainly should have observed the L-conversion line of 175 kev, even if it had only one-fifth of the reported intensity.

Instead of the conversion lines of a 175-kev transition, we detected L- and M- conversion electrons of an unknown transition with an energy (426±2) kev and a half-life of about 5.6 days, which is equal to that of Au^{196}.

From the number of coincidences (which depends upon the amplitude discrimination of the pulses from a photomultiplier) we conclude that this new transition follows a β-decay with a maximum energy between 200 and 300 kev. This conclusion was confirmed by direct observation of the β-spectrum; the Fermi plot indicates a simple spectrum with an energy limit of (270 ± 20) kev. From the intensity of the β-spectrum the following conversion coefficients for the 426-kev transition are deduced: $\alpha_L=(7.0\pm2.5)\times10^{-3}$ and $\alpha_{(M+N)}=(2.0\pm0.8)\times10^{-3}$. They are consistent with electric quadrupole radiation.

The K-conversion electrons of the new 426-kev transition have nearly the same energy as the L-conversion electrons which arise from the 354-kev radiation in the Pt-decay branch of Au^{198}. For that reason the K-conversion line could not be separated in the spectrum of the single counts, but it was revealed in the spectrum of coincidences. Here the intensity ratio for the two lines is more favorable, since every 426-kev transition immediately follows a β-ray, while the 354-kev radiation is only partly in coincidence with the weakly converted 332-kev radiation and a few Auger electrons. The measured energy difference of K- and L-shell conversion electrons confirms that the 426-kev transition occurs in the Hg-decay branch.

A detailed report and new data for the Pt-decay branch of Au^{198} will be published in *Helvetica Physica Acta*. We are indebted to Professor C. J. Bakker at Amsterdam for preparation of the radioactive samples, and to Professor P. Preiswerk for many helpful discussions.

[1] P. Staehelin and P. Preiswerk, Helv. Phys. Acta **24**, 623 (1951).
[2] Steffen, Huber, and Humbel, Helv. Phys. Acta **22**, 167 (1949).
[3] Huber, Humbel, Schneider, and de-Shalit, Helv. Phys. Acta **25**, 3 (1952).

Regular Meson Potentials in Low Energy Proton-Proton Scattering*

H. E. Hart and R. D. Hatcher
New York University, New York, New York
(Received April 8, 1952)

ALTHOUGH low energy proton-proton scattering can be explained quite well by a two-parameter system involving either a boundary condition on the wave function at a finite distance[1] or by means of potentials,[2,3] there exists a discrepancy between the mass of the meson used in the static approximation of meson theories; as, for example, that of Møller and Rosenfeld, by fitting to the experimental scattering results and the directly measured mass of the π-mesons believed largely responsible for nuclear forces. In using a potential of the form

$$\frac{e^2}{r}-\frac{Ce^{-r/a}}{r/a}, \tag{1}$$

Yovits, Smith, Hull, Bengston, and Breit[2] obtained a mass of $m=\hbar/ac=333\pm2$ electron masses, whereas the masses of the π^+, π^-, and π^0 mesons are 277.4 ± 1.1, 276.1 ± 1.3, 264.6 ± 3.2 m, respectively.[4,5] The accuracy in fitting the data is quite high and it seems that something additional is needed to explain the difference. The neutron-proton system seems to give a triplet interaction agreeing with the mass of meson theory, but the error is quite large in the singlet case.[6] A rough estimate of relativistic effects[7] for energies up to 4 Mev indicates that they may cause as much as a 2 percent decrease in the mass. Cutoffs by a straight line parallel to the axis at $r=\hbar/Mc$ where M is the proton mass indicate a meson mass slightly higher, and cutoffs at larger r's would make the mass even higher.

We have investigated the scattering up to 3 Mev, where it is to be expected effects of relativity would be least and angular momenta other than $L=0$ are not significant, by means of a potential form which satisfies certain basic requirements. We require that between protons the potential should be (1) asymptotically equal to the Coulomb potential, (2) finite everywhere, (3) derivable from the static approximation of a relativistically invariant meson theory. Condition (2) was imposed because the infinities associated with the Coulomb and meson potentials can have little physical significance. Condition (3) we required so that there would be some means of comparing the potential with theory.

The potential chosen for calculation,

$$(1-e^{-r/a_0})\left\{\frac{e^2}{r}-\frac{Ce^{-r/a}}{r/a}\right\}, \quad a_0=e^2/mc^2, \tag{2}$$

which is a modification of (1) wherein the comparison of mass values is still possible, may easily be seen to satisfy the postulated requirements. We can consider (2) as consisting of a modified Coulomb term

$$e^2/r-e^2e^{-r/a_0}/r \tag{3}$$

and a modified meson term

$$\frac{Ce^{-r/a}}{r/a}-\frac{Ce^{-(r/a+r/a_0)}}{r/a}. \tag{4}$$

The exponential terms may then be considered as static meson potentials corresponding to different masses. Equation (2) could be easily generalized to bring in arbitrary meson masses so that the change in potential compared to (1) could be explained as being due to heavier mesons which introduce an interaction at short distances similar to that of Enatsu.[8] So as not to introduce a large number of parameters, however, we have restricted ourselves to C, related to the strength of the main meson term, and a, connected to the main meson mass.

The procedure used in relating the potential parameters to scattering results is somewhat similar to that of Breit and Hatcher.[7] Interior solutions were calculated out to $r=3e^2/mc^2$ by numerical integration and matched there to pure Coulomb solutions calculated from the formulas of Yost, Wheeler, and Breit[9] for a range of values of C and a. Values were obtained for the phase shifts and to test the error in neglecting the meson tails several calculations were performed out to $6e^2/mc^2$ where the phase shifts seemed to converge. To estimate analytically the error introduced, a modification of the Born approximation was employed which will be reported on in a forthcoming publication. Our results show that for a value of a corresponding to a meson mass of $274m$ agreement is obtained with experimental results. It is seen then that this theory is a possible explanation of the meson mass disagreement.

It is to be noted that other explanations of the discrepancy have recently appeared. Jastrow[9] has employed a repulsive core with some success, and Breit and Yovits[10] have suggested an internal excitation of the two-particle system which would lead to a possible change of about 10 percent.

* This work supported by the ONR.
[1] G. Breit and W. G. Bouricius, Phys. Rev. **75**, 1029 (1949).
[2] J. D. Jackson and J. M. Blatt, Revs. Modern Phys. **22**, 77 (1950).
[3] Yovits, Smith, Hull, Bengston, and Breit, Phys. Rev. **85**, 540 (1952).
[4] Barkas, Smith, and Gardner, Phys. Rev. **82**, 102 (1951).
[5] Panofsky, Aamodt, and Hadley, Phys. Rev. **81**, 565 (1951).
[6] E. E. Salpeter, Phys. Rev. **82**, 60 (1951).
[7] G. Breit and R. D. Hatcher, Phys. Rev. **78**, 110 (1950).
[8] H. Enatsu, Phys. Rev. **85**, 483 (1952).
[9] Yost, Wheeler, and Breit, Phys. Rev. **49**, 174 (1936).
[10] G. Breit and M. Yovits, Phys. Rev. **81**, 416 (1951); G. Breit, Phys. Rev. **84**, 1053 (1951).

Inelastic Scattering Resulting in Short-Lived Isomers

O. Hittmair
Physics Department, Massachusetts Institute of Technology, Cambridge, Massachusetts
(Received May 28, 1952)

THE angular distribution of the γ-radiation that follows an inelastic scattering process may either provide information concerning spin and parity of the involved levels, or if these data are known, prove the applicability of a certain nuclear model.

We assume that the target nucleus is heavy enough to remain at rest in the center-of-mass system. The z-axis is taken in the direction of the incoming particle. Then the γ-angular distribution, with the outgoing particle unobserved, is given by

$$W(\vartheta)=\sum_{LL'i_4\nu}(-)^{i_2-i_2'+L_1-L_2+L_3+\nu}(2i_2+1)^{\frac{1}{2}}(2i_2'+1)^{\frac{1}{2}}$$
$$\times(2i_2+1)(2i_2'+1)(2L_2+1)^{-1}c_\nu(L_1L_1')c_\nu(L_2L_2')$$
$$\times W(L_1i_2L_1'i_2',i_1\nu)W(i_2i_3i_2'i_3',L_2\nu)W(L_3i_3L_3'i_3',i_4\nu)$$
$$\times S_{L_2i_2L_1'i_1'}{}^{(i_2)*}S_{L_2'i_2'L_1'i_1'}{}^{(i_2')}T_{i_4,i_2}{}^{(L_2)*}T_{i_4,i_2'}{}^{(L_2')}P_\nu(\cos\vartheta).$$

The numbers i_1 to i_4 mean the level spins of the target nucleus, the compound nucleus, the residual nucleus of the scattering process, and the final nucleus which later may coincide with i_1 except for its orientation. The L's are the total angular momenta of the incoming and the outgoing particle and the γ-radiation. The S-matrix elements are the radial parts of the probability amplitudes of the inelastic scattering, i.e., they are independent of magnetic quantum numbers. The relative probability of the γ-radiation is signified by $T_{i_4,i_2}{}^{(L_2)}$. The W's are the Racah coefficients.[1,2] The c_ν's are defined by

$$c_\nu(LL)=\Sigma_\mu(-)^{L'-\mu}(LL'-\mu\mu|\nu 0),$$

where μ is the z-projection of the particle spin and $(LL'-\mu\mu|\nu 0)$ is a Clebsch-Gordan coefficient. The triangular relations of the Racah coefficients restrict the degree of the Legendre polynomials $P_\nu(\cos\vartheta)$ to values $\leq(L+L', i_2+i_2', i_3+i_3', L_3+L_3')$.

The given expression for $W(\vartheta)$ describes the process with full generality. Without making further assumptions about the levels involved and the nature of the transitions, it cannot be simplified any further. In the case when the inelastic scattering process results in a short-lived isomer[3] with mass number >100, two essential simplifications seem to be possible. The γ-transition will, in general, be a pure multipole. Therefore, the product of the radiative transition probabilities $T_{i_4,i_2}{}^{(L_2)}$ can be dropped as a common factor. Furthermore, the statistical assumption[4] may be made for the compound nucleus of the scattering process which cancels interference terms and replaces the product of the S-matrix elements by the transmission for the incoming particle. Using channel spins for the scattering process, we get then for the γ-angular distribution

$$W_E(\vartheta)=\sum_{l_1j_1\nu}(-)^{l_2}T_{l_1}(E)(2i_2+1)^{\frac{1}{2}}(2l_1+1)^{\frac{1}{2}}(2l_2+1)^{-1}$$
$$\times(l_1l_1(00|\nu 0)(L_2L_3-11|\nu 0)W(l_1i_2j_1i_2,j_1\nu)$$
$$\times W(i_2j_2i_2j_2,l_2\nu)W(L_2i_2L_3i_3,i_4\nu)P_\nu(\cos\vartheta),$$

where E is the energy of the incoming particle and $T_{l_1}(E)$ is its transmission.[4]

Since odd Legendre polynomials in $W(\vartheta)$ arise from interference terms, the first requirement for the applicability of the formalism is the symmetry of the angular distribution.

We assume that the inelastic scattering that leads to the isomeric states listed below is neutron scattering. Then the coefficients for the Legendre polynomials of the angular distribution are given in Table I. Proton scattering or scattering of other particles would express itself in changed transmissions $T_{l_1}(E)$.

TABLE I. The coefficients of the γ-angular distribution $W_E(\vartheta)=P_0+a_2P_2(\cos\vartheta)+a_4P_4(\cos\vartheta)$. E is the energy of the incoming neutron; i_3 and i_4 are the spin numbers of the target and the final nucleus; i_2 is the one of the isomeric level.

Target nucleus	Isomeric level (kev)	E (kev)	i_1, i_4	i_2	a_2	a_4
Cd^{111}	247	330	$\frac{1}{2}+$	$\frac{5}{2}+$	−1.26	0.007
Er^{166}	80	170	$0+$	$2+$	1.07	0
Yb^{170}	84	170	$0+$	$2+$	1.07	0
Ta^{181}	134	210	$\frac{7}{2}+$	$\frac{1}{2}+$	0	0
Ta^{181}	345	430	$\frac{7}{2}+$	$\frac{5}{2}+$	−1.99	0
Os^{186}	137	220	$0+$	$2+$	−0.026	0.348
Hg^{197}	133	220	$\frac{1}{2}-$	$\frac{5}{2}-$	−0.279	0.006
Pb^{206}	374	450	$0+$	$2+$	0.071	1.27

The energy of the incoming neutron was chosen to be about 80 kev above the threshold. This means that l_2 is restricted to the values 0 and 1. Higher energies would quickly increase the number of l-values and would complicate the computation of $W_E(\vartheta)$ considerably.

Since the spin and parity assignments are well established by other experiments, an experimental check of the given angular distributions would show how well the statistical model accounts for the given situation.

The author wishes to thank Professor Feshbach sincerely for suggesting this problem.

[1] G. Racah, Phys. Rev. **62**, 438 (1942).
[2] Biedenharn, Arfken, and Rose, Phys. Rev. **83**, 586 (1951).
[3] M. Goldhaber and A. W. Sunyar, Phys. Rev. **83**, 906 (1951).
[4] H. Feshbach and V. F. Weisskopf, Phys. Rev. **76**, 1550 (1949).

Internal Absorption of Fluorescent Light in Large Plastic Scintillators*

C. N. CHOU
Department of Physics, University of Chicago, Chicago, Illinois
(Received June 2, 1952)

THE preparation and performance of comparatively small plastic scintillators have been reported by several authors.[1-3] We have made some plastic scintillators of large dimensions by impregnating styrene monomer with various fluorescent substances

TABLE I. Pulse sizes (in arbitrary units) observed with a Co^{60} source.

	Phosphor	Distance of the path of radiation through the sample from the surface of the photomultiplier: 1 cm	10 cm	20 cm
a	Anthracene in polystyrene	0.6	0.5	0.5
b	p-terphenyl in polystyrene	1.4	0.8	0.5
c	Phenylcyclohexane solution	1.6	1.6	1.5

before polymerization. No catalyst was used in the process. In a series of experiments, the samples had the form of a cylindrical rod 3.5 cm in diameter and 20 cm long. The pulse sizes were observed in an oscilloscope from the output of a 5819 photomultiplier attached to one end of the rod. Except for this end, the rod was wrapped with 0.133-mm thick aluminum foil as a reflecting surface in order to improve light collection. A narrow beam of γ-ray from a Co^{60} source passed through the rod perpendicularly to its axis at various distances from the surface of the photomultiplier. The results are summarized in Table I. Cosmic rays from a coincident counter telescope and a soft x-ray beam from a dental machine were also used as sources of irradiation and gave similar results. From the table we can see that there is little internal absorption of fluorescent light in the cases of a and c, while b shows considerable absorption at greater lengths. The concentration of the anthracene in polystyrene was about 3 percent. No great difference in internal absorption was observed in varying the concentration from 2–5 percent. The concentration of p-terphenyl in polystyrene was about 2 percent. The addition of about 0.01 percent diphenylhexatriene made no significant difference in the large internal absorption as shown in Table I. When the concentration of p-terphenyl was raised to 4 percent, some part of the plastic became less transparent in appearance. In the table the results for liquid phenylcyclohexane solution (plus 0.3 percent p-terphenyl and 0.001 percent diphenylhexatriene) of the same dimensions as the plastic rods are also included. An anthracene crystal 3 cm in diameter and 3.3 cm in length was also used and gave a pulse size of 5.4 (in the same units as used in Table I). A plastic scintillator consisting of 3 percent anthracene in polystyrene, 4.1 cm in diameter and 30 cm long (this is the maximum length that has been investigated), showed relatively small absorption (less than 15 percent) of the light output throughout the

whole length. This makes it possible to use scintillators of this kind (a) in cosmic-ray telescopes, (b) for triggering cloud chambers, and (c) for locating weak radioactive sources, etc. It might be mentioned that a sample of 2 percent pyrene in polystyrene was found to be comparable in performance to anthracene in polystyrene for small thicknesses of the scintillator. However, it showed greater internal absorption at greater lengths.

The author wishes to express his sincere thanks to Professor Marcel Schein for the hospitality extended to him to work in the Cosmic Ray Laboratory. He also thanks the Department of State for a grant.

* Assisted by the joint program of ONR and AEC.

[1] M. G. Schor and F. L. Torney, Phys. Rev. **80**, 474 (1950).
[2] M. G. Schor and E. C. Farmer, Phys. Rev. **81**, 891 (1951).
[3] W. S. Koski, Phys. Rev. **82**, 230 (1951).

Relative Yields of Photonuclear Reactions

L. S. EDWARDS AND F. A. MACMILLAN
Synchrotron Laboratory, Queen's University, Kingston, Ontario
(Received June 2, 1952)

RELATIVE yields for 41 photonuclear reactions have been measured by the method of radioactive end-products. The yields were defined, following Perlman and Friedlander,[1] as "yield = saturation activity of product per milligram atom of parent isotope, divided by saturation activity of monitoring reaction."

The materials, in the form of thin metal foils, were irradiated in the x-ray beam from the 70-Mev Queen's synchrotron. Each foil was sandwiched between two thin polystyrene sheets, which monitored the exposure through the $C^{12}(\gamma, n)C^{11}$ reaction. Activities of the foils and monitors were measured by a thin end-window G-M tube in a standard geometry. The chemical purity of all samples was checked by spectrographic analysis. Some materials were used as simple compounds in powder form. Yields determined in the powder and foil arrangements were related by observing the $C^{12}(\gamma, n)C^{11}$ reaction in powdered and solid graphite and the $In^{115}(\gamma, n)In^{114}$ reaction in indium sesqui-oxide and indium foil. Short-lived activities were investigated with an apparatus which dropped the sample to a well-shielded counter below the x-ray beam.

Saturation activities were corrected for self-absorption of β-rays in the sample, absorption in the counter end-window, for alternative modes of decay such as K-capture, and for counts due to nuclear γ-rays, internal conversion electrons, etc. An estimation of the accuracy of the yields is sometimes very difficult due to the varied factors affecting each result. By giving careful attention to good monitoring, thorough determination of all activities present, reproduction of geometry, and accurate analysis for saturation activities, the standard deviation from the mean for individual runs was reduced to less than ± 3 percent (often for foil weights differing by as much as a factor of six). As each reported yield is the result of about eight experiments, the yield values should be accurate to about ± 2 percent. However, allowance must be made for possible large errors in individual cases due to poor corrections for K-capture, etc.

73 reactions were identified in these 22 elements; uncertainties or complications in decay schemes confined yield calculations to 44 of them. These yields are listed in Table I.

The definition of yield given above leads to the following expression for the relative yields Y_1 and Y_2 of two reactions:

$$\frac{Y_1}{Y_2}=\frac{{}^{P}R_1 \int \sigma_1 dE}{{}^{P}R_2 \int \sigma_2 dE},$$

where ${}^{P}R$ represents the relative number of photons/Mev at the reaction resonance energy in the x-ray spectrum, and $\int \sigma dE$ is the integrated cross section of the reaction. A determination of the x-ray spectrum of this thick-target synchrotron, recently made by McDiarmid[3] using emulsion techniques, indicated that the photon spectrum is essentially flat in the region 10–30 Mev. Since this range includes the resonance energies of the common photonuclear reactions, the quantities ${}^{P}R_i$ should then be equal and the yields directly proportional to integrated cross sections. Assuming this to be the case, the value of $\int \sigma dE = 0.047$ Mev barns for the $C^{12}(\gamma, n)C^{11}$ reaction, as measured by Haslam, Johns, and Horsley,[3] was used to calculate cross sections for all reactions (see Table I). Use of this reference standard and of the empirical spectrum introduces an added probable error of roughly ± 15 percent in the absolute values of the cross sections. The good agreement of our values with the best independently measured cross sections (column 6, Table I) is additional evidence for the flat photon spectrum.

TABLE I. Relative yields and integrated cross sections.

Z	Reaction	Half-life	Relative yield	Calculated values $\int \sigma dE$ (Mev-barns)	Previous values $\int \sigma dE$ (Mev-barns)
6	$C^{12}(\gamma, n)C^{11}$	20.5 min	0.100	0.047	0.047[a,b]
7	$N^{14}(\gamma, n)N^{13}$	10.1 min	0.035	0.017	
8	$O^{18}(\gamma, n)O^{17}$	118 sec	0.400	0.18	
9	$F^{19}(\gamma, n)F^{18}$	112 min	0.382	0.11	
12	$Mg^{26}(\gamma, n)Mg^{25}$	11.4 sec	0.152	0.072	
13	$Al^{27}(\gamma, n)Al^{26}$	6.3 sec	0.170	0.080	
17	$Cl^{37}(\gamma, n)Cl^{36}$	33 min	0.123	0.058	
19	$K^{39}(\gamma, n)K^{38}$	7.5 min	0.162	0.076	
22	$Ti^{48}(\gamma, n)Ti^{47}$	2.9 hr	0.925	0.44	
26	$Fe^{56}(\gamma, n)Fe^{55}$	8.9 min	0.836	0.39	0.42[c]
28	$Ni^{58}(\gamma, n)Ni^{57}$	36.7 hr	0.497	0.23	0.33[c]
29	$Cu^{63}(\gamma, n)Cu^{62}$	10.1 min	1.37	0.64	0.63[a,b]
	$Cu^{65}(\gamma, n)Cu^{64}$	12.9 hr	2.47	1.16	1.2[a,d]
30	$Zn^{64}(\gamma, n)Zn^{63}$	38 min	1.27	0.60	0.83[c]
41	$Nb^{93}(\gamma, n)Nb^{92}$	10.1 day, 21.6 hr	0.111	0.052	
42	$Mo^{92}(\gamma, n)Mo^{91}$	15.5 min	2.28	1.07	
	$Mo^{100}(\gamma, n)Mo^{99}$	68 hr	3.54	1.67	
45	$Rh^{103}(\gamma, n)Rh^{102}$	210 day	>1.42	>0.67	
46	$Pd^{110}(\gamma, n)Pd^{109}$	13.8 hr	8.64	4.1	
47	$Ag^{107}(\gamma, n)Ag^{106}$	24.0 min	3.27	1.54	
	$Ag^{109}(\gamma, n)Ag^{108}$	2.4 min	3.53	1.66	1.65[a,d]
49	$In^{115}(\gamma, n)In^{114}$	72 sec, 50 day	7.10	3.3	
78	$Pt^{198}(\gamma, n)Pt^{197}$	3.4 day, 18 hr	10.2	4.8	
79	$Au^{197}(\gamma, n)Au^{196}$	5.6 day, 14 hr	8.65	4.1	
12	$Mg^{26}(\gamma, p)Na^{25}$	59 sec	0.196	0.092	
12	$Mg^{26}(\gamma, p)Na^{25}$				
22	$Ti^{46}(\gamma, pn)Na^{24}$	14.9 hr	0.486	0.23	
22	$Ti^{46}(\gamma, p)Sc^{45}$	3.4 day	0.416	0.20	
22	$Ti^{50}(\gamma, p)Sc^{49}$	54 min	0.244	0.12	
26	$Fe^{57}(\gamma, p)Mn^{56}$	2.8 hr	0.586	0.28	
28	$Ni^{62}(\gamma, p)Co^{61}$	1.7 hr	0.378	0.18	
30	$Zn^{68}(\gamma, p)Cu^{67}$	58 hr	0.40	0.19	
42	$Mo^{100}(\gamma, p)Nb^{99}$	68 min	0.359	0.17	
46	$Pd^{108}(\gamma, p)Rh^{107}$	25.7 min	0.326	0.15	
26	$Fe^{56}(\gamma, pn)Mn^{55}$	21 min	0.222	0.11	
30	$Zn^{64}(\gamma, pn)Cu^{63}$	10.1 min	0.25	0.12	
30	$Zn^{64}(\gamma, pn)Cu^{63}$	12.9 hr	0.65	0.31	
42	$Mo^{92}(\gamma, pn)Nb^{91}$	16.5 hr	0.622	0.29	
29	$Cu^{63}(\gamma, 2n)Cu^{61}$	3.4 hr	0.154	0.073	
30	$Zn^{64}(\gamma, 2n)Zn^{62}$	9.5 hr	0.073	0.034	
13	$Al^{27}(\gamma, 2p)Na^{25}$	59 sec	0.00476	0.0022	
45	$Rh^{103}(\gamma, 2p)Tc^{101}$	16 min	0.0050	0.0024	
13	$Al^{27}(\gamma, 2pn)Na^{24}$	14.9 hr	0.0065	0.0031	
27	$Co^{59}(\gamma, 2pn)Mn^{56}$	2.7 hr	0.0047	0.0022	

[a] Independent absolute determinations.
[b] Haslam, Johns, and Horsley, Phys. Rev. **82**, 270 (1951).
[c] L. Katz *et al.*, Phys. Rev. **82**, 271 (1951).
[d] B. C. Diven and G. M. Almy, Phys. Rev. **80**, 407 (1950).

A striking feature of these results is that (γ, pn) yields, previously considered to be small,[4] are of the same order as (γ, p) yields; similarly, $(\gamma, 2pn)$ yields are of the same order as $(\gamma, 2p)$ yields.

A more detailed account of these experiments will be published in the near future. The work was carried out at the suggestion of Dr. J. A. Gray, and grateful acknowledgment is made for his interest and advice throughout; also to the National Research Council of Canada and the Ontario Research Council for bursaries held by the authors.

[1] M. L. Perlman and G. Friedlander, Phys. Rev. **74**, 442 (1948).
[3] I. B. McDiarmid (to be published).
[3] Haslam, Johns, and Horsley, Phys. Rev. **82**, 270 (1951).
[4] A. G. W. Cameron, Phys. Rev. **82**, 272 (1951).

Angular Correlation in the Reaction $B^{11}(p;\gamma_1,\gamma_2)C^{12}$†

THOMAS P. HUBBARD, JR.,* EDWARD B. NELSON, AND JAMES A. JACOBS
The State University of Iowa, Iowa City, Iowa
(Received June 2, 1952)

THICK targets of natural boron have been bombarded with 170-kev protons from the kevatron[1] at the State University of Iowa. The excited state of C^{12} resulting from this bombardment decays among other ways by the successive emission of 11.8- and 4.5-Mev gamma-rays. The angular correlation of these gamma-rays and the angular distribution of the 11.8-Mev gamma-ray has been measured. RCA 5819 photomultiplier tubes and NaI(Tl) scintillation crystals were used as the gamma-ray detectors.

The angular distribution of the 11.8-Mev gamma-ray was found to be proportional to $1+(0.23\pm0.04)\cos^2\theta$. This implies that p-wave protons are predominant in the formation of the compound nucleus. Thus, the triple angular correlation theory of Biedenharn, Arfken, and Rose[2] is applicable.

The angular correlation of the successive gamma-rays was measured in two counting geometries. In the first geometry the 4.5-Mev gamma-ray was counted parallel to the proton beam and the 11.8-Mev gamma-ray at an angle θ with respect to the proton beam. The resulting angular correlation function was found to be proportional to $1+(0.39\pm0.15)\cos^2\theta$. In the second geometry the 4.5-Mev gamma-ray was counted at right angles to the proton beam and the 11.8-Mev gamma-ray at an angle θ with respect to the proton beam and in the plane defined by the fixed counter and the proton beam. The resulting angular correlation was found to be proportional to $1-(0.2\pm0.1)\cos^2\theta$.

The spins of the proton, the ground state of B^{11}, and the ground state of C^{12} are known[3] to be 1/2, 3/2, and 0, respectively. The spin[2] of the 16.3-Mev excited state of C^{12} is 2 since this state decays[4] by both gamma-ray emission and alpha-particle emission. This leaves only the spin of the 4.5-Mev excited state of C^{12} and the relative angular momenta of the two gamma-rays unknown. The three independent measurements on the gamma-rays (the 11.8-Mev gamma-ray angular distribution and the angular correlation with two geometries) should then give experimental values for these unknown quantities. Using the theory of Biedenharn, Arfken, and Rose,[2] Professor J. M. Jauch of this department has shown that the above measurements are consistent with the spin of the 4.5-Mev excited state of C^{12} being 2, the 11.8-Mev gamma-ray being dipole radiation, and the 4.5-Mev gamma-ray being quadrupole radiation. This is in agreement with Haefner's[5] analysis of the alpha-particle model of C^{12}.

† This work was supported in part by the AEC.
* Now at Well Surveys, Inc., Tulsa, Oklahoma.
[1] W. R. Arnold, Rev. Sci. Instr. **21**, 796 (1950).
[2] Biedenharn, Arfken, and Rose, Phys. Rev. **83**, 586 (1951).
[3] See, for example, J. E. Mack, Revs. Modern Phys. **22**, 64 (1950).
[4] A. H. Morrish, Phys. Rev. **76**, 1651 (1949).
[5] R. R. Haefner, Revs. Modern Phys. **23**, 228 (1951).

High Energy Nuclear Collisions and the Fermi Model

H. MESSEL AND H. S. GREEN
University of Adelaide, Adelaide, South Australia
(Received June 3, 1952)

WE have recently[1] considered the question of correlating the differential cross section for inelastic nucleon-nucleon collisions with experimental data on the angular and radial spread of the nucleon component of the cosmic radiation. Since our results were communicated, other results[2] have been published which bear on this topic, from a different point of view. It appears to us of great interest to compare the conclusions thus reached by independent methods.

Our results showed that neither the Fermi-model,[3] nor an alternative model[4] with a differential cross section quasi-isotropic in the center-of-mass coordinates, could explain the relatively small angular and radial spreads[5–9] of the nucleon component of the cosmic radiation in the atmosphere. By a detailed mathematical analysis of the cascade processes in the nucleus and the atmosphere, we found that theory could be reconciled with experiment only by supposing that the scattered nucleons in nuclear collisions are confined to a much narrower cone than that required by the relativistic transformation. Moreover, the differential cross section must decrease something like exponentially from the forward direction to ensure that not too many particles escape at wide angles.

Hazen, Heineman, and Lennox[2] have attempted to compare the predictions of the Fermi-model with experimental data. They considered nucleon-nucleus collisions, but they did not employ a quantitative cascade theory, with the result that their numerical comparisons were of a qualitative nature only. Nevertheless, their conclusions do not differ essentially from our own. Under the most favorable conditions that they could envisage, there remained a discrepancy of almost an order of magnitude between the half-width predicted by the Fermi-model and that required by experiment.

This discrepancy would have been increased if the moments of the angular distribution had been considered instead of the number of particles within a given angle. The singularities of the Fermi distribution at 0° and 180° in the center-of-mass frame are of a very weak type which results in moments not very different from those of a quasi-isotropic distribution.[4]

Hazen *et al.* were concerned to a greater extent with the mesons than the nucleons that are generated in nuclear encounters. However, it is obvious that the distributions in the atmosphere of the two components cannot be very different.

There is thus an increasing amount of evidence that neither the quasi-isotropic distribution[4] nor the Fermi distribution can even approximately describe the facts and that some unknown process is in operation at very high energies, which results in an intense concentration of the particles scattered in nuclear collisions in the forward and backward directions.

[1] H. Messel and H. S. Green, Phys. Rev. (to be published).
[2] Hazen, Heineman, and Lennox, Phys. Rev. **86**, 198 (1952).
[3] E. Fermi, Phys. Rev. **81**, 683 (1951).
[4] H. S. Green and H. Messel, Proc. Phys. Soc. (London) **A64**, 1083 (1951).
[5] Cocconi, Cocconi Tongiorgi, and Griesen, Phys. Rev. **76**, 1020 (1949).
[6] Eidus, Alymova, and Videnskii, Dokl. Akad. Nauk (S.S.S.R.) **75**, 669 (1950).
[7] Vernov, Grigorov, and Charaklchyan, Izvest. Akad. Nauk (S.S.S.R) Ser. Fiz., **14**, 51 (1950).
[8] Eidus, Blinova, Videnskii, and Suvorov, Dokl. Akad. Nauk (S.S.S.R) **74**, 477 (1950).
[9] G. M. Branch, Phys. Rev. **84**, 147 (1951).

Measurement of Short Beta-Decay Lifetimes*

R. B. HOLT,† R. N. THORN, AND R. W. WANIEK
Cyclotron Laboratory, Harvard University, Cambridge, Massachusetts
(Received May 28, 1952)

A NEW method for measuring the lifetimes of isotopes has been developed. The isotopes are produced in the bombardment of various targets by the internal proton beam of the Harvard FM cyclotron. The decay particles are detected by a crystal, Lucite probe, and photomultiplier arrangement. The target is located in the median plane about four inches directly below the detecting crystal. Many of the decay particles follow helical paths in the magnetic field through an opening cut in a one-inch thick brass cap shielding the anthracene crystal. An eight-foot long Lucite probe enclosed in a vacuum-tight tube collects the light flashes and conveys them to a RCA 5819 photomultiplier located outside the vacuum tank. The signal is fed from the photomultiplier to a cathode follower and from there to a linear amplifier in the control room. The pulses from the discriminator output go into an integrating circuit; the resulting current is registered on

linear roll paper by a fast recorder. All circuits are left on continuously. The target is irradiated, the cyclotron is turned off, and the excitation is observed immediately.

With this arrangement measurements were taken using a one-sixteenth-inch thick carbon plate as a target. Runs were made at twelve different proton energies chosen in the range between 20 and 110 Mev by varying the distance of the target from the center of the cyclotron tank. Owing to the occurrence of simple and spallation reactions, a variety of modes of disintegration was observed. By pulse-height analysis and varying the time of irradiation, additional discrimination was obtained. Previously known lifetimes as well as some new ones appeared with great consistency over various bombarding energies.

The first part of our investigation was aimed at the detection of the Li^9 isotope. The activity has been first tentatively reported by Gardner *et al.* on the basis of the detection of delayed neutrons produced according to the following scheme:[1]

$$Li^9 \rightarrow (Be^9)^* + \beta, \quad (Be^9)^* \rightarrow Be^8 + n, \quad \text{and} \quad Be^8 \rightarrow 2\alpha.$$

The half-life obtained was 168±4 msec.

By this first direct detection of the beta-decay particles a half-life of 170±5 msec has been obtained, thereby corroborating the California results. The spallation reaction leading to Li^9 is $C^{13}(p, 4p)Li^9$, with a threshold energy of about 47.5 Mev in the laboratory system.

We wish to thank Mr. R. Brown and Mr. M. Hurley for their help in evaluating the large number of decay curves.

* This work has been supported by the ONR.
† Now at the Scientific Specialties Corporation, Cambridge, Massachusetts.
[1] Gardner, Knable, and Moyer, Phys. Rev. **83**, 1054 (1951).

Atomic Beam Resonance Method for Excited States

I. I. RABI
Columbia University, New York, New York
(Received June 4, 1952)

THUS far, only long-lived or metastable states of atoms or molecules have been studied by molecular beam resonance methods. The purpose of this letter is to indicate that excited atomic or molecular levels are accessible to experimental methods quite similar to those which have been used for the ground states.[1] There is the inevitable loss in precision which arises from the fact that excited states have lifetimes of the order of 10^{-8} sec, which brings with it an inevitable line width of approximately 10 megacycles. It will, therefore, be difficult to measure hyperfine structure intervals to a higher accuracy than a fraction of a megacycle.

In essence, this new method is similar to the original investigations. However, in addition to the radio frequency field, the region of the "*C*" field is also illuminated with radiation of the principal series of the atoms under investigation. This resonance radiation brings a substantial fraction of the atoms into an upper level in which they have a lifetime of about 10^{-8} sec. When they return to the lower state by radiation there is a preference for the original hyperfine structure state from which they started, as can be shown by a simple calculation. The application of an rf field of sufficient amplitude and of appropriate resonance frequency causes transitions among the upper hyperfine structure or magnetic levels and "scrambles" the population in the upper state. Since the atoms are essentially "tagged" atoms by the deflection which they have suffered in the "*A*" field this scrambling will cause a change in refocused intensity at the detection.

To reduce background, the "*A*" and "*B*" fields are so arranged as to produce equal deflections and of the same sign at the detector. In this way only very few atoms reach the detector. However, when the beam is illuminated with the optical radiation, some of the atoms which have absorbed this radiation come down to the ground state with moments pointing in a direction opposite to the original and are, therefore, focused onto the detector by the "*B*" field. When the rf is resonant, this beam intensity is changed.

By the interposition of slits or obstacles right after the "*A*" or after the "*B*" field, or both, one can select certain specific states which are to be subjected to the optical excitation, or shut out atoms which have undergone specific transitions, procedures which should prove to be helpful in the interpretation of results, or in the resolution of overlapping lines.

These general methods are capable of wide extension. To mention a few, it should be possible to study isotope shifts by these methods by illuminating with the line of one isotope and, by means of magnetic or electric fields, moving the line of the other isotope into a frequency region which can absorb this radiation; it should be possible to produce atomic states which are too high for temperature excitation by illuminating the ground state with appropriate radiation and studying the atoms which fall into this upper state; double optical excitation can make accessible states other than those which can be reached by absorption of the series alone.

The method here suggested is related to the methods which use the depolarization of resonance radiation.[2] Our present method, however, has the general advantages which atomic and molecular beam methods have of greater simplicity and control of the details of the complicated processes which are involved when a multiplicity of states exists as in hyperfine structure, as well as a better ratio of signal to noise.

This method is being applied to the study of the alkalis, particularly Rb in the first *P* level. It has already been found quite easy to cause 20 percent of the atoms to make transitions by optical excitation with a very simple source of resonant radiation.

Further details will be published in a later paper.

[1] Kellog, Rabi, and Zacharias, Phys. Rev. **50**, 472 (1936); Rabi, Millman, Kusch, and Zacharias, Phys. Rev. **55**, 526 (1939); Kusch, Millman, and Rabi, Phys. Rev. **57**, 765 (1940).
[2] E. Fermi and F. Rasetti, Nature **115**, 764 (1925); Z. Physik **33**, 246 (1925); F. Bitter, Phys. Rev. **76**, 833 (1949); J. Brossel and A. Kastler, Compt. rend. **229**, 1213 (1949); M. L. Pryce, Phys. Rev. **77**, 136 (1949); Brossel, Sagalyn, and Bitter, Phys. Rev. **79**, 196, 225 (1950); F. Bitter and J. Brossel, Phys. Rev. **85**, 1051 (1952); J. Brossel and F. Bitter, Phys. Rev. **86**, 308 (1952).

The Directional Correlation of the Ni^{60} γ-γ Cascade

H. AEPPLI, H. FRAUENFELDER,* E. HEER, AND R. RÜETSCHI
Swiss Federal Institute of Technology, Zürich, Switzerland
(Received May 26, 1952)

THE directional correlation of the γ-γ cascade of Ni^{60} was first investigated by Brady and Deutsch,[1] who report their measurements to be consistent with the correlation function $W(\theta)$ for the cascade $4(E2)2(E2)0$: $W(\theta) = 1 + \frac{1}{8}\cos^2\theta + (1/24)\cos^4\theta$; anisotropy $A = [W(180°)/W(90°)] - 1 = 0.167$. The assignment of the radiation type, *E2*, stems from the measurement of the direction-polarization correlation[2] and from the determination of the internal conversion coefficients.[3] The conclusions of Brady and Deutsch were confirmed by several other investigators.[4–7]

Using the apparatus described in a forthcoming paper,[8] we remeasured the directional correlation of the Ni^{60}-cascade. The scintillation counters were shielded with lead (0.5 cm in front, 1.0 cm laterally) against scattered quanta and annihilation radiation from internal pair production. The scattering correction for the anisotropy, calculated and tested experimentally with Fe^{59} γ-rays,[9] amounts to less than 0.003.

The measurements made with the radioactive source consisting of a spherical piece of pile-irradiated metallic cobalt (diameter ~0.02 cm) yield an anisotropy $A = 0.148 \pm 0.003$. Additional measurements with sources prepared chemically [$CoSO_4$, solid and in solutions; $K_4Co(CN)_6$], with the double stream method (imbedding materials Ag and Ni), and by electrolysis on a thin Ag wire, are all consistent with this value of the anisotropy. The weighted mean value of the anisotropy, taking into account all measurements, is $A = 0.148 \pm 0.002$. (Inspection of the investiga-

tions[1,4,6,7] shows that the values and curves reported there are also consistent with this value of the anisotropy.)

Our experimental value for the anisotropy differs from the theoretical value for the cascade $4(2)2(2)0$: $A_{\text{theor}}=0.167$. To explain the discrepancy, we considered two possibilities:

1. The assignment $4(E2)2(E2)0$ is wrong. We tried to fit all experimental data together with our value of A by assuming other spin- and parity-assignments and by taking into account mixtures of different multipole radiations. No other assignment, however, seems compatible with all known facts.

2. The directional correlation is influenced by the electron shell.[10,11] To test this assumption, we applied an external magnetic field H in the direction of the fixed counter. According to Goertzel,[12] such a field should restore the undisturbed correlation if the field strength H satisfies the relation $\mu H \gg \hbar\omega$, where μ and $\Delta\nu=\omega/2\pi c$ are the magnetic moment and the hyperfine splitting of the atom if the nucleus is in the intermediate level. (Goertzel's statement is only valid for magnetic interactions. We assume, however, that other interactions are too weak to have an appreciable effect.) The directional correlation of Ni^{60} remains, however, unchanged for field strengths H up to 8000 oersted (corresponding to inner fields of $\sim$15,000 gauss in the metallic source). This allows an estimate of the lifetime T of the intermediate nuclear state. The existence of an attenuation by the shell implies $\omega T\sim 1$. The failure of the external magnetic field H to restore the directional correlation means $\hbar\omega \gtrsim \mu H$. These two conditions (with $\mu\sim\mu_{\text{Bohr}}$) give an upper limit for T: $T\lesssim 10^{-11}$ sec. If one assumes further an upper limit for the magnitude of the hyperfine splitting, $\Delta\nu<1$ cm^{-1}, one gets $T\sim 10^{-11}$ sec. This value for the lifetime of the first excited state of Ni^{60} is in essential agreement with the value calculated from the Weisskopf formula[13] for an electric quadrupole transition.

From the present experiments it is, however, impossible to decide if the discrepancy between theoretical and experimental anisotropy is caused by the influence of the electron shell or if other effects have to be considered. Before definite conclusions can be drawn, the measurements have to be repeated with stronger external magnetic fields. The precise determination of the directional correlation of other $4(E2)2(E2)0$ cascades would perhaps also give more information.

We wish to thank Professor P. Scherrer for his continued interest, Dr. M. R. Schafroth and Mr. K. Alder for many valuable discussions, and Mr. R. Hiltbrunner for his assistance during the measurements.

* Now at the University of Illinois, Urbana, Illinois.
[1] E. L. Brady and M. Deutsch, Phys. Rev. **78**, 558 (1950).
[2] F. Metzger and M. Deutsch, Phys. Rev. **78**, 551 (1950).
[3] Waggoner, Moon, and Roberts, Phys. Rev. **80**, 420 (1950).
[4] J. R. Beyster and M. L. Wiedenbeck, Phys. Rev. **79**, 411 (1950).
[5] R. M. Steffen, Phys. Rev. **80**, 115 (1950).
[6] H. E. Petch and M. E. Johns, Phys. Rev. **80**, 478 (1950).
[7] B. L. Robinson and L. Madansky, Phys. Rev. **84**, 604 (1951).
[8] Aeppli, Albers-Schönberg, Frauenfelder, and Scherrer, Helv. Phys. Acta (to be published).
[9] F. R. Metzger, Phys. Rev. **85**, 727 (1952).
[10] H. Frauenfelder, Phys. Rev. **82**, 549 (1951).
[11] Aeppli, Bishop, Frauenfelder, Walter, and Zünti, Phys. Rev. **82**, 550 (1951).
[12] G. Goertzel, Phys. Rev. **70**, 897 (1946).
[13] V. F. Weisskopf, Phys. Rev. **83**, 1073 (1951).

Superconductivity in the Cobalt-Silicon System

B. T. Matthias
Bell Telephone Laboratories, Murray Hill, New Jersey
(Received June 4, 1952)

A COBALT–SILICON melt with 75 atomic percent Si has been found to become superconducting at 1.33°K. This was determined both by measuring the magnetic flux change and by observing the Meissner effect. The bulk properties thus obtained indicate that about half of the sample becomes superconducting. X-ray analysis[1] shows two phases: pure silicon and $CoSi_2$ in roughly equal proportions.

Whereas it has been impossible to detect superconductivity at temperatures above 1.27°K in pure $CoSi_2$, measurements on melts with more than 75 atomic percent Si indicate, from the volume of the sample which becomes superconducting, that $CoSi_2$ is the superconducting phase. This suggests that the transition temperature in $CoSi_2$ has been slightly raised in our samples by the strain resulting from its rapid crystallization into the $CoSi_2$ in an excess of silicon. This suggestion is further supported by the fact that annealing a melt with 75 atomic percent Si lowered the transition temperature.

As cobalt is ferromagnetic and silicon is a semiconductor at best, the probability is low that either element is a superconductor, even at the lowest temperatures. Superconducting compounds of nonsuperconducting elements have thus far been limited to some borides, carbides, nitrides of molybdenum and tungsten, CuS, and a large number of Bi-compounds. In the periodic system, however, Mo, W, Cu, and Bi are very close to the two groups of superconducting elements. This has given rise to the hypothesis[2] that superconducting elements or compounds are essentially confined to these two regions in the periodic table. The present example indicates that this hypothesis is not reliable.

[1] I want to thank Dr. E. A. Wood and Professor W. H. Zachariasen for their help and advice in this analysis.
[2] B. T. Matthias and J. K. Hulm, Phys. Rev. (to be published).

A Quantitative Determination of the Abundance of Telluric CO above Columbus, Ohio*

J. H. Shaw and J. N. Howard
Department of Physics and Astronomy, Ohio State University, Columbus, Ohio
(Received April 9, 1952)

LINES of the 0–1 absorption band of CO at 4.7μ have been observed in solar spectra recorded at Columbus, Ohio,[1,2] and at the Jungfraujoch, Switzerland,[3,4] and it has been shown that the absorption is of telluric origin. However, recent measurements made by Goldberg, McMath, Mohler, and Pierce[5,6] at Lake Angelus, Michigan, and Mt. Wilson, California, who have studied the solar spectrum in the CO overtone region at 2.3μ, have so far failed to reveal any absorption which can be ascribed to telluric CO. Thus, estimates of the average amount of telluric CO above these various geographic locations vary very widely, and in addition daily variations in the amount of CO present has also been reported.[1,4]

In order to make an accurate measurement of the amount of atmospheric CO above Columbus, Ohio, observations on the line $R(2)$ of the fundamental band of CO in the solar spectrum were made on several days during January and February, 1952. The region of the solar spectrum studied is shown in Fig. 1, and it is seen that the $R(2)$ line, marked with an arrow, appears to be free of other strong interfering lines. Measurements of the total absorption of this line for various solar altitudes are shown in Fig. 2.

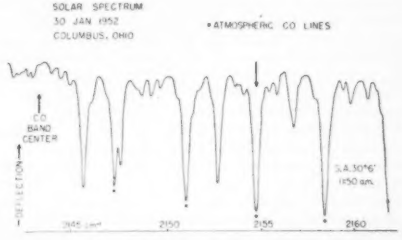

FIG. 1. The solar spectrum near 4.7μ.

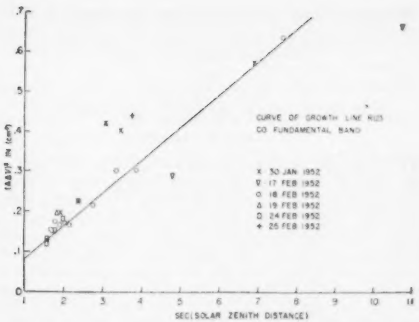

FIG. 2. Curve of growth of line $R(2)$ of the CO fundamental band.

The scatter of the points is due in part to experimental error, but it may also be due to variations in the amount of CO.

If laboratory data are available it is possible to calculate the amount of atmospheric CO from the curve shown in Fig. 2, assuming that the CO is uniformly distributed in a suitable model atmosphere. Goldberg[7] has described in detail how such a calculation can be performed, and we have made the necessary laboratory studies. Our measurements indicate that the average amount of telluric CO above Columbus, Ohio on the days when spectra were obtained was 0.09 atmos-cm per air mass. This is somewhat less than the amount suggested by Goldberg *et al.*[6] from an inspection of our published tracings.[2]

The solar spectrum from 4.5 to 5μ is being remapped using considerably higher resolution than previously reported, and a large number of new lines have been observed. Many of these lines are weak and do not vary in intensity with solar altitude, a result which indicates that they are of solar origin. The frequencies of most of these solar lines agree well with the calculated frequencies of lines of CO bands near 5μ due to solar CO recently predicted by Goldberg *et al.*[6] These calculated frequencies were obtained from the improved constants of the CO molecule published by Plyler, Benedict, and Silverman.[8]

It should be noted here that, if one assumes the amount of solar CO estimated by Goldberg *et al.*, it can be shown that the solar contribution to the observed absorption of the line $R(2)$ is negligible compared with the telluric absorption.

* Supported in part by a contract between the Geophysics Research Division of the Air Force Cambridge Research Center and the Ohio State University Research Foundation.
[1] M. Migeotte, Phys. Rev. **75**, 1108 (1949).
[2] Shaw, Chapman, Howard, and Oxholm, Astrophys. J. **113**, 268 (1951).
[3] M. Migeotte and L. Neven, Physica **16**, 123 (1950).
[4] M. Migeotte and L. Neven, "Zwanzig Jahre Hochalpine Forschungsstation Jungfraujoch," Station Scientifique du Jungfraujoch, Switzerland, (1951).
[5] Goldberg, McMath, Mohler, and Pierce, Phys. Rev. **85**, 140 (1952).
[6] Goldberg, McMath, Mohler, and Pierce, Phys. Rev. **85**, 481 (1952).
[7] L. Goldberg, Astrophys. J. **113**, 567 (1951).
[8] Plyler, Benedict, and Silverman, J. Chem. Phys. **20**, 175 (1952).

Second Sound in He^3-He^4 Mixtures*

P. J. PRICE
Department of Chemistry, Duke University, Durham, North Carolina
(Received June 2, 1952)

THE hydrodynamics of superfluid mixtures of He^3 and He^4 has been worked out on the assumptions: (a) that the two-fluid dynamics still applies; and (b) that the He^3 atoms have the average velocity $\mathbf{v}_n$, i.e., move entirely with the normal fluid. The acceleration of the superfluid is then given by the gradient, not of the Gibbs function, but of the chemical potential of the He^4 component. For large concentrations of He^3, an appreciable coupling of the temperature and pressure waves is predicted. If we make use of Henry's law[1] for the partial vapor pressures p_3 and p_4, then for small concentrations X the general formula for the velocity u_2 of second sound reduces to

$$u_2^2=\left(\frac{\rho_s}{\rho_n}\right)\left\{\frac{T}{C}\left[S(0)+\frac{kX}{m_4}\frac{d}{dT}(a_4T)\right]^2+\frac{kTX}{m_4}\right\}, \qquad (1)$$

where $C=C(X)$, $\rho_n=\rho_n(X)$, etc., and $a_4=(p_4^0-p_4)/p_4^0X$. This result reduces to Pomeranchuk's[2] if we set $a_4=1$, that is, assume perfect ideality of the solution. However, analysis of the experimental values[1] of vapor pressures shows this assumption to be far from the truth. Using these data, and those of Lynton and Fairbank[3] for $u_2(X)$, we find that for $X=5.8\times10^{-2}$ the effect of the He^3 on ρ_n may be represented, from 1.3° to 1.6°, by the formula

$$\frac{\rho_n(X)}{\rho(X)}=\frac{\rho_n(0)}{\rho(0)}+\frac{\rho_s(0)}{\rho(0)}\left(\frac{\mu}{m_4}\right)X, \qquad (2)$$

where $\mu=5.7m_4$. The mixture evidently behaves in this temperature range as though five He^4 atoms were "condensed" on each He^3 atom, and the rest of the liquid were unaffected. A detailed account of the theory will be published in due course.

* Under contract with the ONR.
[1] H. S. Sommers, Jr. (to be published). (Kindly communicated, in advance of publication, by the author to Professor I. London.)
[2] I. Pomeranchuk, J. Exptl. Theor. Phys. (U.S.S.R.) **19**, 42 (1949).
[3] E. A. Lynton and H. A. Fairbank, Phys. Rev. **80**, 1043 (1950).

Interpretation of the Long-Range Protons from the Deuteron Bombardment of Be^9

W. W. TRUE AND L. DIESENDRUCK
Department of Physics, University of Rhode Island, Kingston, Rhode Island
(Received June 4, 1952)

THE experimental curves of the angular distribution of the long-range protons resulting from the deuteron bombardment of Be^9 at energies from 1.00 Mev to 2.20 Mev have been obtained by Canavan.[1] Analysis of the curves into a cosine power series or a series of Legendre polynomials shows that they can be fitted within experimental error only by employing both even and odd power terms and by including the sixth power.

The assumption of deuteron penetration and compound nucleus formation results in four spin states with negative parity and five spin states with positive parity which are possible for the compound nucleus, if no values of orbital angular momentum quantum number higher than 4 are included for the initial and final systems and the following properties are assumed:

$$_4Be^9: \quad I=3/2, \quad \text{odd parity}$$
$$_4Be^{10}: \quad I=0, \quad \text{even parity.}$$

At least two states of the compound nucleus must be considered and the number of combinations which give the necessary complexity of the angular distribution curves is severely limited by the requirement that the quantum numbers of the orbital angular momenta of the initial state, the spins of the compound state, and the orbital angular momenta of the final state each add at least to six.[2]

Calculation of the barrier penetration factors for the orbital angular momenta involved shows that the ratio of the factors for the terms giving the higher complexity to those giving the lower complexity is of the order 10^{-2} or 10^{-4} in the lower energy region. In order to obtain the necessary complexity in the final angular distribution it is, therefore, necessary to assume that the other factors of the term, which essentially involve the matrix elements of the interaction of the incoming and outgoing nucleons with the nucleus, differ in an inverse ratio. The assumption that there

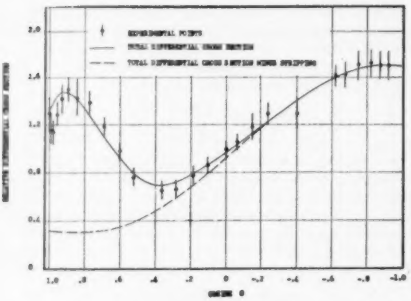

FIG. 1. Comparison of long range proton differential cross section from $Be^9(d, p)Be^{10}$ with calculated stripping curve for $l_n = 1$.

are such unusually large ratios of the matrix elements to compensate for the decreased penetrability of the necessary higher orbital angular momenta can be avoided by considering the possibility of a stripping process for the deuteron. In a stripping process neither the incoming deuteron nor the outgoing proton need penetrate as far into the potential barrier, and higher orbital angular momenta can participate.

The angular distribution of the protons from a deuteron stripping process has been calculated by Butler[3] neglecting the effects of the Coulomb potential. The distribution obtained depends, in addition to the energies involved, on the angular momentum l_n which the absorbed neutron adds to the initial nucleus. The alpha-particle model for the Be nuclei under consideration has recently been discussed by Haefner,[4] and provides the assumption that the angular momentum quantum number of the additional neutron which is added to Be^9 to give Be^{10} in this reaction must be 1, since this, together with the neutron spin, provides for the change from spin 3/2 to 0 and for the parity change. Calculation of the proton angular distribution curves by Butler's methods for the values of the energy and Q involved, and for $l_n = 1$, gives curves which have a characteristic maximum at a small forward angle and agree well with the initial peak observed in the curves obtained by Canavan. Using an arbitrary constant multiplicative factor the calculated stripping curve can be subtracted from the experimental points and the resulting smooth remainder curve shows a marked decrease in complexity from the sixth to the fourth power of the cosine. Figure 1 shows a comparison between the curve obtained by adding the calculated stripping curve to the smoothed-out remainder curve, designated as Total Differential Cross Section, and the experimental points. The agreement is good and it may be noted that the maximum of the experimental curve is shifted towards larger angles by a few degrees.

A recent investigation of the same reaction by Black[5] at much higher energies confirms the result that the angular momentum quantum number of the added neutron is 1 and also shows a shift between the calculated and observed maxima which may be interpreted as the effect of the Coulomb repulsion neglected in the calculations. It may, therefore, be concluded that the forward peak observed in the angular distributions even at low energies is due to the stripping reaction and that the remaining curve, which represents a sum of a term referring only to compound nucleus formation and one due to interference between compound nucleus formation and stripping, is lowered in complexity and therefore not as severely affected by penetrability difficulties.

[1] F. L. Canavan, S. J., thesis, Catholic University of America (1952); Phys. Rev. **87**, 136 (1952).
[2] L. Diesendruck, thesis, Johns Hopkins University (1950); C. N. Yang, Phys. Rev. **74**, 764 (1948).
[3] S. T. Butler, Proc. Roy. Soc. (London) **A208**, 559 (1951).
[4] R. R. Haefner, Revs. Modern Phys. **23**, 228 (1951).
[5] C. F. Black, Phys. Rev. **87**, 205 (1952). The value $l_n = 0$ for the ground state of the $Be^9(d, p)Be^{10}$ reaction given in this abstract is a misprint. Private communication confirms that $l_n = 1$ is the correct result.

Neutrons from Deuteron Bombardment of N^{14}†

WILLIAM B. ROSE AND EMMETT L. HUDSPETH,
University of Texas, Austin, Texas,
AND
N. P. HEYDENBURG,
Department of Terrestrial Magnetism, Carnegie Institution of Washington, Washington, D. C.
(Received May 12, 1952)

THE neutron spectrum from the reaction $N^{14}(d, n)O^{15}$ has been recently studied by Gibson and Livesey,[1] who found only one group of neutrons from this reaction at a bombarding energy of 930 kev. Earlier work[2,3] had led to the conclusion that two groups of neutrons were emitted in this reaction, corresponding to Q-values of 5.1 and 1.1 Mev. Subsequently, it was concluded by Hudspeth and Swann[4] that the low energy group reported by them was actually produced by deuteron bombardment of aluminum, and the neutrons from $N^{14}(d, n)O^{15}$ were found to be associated with only one Q-value for Q greater than a few tenths of a Mev. The value of this reaction as a source of neutrons intermediate in energy to those produced in the $d-d$ and $d-t$ reactions has been emphasized.[5]

We have now made a more complete study of this reaction, utilizing the statitron at the Carnegie Institution of Washington. Targets of NH_4NO_3 of thickness about 300 kev were bombarded with deuterons for approximately 15,000 microcoulombs at 1.7 Mev. The neutrons produced in the reaction were recorded in Ilford C-2 photographic emulsions, which were placed at 0° and at 90° to the bombarding beam. The plates were developed and analyzed with a microscope in the conventional manner; all recoil proton tracks within 12° of the direction of the neutrons emitted by the target were counted. Corrections were applied for the variation of the $n-p$ cross section with energy, for the probability that tracks remain in the emulsion over their entire lengths, and for inverse square decrease of track density with distance from target. The resulting data are shown in Fig. 1. The errors indicated are probable errors based on number of tracks observed in the corresponding energy interval.

It is believed that two groups of neutrons were observed at our bombarding energy which may be ascribed to $N^{14}(d, n)$. These correspond to Q-values of approximately 5.1 and 0.2 Mev, indicating an excited state in O^{15} at approximately 4.9 Mev. (The lowest excited level in the mirror nucleus N^{15} is at 5.5 Mev.) The low energy group which we found would not have been observed by Gibson and Livesey[1] at their bombarding voltage.

The lowest energy group found at both 0° and 90° is thought to come from the reaction $C^{13}(d, n)$, since this is the expected energy of the neutrons from this reaction and since carbon is apparently a universal contaminant in such systems. In a separate experiment, we checked this point by bombarding a pure carbon target of known thickness and observing the density of recoil proton

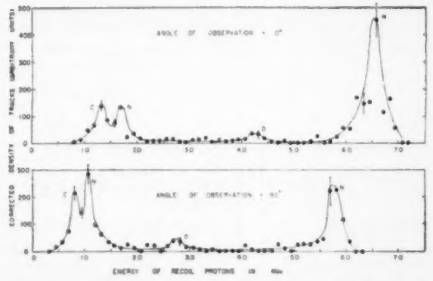

FIG. 1. Neutron groups observed from bombardment of NH_4NO_3. The groups marked C, N, and D are thought to arise from $d-n$ reactions in carbon, nitrogen, and deuterium, respectively.

tracks produced in photographic plates; the N^{13} activity of the bombarded target was also quantitatively followed. When targets of NH_4NO_3 were bombarded, the N^{13} activity (produced by bombardment of carbon contaminant) was again followed. The activity found in the latter case was in satisfactory correspondence to the density of the proton recoil tracks in the lowest energy group shown at 0° and at 90° in Fig. 1. We therefore conclude that our assumptions are correct regarding carbon.

A group of tracks was also observed with maximum energy of 4.5 Mev in plates placed at 0° and at approximately 3.0 Mev in plates at 90°. These apparently represent neutrons which come from the $d-d$ reaction. A deuterium target is of course built up during bombardment, but absorption of deuterium on the surface of the silver plate is probably more important. The "effective bombarding voltage" can be computed by assuming the 4.5-Mev group in the 0° plate does arise from $d-d$; this implies an effective bombarding voltage of 1.3 Mev (which is nearly equal to our bombarding voltage less the target thickness). Using this value, one may compute the energy of the neutrons from $d-d$ which should be observed at 90°; this is 2.8 Mev, in satisfactory agreement with our observations at this angle. The error associated with the number of tracks which we observed in this region make angular distribution comparisons of little value.

We conclude that the Q-values associated with $N^{14}(d, n)$ are 5.1 and 0.2 Mev, and that no other Q-value which leads to neutron yields of more than about 5 percent of the yield corresponding to $Q=5.1$ Mev is present.

Frequent changing of the easily prepared NH_4NO_3 targets would probably enable one to reduce considerably the neutron yield from both carbon and deuterium. Further studies regarding yield and angular distribution are planned with the statitron at the University of Texas.

† Assisted by the AEC.

[1] W. M. Gibson and D. L. Livesey, Proc. Phys. Soc. (London) **60**, 523 (1948).
[2] Stephens, Djanab, and Bonner, Phys. Rev. **52**, 1079 (1937).
[3] E. L. Hudspeth and C. P. Swann, Phys. Rev. **76**, 464 (1949).
[4] Unpublished progress report from Bartol Research Foundation to ONR (1949).
[5] Hanson, Taschek, and Williams, Revs. Modern Phys. **21**, 635 (1949).

The Reactions $p+d\rightarrow\pi^++H^3$ and $p+d\rightarrow\pi^0+He^3$†

M. RUDERMAN
Radiation Laboratory, Department of Physics, University of California, Berkeley, California
(Received June 2, 1952)

THE production of positive and neutral mesons from the bombardment of deuterons by protons is a sensitive test of the charge independence hypothesis.

The isotopic spin of a nucleon (p, n) is 1/2; that of the meson (π^+, π^0, π^-) is 1. Charge independence is the assumption that the total isotopic spin is conserved so that all matrix elements are invariant to rotations in isotopic spin space. An immediate consequence is the charge independence of nuclear forces. Further consequences have been derived by various authors.[1]

The total isotopic spin of a deuteron is 0. Therefore, the initial state $p+d$ is $(J=\frac{1}{2}, m=\frac{1}{2})\equiv W_{\frac{1}{2}}^{\frac{1}{2}}$. For the reaction $p+d\rightarrow$deuteron $(T_0^0)+$nucleon $(U_{\frac{1}{2}}^{\alpha})+$meson (V_1^{β}), in order that the final state transforms like $W_{\frac{1}{2}}^{\frac{1}{2}}$, we have

$$W_{\frac{1}{2}}^{\frac{1}{2}}\rightarrow T_0^0(\sqrt{\tfrac{2}{3}}U_{\frac{1}{2}}^{-\frac{1}{2}}V_1^1+\sqrt{\tfrac{1}{3}}U_{\frac{1}{2}}^{\frac{1}{2}}V_1^0). \quad (1)$$

It follows that (as has been pointed out by Garwin[2])

$$d\sigma(p+d\rightarrow p+d+\pi^0)/d\sigma(p+d\rightarrow n+d+\pi^+)=1/2. \quad (2)$$

The isotopic spin of (H^3, He^3) is assumed to be 1/2, which is the same as the (p, d) system. Consequently,[3]

$$d\sigma(p+d\rightarrow He^3+\pi^0)/d\sigma(p+d\rightarrow H^3+\pi^+)=1/2. \quad (3)$$

A measurement of the ratio (3), which involves the ratio of H^3 to He^3 at any energy and angle, seems more feasible.

The cross section and angular distribution for the reactions (3) involve a more detailed description of meson production than is available at present. The gross features can be extracted from the known cross section for $p+p\rightarrow\pi^++d$. The smallness of the π^- yield from $p+d$ at 90° [4] and $p+C$ at 0° [5] implies that almost all of the π^+ production in $p-d$ collisions arises from $p-p$ rather than $p-n$ interactions.

With 345-Mev incident protons the π-meson will have 90 Mev in the center-of-mass system, and the triton will have 15 Mev. The exchange of momentum between the two protons engaged in the meson production will be about two times as large as the relative momentum between the two deuterium nucleons. This is because a triton will be produced only when, in the center-of-mass system, the incident and struck protons have roughly opposite momenta, while the neutron that does not participate in the collision directly is almost at rest. The differences in the momentum transfer and hence in distance of approach imply that the incident proton interacts more strongly with the proton of deuterium than either proton interacts with the neutron. Since the final proton and neutron of the triton that participated directly in the production are so close, we can approximate the relevant triton wave function in terms of the deuteron wave function:

$$\psi_T\left(x_1-x_2, x_3-\frac{x_1+x_2}{2}\right)\sim\frac{\psi_D(x_1-x_2)}{\psi_D(0)}\psi_T(0, x_3-x_1), \quad (4)$$

where 1 and 3 are neutron coordinates. ψ_T is chosen appropriately antisymmetrized in spin and space coordinates 1, 3 in accordance with the exclusion principle. The ratio

$$\psi_T(0, x)/\psi_D(0)$$

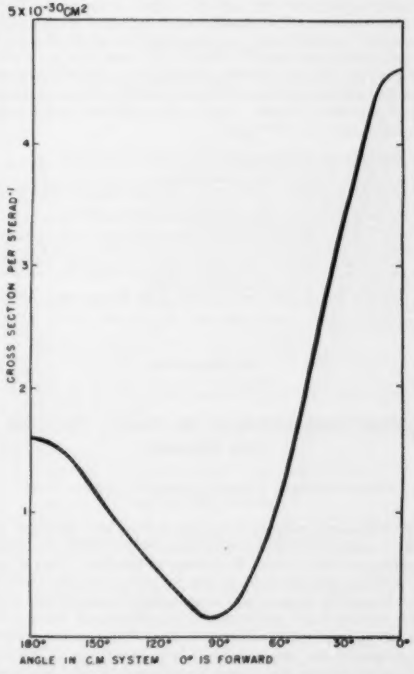

FIG. 1. Differential cross section for meson in the center-of-mass system for $p+d\rightarrow H^3+\pi^+$ with 345-Mev incident protons.

should be evaluated for d-states between 1 and 2 since the predominantly $\cos^2\theta$ angular distribution from the $(p+p\rightarrow\pi^++d)$ interaction shows that the final nucleons are mostly in d-states. In the calculations, s-state wave functions were used for simplicity in view of the crude nature of other approximations.

If one assumes that the deuterium neutron does not influence the production except for the momentum distribution it gives to the deuterium proton[6] and the interactions among the three nucleons in a triton, the cross section $\frac{d\sigma}{d\Omega}(p+d\rightarrow H^3+\pi^+)$ can be estimated in terms of $\frac{d\sigma}{d\Omega}(p+p\rightarrow\pi^++D)$ as

$$\frac{1}{3\pi_{PD}}\left|\int d\mathbf{x}\frac{\psi_T(0,x)}{\psi_D(0)}\exp\left[i\left(\frac{\mathbf{k}}{2}-\frac{\mathbf{q}}{3}\right)\cdot\mathbf{x}\right]\psi_D(x)\right|^2\frac{E_T}{E_\pi+E_T}\times\left[\frac{d\sigma}{d\Omega}(p+p\rightarrow\pi^++D)\frac{v_{PP}(E_\pi+E_D)}{E_D}\right]. \quad (5)$$

E is the total energy in the center-of-mass system including rest mass; $\mathbf{k}$ is the momentum of the incident proton in the center of mass system; $\mathbf{q}$ is the meson momentum. The quantities in the bracket are evaluated at that energy which gives mesons of momentum q. The factor 1/3 arises from the various spin sums.

We choose for the spatial part of the wave functions:

$$\psi_D(r)=\frac{e^{-\beta r}-e^{-\gamma r}}{r}\left(\frac{\beta\gamma(\beta+\gamma)}{2\pi(\beta-\gamma)^2}\right)^{\frac{1}{2}} \quad (6)$$

and[7]

$$\psi_T(0,r)=(\alpha^3/8\pi)e^{-\alpha r}, \quad (7)$$

with $\gamma=6\beta$, $\beta=0.32/\lambda$, $\alpha=1.6/\lambda$, $\lambda=1.4\times10^{-13}$ cm.

The differential cross section in the center-of-mass system for 345-Mev incident protons is given in Fig. 1. $\sigma(p+p\rightarrow\pi^++D)$ for 90-Mev center-of-mass mesons was extrapolated from detailed balancing on lower energy π absorption[8] to be about $6.4(0.07+\cos^2\theta)\times10^{-28}$ cm^2 sterad^{-1}, which is 20 times $\sigma(p+p\rightarrow\pi^++D)$ for 345-Mev incident protons. Although this estimate is uncertain the very large increase of this cross section with meson energy, which is certainly present, makes $\sigma(p+d\rightarrow H^3+\pi^+)$ fairly large, approximately 1.3×10^{-29} cm^2.

† This work was performed under the auspices of the AEC.
[1] K. Watson, Phys. Rev. **85**, 842 (1952).
[2] R. L. Garwin, Phys. Rev. **85**, 1045 (1952).
[3] Since the completion of this work, this result has been published by A. M. L. Messiah, Phys. Rev. **86**, 430 (1952).
[4] Fraasman, Block, and Havens, Phys. Rev. **85**, 370 (1952).
[5] W. Dudziak, private communication.
[6] The use of an impulse approximation is better here than in the deuterium pick-up calculations [G. F. Chew and M. L. Goldberger, Phys. Rev. **77**, 470 (1950)], where the momentum transfer between the incident and struck nucleon is about equal to the internal momentum that the struck deuteron must have for pick-up to be probable.
[7] Fröhlich, Huang, and Sneddon, Proc. Roy. Soc. (London) **A191**, 61 (1947).
[8] Durbin, Loar, and Steinberger, Phys. Rev. **84**, 581 (1951).

Some Observations on the Gamma-Radiation from Polonium

R. W. Pringle, H. W. Taylor, and S. Standil
Physics Department, University of Manitoba, Winnipeg, Canada
(Received May 12, 1952)

THE gamma-radiation from polonium has been the object of a number of recent investigations,[1-5] but the present understanding of the situation is far from satisfactory. This is particularly so with regard to the soft radiation of energy about 80 kev, thought by Zajac *et al.*[2] to be nuclear in origin. Grace *et al.*[3] have recently found evidence that this component seems to be almost entirely the x-radiation of lead following the internal conversion of the well-established hard component at 800 kev, and have estimated the internal conversion coefficient by a study of the internal conversion electrons involved as being 6.7 percent.

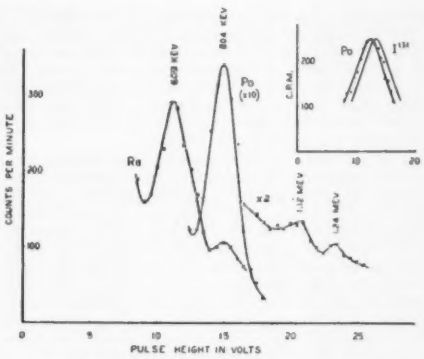

FIG. 1. Pulse-height distribution for the gamma-radiation from polonium 210.

With this interpretation the measurements of Zajac *et al.* would have given a value close to 100 percent. Further information comes from Alburger and Friedlander,[4] who investigated the secondary electrons with a beta-ray spectrometer and concluded that the conversion coefficient must lie in the range 1 to 5 percent. De Benedetti and Minton, as a result of alpha-gamma angular correlation experiments, have shown that the 800-kev component is probably $E2$, and thus imply that the conversion coefficient is less than 1 percent.

In an attempt to clarify this confusing situation certain observations have been made on the radiations involved, using a coincidence scintillation spectrometer and a weak source of polonium in solution from which all traces of Ra and RaD had been removed. Single channel pulse height distribution analysis (Fig. 1) gave a value of 804 ± 5 kev for the energy of the hard component, considerably above the Siegbahn value of 773 kev, but in excellent agreement with the Alburger and Friedlander value of 800 ± 6 kev obtained with a beta-ray spectrometer. Several standard gamma-ray energies were used for purposes of calibration, and the value of 804 kev is a mean for a number of experiments. The calibration source used for the Fig. 1 distribution was a Ra contaminated Po source, so that a residue of the Po line can be seen in the calibration curve. No evidence could be found to suggest the presence of any other component in the gamma-radiation from Po in the range 100 kev to 2 Mev.

Single channel analysis of the soft component failed to reveal any structure because of the limited resolution available at this energy in a scintillation spectrometer, but careful measurements relative to the I^{131} 80.1-kev gamma-ray gave an average energy of 77 ± 2 kev (see Fig. 1). This result is the mean of a number of determinations made with a five-channel kicksorter and also by means of the now conventional photographic storage methods employing a cathode-ray oscillograph. The value is not in disagreement with the observations of Grace *et al.*, for, although the mean energy is significantly above the value of 73 kev given by them for the main component, it agrees well with the conclusions of their critical absorption experiments that one-third of the radiation has an energy higher than 76.5 kev, and most of this is higher in energy than 78.6 kev. On the other hand, the value obtained in this investigation disagrees with the conclusion of Zajac *et al.* that no significant component of the soft radiation lies between 69.4 and 80.7 kev.

An estimate has been made of the intensity of the soft component relative to the hard component from a knowledge of the relative counting rates in the apparatus and the detection efficiencies for the two radiations. On the assumption that the soft component is entirely x-radiation following internal conversion of

the 804-kev gamma-ray, a conversion coefficient is obtained for this radiation of 20 to 30 percent. This value of the conversion coefficient would require the 804-kev gamma-radiation to be $M4$, but considerations of parity and angular momentum[5] in this transition between two even-even nuclei indicate the radiation must be electric.

If, in fact, the internal conversion coefficient for the 804-kev gamma-ray is about 5 percent and the soft component is K-radiation, the above intensity measurements indicate that most of the K-shell ionization is due to processes other than internal conversion, for example, ionization by alpha-particles.[6]

In an attempt to resolve these difficulties a search was made for a possible time association between the two components. A spectrum of coincidences was plotted in the region of 80 kev, with one channel set on the high energy component only. No significant coincidences to the 77-kev component were observed with a resolving time of 0.3 microsecond, and it was concluded that less than 1 percent of the soft radiation is in coincidence with the 804-kev component. This was taken as evidence that, even if part of the soft radiation is nuclear in origin, a prompt cascade de-excitation process does not exist.

[1] K. Siegbahn and S. H. E. Slätis, Nature **159**, 471 (1947).
[2] Zajac, Broda, and Feather, Proc. Phys. Soc. (London) **60**, 501 (1948).
[3] Grace, Allen, West, and Halban, Proc. Phys. Soc. (London) **64**, 493 (1951).
[4] D. Alburger and G. Friedlander, Phys. Rev. **81**, 523 (1951).
[5] S. De Benedetti and G. H. Minton, Phys. Rev. **85**, 944 (1952).
[6] Since the completion of the above work, W. C. Barber and R. H. Helm have reported similar results [Phys. Rev. **86**, 275 (1952)]. They find the ratio of the number of soft rays to the number of 800-kev gamma-rays to be 0.134 ± 0.025 to 1, and suggest that only about one-third or one-half of the K-shell ionization is due to internal conversion, the remaining ionization being a direct result of alpha-emission.

Wall Energy of Ferroelectric Domains

W. KÄNZIG
Swiss Federal Institute of Technology, Zürich, Switzerland
(Received May 12, 1952)

THE present paper will give a simple tentative explanation of the behavior of small ferroelectric particles reported in a previous letter.[1]

The stable domain configuration of an isolated and non-conducting ferroelectric crystal corresponds to a minimum of the sum of wall energy and volume energy. The arrangement of the domains which has to be expected for a KH_2PO_4-crystal is shown in Fig. 1.[2] Assuming a cube-shaped crystal with edges D, consisting of n domains and imbedded in a medium with the dielectric constant ϵ, the depolarization energy is[3]

$$W_{dep} = 1.7 P_s^2 D^3/n\epsilon. \tag{1}$$

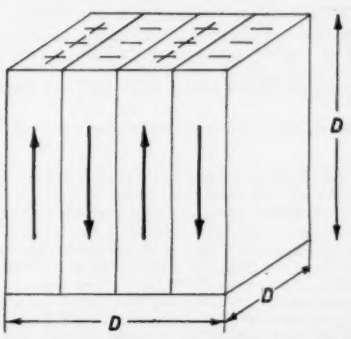

FIG. 1. Expected arrangement of the domains for a KH_2PO_4 crystal.

For the surface energy density of the domain walls, we may put $\sigma = \alpha P_s^2$. Hence,

$$W_{wall} = (n-1)\alpha P_s^2 D^2. \tag{2}$$

These energies are now introduced into the well-known Mueller interaction theory.[4] According to Mueller the free energy density of the shorted (single domain) crystal is

$$A = (T-T_C)P^2/2C + \tfrac{1}{4}\xi' P^4 + \cdots, \tag{3}$$

where T_C is the Curie temperature ($=123°K$), C is the constant of the Curie-Weiss law ($=260°C$),[5] and the coefficients ξ', $\cdots$ are assumed to be independent of temperature.

Introducing W_{dep} and W_{wall} into Eq. (3), the total free energy of the free energy of the crystal described above turns out to be

$$Aa^3 = a^3\{P^2[T-T_C+3.4C/n\epsilon+2(n-1)\alpha C/D]/2C + \xi' P^4/4+\cdots\}. \tag{4}$$

Comparing this expression with (3), we find that the Curie temperature is lowered by

$$\Delta T_C = -\{3.4C/n\epsilon+2(n-1)\alpha C/D\}. \tag{5}$$

The stable domain number n corresponds to a minimum of $|\Delta T_C|$. Hence, for given ϵ and D, the relation between ΔT_C and α is unique.

For small particles the second term in (5) becomes important. The measurement of the Curie temperature of small isolated particles allows, therefore, the evaluation of the wall energy coefficient α. The previously reported investigations on colloidal KH_2PO_4 have now been completed by dielectric measurements with an improved sample technique.[6] A lowering of the Curie temperature with decreasing ϵ and decreasing D has been observed. For $\epsilon \sim 5$ and $D \geq 4000$A the Curie point was found to be above the temperature of liquid nitrogen (i.e., $|\Delta T_C| < 46°C$). From this an upper limit for α can be deduced:

$$\alpha < 26 \times 10^{-8} \text{ cm}.$$

On the other hand, for $\epsilon \sim 5$ and $D \leq 1500$A the Curie point is below the temperature of liquid nitrogen (i.e., $|\Delta T_C| > 46°C$), indicating a lower limit

$$\alpha > 9 \times 10^{-8} \text{ cm}.$$

These limits are consistent with the assumption of classical dipole-dipole interaction together with a domain wall thickness of a few lattice constants.[6]

The value of the spontaneous polarization being[3] 5×10^{-6} coulomb/cm^2, the limits for the surface energy density of a domain wall are

$$20 < \sigma < 58 \text{ erg/cm}^2.$$

The author is indebted to Professor P. Scherrer for illuminating discussions.

[1] W. Känzig and M. Peter, Phys. Rev. **85**, 940 (1952).
[2] See, e.g., Baumgartner, Jona, and Känzig, Ergeb. Exakt. Naturwiss. **23**, 235 (1950).
[3] C. Kittel, Revs. Modern Phys. **21**, 541 (1949).
[4] See, e.g., W. G. Cady, *Piezoelectricity* (McGraw-Hill Book Company, Inc., New York, 1946), p. 580.
[5] The dielectric measurements reported in the first paper (see reference 1) are not conclusive, as the colloid had undergone a change from being pressed into disks.
[6] C. Kittel, Phys. Rev. **82**, 965 (1951).

Anomalous Magnetic Resonance Absorption of Cu^{++}

HIROO KUMAGAI, HIDETARŌ ABE, AND JUNJI SHIMADA
Institute of Science and Technology, University of Tokyo, Meguroku, Tokyo, Japan
(Received February 25, 1952)

IN magnetic resonance absorption of salts containing Cu^{++}, no structure is observed in the resonance lines except for hyperfine structure. The reason is that the ion is in a ^2D state and

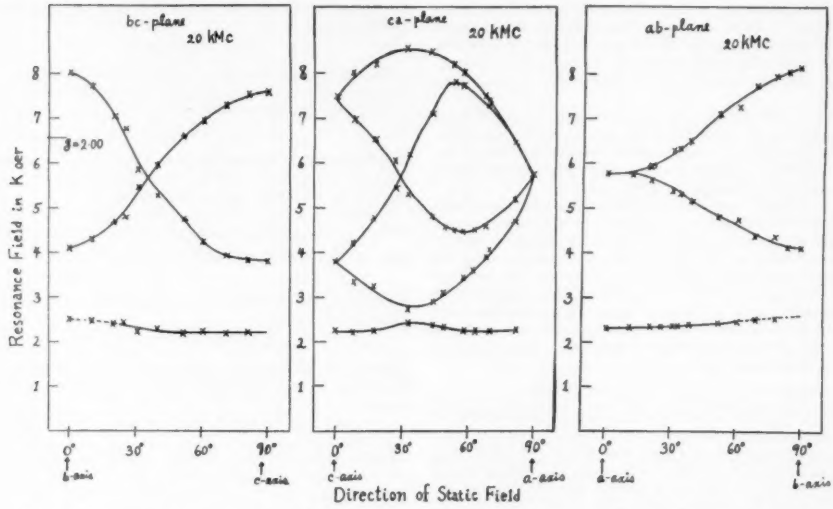

FIG. 1. Peak resonance field strengths observed at 20 kMc when the static magnetic field is in the *bc*, *ca*, and *ab* planes, respectively. The *a*, *b*, and *c* axes are magnetic axes.

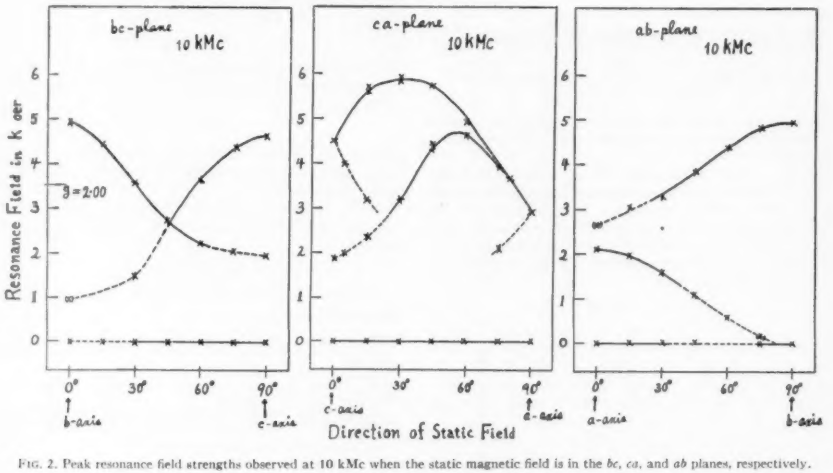

FIG. 2. Peak resonance field strengths observed at 10 kMc when the static magnetic field is in the *bc*, *ca*, and *ab* planes, respectively.

the ground state in crystalline fields is split only by an external magnetic field, the upper levels being far above the ground state. The *g*-value is affected by the upper level and varies with the orientation of the static magnetic field. It ranges from 2.05 to 2.20 as in $CuSO_4 \cdot 5H_2O$,[1-3] $CuK_2Cl_4 \cdot 2H_2O$, etc.[4,5]

Recently, however, Lancaster and Gordy[6] have pointed out anomalous resonance absorption in copper acetate powder. We have measured the absorption in single crystals of this salt at 10 and 20 kMc. The composition of this salt is $Cu(CH_3COO)_2 \cdot H_2O$, the number of water molecules being determined by chemical analysis.

The field strengths at the observed peaks are shown in Figs. 1 and 2. The *a*, *b*, and *c* axes in the figures are magnetic ones, and not axes of crystal forms. The data observed at 20 kMc are shown in Fig. 1, and the corresponding data at 10 kMc, observed by Hayashi and Ôno in our laboratory, are shown in Fig. 2. Up to five peaks are observed, whose *g*-values are distributed in a wide range. At 10 kMc, a peak seems to exist at about zero magnetic field, showing that the salt has a zero-field splitting of about 10 kMc. The peaks in the *a*-direction in the second and third parts of Fig. 2 do not coincide; this point is under examination now. Dotted lines show that the absorption is

weak. The microwave magnetic field is always perpendicular to the static field.

Such anomalous absorptions cannot be explained by a single ion in the ^2D state in any allowable crystalline field. The first possibility for the origin of this anomaly may be that ions are not in the ^2D state in this case of very strong crystalline fields. The second possibility is that the absorption is not effected by a single Cu^{++} ion, but by a molecule containing Cu^{++} and other atoms. The third one is that a number of Cu^{++} ions are located at small distances from each other so that their electron spins mutually interact strongly. We note that the absorption of $Mn(CH_3COO)_2 \cdot 4H_2O$ shows a single peak with $g=2.0$.

The authors' thanks are due to Assistant Professors K. Kambe and E. Ishiguro for their discussions. A more detailed report will appear in J. Phys. Soc. Japan.

[1] D. M. S. Bagguley and J. H. E. Griffiths, Proc. Roy. Soc. (London) **201**, 366 (1950).
[2] R. D. Arnold and A. F. Kip, Phys. Rev. **75**, 1199 (1949).
[3] J. Wheatley and D. Halliday, Phys. Rev. **75**, 1412 (1949).
[4] Itoh, Fujimoto, and Ibamoto, Phys. Rev. **83**, 852 (1951).
[5] H. Kumagai *et al.* (to be published).
[6] F. W. Lancaster and W. Gordy, J. Chem. Phys. **19**, 1181 (1951).

Electron-Hole Recombination in Germanium

R. N. Hall
General Electric Research Laboratory, Schenectady, New York
(Received May 8, 1952)

POWER rectifiers have been described that consist of thin wafers of high purity germanium whose opposite faces are heavily doped with donor and acceptor impurities.[1] Since the current flow depends largely upon the generation and recombination of holes and electrons within the high purity region, this geometry is well adapted to the study of the recombination process. A two-body collision mechanism leads to a rate that is proportional to the square of the carrier concentration at high levels of injection where holes and electrons are present in nearly equal numbers. Measurements show, however, that the rate varies linearly with concentration over a wide range of concentration and temperature.[2] These observations can be accounted for by assuming that recombination takes place largely through the agency of recombination centers distributed throughout the germanium.

A steady-state recombination rate given by[3]

$$R=(np-n_i^2)/[t_p(n+n_0)+t_n(p+p_0)], \qquad (1)$$

results from a simple model in which the centers give rise to an energy level lying in the forbidden band. The electron and hole concentrations are given by n and p, their product under equilibrium conditions being n_i^2. The lifetime for electrons when the centers are completely empty is given by t_n; t_p is the hole lifetime with all centers occupied by electrons. The recombination centers lie at an energy level defined by n_0 and p_0 which are the equilibrium electron and hole concentrations in a sample whose Fermi level coincides with the position of the recombination centers.

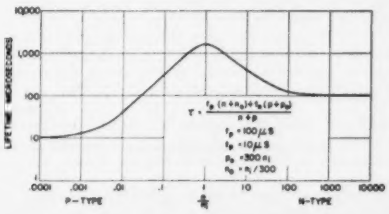

FIG. 1. Variation of lifetime with impurity content.

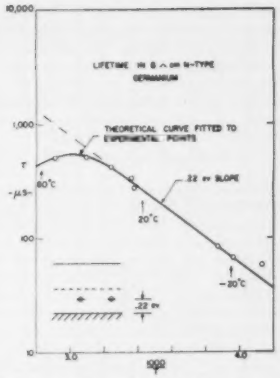

FIG. 2. Variation of lifetime with temperature.

In the derivation of Eq. (1), it is assumed that the rate of capture of electrons is proportional to the number of empty centers and to the number of free electrons. The rate at which electrons are emitted by these centers is proportional to the number of occupied centers. Analogous statements apply to the capture and emission of holes.

It is readily seen that Eq. (1) can account for the linear relation between carrier concentration and recombination rate mentioned in the first paragraph. With high level injection, n and p become equal and much greater than n_i, n_0, or p_0 so that $R \cong n/(t_n+t_p)$. Rectifier characteristics calculated on the basis of Eq. (1) can be fitted to the data in a very satisfactory manner.[4] The lifetime for holes and electrons at high level injection (t_n+t_p) is usually found to be approximately 100 μsec.

The equilibrium lifetime which results from Eq. (1) is

$$\tau=\mathrm{Lim}_{\delta n\to 0}(\delta n/\delta R)=[t_p(n+n_0)+t_n(p+p_0)]/(n+p). \qquad (2)$$

The variation of τ with impurity content is illustrated in Fig. 1 for a choice of parameters which gives reasonable agreement with lifetimes observed in samples of germanium at room temperature.

Since n_0 and p_0 vary exponentially with $1/T$ while t_n and t_p should be relatively insensitive to temperature, the lifetime should assume its limiting values t_n and t_p for p- and n-type samples at low temperatures. At higher temperatures, the lifetime increases with temperature as long as the sample remains extrinsic and then decreases again in the intrinsic range. Measurements of lifetime illustrating the variation with temperature in the upper two temperature ranges are shown in Fig. 2. The slope indicated on the graph gives a tentative value of 0.22 electron volt for the position of the recombination centers above the valence band or below the conduction band.

[1] R. N. Hall and W. C. Dunlap, Jr., Phys. Rev. **80**, 467 (1950).
[2] R. N. Hall, Phys. Rev. **83**, 228 (1951).
[3] This expression was presented in the text of reference 2, using somewhat different notation. Shockley has derived it as a special case of a more general treatment which has been submitted for publication.
[4] A detailed treatment of the germanium power rectifier will be published shortly.

An Experimental Test of the Shell Model

W. C. Parkinson, E. H. Beach, and J. S. King
H. M. Randall Laboratory of Physics, University of Michigan, Ann Arbor, Michigan
(Received June 3, 1952)

IN a recent letter, Bethe and Butler[1] proposed an experiment to give direct information on the accuracy of the shell model of nuclear structure in ascribing definite orbital angular momen-

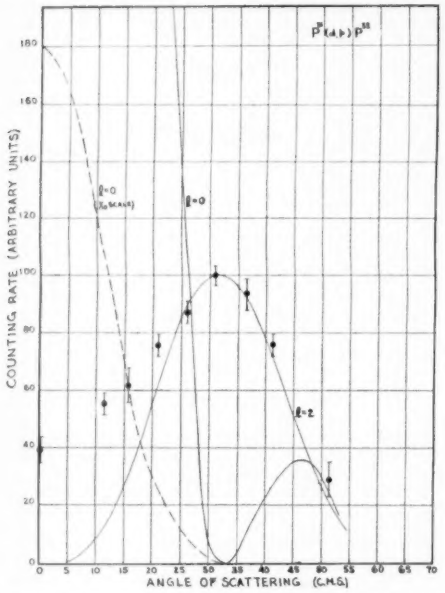

FIG. 1. The angular distribution of the protons associated with the ground state in the reaction $P^{31}(d, p)P^{32}$. The solid curves are calculated from the Butler theory.

tum states to nucleons in a nucleus. According to the Butler[2] interpretation of (d, p) and (d, n) reactions, the angular distribution of the outgoing particle is characterized by the angular momentum l with which the captured particle can be accepted into the appropriate final state. If, for a particular nucleus, the selection rules allow more than one value of l, the target nucleus might be indifferent to which of these it accepts. According to the shell model, however, the target nucleus will accept a particle in one definite orbital angular momentum state only. In the case of phosphorus, the selection rules allow l values of 0 and 2, while the shell model requires an l of 2 only.

We have measured the angular distribution of the protons from the reaction $P^{31}(d, p)P^{32}$ and, although more accurate data are desired, the results are of sufficient interest to warrant a brief note at this time. In Fig. 1, the experimental points for the angular distribution of the protons associated with the ground state are indicated along with the curves for the angular distributions predicted by the Butler theory for l values of 0 and 2. In computing these curves from the expression given by Butler, the following values were used: $r_0 = 5.7 \times 10^{-13}$ cm, $a = 0.23 \times 10^{13}$ cm^{-1}, $b = 1.4 \times 10^{13}$ cm^{-1}. The incident deuteron energy was 7.20 Mev (c.m. sytem). The Q of the reaction was measured to be 5.5 Mev which is in reasonable agreement with that of 5.8 ± 0.3 given by Pollard.[3]

The target consisted of a thin coating of pure phosphorus on a backing of 0.0001-inch silver foil. The background due to the silver was negligible at all angles except 0° where the correction was approximately 10 percent. The vertical lines through the measured points represent the standard deviation determined from the total number of counts and are not a measure of the over-all uncertainty in the data. In particular, we believe that the values indicated at small angles (0° to 15°) represent an upper bound to the true situation. No correction has been applied for the finite solid angle of the detector system. In addition, the "tail" of the first excited state of P^{32} overlapped the ground state peak and at small angles produced much the larger counting rate. The correction for this tail was somewhat uncertain, and we were conservative in applying it.

These results indicate that the neutron is captured mainly into a D state, as is predicted by the shell model, rather than an S state, with an amount of admixture not exceeding 5 percent and probably less than 2 percent.[4] It is worth noting that this is also in agreement with the observations on the beta-decay of P^{32}, which presumably decays by means of an "l-forbidden" transition for which $\Delta l = 2$ with no change in parity.

The measurements on P^{32} and similar nuclei are being continued. A more detailed report, including a discussion of the techniques of measurement, will be given in the near future.

[1] H. A. Bethe and S. T. Butler, Phys. Rev. **85**, 1045 (1952).
[2] S. T. Butler, Phys. Rev. **80**, 1095 (1950); Proc. Roy. Soc. (London) **A208**, 559 (1951).
[3] E. Pollard, Phys. Rev. **57**, 1086 (1940).
[4] Since the ground-state doublet was not resolved, both members are presumably D-states. This does not alter the implications with respect to the shell model.

Electron Capture in Tl^{204}†

ALLAN C. G. MITCHELL AND ROBERT S. CAIRD
Physics Department, Indiana University, Bloomington, Indiana
(Received May 15, 1952)

DURING the course of an investigation of the radiations from Tl^{204} carried out in this laboratory,[1] the spectrum of photoelectrons ejected from Pb and U radiators by photons from Tl^{204} was measured. While the radiation was quite weak, two photopeaks each were found with Pb and U radiators. The peaks came at photoelectron energies of 51 and 66 kev for U and 55 and 69 kev for Pb. If it is assumed that these peaks are due to photoelectrons ejected from the L and M shells of Pb and U, respectively, the energy of the radiation responsible for these photoelectrons is 72.0 ± 0.9 kev. Since this is approximately the energy of the K_α line of Hg, it appeared likely that Tl^{204} decays to Hg^{204} by orbital electron capture as well as to Pb^{204} by beta-ray emission.

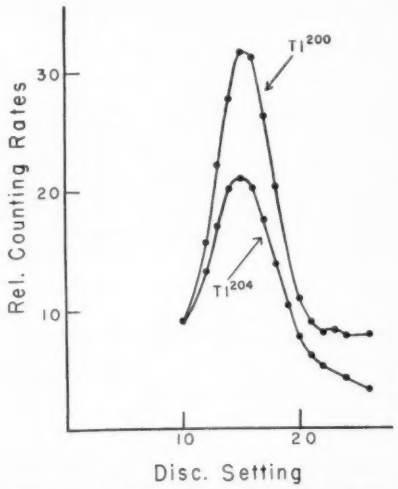

FIG. 1. Pulse-height analysis of the x-rays from Tl^{204} and Tl^{200} using scintillation counters.

The experiments were put aside at that time owing to the press of other work and approximately a year later they were again investigated with the help of a scintillation counter. In the present work two sets of experiments were performed.

In the first set of experiments, in order to get a good calibration point for this low energy radiation, the low energy radiations from Tl^{204} were compared with those of Os^{185}, a known K-capturer.[2,3] By using the line produced by Os^{185} (K_α of Re) as a calibration point, the radiation from Tl^{204} had an energy of 68 kev.

In a second set of experiments, the photon radiations from Tl^{204} were compared directly with those from Tl^{200}, which is known to decay to Hg^{200} by electron capture.[4] The results of these experiments, taken with a scintillation counter are shown in Fig. 1. It will be seen that the peak of the curve, owing to the K_α x-rays of Hg from Tl^{200}, falls at exactly the same place as that of the photons from Tl^{204}.

From the above experiments, it is to be concluded that the photons from Tl^{204} are the K_α x-rays of Hg and that Tl^{204} decays to Hg^{204} by K-electron capture. While these experiments were in progress, a similar conclusion was obtained by Lidofsky, Macklin, and Wu.[5]

† Supported by the joint program of the ONR and AEC.
[1] Mitchell, Canada, and Cuffey (unpublished).
[2] Bunker, Canada, and Mitchell, Phys. Rev. **79**, 610 (1950).
[3] M. M. Miller and R. G. Wilkinson, Phys. Rev. **83**, 1050 (1951).
[4] H. I. Israel and R. G. Wilkinson, Phys. Rev. **83**, 1051 (1951).
[5] Lidofsky, Macklin, and Wu, Phys. Rev. **87**, 204 (1952).

A Proposed Re-Interpretation of Quantum Mechanics

OTTO HALPERN
University of Southern California, Los Angeles, California
(Received April 18, 1952)

IN two recently published extensive papers,[1] Bohm has given a full discussion of an alternative interpretation of nonrelativistic quantum mechanics proposed by him. It is Bohm's opinion that there exists the possibility of looking on nonrelativistic quantum mechanics as a form of classical mechanics involving special quantum forces. While the bulk of the papers is devoted to various applications of this view, the fundamental point is contained in a few remarks concerning the solution of Schrödinger's equation, at the beginning of Bohm's first note.

Writing, as customarily,

$$\psi = R(x, y, z, t)\exp(iS/\hbar) \quad (R, S \text{ real}), \tag{1}$$

the Schrödinger equation is split into two equations:

$$(\partial R/\partial t) + (1/2m)(R\Delta S + 2\,\mathrm{grad}R\cdot\mathrm{grad}S), \tag{2a}$$

$$(\partial S/\partial t) + (1/2m)(\mathrm{grad}S)^2 + V(x, y, z, t) - \frac{\hbar^2}{2m}\frac{(\mathrm{grad}R)^2}{R}. \tag{2b}$$

Equation (2b) is looked upon as the Hamilton-Jacobi equation of the quantum-mechanical problem, in which the terms containing R and its derivatives are a sort of quantum potential energy. Since it is necessary to satisfy also (2a), Bohm simply suggests the use of an arbitrary solution ψ of the Schrödinger equation. One is then certain that both (2a) and (2b) will be satisfied.

We do not want to enter here into a discussion of the individual cases treated by Bohm. It is the thesis of the present letter that so far no possibility of a mechanical interpretation has been demonstrated.

To obtain the solution of a mechanical problem, it is necessary to have a solution S which depends on the coordinates of the system, the physical parameters entering into the expression for kinetic and potential energy and f nonadditive integration constants. Bohm has failed to show that such a function can be found.[2]

It is, of course, true that, thanks to the infinite number of eigenstates, as many constants as one wishes can be introduced into S; but these are not integration constants in the sense of the Hamilton-Jacobi theory, since they will in general also be present in the "quantum potential" described by R and its derivatives. There does not seem to exist a general formulation by which (2a) and (2b) can be satisfied and S still be made to contain f (nonadditive) integration constants that are not present in R. Until a way to find these integration constants has been devised, the similarity with the Hamilton-Jacobi theory is purely extraneous, and one cannot talk about a mechanical interpretation of the wave equation.

It may perhaps be kept in mind that the whole procedure suggested by Bohm is, even in its present incomplete form, strictly limited to nonrelativistic quantum mechanics and there is no indication given as to how it could possibly be extended to include relativistic (spin) phenomena; nor has an attempt been made in any of the examples to analyze the fundamental relativistic questions of observables and their measurability.[3]

Keeping in mind these factors together with the difficulties in the purely mechanical part of the interpretation, one may feel justified in concluding that no alternative interpretation of quantum mechanics has been offered.

[1] D. Bohm, Phys. Rev. **85**, 166; **85**, 180 (1952).
[2] To put the momentum vector equal to the gradient of S (as defined by Bohm) disposes of f integration constants in a nonmechanical manner which may be compared to the quantization of the phase-integrals in the old quantum theory.
[3] O. Halpern and M. H. Johnson, Phys. Rev. **59**, 896 (1941).

Reply to a Criticism of a Causal Re-Interpretation of the Quantum Theory

DAVID BOHM
Faculdade de Filosofia, Ciências e Letras, Universidade de São Paulo, São Paulo, Brasil
(Received May 22, 1952)

IN a letter[1] criticizing a causal re-interpretation of the quantum theory proposed by the author,[2] Halpern comes to the conclusion that "no alternative interpretation of the quantum theory has been offered." In the present letter, the author wishes to discuss in some detail the arguments by which Halpern is led to this conclusion.

Halpern's first objection is that because the function, $S(\mathbf{x})$, appearing in paper I, Eq. (6), does not depend on f nonadditive integration constants, one has not yet obtained a solution of the mechanical problem. It was stated in paper I, Sec. 4, however, that the Hamilton-Jacobi theory was being used only for the purpose of indicating in a simple way how one might arrive at a causal interpretation of the quantum theory; while the theory itself was to be based directly on the equations of motion [paper I, Eq. (8a)]:

$$m d^2\mathbf{x}/dt^2 = -\nabla\{U(\mathbf{x}) + V(\mathbf{x})\},$$

where $V(\mathbf{x})$ is the classical potential, and $U(\mathbf{x})$ is the "quantum-potential." Now, the solution of these equations by the Hamilton-Jacobi technique would certainly require the f nonadditive integration constants referred to by Halpern, but the author intended to employ another method of solution in his papers; namely, that of guessing a function and verifying it by direct substitution in the differential equations. Since the treatment given in the papers is perhaps not completely explicit, it may be useful to amplify it here. Guided by the Hamilton-Jacobi theory, we guess tentatively that if the momentum were equal to $\mathbf{p} = \nabla S(\mathbf{x})$, this function would satisfy the equations of motion. Now,

$$d\mathbf{p}/dt = \partial\mathbf{p}/\partial t + (\mathbf{v}\cdot\nabla)\mathbf{p} = \partial(\nabla S)/\partial t + \nabla(\nabla S)^2/2m.$$

But since S is defined as the phase of the wave function, we have (paper I, Eq. (6))

$$\partial S/\partial t = -(\nabla S)^2/2m - V - U, \quad d\mathbf{p}/dt = -\nabla\{V + U\}.$$

Thus, we verify that a particle traveling with velocity $\mathbf{v}=\nabla S/m$ will satisfy our equations of motion.[3] This means that the condition $\mathbf{p}=\nabla S(\mathbf{x})$ is a consistent subsidiary condition. It was then pointed out in paper I, Secs. 4 and 9 that if we assumed this subsidiary condition to be satisfied initially, we would be able to obtain a mechanical explanation of the results of the quantum theory; if not, we obtained a wider theory. Since it was shown to be possible to choose this wider theory in such a way that $\mathbf{p}$ approached $\nabla S(\mathbf{x})$ at the atomic level, but differed significantly from it at the level of 10^{-13} cm, it was concluded that the wider theory might be needed in the domain of very small distances, where present theories seem to be inadequate.

Halpern then objected that the suggested reinterpretation was not relativistic and did not deal with spin phenomena. The author has, however, recently developed an extension of the causal interpretation which applies to the Dirac relativistic wave equation and therefore also takes care of spin phenomena. This interpretation will soon be submitted for publication.

As for Halpern's statement that no attempt has yet been made to analyze the question of the measurability of observables from a relativistic point of view, the answer is, of course, that this will now be done with the aid of the causal interpretation of Dirac's relativistic wave equation.

It is therefore the author's feeling that his previous articles[2] do in fact present a causal reinterpretation of quantum mechanics.

[1] O. Halpern, preceding letter, Phys. Rev. **87**, 389 (1952).
[2] D. Bohm, Phys. Rev. **85**, 166 (1952) (Paper I); **85**, 180 (1952) (Paper II).
[3] To solve for $\mathbf{x}$, one must, of course, integrate the differential equations $d\mathbf{x}/dt=\nabla S(\mathbf{x})/m$ with the appropriate initial position of the particles.

The Decay Scheme of the V^0-Particle*

K. A. Brueckner and R. W. Thompson
Physics Department, Indiana University, Bloomington, Indiana
(Received May 22, 1952)

OBSERVATIONS of the V^0-particle are based on the detection of two charged decay fragments which in many cases are probably a proton and a negative pion.[1-3] Accordingly, the tentative decay scheme

$$V^0\rightarrow p+\pi+Q^* \tag{1}$$

has been assigned with a Q^*-value given by various groups as ranging from 10 to 250 Mev, the majority of the Q^*-values falling between 30 and 50 Mev. A neutral decay product cannot be directly observed in the cloud chamber,[4] but would be expected to produce detectable dynamic effects on the observed decay fragments and their orientation with respect to the apparent origin of the V^0-particle.

If the V^0-particle decays according to the scheme

$$V^0\rightarrow p+n_0+\pi+Q, \tag{2}$$

where n_0 is a neutral decay product, then the energy carried off by the charged particles and accordingly the apparent Q^*-value calculated for the assumed 2-particle decay scheme of Eq. (1) will depend on the energy taken up by the neutral particle. The relation between the true energy release Q and the apparent energy release Q^* is

$$Q^*=\frac{2(M+\mu)+Q}{2(M+\mu)+Q^*}\left(1-\frac{T_0}{T_{0\max}}\right)Q, \tag{3}$$

where M and μ are the masses of the proton and pion, respectively, T_0 is the kinetic energy of the neutral particle in the true c.m. system, and $T_{0\max}$ is the maximum possible value of T_0. In case $Q\ll 2(M+\mu)$, this exact expression can be approximated by the relation

$$Q^*=[1-(T_0/T_{0\max})]Q. \tag{4}$$

In this approximation, since the proton is of large mass compared to the other decay fragments, it takes up very little kinetic energy and $Q^*=T$, the kinetic energy of the pion in the true c.m. system. Thus the probability distribution for Q^* is identical to that for T, which can be easily obtained if it is assumed that the partition of energy among the decay products is determined by the statistical factor alone, i.e., that the matrix elements which characterize the decay are constant. Thus, under the approximation that the proton is heavy, the result for the relative probability distribution is

$$P(T)=EqE_0q_0, \tag{5}$$

where E, q, E_0, q_0 are the total energies and momenta of the pion and neutral particle respectively considered to be functions of the pion kinetic energy T with the restriction that $E+E_0=Q+\mu+\mu_0$. The distribution in Q^* is given in Fig. 1 for the cases of zero and mesonic[5] neutral particle mass. The true energy release Q has been adjusted to give a most probable value for Q^* of 35 Mev, to correspond approximately to experiment.

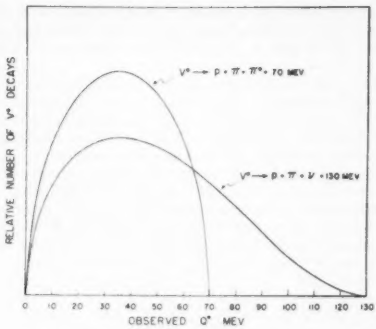

FIG. 1. Probability distribution of observed Q^*-values.

The problem of coplanarity can be treated similarly. If $\mathbf{p}'$ and $\mathbf{q}'$ are the momenta of the proton and pion in the laboratory system, then the angle δ between the plane of the charged particles and the true direction $\boldsymbol{\beta}/\beta$ of the V^0-particle is given by the expression

$$\sin\delta=(\mathbf{q}'\times\mathbf{p}')\cdot\boldsymbol{\beta}/(|\mathbf{q}'\times\mathbf{p}'|\beta). \tag{6}$$

This result can be simplified if, in the numerator, we substitute $\mathbf{p}'=\mathbf{P}_0'-\mathbf{q}'-\mathbf{q}_0'$, where $\mathbf{P}_0'$ is the momentum of the V^0-particle. In the denominator, we make use of the fact that for the decay of a rapidly moving V^0-particle, the velocity and direction of the decay proton are essentially the same as for the V^0-particle, so that $|\mathbf{q}'\times\mathbf{p}'|\cong|\mathbf{q}'\times\boldsymbol{\beta}|\gamma M$, where $\gamma=(1-\beta^2)^{-\frac{1}{2}}$. We then find, for small angles

$$\delta=\frac{1}{\gamma\beta M}\frac{\mathbf{q}'\times\boldsymbol{\beta}}{|\mathbf{q}'\times\boldsymbol{\beta}|}\cdot\mathbf{q}_0'. \tag{7}$$

Aside from the numerical factor $p'=\gamma\beta M$ in the denominator, the right hand side of this expression represents the component $q_{0\perp}'$ of $\mathbf{q}_0'$ perpendicular to the plane defined by the vectors $\mathbf{q}'$ and $\boldsymbol{\beta}$ and may be evaluated in the c.m. system. Thus

$$\delta\cong q_{0\perp}/(\gamma\beta M), \tag{8}$$

and the distribution of δ is identical to that for $q_{0\perp}$ except for the scale factor $1/\gamma\beta M$. In the present approximation that the proton is heavy, the distribution of $\mathbf{q}_0$ with the plane of $\mathbf{q}'$ and $\boldsymbol{\beta}$ considered fixed is spherically symmetric, so that the distribution of $q_{0\perp}$, for a particular magnitude of q_0 is given by

$$\begin{aligned} N(q_{0\perp})&=1/q_0, \quad q_{0\perp}<q_0; \\ &=0, \quad q_{0\perp}>q_0. \end{aligned} \tag{9}$$

The actual distribution in $q_{0\perp}$ is obtained by integration over the

momentum spectrum $P(q_0)$ of the neutral particle

$$P(q_{0T})=\int_{q_{0\perp}}^{q_{0\max}} P(q_0)\frac{dq_0}{q_0},$$

where $P(q_0)$ is readily found from Eq. (5). The resulting distribution is given in Fig. 2 with the neutral particle taken to be of zero or mesonic mass, and the same true Q-values as were assumed in Fig. 1. It is apparent from Fig. 2 that the most probable departure from coplanarity is zero and that the width of the distribution is small for a light neutral decay product and for a fast V^0-particle such as those typically observed. Therefore, even in favorable cases, the observation of V^0-disintegrations which are coplanar to within an experimental uncertainty of a few degrees cannot be considered as evidence for decay schemes involving two bodies only.

An additional quantity of experimental interest is the so-called net transverse momentum of the charged particles relative to the true direction of the V^0-particle and in the plane of the charged particles. Considerations very similar to those involved in the discussion of the coplanarity angle show that the distribution of

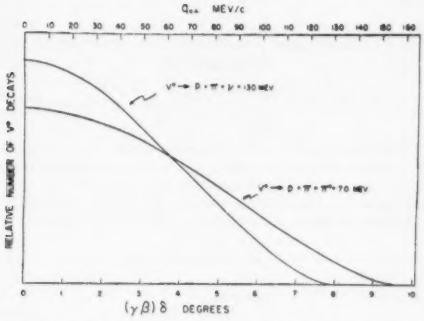
$Q_{\perp\perp}$ MEV/c
0 10 20 30 40 50 60 70 80 90 100 110 120 130 140 150 160
RELATIVE NUMBER OF V^0 DECAYS
$V^0 \to p+\pi^-+\nu+130$ MEV
$V^0 \to p+\pi^-+\pi^0+70$ MEV
0 1 2 3 4 5 6 7 8 9 10
$(\gamma\beta)\,\delta$ DEGREES

FIG. 2. Probability distribution of $q_{0\perp}$ and of the deviation from coplanarity δ.

the net transverse momentum in the plane of $\mathbf{q}'$ and $\boldsymbol{\beta}$ (which is close to the plane of $\mathbf{q}'$ and $\mathbf{p}'$) is identical to that for $q_{0\perp}$ given in Fig. 2. Thus the net transverse momentum also has the most probable value zero, and comparison with experiment, as in the case of the coplanarity angle δ, requires comparison of the observed width of the distribution about zero with the width to be expected from the experimental errors alone.

The three tests for the presence of a neutral particle discussed above are not entirely independent; for example, V^0-disintegrations with low Q^*-values corresponding to large kinetic energies of the neutral particle should, on the average, be less coplanar than the average case.

Of the three tests, the one based on the distribution of Q^*-values is perhaps to be preferred in the sense that it does not depend on assumption of the point of origin of the V^0-particle. Unfortunately, the available experimental data do not appear to be sufficiently accurate at the present time so that the presence of a light neutral particle among the decay fragments can be excluded.

* Assisted by the joint program of the ONR and AEC, by the Office of Ordnance Research, and by grant of the Frederick Gardner Cottrell Fund of the Research Corporation.

[1] Armenteros, Barker, Butler, and Cachon, Phil. Mag. **42**, 1113 (1951).
[2] Leighton, Wanlass, and Alford, Phys. Rev. **83**, 843 (1951).
[3] Thompson, Cohn, and Flum, Phys. Rev. **83**, 175 (1951).
[4] Except in that it produces detectable interactions in plates placed in the cloud chamber.
[5] The neutral pion is included for comparison only, since it is probably excluded by the absence of cascade showers that its disintegration γ-rays would produce in metal plates.

The Evaluation of the Ratio F_n/F_0 in the Theory of Forbidden Beta-Transitions*

P. MACKLIN,† L. LIDOFSKY, AND C. S. WU
Columbia University, New York, New York
(Received June 6, 1952)

THE tables of the Fermi function issued by the National Bureau of Standards are essentially tables of the gamma-function of complex argument, the real part of which is ~ 1. Therefore, these tables may be utilized for the accurate computation of those correction factors[1] corresponding to the various matrix elements in beta-decay which contain the ratio of complex gamma-functions.

Typical of these ratios is the ratio F_n/F_0, where

$$F_n=\left[\frac{(2(n+1))!}{n!\Gamma(2s_n+1)}\right]^2(2\rho\rho)^{2(s_n-n-1)}e^{\pi\gamma W/p}\,|\,\Gamma(s_n+i\gamma W/\rho)\,|^2,$$

where $s_n=[(n+1)^2-\gamma^2]^{\frac{1}{2}}$ and $\gamma=aZ$. The use of the usual recursion relationship $\Gamma(x)=(x-1)\Gamma(x-1)$ yields[2]

$$|\,\Gamma(s_n+i\gamma W/\rho)\,|^2=\left(\prod_{k=1}^{n}[(s_n-k)^2+\gamma W/\rho)^2]\right)\times|\,\Gamma(s_n-n+i\gamma W/\rho)\,|^2.$$

Since $s_n-n\sim 1$, one can define $s'=s_n-n$ and use the National Bureau of Standards tables for the evaluation of the Γ-function. Let

$$|\,\Gamma(s_n-n+i\gamma W/\rho)\,|^2=|\,\Gamma(s'+i\gamma W/\rho)\,|^2=|\,\Gamma(s'+i\gamma' W'/\rho')\,|^2,$$

where

$$s'=(1-\gamma'^2)^{\frac{1}{2}}$$

and

$$W'/\rho'=(\gamma/\gamma')(W/\rho)=(Z/Z')(W/\rho).$$

Thus, for a given Z, ρ, the National Bureau of Standards tables will be entered at the related Z', ρ'.

The National Bureau of Standards tables give the function

$$f(Z,\rho)=\rho^{2s_0}e^{\pi\gamma W/\rho}\,|\,\Gamma(s_0+i\gamma W/\rho)\,|^2.$$

So

$$\frac{F_n}{F}=\frac{[2(n+1)]!}{4(n!)^2}\frac{\Gamma^2(2s_0+1)}{\Gamma^2(2s_n+1)}(2\rho)^{2(s_n-p-s_0)}\times\left(\frac{\rho}{\rho'}\right)^{2(s_n-n)}\frac{f(Z',\rho')}{f(Z,\rho)}\prod_{k=1}^{k=n}[(s_n-k)^2+(\gamma W/\rho)^2].$$

* Partially supported by the AEC.
† Present address: Department of Physics, Middlebury College, Middlebury, Vermont.
[1] E. J. Konopinski and G. Uhlenbeck, Phys. Rev. **60**, 308 (1941).
[2] E. Jahnke and F. Emde, *Tables of Functions* (Dover Publications, New York, 1943).

The Radiations of Tl^{204}†

L. LIDOFSKY, P. MACKLIN,* AND C. S. WU
Columbia University, New York, New York
(Received June 6, 1952)

THE beta decay of Tl^{204} has been reported to have a half-life of 2.7 years and an upper energy of 783 kev.[1] The logft value ~ 10.3 is characteristic of a first-forbidden transition involving the B_{ij} matrix element only ($\Delta J=2$; yes).[2] The shell structure prediction for the spin and the parity of Tl^{204} is $J=1, 2$; odd. The daughter nucleus Pb^{204} is even-even, so the shell structure predictions of the transition include the possibility of $\Delta J=2$; yes.

An investigation of the beta-spectrum has been made which explores the possibilities of source scattering and of inadequate evaluation of the B_{ij} correction factor as possible causes for the reported deviation from the B_{ij} shape at energies below 350 kev.[1] Simultaneously, a search was made with a NaI(Tl) crystal scintillation spectrometer for gamma-radiation which would introduce the possibility that the beta-spectrum was complex.

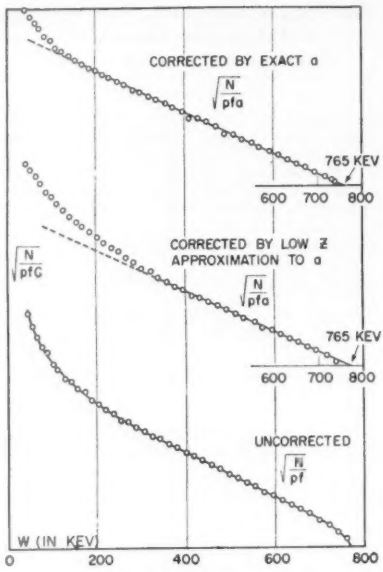

FIG. 1. Kurie plots of Tl^{204} β-spectrum.

The beta-spectrum of Tl^{204} was investigated in the solenoid spectrometer using both chemically deposited and vacuum evaporated sources. An exact evaluation of the B_{ij} correction factor, as formulated by Konopinski and Uhlenbeck,[3] was made utilizing the NBS Tables of the Fermi factor.[4,5]

Three Kurie plots of the beta spectrum from a thin evaporated source are shown in Fig. 1. The first is the conventional Kurie plot and exhibits the typical "B_{ij}" spectrum shape. The second plot using the admittedly poor approximation $\alpha=(1/12)(p^2+q^2)$ is linear at higher energies but deviates below 350 kev. The final plot using the exact evaluation of B_{ij} is linear from the endpoint of 765 kev to about 150 kev.

The spectra from chemically deposited and vacuum evaporated sources of nearly the same strength were compared. The spectrum from the chemical source showed deviation below 350 kev.

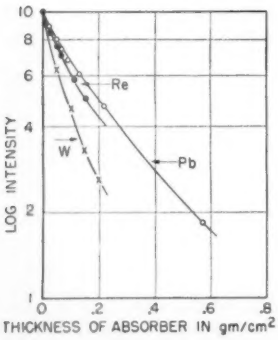

FIG. 2. Critical absorption curves of Tl^{204} γ-radiation.

A search for gamma-rays revealed only the presence of gamma-radiation whose energy was about that for x-rays from elements of $Z\sim81$. W is a critical absorber as compared to Re and Pb for Hg K x-rays, while both Re and W are critical absorbers as compared to Pb for Tl K x-rays. The experimental absorption curve in Fig. 2 showing that W alone is a critical absorber, classifies the radiations as Hg x-rays and indicates that K-capture takes place in Tl^{204}.

A further check made using a proportional counter[6] and W and Ta absorbers confirmed the identification as Hg x-radiation.

The abundance of K-capture was determined as $N_K/N_\beta-\sim2$–3 percent.

† Partially supported by the AEC.
* Present address: Department of Physics, Middlebury College, Middlebury, Vermont.
[1] D. Saxon and J. Richards, Phys. Rev. **76**, 982 (1949).
[2] C. S. Wu, Revs. Modern Phys. **22**, 386 (1950).
[3] E. J. Konopinski and G. Uhlenbeck, Phys. Rev. **60**, 308 (1941).
[4] I. Feister, Phys. Rev. **78**, 375 (1950).
[5] Macklin, Lidofsky, and Wu, preceding letter, Phys. Rev. **87**, 391 (1952).
[6] Kindly loaned by Dr. Rubinson and Dr. Friedlander of Brookhaven National Laboratory.

The Influence of Anisotropy on Ferromagnetic Relaxation*

N. BLOEMBERGEN AND SHYH WANG
Cruft Laboratory, Harvard University, Cambridge, Massachusetts
(Received June 3, 1952)

THE experiments on the relaxation effects in ferromagnetic resonance[1] have been extended to other samples of nickel ferrite, other types of ferrites, and to lower temperatures. It has been found that the saturation curves, giving the imaginary part of the high frequency permeability μ'' and the magnetization M_z

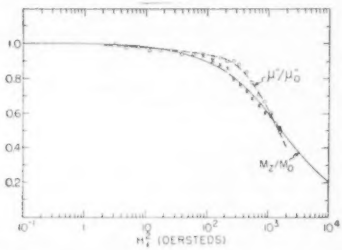

FIG. 1. The saturation effect in a spherical polycrystalline sample of manganese zinc ferrite. The decrease in the high frequency permeability is proportional to the decrease in magnetization, as a function of microwave field strength.

in the direction of the external field as a function of microwave power level, coincide in polycrystalline specimens. The results for a spherical sample of $MnOZnOFe_2O_3$ are shown in Fig. 1. The spin-lattice relaxation time is again a few times 10^{-8} sec. Similar curves have been found for a *powdered* spherical sample of nickel ferrite and for a single crystal of irregular shape. The difference from the previously reported result[1] on a spherical single crystal of the same substance is remarkable. There, the μ'' curve is shifted to values of H_1^2 which are about 500 times lower. The present results seem to be in better agreement with the predictions of simple theoretical models, namely that μ'' is proportional to M_z.

The following explanation is proposed. When power is absorbed by the ferromagnetic spins from the microwave field, the magnetization vector tends to turn away from the direction of the external field H_0. Due to dipolar or pseudo-dipolar interaction[2] between the spins the absorbed magnetic energy is partially trans-

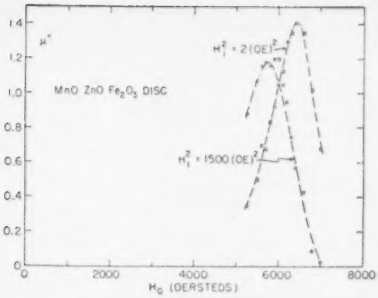

FIG. 2. The position of the resonance depends on the microwave power level in a disk-shaped specimen. No appreciable saturation can be obtained, as the constant field cannot be changed fast enough to satisfy the rapidly changing resonance condition during the microsecond pulse of the magnetron.

formed to exchange energy. This spin-spin damping process tends to keep the spin system in equilibrium within itself and at low microwave power the magnetization vector will always precess in a cone of very narrow opening, determined by the balance between absorbed power and spin-spin relaxation. When the microwave power is increased, the opening angle of the cone will increase. Strictly speaking, the magnetization vector will not even precess uniformly on a conical surface. It can be shown that the effective anisotropy field, i.e., the field which would produce the same torque as the anisotropy, depends on the angular deviation of the magnetization from the axis of the cone. The derivations of Kittel,[3] Van Vleck,[3] and Bickford,[3] of the influence of the anisotropy on the resonance condition, make the assumption that the vertex angle 2φ of the cone is very small. When we take for simplicity the case with H_0 is parallel to the 001 direction of the cubic crystal, the anisotropy will change the resonance value of the field approximately by an amount

$$H_{\text{anis}}{}^{\varphi} = K_1 M_s{}^{-1} \cdot \tfrac{1}{4}(7\cos 2\varphi + 1)\cos\varphi.$$

For very small values of φ this reduces to the well-known expression

$$H_{\text{anis}}{}^{\varphi} = 2K_1/M_s.$$

For $\varphi = \pi/8$, the resonance field would differ by about 80 gauss from the value for $\varphi = 0$, in nickel ferrite at room temperature. As the resonance line is rather narrow, this means that μ'' drops to 15 percent of its maximum value, if the magnetization is forced to precess in a wider cone. On the other hand, the component M_z has decreased by only 7 percent for this opening angle. Thus μ'' can decrease without an essential change in M_z. For other directions of H_0 the calculations become much more complicated, but effects of the same order of magnitude result.

If one starts off resonance at low microwave power, the change in the anisotropy torque with increasing power would produce an approach to the resonance maximum on one side of the absorption line. Although no actual increase of μ'' has been observed off resonance, it has been found that saturation occurs much more readily on one side of the resonance line than on the other.

In polycrystalline or irregularly shaped samples no apparent change in μ'' is caused by this effect, as the effective width of the resonance line is broad in these cases. Here we observe only the regular spin-lattice relaxation mechanism.

In samples of ellipsoidal shape or flat disks the spin-lattice relaxation is difficult to observe. Here the resonance condition depends on M_z through the demagnetizing factors. At the onset of saturation we get off resonance and thus only the initial small decrease of M_z can be observed. The shift in resonance through incipient saturation is shown in Fig. 2.

Saturation experiments in a spherical single crystal of $NiFe_2O_4$ have been carried out at 77°K. Preliminary data show that the decrease in μ'' occurs for microwave power levels which are six times lower than at room temperature. So the spin-spin relaxation time increases with decreasing temperature. The spin-lattice relaxation time is also increased by a factor of about 3, as can be derived from the decrease of M_s.

A prediction of our theory about the influence of anisotropy is that the saturation curves for μ'' and M_z should coincide near the Curie point, where the anisotropy is very small. Experiments at high temperatures to test this point are in the course of preparation.

* This work was supported by the ONR.

[1] N. Bloembergen and R. W. Damon, Phys. Rev. **85**, 699 (1952).
[2] J. H. Van Vleck, Phys. Rev. **78**, 266 (1950).
[3] C. Kittel, Phys. Rev. **73**, 155 (1948); L. R. Bickford, Technical Report XXIII, Laboratory for Insulation Research, Massachusetts Institute of Technology (1949).

First Excited States of Even-Even Nuclides in the Heavy Element Region

FRANK ASARO AND I. PERLMAN
Radiation Laboratory and Department of Chemistry, University of California, Berkeley, California
(Received June 3, 1952)

THIS communication aims to amplify some observations on regularities of the complex spectra of even-even alpha-emitters particularly as they apply to the location of nuclear energy levels.[1,2] Most of the alpha-emitters of this type examined in this laboratory have shown two alpha-groups and the ratio of intensities of the two groups for a particular nuclide is, in good approximation, that expected for the energy difference according to simple alpha-decay theory. For lack of good evidence to the contrary, we have been assuming that the energy level reached by the low energy group is the first excited state and that the laws

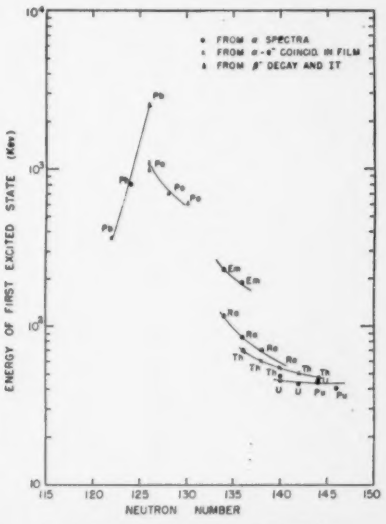

FIG. 1. First excited states of even-even nuclides.

governing the alpha-decay rate are the same as for the ground-state transition with only the energy operating to fix its relative abundance. For the few instances in which but a single alpha-group has appeared, the working hypothesis has been adopted that the first excited state is so high that the correspondingly low abundance of the alpha-group has prohibited its detection. To the extent that these assumptions are valid, the examination of complex alpha-spectra leads to the definition of the first excited states of the even-even nuclides.

The examination with our alpha-particle spectrograph of a number of nuclides in the region of uranium and higher atomic numbers yielded the curious result that the energy levels reached were all in a narrow range. For example, the energy differences between the two alpha-groups for each of the nuclides Cm^{244}, Cm^{242}, Pu^{240}, Pu^{238}, U^{234} all fell between 41 and 47 kev. It was also noted that nuclides of lower mass numbers showed higher energies for their first excited states.

The data are summarized in Fig. 1, in which are plotted the energy levels of the "first excited states" against neutron numbers with isotopes of each element joined. Most of the data were obtained from alpha-spectra taken in this laboratory, others were obtained by Rosenblum and co-workers, and some were measured by conversion electron ranges in photographic emulsions both in this laboratory and elsewhere. Data for excited states of polonium and lead were taken from the literature concerning principally beta-decay processes leading to these states. For the sake of brevity, references are omitted for both the published and unpublished data but these will be included in a later paper.

It is seen that the levels for plutonium, uranium, and the heaviest thorium isotopes are all bunched within a range of about 10 kev. The progressively higher energy for lower elements is consistent with the experienced difficulty of finding such states in alpha-spectra because of the low abundance which would accordingly be expected for the low energy alpha-groups. For example Em^{222}, Em^{220}, and Em^{218} have not yet revealed low energy groups which, according to our present expectations for the energies of the excited states of the corresponding polonium isotopes, would have abundances in the range $\sim 0.03-1$ percent.

The wide level spacing encountered at the region of 126 neutrons is obvious and it is interesting to note that lead isotopes show a decrease going away from 126 neutrons on the low mass side. It is possible that all of these correlations may be based primarily on departures from closed neutron and proton shells. Recently, there have been communications from several sources pointing out this same relationship surrounding closed shells.[2,4]

It is difficult to interpret these data on the single particle model which has been so successful in correlating transitions and energy states of nuclides having odd nucleons. The marked regularity of the first excited states and their low energies suggest some type of excitation involving the nucleus as a whole.

There are a number of apparent steps which may be taken in pursuing further these correlations and their interpretation. One of these, of course, is to extend the data to a wider range and, as one example, to see if energy level spacings increase at still higher mass numbers as might be expected for the approach to a new closed shell. Another point is the examination of the lifetimes of these states and the measurement of conversion coefficients and angular dependence of the gamma-rays. Goldhaber and Sunyar[5] have concluded that the first excited states of most even-even nuclides have spin 2 and even parity. With the low energies encountered for most of these transitions the lifetimes should be in the measurable range.

[1] I. Perlman and T. J. Ypsilantis, Phys. Rev. **79**, 30 (1950).
[2] Asaro, Reynolds, and Perlman, Phys. Rev. **87**, 277 (1952).
[3] P. Stähelin and P. Preiswerk, Helv. Phys. Acta **85**, 690 (1952).
[4] G. Scharff-Goldhaber, Phys. Rev. **87**, 218 (1952).
[5] M. Goldhaber and A. W. Sunyar, Phys. Rev. **83**, 906 (1951).

THE AMERICAN INSTITUTE OF PHYSICS

INCORPORATED

57 East 55 Street, New York 22, N.Y.

MEMBER SOCIETIES:

American Physical Society
Karl K. Darrow, *Secretary*, Columbia University, New York 27, New York

Optical Society of America
Arthur C. Hardy, *Secretary*, Massachusetts Institute of Technology, Cambridge 39, Massachusetts

Acoustical Society of America
Wallace Waterfall, *Secretary*, 57 East 55th Street, New York 22, New York

Society of Rheology
G. J. Dienes, *Secretary*, Brookhaven National Laboratory, Upton, Long Island, New York

American Association of Physics Teachers
R. F. Paton, *Secretary*, University of Illinois, Urbana, Illinois

AFFILIATED SOCIETIES:

American Crystallographic Association
Electron Microscope Society of America
Physical Society of Pittsburgh
Physics Club of Chicago
Physics Club of Philadelphia
Cleveland Physics Society
Physics Club of the Lehigh Valley
Sigma Pi Sigma

ASSOCIATES:

Over seventy-five leading industrial enterprises and other institutions which contribute the support of the Institute.

JOURNALS:

The Physical Review
S. A. Goudsmit, *Editor*, Brookhaven National Laboratory, Upton, Long Island, New York

Reviews of Modern Physics
J. W. Buchta, *Editor*, University of Minnesota, Minneapolis, Minnesota

Journal of the Optical Society of America
Wallace R. Brode, *Editor*, National Bureau of Standards, Washington 25, D. C.

The Journal of the Acoustical Society of America
Floyd A. Firestone, *Editor*, 57 East 55th Street, New York 22, New York

American Journal of Physics
Thomas H. Osgood, *Editor*, Michigan State College, East Lansing, Michigan

The Review of Scientific Instruments
Gaylord P. Harnwell, *Editor*, Randal Morgan Laboratory of Physics, University of Pennsylvania, Philadelphia, Pennsylvania

The Journal of Chemical Physics
Joseph E. Mayer, *Editor*, Institute for Nuclear Studies, University of Chicago, Chicago 37, Illinois

Journal of Applied Physics
Elmer Hoffman, *Editor*, Case Institute of Technology, Cleveland 6, Ohio

Physics Today
Gaylord P. Harnwell, *Editorial Director*; Beatrice M. Hicks, *Managing Editor*, American Institute of Physics, 57 East 55th Street, New York 22, New York

OFFICERS

George B. Harrison, *Chairman*
Massachusetts Institute of Technology
George B. Pegram, *Treasurer*
Columbia University

GOVERNING BOARD:

Karl K. Darrow
G. J. Dienes
S. A. Goudsmit
G. P. Harnwell
George B. Harrison
F. V. Hunt
Rudolph Kingsbury
Hugh S. Knowles
C. C. Lauritsen
F. W. Loomis
William F. Meggers
George B. Pegram
I. I. Rabi
Duane Roller
Frederick Seitz
Frances G. Slack
John C. Stehlin
Richard M. Sutton
Mark W. Zemansky

Consultant on Publications
Melvin Loos

ADMINISTRATIVE STAFF

Henry A. Barton, *Director*
Wallace Waterfall, *Executive Secretary*
Theodore Vermeulen, *Advertising Manager*
Ruth F. Bryans, *Publication Manager*
Betty H. Goldsmith, *Assistant Secretary*
Eileen B. Neumann, *Circulation Manager*
Katherine Seitz, *Assistant Treasurer*

THE American Institute of Physics was established in 1931 as a federation of fourteen societies in the field of Physics. It combines into one operating unit those functions common to all which can best be done for the societies jointly. Its purpose is the advancement and diffusion of physics and its applications to human welfare. To this end it publishes for itself or the Societies the nine journals listed on this page; encourages unity and effectiveness of effort among all who are interested in physics; renders important direct services to physicists and to the public; and cooperates with governmental agencies, national associations, educational institutions, technical industries, and others in such manner as to realize the opportunities and fulfill the responsibilities of physics as an important and constructive human activity.

CONTENTS

The Physical Review

Angular Correlations in the [illegible]

Beta-Spectra and Internal Conversion [illegible]

Energy Levels in Cr, Mn, and [illegible]

Thermodynamic Quantities and [illegible]

Ionospheric Absorption by [illegible]

Complex Alpha-Spectra of [illegible]

Positron-Electron Radiation in [illegible]

Antiferromagnetic Antiparallelism in [illegible]

Angular Correlation between Positron and [illegible]

Neutron-Proton Scattering in the [illegible]

Inelastic Scattering of Neutrons [illegible]

Study of the Electron Trajectories [illegible]

Classical Equations of Motion of [illegible]

Application of the Klein-Nishina [illegible]

Mass Correction to the [illegible]

Decay of a Neutral Meson [illegible]

Ratio of Soft and Hard [illegible]

Nuclear Reaction of Iron with [illegible]

Inelastic Scattering of Neutrons [illegible]

Letters to the Editor:

Zeta Function of Riemann [illegible]

Lowest Excitation Level of [illegible]

Angular Momenta Determination [illegible]

Inelastic Scattering Resonance [illegible]

Internal Absorption of [illegible]

Relative Yields of [illegible]

Angular Correlation in [illegible]

High Energy Electron [illegible]

Measurement of [illegible]

Atomic Beam Resonance [illegible]

Directional Correlation [illegible]

Proportionality [illegible]

Coincidence Detection [illegible]

Neutral Mesons in [illegible]

Interpretation of the [illegible]

Neutrons from Reactions [illegible]

Reactions of [illegible]

Beam Observations [illegible]

Wall Energy of [illegible]

Anomalous Magnetic [illegible]

Neutron-Spin [illegible]

Hyperfine Structure [illegible]

Neutron Capture [illegible]

Proposed Experiment [illegible]

Reply to a Criticism [illegible]

Decay Energies of [illegible]

Reflection of the [illegible]

Reflection of Slow [illegible]

Influence of Atomic [illegible]

Mass Spectrometer [illegible]